GENETIC CONTROL OF ENTERIC NERVOUS SYSTEM DEVELOPMENT AND SUBTYPE SPECIFICATION

Christina Marie Wright

A DISSERTATION

in

Neuroscience

Presented to the Faculties in the University of Pennsylvania

in

Partial Fulfillment of the Requirements for the

Degree of Doctor of Philosophy

2019

Supervisor of Dissertation

_____

Dr. Robert O. Heuckeroth, Professor of Pediatrics and Professor of Cell and Developmental Biology

Graduate Group Chairperson

_____

Joshua I. Gold, Professor of Neuroscience

Dissertation Committee:

Dr. Wenqin Luo, Associate Professor of Neuroscience and Associate Professor of Institute for Regenerative Medicine (IRM)

Dr. Bryan Crenshaw, Adjunct Professor of Otorhinolaryngology: Head and Neck Surgery

Dr. Stewart Anderson, Professor of Psychiatry

Dr. Junhyong Kim, Patricia M. Williams Term Professor and Chair, Biology

Dr. Allan Goldstein, Pediatric Neurogastroenterology Program Director, Mass General Hospital

GENETIC CONTROL OF ENTERIC NERVOUS SYSTEM DEVELOPMENT AND SUBTYPE SPECIFICATION

COPYRIGHT
2019
Christina Marie Wright

This thesis is dedicated to the many patients and organ donors who graciously provided the tissue that make this research possible, and to the many mice sacrificed to better understand bowel motility disorders.

ACKNOWLEDGMENTS

First and foremost, I would like to thank my thesis mentor Dr. Robert Heuckeroth for his unwavering guidance and support throughout the completion of this thesis work. Bob, you have truly been the best mentor I could have asked for these past five years. You have challenged me, supported me and taught me so much about writing, the ENS, and being a scientist. Thank you for taking a chance on me as your first PhD student after you arrived in Philadelphia.

I would also like to thank my committee members: Dr. Wenqin Luo, my committee chair, and Dr. Stewart Anderson, Dr. Bryan Crenshaw, and Dr. Junhyong Kim, for your immensely valuable insight over the years and for challenging me to make this thesis as good as possible. Thank you as well to my external thesis committee member, Dr. Allan Goldstein, for your encouragement and for agreeing to jump in on this project as it was nearing completion.

I am incredibly grateful to the past and present members of the Heuckeroth lab, whose scientific input and friendship have kept me sane throughout this journey: Dr. Marina Avetisyan, Dr. Ellen Schill, Dr. Rajarshi Sengupta, Sabine Schneider, Sohaib Hashmi, Silvia Huerta, Dr. Tao Gao, Beth Maguire, Dr. Kahleb Hashmi, Amanda Lemke, Deepika Kothakapa, Jessica Anderson, Chris Pai, Heather Mentch, Brianna Christophers, Rachel Dvorak, Dr. Jonathan Lake, Dr. Jenny Yang, Alisha Jamil, Rebecca Bradley, and Dr. Josh Eisenberg. Ellen, thank you for mentoring me the year we overlapped, and for unexpectedly leaving me a very interesting unfinished project (and many cages of mice that refused to breed). Thank you, Marina, for many years of mentoring, advice, friendship, and hilarious lab hijinks. Sohaib and Sabine, you have truly been the best lab friends a person could ask for, and I owe you another Vermont trip very soon. Thank you as well to Raj and Bryan, for endless support, friendship, and delicious food; Deepika, for counting more cells than was probably healthy; Silvia, for being all-around awesome; Jessica, for valiantly rabbit-sitting in times of need; Beth, for keeping sane in the face of hordes of mice; Amanda, for

always replying instantly to emails no matter where you are; and Chris, for being an endless fount of statistical wisdom.

Many scientists outside the lab also deserve thanks: Dr. Kristen Edwards, Dr. Brian Davis, Dr. Joel Bornstein, Anita Leembruggen, Dr. Randall Roper, Dr. Heron Baumgarten, Dr. Archana Shenoy, Dr. Benjamin Wilkins, Dr. Fernanda Mafra, Dr. Renata Pellegrino, James Garifallou, Dr. Marthe Howard, Dr. John Grider, Dr. Toshinori Hoshi, Nishi Gheewala, Lucie Ngaba, Melissa Orr, Danielle Pi, Dr. Florin Tuluc, Jennifer Murray, and Lily Wu. Thank you as well to Dr. Emma Furth, Dr. Federico Valdivieso, Jennifer Finan, Lauren Schmucker, Andrew Kromer, and Caitlin Feltcher in HUP pathology, and Dr. Archana Shenoy, Dr. Benjamin Wilkins, and Dr. Ali Naji at CHOP, for helping us coordinate tissue acquisition. And of course, thank you to Maggie Krall, Dr. Skip Brass and the Penn MSTP program, as well as my doctors, Dr. Mary Mullen and Dr. Hans Oettgen, and my undergraduate thesis advisor, Dr. Ethan Graf, for encouraging me to go down this path.

I also wish to thank my friends outside the lab for helping me have a life that is not 100% science: Natania Field, Sneha Narasimhan, Jessica Luo, Rose Weisshaar, Leandro Lichtenfelz, Varsha Viswanath, Stephanie Cheng, Tanya Xu, Christine Chen, Michiko Theurer, Jean Santos, Mingzi Shao, Emma Fink, Dang Trinh, Ambika Kamath, and Arthi Kumaravel. Special thanks to my writing-buddy Natania, without whom assembling this thesis would have been considerably lonelier and more miserable; I'm sorry we will miss each others' defenses.

Of course, this acknowledgements section would not be complete without thanking my wonderful fiancé, Tiancheng Wang. Tian, thank you for your unconditional love and support throughout my PhD. You have unwaveringly listened to me rant about mice, low sequencing read depth, mice, programming difficulties, mice, genotyping, mice, 3 AM labwork, and mice. Even when things looked grim, I am glad we were able to laugh about them together.

Finally, thank you to my parents, Karl and Martha Wright, without whom I would not be alive and writing this thesis. I truly appreciate your lifelong encouragement and support.

Funding for the work described in this dissertation came from the Perelman School of Medicine Medical Scientist Training Grant, the Irma and Norman Braman Endowment, The Children's Hospital of Philadelphia Research Institute, the Suzi and Scott Lustgarten Center Endowment, NIH grants 5 F30 DK117546-02 (CMW), and RO1 DK087715 (ROH), March of Dimes 6-FY15-235 (ROH), the Burroughs Wellcome Fund Clinical Scientist Award in Translational Research (grant no. 1008525) (ROH), and from NIH SPARC Program OT2OD023859 (Marthe Howard PI, Robert Heuckeroth co-I).

ABSTRACT

GENETIC CONTROL OF ENTERIC NERVOUS SYSTEM DEVELOPMENT AND SUBTYPE SPECIFICATION

Christina Marie Wright

Robert O. Heuckeroth

Hirschsprung disease (HSCR) and chronic intestinal pseudo-obstruction (CIPO) are life-threatening bowel motility disorders that cause growth failure, abdominal distention, and sometimes, early death. In HSCR, the enteric nervous system (ENS) does not develop completely, resulting in a region of bowel lacking neurons. HSCR can be treated by surgically removing aganglionic bowel, but many children with HSCR have poor motility even after surgery, especially children with comorbid Down syndrome. In contrast to HSCR, the entire ENS is present in CIPO, but bowel motility is abnormal. Abnormal motility can occur if neurons are present but dysfunctional, or if neuron subtypes are incorrectly specified. Unfortunately, the transcriptional machinery underlying neuron subtype identity in the ENS is poorly understood, and we also know little about genetic causes of dysfunctional motility in CIPO and post-surgical HSCR.

To better understand transcriptional control of ENS development, we characterized the ENS of several mice lacking transcription factors highly expressed in ENS precursors. Mice lacking *Dlx1* and *Dlx2* had a structurally normal ENS but bowel function defects similar to CIPO, and markedly decreased *Vip* expression in enteric neurons (Chapter 2). Mice with an ENS-specific deletion of *Tbx3* had reduced glia density (Chapter 3), and reduced density of a subtype of enteric neurons (Chapter 4). To

determine if *Dlx1, Dlx2,* and *Tbx3* were expressed in subsets of enteric neurons, we performed single-cell and single-nucleus sequencing on neurons from embryonic and adult mouse bowel (Chapter 4). We identified 40 differentially-expressed transcription factors and hundreds of ion channels, signaling molecules, and receptors defining 7 classes of enteric neurons. We also sequenced nuclei from 48 human enteric neurons (Chapter 4). This data confirms *Tbx3* expression in ENS subpopulations and generates numerous hypotheses about other genes involved in subtype specification. Finally, to investigate causes of poor bowel motility in Down syndrome, we characterized two mouse models of Trisomy 21. We found multiple ENS defects, including submucosal plexus hypoganglionosis, distal colon hypoganglionosis, and impaired colon motility (Chapter 5). These studies enhance our understanding of the genetic causes of motility disorders and provide a wealth of data on subtype-specific gene expression in the ENS.

TABLE OF CONTENTS

LIST OF MAIN TABLES

LIST OF MAIN ILLUSTRATIONS

LIST OF SUPPLEMENTARY TABLES

LIST OF SUPPLEMENTARY ILLUSTRATIONS

CHAPTER 1 : GENERAL INTRODUCTION

Relevant sections from our *Annual Review of Physiology* review, "Unexpected roles for the second brain: The ENS as a master regulator of bowel function" (included here in full as Chapter 7: Appendix A) were reprinted here with permission. **Sections directly from the review are in italics. Many sections were rewritten to focus on enteric neuron subpopulations, while the review focused on other cells in the bowel.**

Digesting nutrients that fuel our survival requires complex integration of many bowel functions, and all must run smoothly to maintain a normal quality of life. Food must be broken into small particles and chemically digested for nutrient absorption. Indigestible components must efficiently pass through the gastrointestinal tract for elimination, while fluid and electrolyte balance is maintained. All of these processes occur in the setting of a complex microbiome that aids nutrient absorption but can trigger inflammation and even infection should the system go awry. The intestine could not coordinate these functions without the enteric nervous system (ENS), a complex network of neurons and glia that reside in the bowel wall and send nerve fibers throughout the bowel. Like an orchestra conductor, the ENS is a critical regulator of the many processes described above and interacts with an astounding array of cell types to facilitate bowel function.

The ENS is distributed all the way along the bowel in two layers called the myenteric and submucosal plexus (1). Each plexus is comprised of diverse enteric neuron and glial cell types that interact closely with each other and with other intestinal cells. Myenteric plexus cells cluster into ganglia between the outer longitudinal and inner circular smooth muscle of the bowel.

Myenteric neurons provide the majority of direct innervation to the bowel's motor apparatus and the final output controlling bowel relaxation and contraction. Myenteric neurons interact closely with the tissue-resident macrophages (muscularis macrophages) that influence motility. Submucosal plexus ganglia reside between muscle and epithelium, where they regulate epithelial secretion and local blood flow. In mice and many smaller mammals, submucosal neurons comprise a single layer, while large mammals, such as humans, may have two or more layers of submucosal neurons (2). Neurons in both plexi respond to input from mucosal enteroendocrine cells and the autonomic nervous system. The ENS also interacts with immune and epithelial cells to promote barrier function that protects the bowel from pathogens in the gut lumen. Defects in any one of these processes could lead to a spectrum of bowel disorders, and complete absence of the ENS (i.e. total intestinal aganglionosis) is a uniformly fatal diagnosis (3).

A complex array of neuron subtypes with distinct roles is needed to coordinate the many bowel functions described above. Approximately twenty enteric neuron subtypes and four glial subtypes have been described. Neuron classifications have been made based on neurotransmitter immunohistochemistry, function, axon number, direction of axonal projections, synaptic connectivity, and electrophysiologic signatures (4). Unfortunately, past classification approaches have told us little about the differences in gene expression between neuron classes, nor have they offered much insight into how individual neuron subtypes develop. Single-cell sequencing data will likely redefine our understanding of enteric neuron and glial subtypes in the next few years. Improving our understanding of the developmental processes involved in neuron subtype formation is especially important because some disorders of ENS function involve selective loss or reductions in specific neuron subtypes. A possible treatment for these disorders is stem cell therapy to replace reduced or missing subtypes. To facilitate stem cell replacement therapy, we must first define normal bowel neuron composition and characterize regulatory networks involved in enteric neuron subtype development.

Here, I review the classes of neurons that comprise the mature ENS, with an emphasis on how defects in neuron subgroups could cause disease. I then review major steps in ENS development, with particular focus on transcription factors known to coordinate ENS precursor migration, cell fate decisions, and neuron subtype specification.

1.1 – Types of enteric neurons

Classically, enteric neuron subtypes were described as falling into three major classes: intrinsic primary afferent neurons (IPANs), interneurons, and motor neurons (5, 6). IPANs were thought to sense signals from the environment, including chemicals in the bowel lumen and gut wall stretch, and transduce these signals into appropriate reflex responses. Interneurons receive signals from IPANs and other interneurons, and then signal onto motor neurons and other interneurons. Finally, motor neurons comprising inhibitory and excitatory muscle motor neurons, secretomotor neurons, vasodilator neurons, enteroendocrine-signaling motor neurons, directly affect most other bowel cell types to regulate bowel function (2). Although the motor neuron classification has remained stable over many years, the role of IPANs and interneurons remains a subject of debate, as discussed in detail below.

Enteric neuron subtypes have been described by their chemical coding, their morphology (i.e. Dogiel type I and type II), and their electrophysiological properties (i.e. AH versus S). Important markers for enteric neurons include choline acetyl-transferase (ChAT), neuronal nitric oxide synthase (nNOS), vasoactive intestinal peptide (VIP), substance P (SP), and calcitonin gene related peptide (CGRP). Common neurotransmitter abbreviations are in (**Table 1-1**). Morphologically, enteric neurons are often described as having either Dogiel Type I or Dogiel Type II morphology. Dogiel Type I neurons are mono-axonal, with short, club-like dendrites, while Dogiel Type II neurons have two or more axons and large, smooth cell bodies. In mouse bowel, Dogiel Type II neurons (generally assumed to be IPANS) can be readily identified, and

Table 1-1: Enteric neuron subtype markers	
Abbreviation	**Stands for**
ChAT	Choline acetyltransferase
nNOS	Neuronal nitric oxide synthase
SP	Substance P
VIP	Vasoactive intestinal peptide
SOM	Somatostatin
CGRP	Calcitonin Gene-Related Peptide
NFM	Neurofilament M
GRP	Gastrin-releasing peptide
NMU	Neuromedin U
5-HT	Serotonin

Dogiel Type I neurons can sometimes be identified with biocytin tracing (4, 7). Other Dogiel neuron types are identifiable in the ENS of larger species, which tend to have more elaborate dendritic arbors than mouse (4, 8).

The electrophysiological properties of enteric neurons can also be divided into two categories: after-hyperpolarizing (AH), and S-type neurons. In AH neurons, Ca^{2+} carries part of the action potential, and a delayed afterhyperpolarizing potential (carried by the intermediate conductance potassium channel) follows the action potential (9). Most AH neurons in the bowel are thought to be IPANs. In contrast, interneurons and motor neurons, which are classified as electrophysiologically as S neurons, have narrow action potentials, monophasic repolarizations, and no afterhyperpolarizing potential (5, 10).

1.1.1 – Intrinsic primary afferent neurons (IPANs) and sensory responses in the bowel

Responses to chemical stimuli

Classically, IPANS have been defined as AH neurons with Dogiel Type II morphology; in mouse small intestine, they are large, distinctive neurons that contain the markers Neurofilament M and CGRP (4). Past studies reported that IPANS respond to chemical stimuli within the bowel lumen (5), but it remains unclear if IPANS respond directly to chemical stimuli

Table 1-2: Hypothesized neurochemical code for mouse small intestine enteric neurons.

Modified from: (11)**,** (4)

Submucosal plexus, mouse ileum			Mouse strain: C57BL/6
Putative subtype	**Chemical coding**	**Relative percent**	**Morphology**
Vasodilator neurons	VIP/NPY/calretinin	30%	
Secretomotor neurons	VIP/NPY/calretinin/TH	20%	
Secretomotor neurons	ChAT/CGRP/SOM ± NPY	30%	
Unknown	ChAT alone	10%	
Unknown	Neither ChAT nor VIP	8%	
Myenteric plexus, mouse ileum			Mouse strain: BALB/c
Putative subtype	**Chemical coding**	**Relative percent**	**Morphology**
IPANs	CGRP/NFM/Calbindin/ChAT ± calretinin	26%	Dogiel Type II
Descending interneuron	ChAT/nNOS	3%	Type I
Descending interneuron	ChAT/5-HT	1%	Type I
Descending interneuron	ChAT/SOM/Calretinin	4%	Filamentous
Ascending interneuron	ChAT/SP ± Calretinin	4%	Type I
Excitatory circular muscle motor neurons	ChAT/calretinin ± SP	21%	Small-medium
Excitatory longitudinal muscle motor neurons	ChAT/calretinin ± SP	13%	Small
Inhibitory circular muscle motor neurons	nNOS/VIP ± NPY	23%	Type I
Inhibitory longitudinal muscle motor neurons	nNOS/VIP	3%	Small, Type I
Tyrosine hydroxylase neurons	TH	Rare, < 0.5%	Type I
Intestinofugal neurons	Unknown	Unknown	Unknown

or indirectly to chemicals via enterochromaffin cells (12). Enterochromaffin cells are a subtype of enteroendocrine cell that act as polymodal chemosensors and can activate in response to a wide range of compounds. Enterochromaffin cells produce serotonin and appear to form functional synapse-like contacts with $5HT_3$R-expressing nerve fibers (13). Thus, it seems plausible they could stimulate IPANs in response to chemical stimuli.

Responses to mechanical stimuli

It is already accepted that enterochromaffin cells respond to *mechanical* stimulation by releasing serotonin (5-HT) onto IPANs, and this evokes enteric neural reflexes like peristalsis.

Enterochromaffin cells in the gut share many similarities to mechanosensitive Merkel cells in the skin, including expression of the mechanosensitive ion channel Piezo2, certain transcriptional regulators, and serotonin release onto neurons (14). Mice lacking the enzyme necessary for 5-HT biosynthesis in enterochromaffin cells [tryptophan hydroxylase 1 (*Tph1*)] have altered colon migrating motor complexes and significantly larger fecal pellets (15). This finding suggests that without 5-HT from enterochromaffin cells, a larger degree of stretch is needed to induce contractions (16). However, this topic remains controversial (14, 17, 18). It was surprising that *Tph1-/-* mice survive to adulthood with normal gastrointestinal transit time (19). Moreover, although possibly less frequent, spontaneous colon migrating motor complexes persist despite removal of GI mucosa (20, 21). These new findings may suggest enterochromaffin cells contribute less to mechanically-evoked reflexes than was once thought, and that redundant systems control bowel motility.

One mechanism supporting enterochromaffin cell-independent mechanosensation is direct mechanosensing by enteric neurons. IPANs were originally believed to act as mechanosensors, and in fact to be the main mechanosensitive neurons in the bowel (1, 2, 10). Subsequent research questioned this assumption. A study using voltage-sensitive dye suggested that 25% of neurons in the guinea pig myenteric plexus exhibit rapidly adapting responses to deformation that persists even when excitatory post-synaptic potentials were blocked. These mechanosensitive neurons had a variety of different chemical codes; 72% were cholinergic and 22% were nitrergic (22), suggesting that many classes of neuron may contribute to mechanotransduction in the gut wall. Further research suggests that slowly adapting, and ultra-slowly adapting mechanosensitive neurons also reside in the myenteric plexus (23, 24). This research has given rise to a new model for mechanosensation in the gut which argues that enteric neurons of multiple types may act as multifunctional mechanosensors (24).

1.1.2 – Interneurons

It is generally agreed that ENS interneurons are S-type neurons of Dogiel Type I morphology. Compared to more common IPANS and to motor neurons, individual interneuron subtypes are much rarer. Interneurons appear to interact with all neuron subtypes in the bowel, including other interneurons, and may form chains extending up and down the bowel (5).

The existence of interneurons in the ENS is indicated by the existence of ascending and descending reflexes, as well as from nerve tracing studies showing nerve endings that lie in ganglia proximal or distal to their cell bodies (5, 6). Divided organ baths have been used to evaluate reflex contractions in adjacent segments of bowel and their sensitivity to different antagonists (25, 26). In guinea pig small intestine, one type of ascending (i.e. orally-directed) and three types of descending (i.e. anally-directed) interneurons have been identified (5), and attempts have been made to correlate these interneuron subtypes in mouse small intestine (**Table 1-2**) (4). Interneurons contain complex combinatorial codes of ChAT, somatostatin, calretinin, VIP, GRP, calbindin, and serotonin, among other neurotransmitters (**Table 1-2**). In the guinea pig distal colon, one study described three classes of ascending interneurons and four classes of descending interneuron, some of which project to the submucosal plexus (27). A neurochemical code for mouse distal colon has not yet been elucidated. In the studies mentioned above, considerable inference has been employed in assigning different chemical codes to different types of interneurons, particularly across different regions and across different species. Assumptions are often made that neurons expressing a certain chemical code in one species or region of bowel will have the same function and orientation in other species or bowel region, which may not always be the case (4, 28). There is also an assumption that the chemical code seen in soma perfectly matches the chemical code expressed in varicosities, which could be problematic if immunostaining is patchy or neurotransmitters are expressed at low levels (27). We expect single cell sequencing may help clarify some of these issues in the near future.

1.1.3 – Motor neurons

Inhibitory muscle motor neurons:

Inhibitory enteric neurons are a critical group of uni-axonal neurons that promote bowel relaxation by projecting into the circular and longitudinal smooth muscle layers. In mouse, the cell bodies of these neurons are uniformly in the myenteric plexus, while in larger mammals, some circular muscle innervation may come from submucosal ganglia (2). The muscle layers innervated by inhibitory muscle motor neurons contain smooth muscle cells (SMCs), interstitial cells of Cajal (ICC), and platelet-derived growth factor receptor (PDGFR)α+ cells. These three cell types form a multicellular syncytium commonly known as the "SIP syncytium," *whose name derives from the first letter of each cell type (29). Although SMCs were once considered the main targets of excitatory and inhibitory ENS motor neurons, neural input onto ICC and PDGFRα+ cells is likely also critical for mediating smooth muscle contractility and for generating complex motility patterns necessary for life.*

Diverse motor patterns are required for food to be digested and absorbed and for waste to be eliminated. These motility patterns in human small intestine include peristalsis (waves of contraction and relaxation that propagate down the bowel), segmentation (alternating contraction and relaxation to mix food with digestive enzymes and bile), and the migrating motor complex (MMC) (where strong waves of contraction and relaxation propagate down the bowel during phase III to move luminal contents toward distal bowel for elimination). In the colon, high-amplitude propagating contractions (HAPCs) move stool over long distances toward the rectum and occur only occasionally. Generation and maintenance of these motor patterns require a complex interplay between neural signaling, ICC, PDGFRα+ cells, and SMCs. In broad strokes, ICC continually produce oscillating electrical slow waves in the bowel that set the rhythm for many motor patterns. Slow wave electrical activity propagates from ICC to SMCs, generating rhythmic SMC depolarization and contraction. Neural signaling onto the SIP

syncytium generates and modulates ICC and SMC activity to produce the motor patterns described above. Stimuli from the environment alter ENS activity to determine which motor patterns should occur at specific times (30). For example, segmentation in the small bowel occurs after meals, but phase III MMC predominates once most nutrients are absorbed. Although the ENS is not essential for generating some motor patterns, the ENS is probably the primary inducer of complex motility patterns needed for survival (31).

Inhibitory motor neurons release nitric oxide (NO), VIP, PACAP, and purines onto their targets (**Figure 1-1A**). These neurons may also synthesize gamma-aminobutyric acid (GABA), neuropeptide Y (NPY), and bombesin, although it is unclear if these transmitters have post-synaptic roles (5). NO acts on both ICC and SMCs by binding and activating *nitric oxide-sensitive guanylyl cyclase (NO-GC). Guanylate cyclase converts GTP to cGMP, which activates GMP-dependent protein kinase 1 (PRKG1). PRKG1 in turn phosphorylates serines and threonines on many intracellular proteins, causing hyperpolarizing via mechanisms that remain incompletely understood. A few recent papers have also suggested that PRKG1-independent (but NO-GC and cGMP dependent) NO signal transduction may occur in ICC (32, 33). In addition to NO, inhibitory enteric neurons release vasoactive intestinal peptide (VIP) and pituitary adenylate cyclase–activating peptide (PACAP). These neuropeptides likely signal through VIP receptors VIPR1 and VIPR2 and the PACAP receptor ADCYAP1R1, which are expressed on ICC and SMCs (30). Typically, neuropeptides are released at high-stimulus frequencies, so VIP and PACAP may play less prominent roles in direct motor neurotransmission than NO (30).* Finally, purines released by inhibitory motor neurons probably bind to P2Y1 receptors on PDGFRα+ cells. *The ligand for P2Y1 receptors in the bowel was once thought to be adenosine 5′ triphosphate (ATP), but in recent years, β-nicotinamide adenine dinucleotide (β-NAD) and adenosine 5′-diphosphate-ribose (ADPR) have emerged as more likely candidates (34). Applying β-NAD and ADPR to PDGFRα+ cells activates apamin-sensitive, small-conductance Ca2+-*

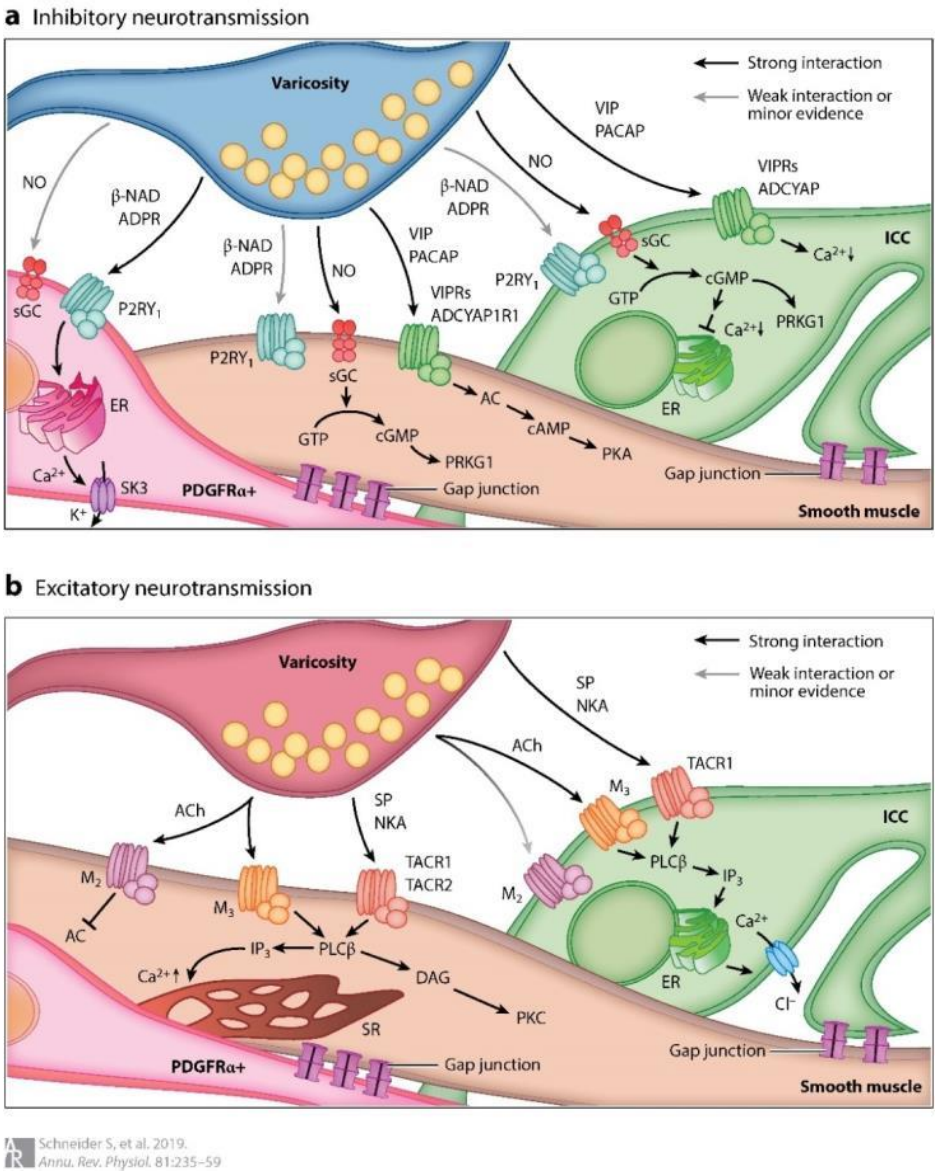

Schneider S, et al. 2019.
Annu. Rev. Physiol. 81:235–59

Figure 1-1: Inhibitory and excitatory muscle motor neuron signaling.
(a) Inhibitory neurotransmission involves a combination of purine, NO, and VIP/PACAP signaling. (b) The primary neurotransmitters involved in excitatory neuromuscular transmission are acetylcholine and tachykinins. Abbreviations: AC, adenylate cyclase; ACh, acetylcholine; ADCYAP1R1, pituitary adenylate cyclase-activating polypeptide type 1 receptor; ADPR, ADP-Ribose; β-NAD, β-nicotinamide adenine dinucleotide; cAMP, cyclic AMP; cGMP, cyclic GMP; DAG, diacylglycerol; GTP, guanosine triphosphate; ER, endoplasmic reticulum; ICC, interstitial cells of Cajal; IP_3, inositol triphosphate; M2, muscarinic receptor 2; M3, muscarinic receptor 3; NKA, neurokinin A; NO, nitric oxide; PACAP, pituitary adenylate cyclase-activating peptide; PKA, protein kinase A; PKC, protein kinase C; PRKG1, protein kinase G; PLCβ, phospholipase C beta; sGC, soluble guanylate cyclase; SK3, small conductance calcium-activated potassium channel 3; SP, substance P; SR, sarcoplasmic reticulum; TACR1, tachykinin receptor 1; TACR2, tachykinin receptor 2; VIP, vasoactive intestinal peptide; VIPR, VIP receptor.

activated K+ (SK) channels, leading to potassium efflux and membrane hyperpolarization (15). The change in membrane potential spreads via gap junctions to nearby SMCs. Purinergic receptors are also expressed on SMCs and ICC, but they are unlikely to mediate the strong fast hyperpolarization associated with the IJP (34, 35).

Excitatory muscle motor neurons

Excitatory motor neurons also project uni-axonally from the myenteric plexus into the circular and longitudinal smooth muscle layers. The major excitatory neurotransmitters involved in direct motor neurotransmission are acetylcholine (ACh) and tachykinins (neurokinin A (NKA) and substance P). *ACh binds muscarinic M2 and M3 receptors on SMCs and ICC, while tachykinins bind tachykinin receptor 1 (TACR1) and 2 (TACR2) receptors on SMCs and TACR1 on ICC (***Figure 1-1b***). In ICC-DMP, signal transduction via M3 receptors likely occurs through Gq, leading to Ca2+ release from the endoplasmic reticulum and activation of CaCCs such as anoctamin 1 (Ano1). Opening of CaCCs causes a depolarizing current predicted to enhance the likelihood of action potential generation and increase contraction amplitude (36, 37). M2 receptors are also expressed on ICC but may play a less important role than M3 receptors (36, 38). In contrast, evidence from knockout mice suggests that both M3 and M2 receptors influence SMC contractility (39).*

Like muscarinic signaling in ICC, tachykinin signaling via TACR1 is hypothesized to act via Gq signaling coupled to Ca2+ release and CaCC opening. Tachykinin signaling may be more important than muscarinic signaling in ICC-DMP. Applying TACR1 antagonists attenuated basal Ca2+ transients in small intestine ICC-DMP, suggesting that ICC-DMP are tonically excited by tachykinins (36). The same may not be true in colonic ICC, which do not express TACR1 as highly (36). In SMCs, tachykinin signaling is transduced by both TACR2 and TACR1 (40).

Second messenger signaling likely occurs through protein kinase C (PKC) and IP3 (30), although other pathways may be involved (40).

Vasodilator neurons

During digestion, blood flow to intestinal mucosa increases as much as twofold, owing in part to dilation of submucosal arterioles. Vasodilation and resulting hyperemia are needed to meet the high metabolic demands of the mucosa and to exchange nutrients, water, and solutes across bowel epithelium. Neurogenic vasodilation of submucosal arterioles is mediated by extrinsic and intrinsic (ENS) innervation. In contrast, vasoconstriction of bowel arterioles is wholly under control of extrinsic sympathetic innervation.

Most studies of submucosal arteriole vasodilation evaluated guinea pig small intestine, using varied preparations including isolated submucosa and full thickness intact bowel. These studies suggest many triggers for ENS-mediated vasodilation, including gently stroking bowel mucosa, distorting the mucosa with puffs of gas, and distending smooth muscle with a balloon. Small distortions of the mucosa (stroking, puffing gas) cause enterochromaffin cells to release 5-HT onto enteric nerve terminals expressing 5-HT3 [myenteric IPANS (38)] and 5-HT4, and/or 5-HT1P [submucosal IPANs (41)]. Stimulating these IPANs by 5-HT activates short (1–2 mm) reflex pathways within the submucosa, as well as longer reflex pathways that span submucosal and myenteric plexus (41). Stretching the bowel activates 5-HT3- and 5-HT4-insensitive mechanotransducers in the myenteric plexus (42) and possibly submucosal plexus (43), leading to vasodilation. Mechanical deformation of the gut activates neurites and soma of a large number of mechanosensitive enteric neurons within the myenteric plexus (24). These mechanosensitive neurons are multifunctional (i.e., they may be afferents, interneurons, or efferents), and their responses to mechanical stimulation may be rapid-adapting, slow-adapting, or ultraslow-adapting (44).

The final common pathway for ENS-mediated vasodilation in guinea pig small intestine is release of acetylcholine onto endothelial cells, which activates muscarinic M_3 receptors, leading to NO release and vasodilation (45). In guinea pig distal colon, substance P and/or VIP release from submucosal plexus neurons may contribute to vasodilation (46). It is unclear if and how these processes differ in mouse. The ENS may also stimulate mast cells to release the vasodilator histamine directly onto submucosal blood vessels (45) via substance P and/or calcitonin gene–related peptide (CGRP)(47).

Secretomotor neurons

At least two classes of secretomotor neurons are found within the submucosal plexus: cholinergic and non-cholinergic (VIP+). Release of 5-HT from enteroendocrine cells in response to mucosal stroking activates IPANs, which in turn synapse onto secretomotor neurons that release acetylcholine or VIP. *Acetylcholine acts via muscarinic receptors and VIP via VIPR1 receptors on crypt epithelial cells to increase intracellular Ca2+ (via phospholipase C and IP3) and cAMP (via Gs), respectively. Cyclic AMP activates the cystic fibrosis transmembrane regulator (CFTR) chloride channel. Calcium activates the HCLCA1 chloride channel, inducing more transient chloride flux. Movement of chloride into the gut lumen is accompanied by sodium and water. The details of these circuits are much better understood than this brief description suggests, and they are beautifully described in reviews (48, 49).*

1.1.4 – Regional, species, and strain differences in bowel neuron composition and function

Although we sometimes discuss these broad categories of enteric neurons as if they are uniformly represented throughout the bowel, neuron density and ENS subtype composition differs significantly between esophagus, stomach, small bowel, and large intestine. Even within different parts of the large intestine, relative ratios of neuron subtypes and their projections can

differ greatly (50) (Chapter 8). ICC localization and receptor expression also differ along the bowel, and selectively deleting parts of the signal transduction pathway (for instance, NO-GC from ICC) has different effects in mouse colon than in mouse fundus (51). Adding to the complexity, many initial studies of chemical coding were performed in guinea pig, but there are considerable differences between guinea pig and mouse, and also between guinea pig and large mammals. For example, in guinea pig small intestine, submucosal plexus contains four types of neuron (2 classes of secretomotor neuron, 1 class of vasomotor neurons, and 1 class of IPANs). In mouse, no evidence of IPANS has been identified in submucosal plexus (11). In contrast, pigs have *fourteen* neuron subtypes in submucosal plexus alone, comprising secretomotor, vasomotor, IPANs, muscle motor, interneurons, intestinofugal neurons (52). These findings illustrate potential issues with making cross-species assumptions for chemical coding, and underscore the importance of ultimately characterizing the chemical and transcriptional coding of human enteric neurons. Neuron subtype ratios have been shown to differ significantly even between mouse strains (53). Microbiome and diet also significantly impact neuron subtype ratios in the bowel (54, 55). It is unclear how much of the discrepancies observed in the mouse literature are due to differences in strain, microbiome, diet, and antibody quality (56).

1.2 – Disorders associated with ENS dysfunction

The ENS relies on the coordinated and balanced activity of its component neurons in order to function appropriately. Perturbations in one or all of the neuron types described above can have serious effects on various aspects of bowel function, including motility, secretion, and intestinal barrier function. We discuss some human diseases that can arise when the ENS is dysfunctional, with particular focus on enteric neuron subtypes.

1.2.1 - Hirschsprung disease

The ENS forms from enteric neural crest–derived precursor cells (ENCDCs) that colonize the bowel during first trimester fetal development. In approximately 1:5,000 children, ENCDCs never reach the distal bowel, resulting in a region where the ENS is completely absent. This problem is called Hirschsprung disease. In children with Hirschsprung disease, the region of bowel that lacks enteric ganglia (i.e., aganglionic bowel) tonically contracts and lacks propagated motility, leading to functional obstruction. Because aganglionic bowel does not efficiently pass stool or air, Hirschsprung disease symptoms include distension, constipation, vomiting, abdominal pain, growth failure, and a predisposition to bowel inflammation (called enterocolitis) that may lead to death from sepsis (57-59). Genetic and environmental factors both play a role in HSCR. Inheritance is multigenic, and many causative mutations and associated gene variants have been identified (60). In about 30% of cases, HSCR occurs as part of a broader genetic syndrome. Vitamin deficiencies and certain medications can also affect bowel colonization and may contribute to HSCR risk (61-63). The developmental processes involved in HSCR, and many key causative genes, are described in more detail later in this introduction.

Surgical resection of the aganglionic segment of bowel is considered the gold-standard treatment for HSCR. However, even after bowel resection surgery, many children with HSCR continue to experience serious bowel problems, including persistent constipation, enterocolitis, and fetal incontinence, sometimes persisting into adulthood (64-69). We now believe some of these issues are due to abnormalities in the unresected neuron-containing bowel. Neuron subtype imbalances have been noted in the ganglia-containing proximal colon of some HSCR mouse models (70-72), and also in human subjects with HSCR (73, 74). Most studies found an increased proportion of nNOS+ neurons in these proximal regions of the colon (70-74). One study using a common mouse model of HSCR ($Sox10^{Dom/+}$) also found increased calretinin+ neurons throughout the small intestine, but decreased calretinin+ neurons in colon (71). Profound abnormalities in bowel motility were also observed in regions with ganglia in HSCR mouse

models, including impaired small intestine transit and reduced or absent colon migrating motor complexes (71, 72).

Intriguingly, the incidence of HSCR is much higher in children with Down syndrome (Trisomy 21) than in the general population. The cause of this increased incidence remains unknown. Several genes on chromosome 21 have been postulated to increase HSCR risk, including Down syndrome cell adhesion molecule (*DSCAM*) and Dual specificity tyrosine-phosphorylation-regulated kinase 1A (*DYRK1A*). DSCAM is a member of the immunoglobulin superfamily of cell adhesion molecules that is expressed in ENS precursors during development (75). Certain *DSCAM* SNPs occur at increased frequency in individuals with HSCR (76, 77), and *DSCAM* is located in a region on chromosome 21 thought to be critical for development of HSCR based on studies with individuals with rare partial trisomy 21 (78). *DYRK1A* is another gene located on in this critical region (78). DYRK1A has many roles in nervous system development, including the regulation of cell cycle control and activation of GLI1, a protein in the Hedgehog signaling pathway whose overexpression was linked to HSCR (79-84). These genes and their association to HSCR are explored further in Chapter 5.

Another unexplained observation is that children with HSCR and Down syndrome tend to have worse bowel problems after corrective surgery than children with HSCR alone. Enterocolitis, severe constipation, and soiling are significantly more frequent in HSCR with coexisting Down syndrome (85, 86). One hypothesis is that children with Down syndrome might have baseline differences in ENS structure, subtype composition, or function. In support of this theory, individuals with Down syndrome who do not have HSCR are more likely than the general population to have other functional gastrointestinal problems, including chronic diarrhea and unexplained severe constipation (87, 88). In Chapter 5, we describe markedly reduced submucosal neuron density and abnormal colon motility in the ENS of Down syndrome mouse models. These findings may be relevant for understanding the functional defects in these patients.

1.2.2 - Chronic intestinal pseudo-obstruction syndrome:

When the ENS is present throughout the bowel, but bowel motility does not consistently support survival or growth without at least intermittent intravenous nutrition, chronic intestinal pseudo-obstruction syndrome (CIPO) is the likely diagnosis. Symptoms of CIPO include repetitive episodes of abdominal distension and pain, vomiting, growth failure, and weight loss (89). CIPO may occur as a primary disorder, or it may be secondary to complications of another disease. CIPO should not be confused with transient bowel motility defects such as ileus (the absence of bowel contractions) that commonly accompany abdominal surgery, pancreatitis, appendicitis, or sepsis.

The etiology of CIPO remains poorly understood, but clues are emerging from human and mouse genetics. Because so many cell types, transmitters, and signaling molecules impact ENS development and intestinal function, there are likely many underlying causes of CIPO, potentially including dysfunction of ENS, SMCs, ICC, and/or PDGFRα+ cells. A significant fraction of CIPO cases are thought to be neuropathic. In neuropathic CIPO, neurons and glia are present throughout the bowel, but damage, dysfunction, or subtype ratio imbalances lead to bowel dysmotility. In a majority of cases, CIPO occurs as an idiopathic disease, but it can also occur secondary to other problems, such as diabetes, hypothyroidism, radiation, autoimmune disease, paraneoplastic syndrome, neurodegeneration, infection, and medications (89).

Unfortunately, even with advanced genetic tools like whole exome sequencing, causative genetic variants remain poorly defined. *Only a few genetic causes of CIPO have been identified. These include mutations in the genes encoding filamin A (FLNA) (90), gamma smooth muscle actin (ACTG2) (91), the double-strand-break repair protein RAD21 (92), leiomodin 1 (LMOD1), myosin heavy chain 11 (MYH11), myosin light chain kinase (MYLK), and SRY-box 10 (SOX10)*

(89, 91, 93). Identifying more genetic causes of CIPO is critical, as it will undoubtedly aid diagnosis.

1.2.3 - Enteric neuropathies involving Nitric Oxide Synthase

Compared to other bowel neurons, nitrergic neurons appear to be especially susceptible to damage. Partial or complete loss of nNOS+ neurons can be seen in a many enteric neuropathies, including esophageal achalasia, diabetic gastroparesis, diabetes-induced colon dysfunction, Chagas' disease, hypertrophic pyloric stenosis, and ischemia with reperfusion injury (94). All of these diseases involve impairments in bowel function, likely due to reduced inhibitory motor neuron input. Although it is unclear why nNOS+ neurons are more susceptible than other subtypes, one hypothesis is that nitric oxide can be converted to damaging free radicals that can produce adducts like cysteine nitrosothiols. Cysteine nitrosothiol formation can sensitize cells to reactive oxygen species-dependent dysfunction and death (95). Nitric oxide can also combine with free-radical oxygen to form peroxynitrite anion, which can cause protein misfolding and post-translational modifications (94).

1.2.4 - Dysfunctional regulation of vasodilation

Impaired vascular control has been implicated in a number of inflammatory conditions, including necrotizing enterocolitis (NEC) and inflammatory bowel disease (IBD). NEC is a dangerous bowel disease in premature neonates, characterized by severe inflammation, ischemic necrosis, and sometimes bowel perforation. It is tempting to hypothesize that neuron dysfunction may contribute to development of necrotizing enterocolitis, for instance through dysregulation of vasodilation that occurs in response to feeding. Indeed, altered microcirculation involving constricted arterioles has been demonstrated in NEC (96), and damage to the ENS also occurs with NEC (97). However, there is not yet convincing evidence that ENS dysfunction is the

primary cause of altered blood circulation in babies with NEC. Arguing against this hypothesis, vessel endothelial cells from bowel with NEC failed to generate NO in response to ACh, but vessels dilated in response to exogenous NO administration, suggesting that dysfunction of endothelial cells may be paramount (98). This is similar to IBD, where vessel endothelium does not appropriately produce NO even when stimulated by ACh (99). Unfortunately, because defects seem intrinsic to endothelial cells, neuromodulators (e.g., AChE inhibitors) are unlikely to have therapeutic value in these disorders, although gut-derived neural stem cells do appear to prevent NEC-like injury in a rodent model (97).

1.2.5 - Dysfunctional regulation of epithelial secretion

Dysfunctional regulation of epithelial secretion may lead to increased stool water content. VIP-producing tumors and serotonin reuptake inhibitor (SSRI)-induced serotonin syndrome cause diarrhea by directly increasing neurotransmitters in the ENS circuit that controls epithelial secretion (100). Cholera, rotavirus, Clostridium difficile, Cryptosporidium, and enterotoxin producing Escherichia coli all cause profuse watery diarrhea at least in part by activating ENS circuits (101, 102).

1.2.6 - Disorders associated with ENS-immune system interactions

In addition to the functions described above, the ENS also plays a significant role in promoting gut immunity by interacting with muscularis macrophages, crypt epithelial stem cells, microbes, and components of the adaptive immune system. These interactions likely contribute to epithelial barrier function, enteric lymphoid proliferation within Peyer's patches, and other aspects of bowel immunity (103-105). Unfortunately, little is known about which neuron (and glia) subtypes mediate these interactions. The crosstalk between the ENS and the immune system is an incredibly complex field that is described in much more detail in our review (106).

1.3 – Transcriptional regulation of ENS development

1.3.1 – Stages of ENS development

The ENS receives minor cellular contributions from various sources, including somite levels 1-2, which contribute to esophagus and stomach; sacral neural crest and pelvic Schwann cell derivatives, which contribute to descending colon and rectum; and possibly cells of endodermal origin, which contribute mainly to the duodenum (107-109). However, most of the ENS is derived from enteric neural crest-derived cells (ENCDC) which originate at somite levels 3-7. In mouse, these cells invade the foregut around embryonic day 9.5 (week 4 in humans), migrate rostro-caudally, reaching the end of the colon by E14 (week 7 in humans). Once migration down the bowel (known as longitudinal migration) is complete, a subset of ENCDCs migrate inward from the region of the myenteric plexus to the region of the submucosal plexus, a process known as radial migration. As migration proceeds, ENCDCs proliferate extensively and differentiate into neurons and glia. Differentiation begins almost immediately after colonization of a region of bowel is complete. The timing of enteric neuron subtype specification is asynchronous, meaning certain neuron subtypes exit the cell cycle earlier than others, and subtype-specific markers are expressed at different ages. Myenteric plexus neurons are generally born before submucosal plexus neurons (110), and glia development may lag behind neuronal development. In mouse, nNOS, calbindin, and CART immunoreactivity is detectable by E11.5 (111). Studies using tritiated choline and tritiated 5-HT showed that cholinergic and serotonergic neurons may be present by E11 and E12 respectively, but immunoreactivity to ChAT and 5-HT are not detectable until E18.5, probably owing to the limitations of available antibodies (112, 113). Neurotransmitters like NPY and VIP (E13.5), Substance P (E14.5), CGRP (E17.5), and calretinin (P0) are not detected until later in development. The time at which a neuron subtype leaves the cell cycle does not appear to correlate with the time that its neurotransmitters are first detected, suggesting that different neuron subtypes may take varying amounts of time to mature,

and/or some marker genes may turn on earlier than others. Most nNOS+ neurons, for example, are also VIP+, but nNOS is typically detected earlier than VIP (111). A low level of neurogenesis likely continues in adulthood, particularly in response to injury (114), but the baseline degree of neuron turnover in the gut remains controversial. A recent report suggested enteric neurons are continually born in adulthood and turn over rapidly (31% of nNOS+ neurons in one week). This finding is difficult to reconcile with published literature and with longer-term lineage tracing experiments performed in our laboratory (113, 115).

A number of signaling pathways are essential for bowel colonization and early patterning. One of the most important pathways involves glial cell-line derived neurotrophic factor (GDNF), the transmembrane tyrosine kinase receptor RET, and RET's co-receptor GFRα1. RET is expressed on the surface of migrating ENCDC, while GDNF is expressed in developing bowel mesenchyme, and GFRα1 is expressed by both ENCDC and mesenchyme (116). RET signaling promotes ENCDC survival, proliferation, and migration (117, 118). Deleting *Gdnf*, *Gfrα1*, or *Ret* causes near-total bowel aganglionosis in mice (119-121). *RET* mutations have been linked to Hirschsprung disease in humans, with an estimated 18% of Hirschsprung disease cases (50% familial and 15-20% sporadic) caused by *RET* coding mutations. Human HSCR is rarely caused by *GDNF* or *GFRA1* mutations, although case reports exist (122, 123). In addition to its importance in early bowel colonization, RET signaling is involved in radial migration (124) and is required for survival of colon ENCDC even after bowel colonization is complete (125). RET signaling may be important for cell fate commitment to a neural lineage, since fewer RET-deficient cells become neurons (126). RET continues to be expressed in many mature neurons, even into adulthood. RET has at least four co-receptors, all members of the *Gfrα* family of genes (*Gfrα1*, *Gfrα2*, *Gfrα3*, and *Gfrα4*), and each preferentially mediates responses to a different ligand (GDNF, neurturin, persephin, and artemin respectively). Although persephin and artemin signaling do not appear to have roles in ENS development, Neurturin signaling via RET and

GFRA2 appears to be important for the development of cholinergic neurons in many parts of the peripheral nervous system, including the ENS (127, 128).

Another signaling pathway critical for normal ENS development involves endothelin 3 (*EDN3*), its receptor endothelin receptor type B (*EDNRB*), and endothelin converting enzyme 1 (*ECE1*), which converts pro-endothelins to biologically active peptides. Mice with homozygous inactivating mutations in *Edn3*, *Ednrb* or *Ece1* usually have bowel colonization through the small intestine and aganglionosis in distal colon (129-131). In humans, mutations in any of these three genes can cause HSCR or a syndromic form of HSCR called Waardenburg Syndrome type 4, a serious neurocristopathy characterized by sensorineural deafness, dysmorphic facial features, pigmentation defects, and HSCR (132, 133).

Many other signaling pathways have been identified whose perturbation critically affects ENS development. These include retinoic acid, which is required for migration of ENCDCs; Sonic and Indian hedgehog, netrins, and BMP4, which control radial patterning of the bowel; and semaphorins, which affect sacral ENCDC migration. These pathways are beautifully summarized in a prior review from our laboratory (134).

1.3.2 - Transcription factors critical for early bowel colonization

A complex transcriptional regulatory network supports migration of ENS precursors into the bowel. Members of this network include SOX10, ZEB2, PHOX2B, and PAX3. Deletion of these transcription factors leads to complete failure of ENCDCs to invade the foregut (SOX10 and ZEB2) (135, 136) or severely attenuated migration of ENCDCs past the foregut (PHOX2B and PAX3) (137, 138). The failure to migrate is due, at least partially, to altered expression of RET (regulated by SOX10, PHOX2B, and PAX3) (138, 139) and EDNRB (regulated by SOX10 and ZEB2) (140, 141). A few of these transcription factors are described in more detail below.

SOX10

The SRY-like high mobility group (HMG)-box transcription factor SOX10 is one of the most well-studied transcription factors involved in early bowel colonization. SOX10 is expressed in neural crest cells as they delaminate from the neural tube and migrate down the bowel, but expression is restricted to enteric glia as the ENS matures. In mice, *SOX10* haploinsufficiency (142) or dominant negative frameshift mutation (135, 143) causes aganglionic megacolon. In humans, heterozygous mutations in *SOX10* can cause Waardenburg syndrome type 4 (144), CIPO (145), and demyelinating disease (145, 146). SOX10 appears necessary for ENCDC survival, since homozygous SOX10 mutants exhibit dramatic ENCDC apoptosis prior to foregut invasion (135), and SOX10 also affects the size of the progenitor pool that initially colonizes the bowel (147). Overexpression experiments suggest SOX10 maintains progenitors in an undifferentiated state with both neurogenic and gliogenic potential (148, 149). Some of SOX10's effects in bowel are undoubtedly mediated through its regulation of *Ret* and *Ednrb* (140).

ZEB2

Zinc finger E-box binding homeobox (Zeb) 2 (a.k.a. *Sip1*, *Zfhx1b*) similarly regulates *Ednrb* expression in developing bowel. Like *Sox10*, *Zeb2* is expressed in glial cells and enteric progenitors, and most cells in the bowel that express *Sox10* also express *Zeb2* (150). In humans, heterozygous *ZEB2* mutations cause Mowat-Wilson syndrome, a serious disease characterized by microcephaly, seizures, dysmorphic facial features, developmental delay, and HSCR in half to two-thirds of children (151-153). Intriguingly, an additional 10% of individuals with *ZEB2* mutations have chronic constipation (153), and children with HSCR and *ZEB2* mutations typically have worse outcomes following pull-through surgery than children with HSCR alone (154). These findings suggest *ZEB2* is required for bowel colonization by ENS precursors, but also may be required for other aspects of ENS development. Mice completely lacking ZEB2 do

not form SOX10+ vagal neural crest and die at E9.5 (136). When *Zeb2* is conditionally deleted from neural crest later in development (*Wnt1-Cre;Zfhx1b*$^{fl/fl}$), ENS precursors do not migrate past the rostral duodenum (155). *Zeb2* heterozygous mice have apparently normal ENCDC migration, but when placed on a C57BL/6 background, many die between birth and weaning age (a timeframe similar to mice with defined enteric neuropathies (156), suggesting exciting future avenues for exploration (150).

While the mechanisms underlying ZEB2's effects on the ENS are not fully defined, some *Zeb2* mutant phenotypes are probably mediated by reduced *Ednrb* expression. For example, *Zeb2* haploinsufficiency increases neuronal differentiation in culture, while the ZEB2 target gene *EDNRB* appears to prevent premature differentiation of ENS precursors (140). Indeed, ZEB2 binds the *EDNRB* promotor, and *EDNRB* luciferase reporter assays suggest ZEB2 and SOX10 interact synergistically to promote *EDNRB* expression (140). Consistent with synergistic interaction, *Sox10;Zeb2* double heterozygotes have fewer ENS progenitor cells, decreased precursor proliferation, increased neuronal differentiation, and more profound defects in bowel colonization by ENCDC compared to single mutant mice (150).

PHOX2B

PHOX2B is a homeodomain transcription factor expressed in the developing ENS, adult enteric neurons, and in mature enteric glia at very low levels (157) (Chapter 4; Chapter 8). In mice lacking PHOX2B, enteric neuron precursors arrive in the foregut, but undergo total apoptosis by E13.5, and RET levels are significantly reduced (137), likely because PHOX2B binds and activates the *Ret* enhancer. PHOX2B non-polyalanine repeat mutations in humans are associated with congenital central hypoventilation syndrome (CCHS), and Haddad syndrome (CCHS + HSCR) (158). Introducing these same non-polyalanine mutations into the mouse *Phox2b* gene locus resulted in colon hypoganglionosis, impaired proliferation of immature

ENCDCs, and abnormally elevated SOX10 levels due to aberrant transactivation of *SOX10* by mutant PHOX2B (159).

PAX3, HOXB5, NKX2-1, HLX, and FOXD3

Several other transcription factors affect bowel colonization, but their roles are less well-studied. PAX3, a member of the paired-box–containing family of nuclear transcription factors, is associated in humans with Waardenburg syndrome without HSCR. However, homozygous deletion of *Pax3* in mouse leads to near-total bowel aganglionosis (138). PAX3 works synergistically with SOX10 to activate *RET* expression and may help recruit SOX10 to the *RET* promoter (138, 160). Two other transcription factors, HOXB5 and NKX2-1 also trans-activate the *RET* promoter (139, 161-163), and variants of these genes have been detected in HSCR patients (164, 165). Although homozygous mutations in *Hoxb5* do not lead to ENS pathology, possibly due to functional redundancy with *Hoxb6* (166), mice with ENCDC-specific dominant negative HOXB5 expression have megacolon due to incomplete bowel colonization by ENCDCs (167). NKX2-1 effects on mouse ENS have not been studied. Finally, mice lacking the homeobox transcription factor HLX, or conditionally lacking the transcriptional repressor FOXD3 fail to develop an ENS (168, 169), although the mechanisms behind this colonization failure have not been elucidated. Taken together, the above findings paint a picture of a complex regulatory network in which many genes act in concert to promote colonization of fetal bowel by ENCDC.

1.3.3 - Transcription factors, self-renewal, and differentiation into neurons and glia

Since complete bowel colonization depends on adequate proliferation of migrating ENCDCs, it is only logical that many transcription factors important for early ENS colonization also regulate the self-renewal and differentiation capacities of ENS progenitors. In neural crest stem cells, SOX10 appears to be important for preserving the potential of cells to become

neurons, since it is responsible for the initial induction of PHOX2B and the pro-neural transcription factor ASCL1. However, high levels of SOX10 inhibit neuronal differentiation (148) while remaining permissive for glial differentiation. As mentioned earlier, ZEB2 also inhibits neuronal differentiation, and it is likely ZEB2 and SOX10 act via EDNRB to maintain cells in an undifferentiated, or at least non-neuronal, state (140, 141, 149, 170). Interestingly, although they are co-expressed in ENCDC early in bowel development, PHOX2B acts as a *Sox10* repressor (148, 159). It is tempting to speculate that stochastic imbalances between SOX10 and PHOX2B levels in individual ENCDCs contribute to specification of a neuronal versus glial fate, although the fact that PHOX2B expression is also seen at low levels in enteric glia challenges this model (157) (Chapter 8).

Hedgehog pathway signaling is strongly implicated in glial cell differentiation (171). Perturbations of the transcription factors *Gli1-3*, key mediators of Hedgehog signaling, lead to altered neuron-glia ratios. Specifically, the ratio of the transcriptional activator GLI2 to the repressor GLI3 appear crucial for controlling the neuron-glia ratio in small intestine (80). GLI proteins upregulate expression of *Sox10*, and *Sox10* mutant cells show elevated SUFU, a negative regulator of *Gli* genes (80). Taken together, these findings suggest a bidirectional loop regulating SOX10 levels (80). Increasing GLI activity have also been associated with HSCR, likely as a result of premature gliogenesis (80), and mice forced to overexpress human *GLI1* had a HSCR-like phenotype (81). In addition to canonical signaling via the Patched, Smoothened, and Gli pathway, Sonic Hedgehog also promotes expression of the Notch ligand *Dll1* and its downstream effector *Hes1*. DLL1 activity is necessary for Sonic Hedgehog to induce proliferation of ENCDCs in culture. Conditionally deleting Patched from a subset of ENS precursors leads to elevated *Dll1* and *Hes1* expression, significantly more HES1+ cells, reduced ENCDC proliferation, and premature gliogenesis. Further research is needed to determine if gliogenesis in these mutants occurs via signaling through GLI proteins, HES1, or both (171).

Other novel and poorly-understood players in ENS gliogenesis include FOXD3, the orphan receptor NR2F1, and the T-box transcription factor TBX3. FOXD3 is expressed in developing ENCDC but its expression becomes restricted to glial cells as the ENS matures. When *Foxd3* was deleted from a subset of ENCDC using a late-acting *Ednrb-iCre* driver, enteric glia were much more severely affected than neurons, suggesting that FOXD3 may be important in glial cell differentiation or survival (172). Mutations in *Nr2f1* (known to promote gliogenesis in the CNS) lead to symptoms resembling Waardenburg-Shah syndrome in mice due to premature gliogenesis, although the cause of premature differentiation is unknown (173, 174). Finally, our lab recently identified the T-box transcription factor *Tbx3* as necessary for normal glia maturation in mouse small intestine. This work is further described in Chapter 3 (175).

Neuronal differentiation in the ENS is less well-understood than glial cell differentiation, but is known to rely, at least in part, on expression of the basic helix-loop-helix protein HAND2. HAND2 conditional deletion mutants have a colonized ENS with few terminally-differentiated neurons but normal glia development, suggesting that HAND2 is necessary for neurogenesis but not for precursor migration or glia formation (176, 177). HAND2 appears to have a dose-dependent effect on neurogenesis since heterozygotes have hypomorphic ENS, and *HuD* transcript numbers correlate with the amount of available HAND2 (178). In addition, *Hand2* deletion results in profound structural changes in ENS architecture (179). Interestingly, HAND2 is nuclear during development but becomes cytoplasmic in adulthood, suggesting that once differentiation is completed, HAND2 may be functionally inactive as a transcription factor (176).

PHOX2B and the basic helix-loop-helix transcription factor ASCL1 (a.k.a. MASH1) may also be involved in neuron differentiation in the ENS (148). *Phox2b* is expressed highly in both enteric precursors and mature neurons and is a known activator of *Ret*, which promotes a neuronal fate (126). *Ascl1* has a neurogenic role in other parts of the nervous system, including retina, CNS, and dorsal horn interneurons (180-182). In cultured neural crest stem cells,

overexpression of ASCL1 and PHOX2B reduced expression of SOX10, and this reduction was especially pronounced in cells infected with ASCL1 (148). In addition to possible roles in neuron differentiation, multiple studies have shown ASCL1 as an important mediator of enteric neuron subtype specification; this role for ASCL1 is described more in the next section.

1.3.4 - Transcription factors involved in ENS neuron subtype specification

In the CNS and other parts of the peripheral nervous system, it is generally accepted that a combinatorial code of transcription factors mediates neuron subtype specification (183, 184). Unfortunately, few studies thus far have described TFs with roles in ENS subtype specification. This is likely due to difficulties detecting subtle defects in ENS morphology (i.e. it is easier to identify total colon aganglionosis than a 10% decrease in VIP+ neurons), and challenges linking these genes to human disease phenotypes. Known transcription factors involved in subtype specification include *Hand2, Ascl1, Smad1*, and *Sox6*. Haploinsufficiency of *Hand2*, in addition to affecting neurogenesis as described above, dramatically reduced the relative proportions of nNOS+ and calretinin+ neurons in certain bowel regions, but had no effect on substance P levels (178). *Ascl1* was originally believed necessary for production of 5-HT-producing enteric neurons (185). However, a new study published in 2016 paints a much more complex picture, with delayed neurogenesis; anterior reductions in neuron density; posterior reductions in glia density; reduced ratios of calbindin+, VIP+, and TH+ neurons; and increased ratios of NOS1+ neurons in *Ascl1-/-* mice (186). The bone morphogenetic protein 2 (BMP2) literature in the ENS is complex, but BMP2, acting through the SMAD family of transcription factors, seems to promote differentiation of enteric neurons preferentially into nitrergic and catecholinergic subtypes (187, 188). Finally, *Sox6* was recently shown to be important for development of tyrosine hydroxylase (TH) + neurons in mouse stomach. Conditional deletion of *Sox6* led to a 70% reduction in TH+ neurons lasting into adulthood, with significantly impaired gastric emptying (189).

It is also interesting to note that a *Sox10* dominant negative heterozygous mouse model of HSCR had neuron subtype imbalances, including increased calretinin+ neurons in small intestine and decreased calretinin+ neurons in colon (71). These findings suggest *Sox10* could play a role in subtype specification, in addition to its previously-described roles in inhibiting neuron differentiation. Another possibility is that time of neuronal differentiation is dysregulated in *Sox10* dominant negative mutants, and altered differentiation timing results in altered subtype ratios in the bowel.

1.3.5 - Transcription factors and positional specification

Profound regional differences exist between the ENS of the stomach, small bowel, and colon, and it is likely these differences occur because of changes in transcriptional regulatory control. Very little is known about this subject, but new findings may offer some insights. A subset of mice lacking *Tlx2* (also known as *Ncx* and *Hox11L.1*) exhibit paradoxical hypoganglionosis of distal ileum and hyperganglionosis of the proximal colon at 3 weeks of age. The cause is unknown, but one possibility is that TLX2 is important for positional specification and proliferation of enteric neurons (190, 191). In Chapter 4, we describe another transcription factor, *Pou3f3*, that is exclusively expressed in colon neurons but is absent from stomach or small intestine. Homozygous *Pou3f3* deletion mutants die one day after birth due to kidney agenesis (i.e. at an age too young for megacolon to become obvious). To our knowledge, bowel function in these mice has never been examined (192).

1.3.6 – Other processes involved in neuron subtype specification

It is tempting to focus solely on transcriptional regulatory networks when considering ENCDC cell fate decisions. However, no discussion of ENS subtype specification would be complete without acknowledging the many diverse genetic and environmental factors that affect

neuron subtype ratios in the bowel. One process that critically affects neurochemical coding is neuron activity levels. Depolarization with potassium chloride, veratridine, or electrical field stimulation significantly increased expression of tyrosine hydroxylase in cultured rat ENS (193). In cultured mouse hindgut explants, blocking voltage-gated sodium channels using tetrodotoxin dramatically reduced the proportion of NOS+ neurons but did not affect total neuron number (194). Consistent with the idea that nerve activity may affect subtype development, certain neurotransmitters dramatically affect the development of neuron subgroups. Loss neuronal serotonin results in decreased proportions of dopaminergic and GABA-ergic neurons in the ENS (19), while mice mutant for the norepinephrine transporter had decreased numbers of serotonergic and calretinin-expressing neurons (195).

Interactions with the extracellular matrix also affect cell fate decisions in enteric neurons. Cells plated on engineered smooth muscle sheets with collagen I are more likely to be ChAT+ and nNOS-, while smooth muscle sheets with collagen IV have significantly higher nNOS expression (196). Mice lacking the cellular adhesion molecule L1 had a decreased number of CGRP+ neurons, in addition to general enteric neuron differentiation delays (197). A growing body of evidence also implicates diet and the microbiome in neuron subtype development after birth. Several studies have reported nitrergic neuron imbalances in mice raised in germ-free conditions (54, 55). These imbalances may be mediated by Toll-like receptor signaling, since deletions of *Tlr2*, *Tlr4*, and *Myd88* (a mediator of TLR4 signaling) also reduce nitrergic neuron numbers in the ENS (55, 198). High-fat diet induced microbial dysbiosis and decreased nitrergic neuron numbers, while delaying colonic transit in mice (199). In contrast, daily butyrate enemas in rat pups increased the proportions of nitrergic and cholinergic neurons (200). It is difficult to determine if these nutrients affect enteric neuron subtype numbers directly or via microbiome dysbiosis. Direct application of nutrients to the bowel lumen changes bowel motility patterns

(201), so it is not unreasonable to hypothesize that nutrients may alter bowel neuron phenotypes without the intervention of gut microbes.

1.3.7 - Transcriptomics and novel regulatory gene discovery

In the last two years, advances in transcriptomics have revealed expression of hundreds of previously unidentified regulatory genes in the developing ENS. These include *Dlx1, Dlx2, Ebf1, Etv1, Meis2, Pbx2, Pbx3, Satb1, Satb2, Tbx2, Tbx3, Tlx3, Tshz3,* a plethora of *Hox* genes, and many others (175, 189, 202). Most of these studies used microarray or RNA sequencing to compare gene expression in ENCDC with surrounding bowel mesenchyme at young ages (175, 189), or to compare gene expression in whole bowel with ENS to whole bowel lacking ENS (202). These approaches have several limitations. For one thing, bulk RNA sequencing does not always permit detection of genes expressed in very small cell populations (i.e. rare subtypes). Furthermore, the only genes detected in these studies are highly expressed in ENCDC relative to bowel mesenchyme, but some genes important for ENS development may also be expressed in bowel mesenchyme (for instance, *Etv1* is expressed in ENS and also interstitial cells of Cajal, and *Gfra1* is abundant in gut mesenchyme when ENCDC migrate through fetal bowel). Finally, bulk RNA sequencing does not allow us to determine which genes are differentially expressed in different neuron subtypes.

Despite these limitations, several recent studies significantly advanced our understanding of transcription factor expression in the ENS. The most comprehensive study, published in *Gastroenterology* early last year, used immunohistochemistry to validate expression of dozens of transcription factors identified as highly expressed in mouse ENS at E11.5 and E15.5. Identified transcription factors included some expressed early (*Ebf1-3, Etv1, Klf7, Hmx1, Hoxb3, Pbx3, Alx1, Oc2, Zfhx4, Tlx3, Hdx, Foxd1, Neurod4*), and late (*Cux1, Zeb1, Tshz3*) in neuronal development. Transcription factor expression was validated in mouse and human embryos using

immunohistochemistry and *in situ* hybridization. Encouragingly, many transcription factors expressed in mouse ENCDC were also expressed in human ENCDC, supporting the hypothesis that developmental pathways are conserved. Attempts were made to correlate expression of select transcription factors with enteric neurotransmitters and neuropeptides at E18.5 (189). Unfortunately, subtype analysis was limited by a lack of quantitative data and by the use of two-dimensional sections, which can give incomplete or misleading views of cellular architecture, particularly when proteins of interest (i.e. transcription factors) are expressed in distinct cellular compartments from the neurotransmitters with which they 'colocalize'. We have had far better success using whole mount immunohistochemistry in conjunction with tissue clearing methods in human tissue (described further in Chapter 8: Appendix B), and delicate dissection techniques in young mice (Chapters 2 and 3) than when we use tissue sections.

Single-cell and single-nucleus sequencing are expected to revolutionize our understanding of ENS subtype classification and specification in the near future. Single-cell sequencing of adult ENS neurons is challenging owing to the sparsity of neurons relative to other cell types, as well as their proximity to fibrous, hard-to-dissociate muscle. Dissociating tissue from young bowel is easier, but may be harder to interpret owing to the lack of defined neuron subpopulations at younger ages and cells at varying stages in development. In an ideal world, we would sequence from multiple ages in mouse (i.e. E12.5, E14.5, E17.5, P0, P5, adulthood) and multiple bowel regions (stomach, proximal and distal small intestine, colon) and use the data to construct region-specific pseudo-timelines of neuron subtype development (203, 204). Unfortunately, this approach is prohibitively expensive and labor-intensive, so for now, we are forced to rely on what data we can from adult bowel and from carefully-selected developmental timepoints. So far, one group has successfully performed single-cell sequencing at E12.5, which showed undifferentiated precursors, cells on a neurogenic trajectory, and cells on a glial trajectory; however, findings were limited by low cell count (126). Another group performed

single-cell sequencing of neurons in adult mouse small intestine along with many other neurons in mouse (126); however, no published study has yet attempted to correlate this data to known subgroups of neurons. To our knowledge, we are the first group to sequence enteric neurons in mouse distal colon, the region most likely to be affected in HSCR (Chapter 5).

1.4 – Summary

It is increasingly accepted that ENS dysfunction may underlie many dangerous medical problems including CIPO and HSCR (both before and after pull-through surgery), achalasia, and gastroparesis. ENS defects are also likely to cause symptoms in necrotizing enterocolitis, irritable bowel syndrome, slow transit constipation and in bowel symptoms that occur early in the course of Parkinson's disease, and later in the course of diabetes. New genetic and sequencing techniques are poised to revolutionize this field of biology and these areas of medicine. Although substantial progress has been made in understanding ENS disorders, many questions remain. These fall into several broad themes, which are explored in more detail in the body of this thesis:

1) *Subtle ENS structural and functional defects and their contribution to disease* (Chapters 2-5). New ENS transcriptomics data has led to the discovery of many genes involved in development. However, understanding the function of these genes is challenging, as many may play subtle roles in development. Some genes, including several described in this thesis, are associated with small but important defects in structure and function, such as reductions in subsets of cells, or functional defects despite apparently normal ENS structure. Understanding outcomes in patients with HSCR and Down syndrome also requires us to explore the contributions of trisomic genes to ENS structure and function.

2) *Neuron subtype classification and development* (Chapter 4). Substantial confusion remains about how enteric neuron subtypes should be defined, the roles of these neuron classes, the receptors that they express and the mechanisms that guide the development of these cell types. The traditional approach for defining enteric neuron subtypes used a limited set of markers in guinea pig, but most genetic experiments are now performed in mouse, which may have minor but important differences in neuron subtype composition. There is a strong need to integrate single-cell sequencing data with our current understanding of neuron subtypes to better understand the subtype composition of 'normal' bowel and the process of neuron subtype development.

3) *Transcriptional control of ENS development* (Chapters 2-4). Transcriptional control of enteric neuron subtype specification is very poorly understood. A few transcription factors driving subtype specification (*Ascl1, Hand2, Sox6, Smad1*) have been described in the literature, but many remain to be discovered. Understanding the genetics involved in neuron fate decisions will help guide stem cell regenerative therapies and will also help us identify novel genes causing CIPO and HSCR.

.

CHAPTER 2 : DLX1/2 MICE HAVE ABNORMAL ENTERIC NERVOUS SYSTEM FUNCTION

This manuscript is currently under review at *JCI Insight*, and we are in the process of performing additional experiments based on reviewer feedback. Authors: Christina M. Wright, James P. Garifallou, Heather L. Mentch, Deepika R. Kothakapa, Beth A. Maguire, and Robert O. Heuckeroth.

2.1 ABSTRACT

Decades ago, investigators reported that mice lacking DLX1 and DLX2, transcription factors expressed in the enteric nervous system (ENS), die with possible bowel motility problems. These problems were never fully elucidated. We found that mice lacking DLX1 and DLX2 (*Dlx1/2-/-* mice) had slower small bowel transit and reduced or absent neurally-mediated contraction complexes. In contrast, small bowel motility seemed normal in adult mice lacking DLX1 (*Dlx1-/-*). Even with detailed anatomic studies, we found no defects in ENS precursor migration, neuron or glia density, or neuron subtype ratios in *Dlx1/2-/-* or *Dlx1-/-* mice. However, RNA sequencing of *Dlx1/2-/-* ENS revealed dysregulation of many genes, including vasoactive intestinal peptide (*Vip*). Our study reveals a novel connection between *Dlx* genes and *Vip* and highlights the observation that dangerous bowel motility problems can occur in the absence of ENS structural defects. These findings may be relevant for disorders like chronic intestinal pseudo-obstruction (CIPO) syndrome.

2.2 INTRODUCTION

Chronic intestinal pseudo-obstruction (CIPO) is a serious digestive disorder characterized by profound bowel motility defects, leading to severe constipation, abdominal distention, and life-threatening malnutrition requiring total parenteral nutrition (TPN). Although rare, CIPO is a

leading cause of intestinal failure (89), accounting for ~10-14% of small bowel transplants (205). Many CIPO cases are believed to be caused by defects in the enteric nervous system (ENS), a complex network of neurons and glia within the bowel wall (134). The ENS develops from enteric neural crest-derived cells (ENCDC) that migrate through the bowel during fetal development (107). ENCDC give rise to diverse neuron and glia subtypes that control nutrient absorption, epithelial secretion, intestinal mixing, and (critically) transport of contents down the bowel (106). In neuropathic CIPO, neurons and glia are present, but damaged or dysfunctional, leading to dysmotility. Neuron dysfunction in CIPO has many etiologies, including infection, autoimmune disease, neurodegeneration, and gene mutations (89, 206). Genetic causes of CIPO are poorly understood. Although genes like *SOX10* and *POLG* have been linked to neuropathic CIPO (93, 207), we believe many CIPO-linked genes remain to be discovered (208). Here, we examine the role of *Dlx1* and *Dlx2*, two transcription factors expressed in developing ENS. We discovered that loss of these genes in mice causes profound intestinal dysmotility despite normal-appearing ENS anatomy.

Dlx1 and *Dlx2* are highly conserved homeobox transcription factors located in a tail-to-tail configuration on mouse chromosome 2. They are essential for craniofacial, palate (209), tooth (210), and central nervous system (CNS) morphogenesis (209, 211-213). In CNS, *Dlx1* and *Dlx2* are critical for subpallial interneuron differentiation and migration into the cortex and olfactory bulb (212). *Dlx1-/-* and *Dlx2-/-* mice exhibit milder defects than *Dlx1/2* double mutants, implying functional redundancy for DLX1 and DLX2 in some developmental contexts (213).

Dlx1 and *Dlx2* were hypothesized to be important for ENS development over 20 years ago, but their role in the ENS was never carefully evaluated. *Dlx2-/-* mice die as neonates with massive proximal bowel distention attributed to abnormal motility (209). Unsurprisingly, *Dlx1/2-/-* mice have a similar phenotype due to a deletion encompassing *Dlx1, Dlx2* and the intergenic region. In contrast, *Dlx1-/-* mice on some genetic backgrounds were reported to die by one month

of age (213, 214), a timeframe similar to mouse models with defined enteric neuropathies (156, 211). Consistent with the hypothesis that *Dlx1* and *Dlx2* mutations affect ENS function or development, both genes are expressed in developing ENS at ages when ENCDCs are migrating, proliferating, and differentiating into neurons and glia, including embryonic days (E) 12.5 (202, 209), E14.5 (215, 216), E17.5 (217), and postnatal day (P)0 (215). Further supporting a role in ENS development, *Dlx2* enhances expression of the transcription factor *Zfhx1b* in CNS (218), and *ZFHX1B* mutations can cause Hirschsprung disease (a problem where distal bowel lacks ENS) (136, 219). Given the compelling evidence implicating DLX1 and DLX2 in ENS development, we were surprised to find no studies thoroughly characterizing the ENS in mice lacking these proteins.

To evaluate DLX1 and DLX2's role in ENS development, we analyzed bowel structure and function in *Dlx1/2-/-* mice, which die at P0, and *Dlx1-/-* mice, which survive to adulthood in our mouse colony. We observed serious bowel function defects in *Dlx1/2-/-* mice at P0, including slower transit and absence of neurally-mediated contractions. Given the critical role of DLX1 and DLX2 in CNS interneuron migration, we initially hypothesized that ENS precursor migration might also be defective in *Dlx1/2-/-* mice causing Hirschsprung-like disease (absent distal ENS) that explained dysfunctional bowel. To our surprise, ENCDC migration, neuron and glia density, and ratios of neuron subtypes were normal in *Dlx1/2-/-* mice. To define mechanisms causing defective bowel function, we performed RNA sequencing on E14.5 and P0 *Dlx1/2+/+* and *Dlx1/2-/-* ENCDC. We identified dysregulation of many genes, including the neurotransmitter vasoactive intestinal peptide (*Vip)*, which may explain the functional defects in *Dlx1/2-/-* mice. To our knowledge, this study is the first linking *Dlx* genes to *Vip* expression.

2.3 METHODS

Animals

All mouse experiments were performed in accordance with the Children's Hospital of Philadelphia Institutional Animal Care and Use Committee. *Del(Dlx1-Dlx2)^{1Jlr}/Mmucd* mice and *B6.129X1-Dlx2^{tm1Jlr}/Mmucd* mice (referred to as *Dlx1/2* and *Dlx2* mice respectively) (209, 211) were obtained from the MMRRC (RRID:MMRRC_036673-UCD and RRID:MMRRC_015870-UCD) and were maintained on a CD1 or C57BL/6J background, respectively. *B6;129S4-Dlx1$^{tm1(cre/ERT2)Zjh}$/J* (referred to as *Dlx1-Cre^{ERT2}*) mice were ordered from The Jackson Laboratory (RRID:IMSR_JAX:014551) and were maintained on a C57BL/6J background. *EDNRB-EGFP-L10a* mice (220) were bred into *Dlx1/2* mice and maintained on a mixed C57BL6/J X CD1 background. *ChAT-EGFP-L10a* mice (RRID:IMSR_JAX:030250; C57BL/6J) were a kind gift from Joseph Dougherty at Washington University School of Medicine in St. Louis. *Dlx1/2;ChAT-EGFP-L10a* mice were obtained by breeding homozygous *ChAT-EGFP-L10a* mice to *Dlx1/2* heterozygotes and were maintained on a mixed C57BL/6J x CD1 background. *Dlx1/2;Ret* mice were generated by breeding *Dlx1/2* mice to *Ret^{TGM}* mice (referred to as *Ret* mice in paper; C57BL/6J) (221) and were maintained on a C57BL/6J x CD1 background. *Tg(Wnt1cre)11Rth* mice (referred to as *Wnt1-Cre*; RRID:IMSR_JAX:003829) and Gt(ROSA)26Sortm9(CAGtdTomato)Hze mice (referred to as *R26R-TdTomato*; RRID:IMSR_JAX:007909) were obtained from The Jackson Laboratory (Bar Harbor, ME). *Wnt1-Cre; R26R-TdTomato* mice on a mixed C57BL/6J x CBA/J)F1 background were bred into *Dlx1/2* mice and maintained on a mixed C57BL/6J x CD1 x CBA/J)F1 background. Genotyping was performed using previously published and novel primers (Supplementary Table 1). Vaginal plug day was considered E0.5.

Preparation of whole gut samples

Adult mice were euthanized in CO_2 for 5 minutes and cervically dislocated. P0 mice were euthanized by decapitation. Stomach, small bowel, and colon were removed and quickly

dissected in cold PBS. Small bowel and colon were opened along the mesenteric border and pinned onto Sylgard® 184 Silicone Elastomer (Dow Corning, Midland, MI), serosal side up using stainless steel insect pins. Tissue was fixed in 4% paraformaldehyde for 20-30 minutes at 25° C and transferred to cold PBS. The muscle layer was carefully peeled away from the mucosa and submucosa to separate the myenteric and submucosal plexus. Peeled gut was equilibrated at room temperature for 30 minutes in 50% glycerol/50% PBS and then stored at -20°C until staining.

To prepare E12.5 bowel, pregnant dams were euthanized in CO_2 for 5 minutes and embryos were dissected in Leibovitz's L-15 medium (ThermoFisher, Waltham, MA; Cat# 41300039). Stomach, small bowel, and large bowel were carefully removed, fixed in 4% paraformaldehyde for 30 minutes, equilibrated at room temperature for 30 minutes in 50% glycerol/50% PBS, and stored at -20°C until staining.

E12.5 Neuron Culture

Pregnant dams were euthanized in CO_2 for 5 minutes, and E12.5 embryos were dissected in Leibovitz's L-15 medium. Stomach, small bowel, and large bowel were carefully removed and placed for 15 minutes at 37°C in dispase (0.2 mg/mL; ThermoFisher, Cat#17105-041) and collagenase (0.2 mg/mL; Sigma-Aldrich, St. Louis, MO; Cat# C-6885) in PBS. Bowels were rinsed with cold PBS using a cell strainer and dissociated by triturating 35x through a P1000 pipet, then centrifuged and resuspended in Neurobasal Media (Invitrogen, Carlsbad, CA; Cat# 21103049) supplemented with L-glutamine (2 mM; Invitrogen, Cat# 25030081), B27 (1X; Invitrogen, Cat# 12587010), penicillin/streptomycin (1X; Invitrogen, Cat# 15140122), and 50 ng/mL 6XHis-GDNF prepared as described (222) and plated on Nunc™ Lab-Tek™ 8-well chamber slides (ThermoFisher, Cat# 177402). After two days, they were fixed for 15 minutes with 4% paraformaldehyde and immunostained.

Immunofluorescent and enzymatic staining of whole mount

Whole mount bowel stored in 50% glycerol/50% PBS at -20ºC was rinsed once in PBS. To prevent tissue curling, fixed P0 samples were pinned serosal side up on 48-well plates treated with Sylgard® 184 Silicone Elastomer (Dow Corning), and solutions were added directly to wells containing pinned tissue. Fixed E12.5 bowel was maintained in 48-well plates for the duration of immunostaining. Samples were blocked for 2 hours in PBS + 0.1% or 0.5% Triton X-100 (PBST) with 5% Normal Donkey Serum (NDS; Jackson Immuno Research Laboratory, West Grove, PA) and then incubated in primary antibody with gentle rocking at 4°C overnight, except for HuC/D (ANNA-1) antibody, where we incubated tissues for two hours at room temperature. Primary antibody concentrations and sources are in Supplementary Table 2. Tissues were washed 3 x 5 minutes each in PBST and incubated in secondary antibody (Supplementary Table 2) at room temperature with gentle rocking for 1 hour. After 3 additional 5-minute washes in PBS, samples were mounted serosal side up in 50% glycerol/50% PBS on glass slides. NADPH diaphorase staining was performed as described (223). Briefly, NADPH (Sigma-Aldrich) and Nitro Blue Tetrazolium were dissolved in PBS with 0.2% Triton-X-100. Samples were incubated in this solution at 37°C for 7-15 minutes, rinsed in PBS, and then stained with antibodies as described above.

Immunofluorescent staining of cultured cells

Slides were rinsed once in PBS, blocked for 1 hour in PBS + 0.1% or 0.5% Triton X-100 (PBST) with 5% NDS, and incubated with primary antibody (Supplementary Table 2) at 4°C overnight. Tissues were washed 3 x 5 minutes each in PBS and incubated in secondary antibody (Supplementary Table 2) at RT for 1 hour. After 3 additional 5-minute washes in PBS, samples were mounted in 50% glycerol/50% PBS + DAPI on glass slides.

Microscopy

Zeiss Axio Imager.A2, Axio Observer.A1, or LSM 710 microscopes and Zeiss Zen software were used to acquire images. Confocal images show single optical projections or maximum intensity projections as indicated in figure legend. For image processing, ImageJ and Photoshop were used to rotate, crop, and uniformly color adjust images.

Quantitative analysis of antibody-stained bowel

Using whole mount stained samples, we determined the density of enteric neurons (HuC/D+ cells), enteric glia (SOX10+S100β+ cells), and SOX10+ cells (a mix of glia and ENS precursors) in bowel by counting the number of stained cell bodies from 5-10 randomly selected 20x fields (a 0.045 mm^2 region). Enteric neuron subtype proportions were determined by counting the number of HuC/D+, GFP+, nNOS+, calretinin+, NADPH-diaphorase+, GABA+, VIP+, or somatostatin+ cell bodies from 5-10 randomly selected 20x fields from each gut sample. Observers were blinded to genotype for all quantitative analyses.

Quantitative Analysis of Neurites in Culture

One large (at least 12 mm^2) image was taken within a well (2 separate wells per embryo). Neurites from intact cells were traced, and cell bodies were counted using the Simple Neurite Tracer plugin in ImageJ (NIH) by investigators blinded to genotype. Because neurites sometimes crossed making tracing difficult, we determined average total neurite length per cell by dividing the sum of all neurite lengths by the number of nerve cell bodies. When neurites could be traced unambiguously, we measured the length of all neurites, added these lengths together to determine total neurite length, and plotted data in a histogram.

Delivery by Cesarean Section

Pregnant mouse mothers (E18.5) were injected subcutaneously with 2 mg of progesterone (Sigma-Aldrich, #P3972-5G). The following morning (E19.5), mice were euthanized via cervical dislocation and decapitation. An incision was made across the lower abdomen and pups were removed from the mother as previously described (224). Pups were placed on a warming pad (DCT-20, Kent Scientific, Torrington, CT) set initially to 35°C. After 30 minutes, the warming pad temperature was reduced to 30°C. Pups appeared similar to mice born by spontaneous vaginal delivery.

Intestinal Transit Assay

P0: At 1-3 hours after Cesarean section, pups were gavage fed 7 µL of a solution containing 50 mg/mL FITC-Dextran (70 kiloDalton; Sigma-Aldrich, Cat#46945) plus 2% methylcellulose (Sigma-Aldrich, Cat#274429) in water. Pups were kept on a 30ºC warming pad for the duration of the study (217). After 3 hours, pups were euthanized by decapitation and whole bowel was dissected, cut into 10 segments (esophagus, stomach, 6 small intestine pieces, cecum, and colon), minced with a scissors, and placed in Eppendorf® tubes containing 100 uL of PBS. Tubes were vortexed and then centrifuged at 4000 RCF for 10 minutes. 50 uL of supernatant fluid was analyzed for FITC fluorescence using a fluorometer (Turner Biosystems Modulus II Microplate Multimode Reader). A weighted average (geometric mean) was computed by multiplying fluorescence values by segment number, summing the results, and dividing by total fluorescence (225).

P35: P35 mice were food-deprived for 14 hours and gavage-fed 100uL of 10 mg/mL FITC-Dextran (70 kiloDalton) plus 2% methylcellulose in water. After 1 hour, mice were euthanized by CO_2 and whole bowel was dissected, cut into 16 segments (stomach, 10 small intestine pieces, 2 cecum pieces, and 3 colon pieces), and placed in Eppendorf® tubes containing 400 uL of PBS. Tubes were vortexed and centrifuged at 4000 RCF for 10 minutes. 50 uL of supernatant fluid was

combined with 50 uL of PBS and analyzed using a fluorometer.

Bowel Physiology

Between 1-3 hours after Cesarean section, pups were decapitated and the bowel was gently and rapidly removed. Bowel was immediately placed in warmed (37°C), oxygenated (95% O_2, 5% CO_2) Krebs-Ringers solution (118 mM NaCl, 4.6 mM KCl, 2.5 mM $CaCl_2$, 1.2 mM $MgSO_4$, 1 mM NaH_2PO_4, 25 mM $NaHCO_3$, 11 mM D-Glucose, pH 7.4) in a horizontal organ bath (Hugo Sachs Elektronik Harvard Apparatus, March, Germany; Cat# D-79232) with fluid continually replaced at a rate of 6.15 mL/min. Proximal SI was isolated by making one cut just distal to the stomach and a second cut ~2 cm proximal to the cecum. The proximal end of the SI was cannulated and tied to a P2/P10 Ultra Micro Pipet Tip (ThermoFisher, Cat# 02-707-438) connected using an L-shaped connector (Harvard Apparatus, Cat# 72-1407) and tubing to an upright 3mL syringe (Beckton Dickerson, Franklin Lakes, NJ; Cat# 309657). Fluid level in the syringe was maintained at 1.3 cm above the proximal end of the bowel. Proximal and distal bowel were at the same elevation. Bowel was pinned loosely on a secure piece of Sylgard 184 Silicone Elastomer (Dow Corning), illuminated to contrast with background, and filmed with a camera (Olympus, Center Valley, PA; PEN Mini E-PMI) connected to a dissecting microscope (Olympus SZ-PT SZ40). After an initial 20 minute video, 1 mM tetrodotoxin stock solution (Abcam, Cambridge, UK; Cat# ab120054) dissolved in sodium citrate buffer (40 mM citric acid monohydrate and 60 mM trisodium citrate dihydrate, pH 4.8) was diluted in Krebs-Ringer to a concentration of 1 µM. The resulting solution was oxygenated and pumped into the organ bath, and then another 20 minute video was recorded.

Analysis of bowel motility patterns

Videos were converted to .wmv format using Movie Maker and saved at 1x and 16x

speeds. In-house MatLab (MathWorks, Natick, MA) scripts (https://github.com/christinawright100/BowelSegmentation) were used to threshold the movies, generate kymographs, and perform Fourier transform analysis. Peak frequency was determined by calculating the Fourier transform at each vertical slice of the kymograph, averaging these, and plotting the averages to determine the peak frequency. Investigators blinded to genotype and condition quantified neurally-mediated contractions in kymographs and recorded if contractions were rhythmic or non-rhythmic. To quantify bowel width and tortuosity, 10 random frames were saved from each video and analyzed in ImageJ. For each frame, we measured 5 random widths (randomly generated using a MatLab script) along the proximal bowel (50 widths per bowel). For tortuosity, total bowel length was divided by straight-line distance.

RNA extraction

E14.5 dams were euthanized with CO_2. P0 pups were delivered by Cesarean section as described above. Pups were rapidly removed from the mother. E14.5 small intestine was dissected in ice-cold Leibovitz's L-15 medium (Life Technologies, Cat# 41300039) and dissociated for 15 minutes at 37°C in dispase (0.2 mg/mL; ThermoFisher, Cat# 17105-041) and collagenase (0.2 mg/mL; Sigma, Cat# C-6885) in PBS with P1000 trituration. P0 small intestine was dissected in Leibovitz's L15 medium, snipped into small pieces using insulin needles (Beckton Dickerson, Cat# 08290-3284-18), and dissociated for 30 minutes at 37°C in Liberase (Sigma-Aldrich, Cat# 5401135001) supplemented with DNase I (Roche, Basel, Switzerland; Cat# 04716728001), $MgCl_2$ (6 mM) and $CaCl_2$ (1 mM) in HBSS with repeated P1000 trituration. Fluorescent EGFP-L10a+ cells (E14.5) or Tdtomato+ cells (P0) were sorted on a BD FACSJazz and collected in Neurobasal medium (Invitrogen, Cat# 21103049). RNA was extracted using the Qiagen RNeasy Plus Micro kit (Qiagen, Hilden, Germany; Cat# 74034) combined with Qiagen's RNase Free DNase Set (Qiagen, Cat# 79254). Samples were run on an Agilent Bioanalyzer and used if RNA Integrity Number (RIN) was > 7.0.

Quantitative PCR (qPCR) Analysis

Quantitative real time-polymerase chain reaction (qRT-PCR) was performed using previously described primers which we validated (**Supplementary Table 2-3; Supplementary Figure 2-3**) and SSoFast Evagreen (Bio-Rad, Hercules, CA; Cat# 172-5211). Fold change relative to control was computed using the ΔΔCt method with normalization to *Gapdh* mRNA levels.

RNA sequencing

RNA was extracted as described above. cDNA libraries were generated from samples with RIN > 8.0 using the SMARTer Stranded Total RNA-Seq Kit v2 - Pico Input Mammalian (Takara Bio, Kusatsu, Japan; Cat# 634411) designed to work with very low input RNA. Libraries were sequenced on a HiSeq2500 to a read depth of 17-26 million paired-end reads per sample. Reads were mapped to the genome using the STAR RNA-seq aligner (226), normalized using Pipeline of RNA-seq Transformations (PORT) (227) and analyzed in R (The R Foundation, Vienna, Austria) using Limma's Voom method (228, 229). Datasets will be made available on the GEO database pending publication of the paper.

Statistics

We used Prism 7.03 (GraphPad Software, San Diego, CA) and SigmaPlot 11.0 (Systat Software, Chicago, IL) for statistical analysis. A two-sided Student's t-test or Mann-Whitney Rank Sum Test (MWRST) was used when comparing two groups. When comparing multiple groups, a one-way ANOVA with *post hoc* multiple comparisons tests (Tukey) was used unless assumptions were not met, in which case we used a Kruskal-Wallis test with Dunn's *post hoc* multiple comparisons test. When comparing weight across multiple time points and groups, a two-way repeated measures ANOVA was used with *post hoc* multiple comparisons tests (Tukey).

A cutoff of $p < 0.05$ was considered significant. For RNA-seq analyses, a false discovery rate-adjusted p-value (i.e. q-value) of 0.10 was considered significant. Data represent mean ± standard error of the mean (SEM). Investigators were blinded to condition for all quantifications.

Study approval

All animal experiments were approved by the Children's Hospital of Philadelphia IACUC.

2.4 RESULTS

Dlx1/2-/- and *Dlx2-/-* mice die as neonates with massive abdominal distention due to gas accumulation in the bowel

To evaluate the role of *Dlx1* and *Dlx2* in bowel development, we bred to generate *Dlx1-/-*, *Dlx2-/-*, and *Dlx1/2-/-* mice. The *Dlx1/2-/-* mice appeared ill as neonates, lacked a milk spot, and died within 24 hours of birth with massive abdominal distention (**Figure 2-1A-D**). *Dlx2-/-* mice also died early with a similar phenotype to *Dlx1/2-/-* mice, but survival was not tracked as closely; *Dlx2-/-* mice were never recovered at weaning (P30). Gross anatomic analysis demonstrated marked accumulation of gas within the proximal small bowel (**Figure 2-1E**). In contrast, *Dlx1-/-* mice, *Dlx2+/-* mice, *Dlx1/2+/-* mice and wild type (WT) mice appeared healthy as neonates. Furthermore, although *Dlx1-/-* mice were previously reported to grow slowly and die by one month of age (211), we did not observe excess perinatal death of our *Dlx1-/-* mice (**Figure 2-1F**) despite a slow growth trajectory (**Figure 2-1G-H**). To test if *Dlx1-/-* mice had poor bowel motility which can lead to slow growth, we gavage-fed 37-day-old *Dlx1-/-* mice with fluorescein isothiocyanate–dextran (FITC-dextran) and evaluated transit through the bowel lumen. FITC-dextran is poorly absorbed across bowel epithelium, and transit of FITC-dextran through the bowel lumen is a well-established method to assess bowel motility (217, 225). However, we observed no delays in small bowel transit (**Figure 2-1I-J**).

We noted that *Dlx2-/-* and *Dlx1/2-/-* mice have cleft palate as previously reported (209, 211, 230) and that this might cause poor feeding and air swallowing, but the marked accumulation of air in the proximal small bowel suggested that bowel dysmotility may slow gas transit. We decided to focus our analysis on *Dlx1/2-/-* mice that lack both DLX1 and DLX2 proteins since some functional redundancy has been reported for *Dlx1* and *Dlx2* in the CNS.

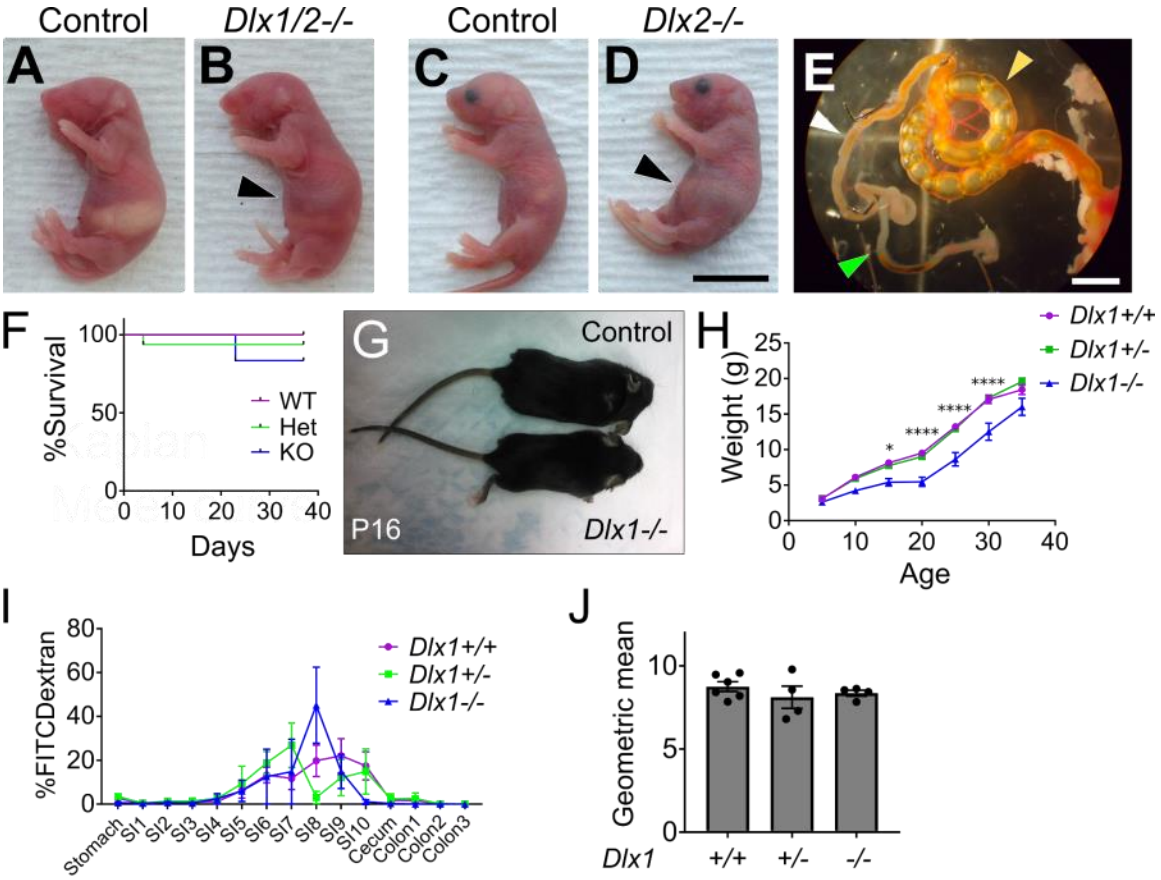

Figure 2-1: *Dlx1/2-/-* and *Dlx2-/-* mice have obvious abdominal distention at P0 due to bowel air accumulation, while *Dlx1-/-* mice exhibit poor weight gain but normal SI transit.
(A-D) *Dlx1/2-/-* (A-B) and *Dlx2-/-* (C-D) mice exhibited dramatic bowel distention. Scale bar = 1 cm. (E) Bowel of *Dlx2-/-* mouse viewed under dissecting microscope. Note air-filled proximal small intestine (yellow arrowhead) with absence of air in distal small intestine (white arrowhead) and colon (green arrowhead). Scale bar = 5mm. (F) Kaplan-Meier curve indicates most *Dlx1-/-* mice survived past 1 month of age (p=0.4665; Log-rank Mantel-Cox; n=9(+/+), 16(+/-), 6(-/-)). (G-H) *Dlx1-/-* mice were small and weighed significantly less than their WT littermates at P15 (p = 0.0433), P20 (p<0.0001), P25 (p<0.0001), and P30 (p<0.0001; n=9(+/+), 14(+/-), and 5(-/-); 2-way repeated measures ANOVA). We include only mice that lived to P35. (I) % FITC-dextran in distinct bowel regions 1 hour after oral FITC-dextran administration. SI1 to SI10 indicate sequential small intestine segments. (J) Weighted average of FITC bowel transit showed normal small intestine transit times in *Dlx1-/-* mice (p= 0.5182; one-way ANOVA, n=6(+/+), 4(+/-), and 4(-/-)). *p<0.05, ****p<0.0001.

Dlx1/2-/- mice have bowel dysmotility

To determine if bowel dysmotility at P0 contributes to bowel distension in *Dlx1/2-/-* mice, we fed neonatal mice FITC-dextran and evaluated transit through the bowel lumen. To ensure conditions for testing were as similar as possible between genotypes, we delivered mice by Cesarean section (C-section) at E19.5 (the usual day of delivery). Cesarean delivery prevented

WT and *Dlx1/2+/-* from feeding and permitted evaluation at a well-defined interval after birth. To delay spontaneous delivery but test bowel transit in full term pups, mothers were treated with progesterone at E18.5. Between 1-3 hours after delivery, each pup received a small bolus of FITC-dextran delivered directly into the oral cavity. All mice swallowed FITC-dextran even when they had cleft palate. Three hours later, pups were euthanized and intraluminal FITC fluorescence intensity was measured for defined bowel regions. In WT and *Dlx1/2+/-* mice, most FITC-dextran reached mid-small intestine after 3 hours. In contrast, *Dlx1/2-/-* mutants retained most FITC-dextran in their stomach with small amounts in the proximal small bowel (**Figure 2-2A**). A weighted average of fluorescence intensity (i.e., geometric mean) confirmed significant delays in bowel intraluminal transit for newborn *Dlx1/2-/-* mutant mice (**Figure 2-2B**), suggesting abnormal bowel motility.

Despite our attempts to control for presence of bowel air, many *Dlx1/2-/-* mice accumulated air in their bowel during the assay. Intriguingly, a subset of *Dlx1/2+/-* heterozygotes also spontaneously accumulated air in their GI tracts in the absence of cleft palate. Compared to these *Dlx1/2* heterozygotes with intraluminal air, *Dlx1/2-/-* mice still had significantly slower FITC-dextran transit (**Figure 2-2C**; $p < 0.05$), confirming poor gut motility in *Dlx1/2-/-* mutant mice.

One possibility was that delayed FITC-dextran transit in *Dlx1/2-/-* mice could reflect poor health of the *Dlx1/2-/-* neonates (i.e., ileus as a result of systemic illness). In fact, *Dlx1/2-/-* mice showed signs of poor health and four *Dlx1/2-/-* pups died during the experiment. We excluded these animals and an additional two pups from our analysis due to lack of activity after the 3 hour study was complete. *Dlx1/2-/-* pups included in the experiment were more likely to be pale-appearing and exhibited fewer movements in the first few hours of life (**Supplementary Figure 2-1A-B**). These concerns prompted us to perform an *in vitro* motility assay to complement our *in*

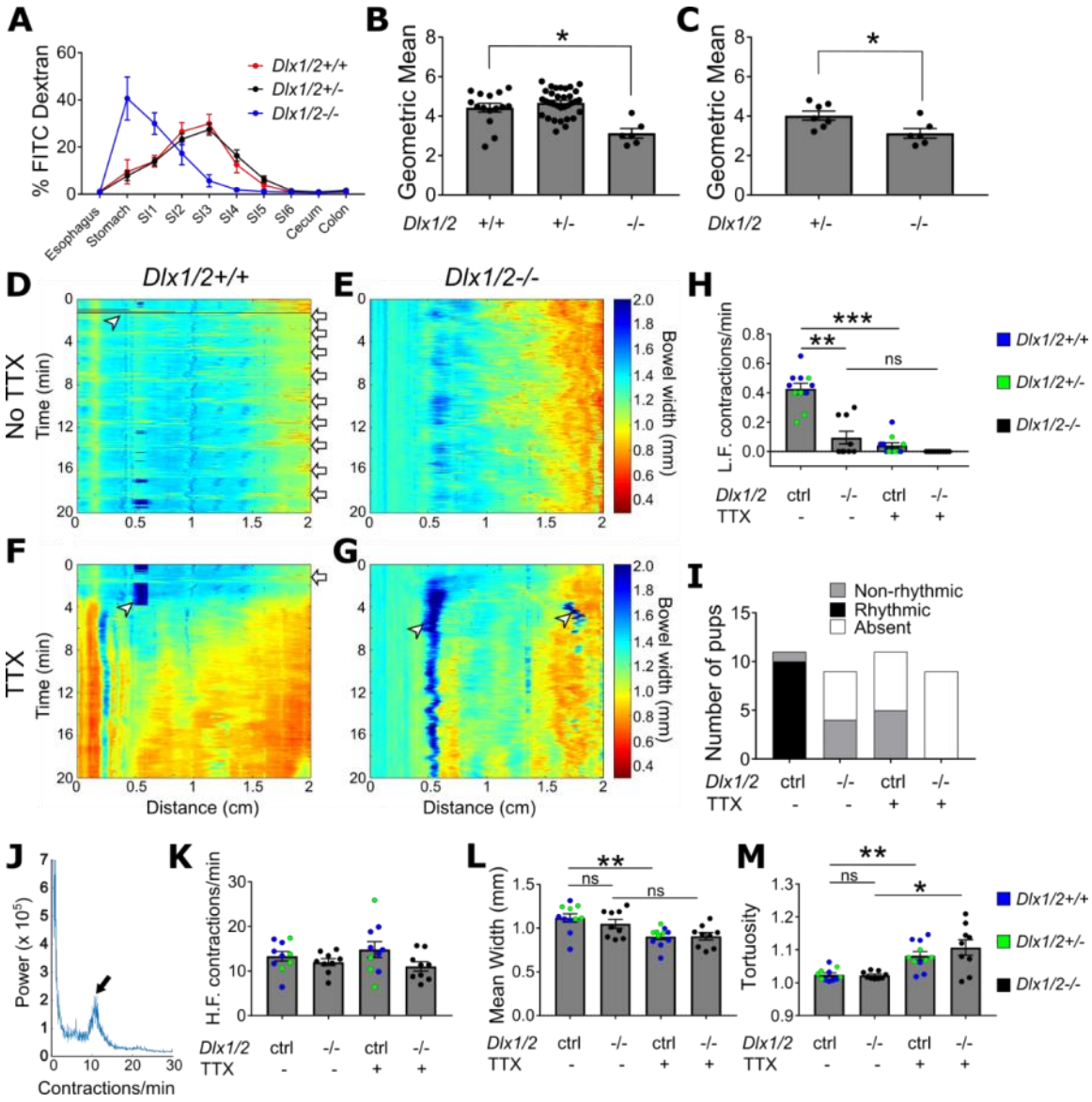

Figure 2-2: *Dlx1/2-/-* mice have abnormal bowel motility.
(A) Percent FITC-Dextran in distinct bowel regions 3 hours after oral FITC administration. SI1 to SI6 indicate sequential small intestine segments. (B) Weighted average of FITC bowel transit, represented by geometric mean, shows significant delays in transit for P0 *Dlx1/2-/-* mice, but not for heterozygous *Dlx1/2+/-* mice (p=0.0188; Kruskall-Wallis with Dunn's multiple comparisons test; n = 15 (+/+), 33 (+/-), 6 (-/-)). (C) A subset of heterozygotes spontaneously accumulated bowel air, but transit in *Dlx1/2-/-* mutants was still slower than in *Dlx1/2+/-* mice. (p=0.0228; Student's t-test; n=7 (+/-), n=6 (-/-)). (D-G) Representative kymographs depicting bowel width (color axis) over time (y-axis) at specific distances along the small intestine (x-axis) in control and *Dlx1/2-/-* bowels in the absence (D-E) or presence (F-G) of tetrodotoxin. White arrows indicate contraction complexes in control mice, but similar contraction complexes could not be identified in *Dlx1/2-/-* bowel; white arrowheads indicate artifacts such as air bubbles on the surface of bowel. (H) *Dlx1/2-/-* mice had fewer low-frequency (L.F.) contraction complexes than controls (p=0.0055; Kruskal-Wallis with Dunn's multiple comparisons test; n=10 (ctrl), n=9 (-/-)). (I) Low-frequency contraction complexes generally occurred in rhythmic patterns in controls

but not in mutants. (J) Representative Fourier plot from control mouse, with black arrow highlighting peak contraction frequency for TTX-insensitive contractions; note that contraction frequency for neurally-mediated contractions is too low to be reliably identified on the Fourier graph. (K) High-frequency (H.F.) TTX-insensitive contractions occurred at normal rates in *Dlx1/2-/-* mice (p=0.181; one-way ANOVA; n=10 (ctrl), n=9 (-/-)). (L-M) In controls, average bowel width decreased significantly with addition of TTX (L; p=0.0043; one-way ANOVA with Tukey's multiple comparisons test), while tortuosity increased with TTX (M; p=0.0087; Kruskal-Wallis with Dunn's multiple comparisons test). In mutants, bowel width did not significantly change with TTX addition (L; p=0.1423), but tortuosity increased with TTX (M; p=0.0276). *p<0.05; **p<0.01; ***p<0.001. Error bars represent S.E.M.

vivo studies. We again treated dams with progesterone and delivered pups via Cesarean section to control for food and air in the bowel. Bowel was carefully removed from neonates shortly after delivery and was placed in warmed, oxygenated Krebs-Ringers solution in a continuously-perfusing organ bath. Small intestine was cannulated at the proximal end and perfused with oxygenated Krebs-Ringers using an oral pressure of 1.3 cm H_2O above the bowel lumen. Videos of bowel contractions were recorded in the presence or absence of tetrodotoxin (TTX; see **Supplementary Videos 2-1 and 2-2** for representative videos). The videos were converted to spatiotemporal maps or "kymographs" depicting bowel width (color axis) over time (y-axis) for the first 2 cm of small intestine (**Figure 2-2D-G**). In control bowel, we observed low-frequency (~0.4 contractions/minute) and high-frequency (6-18 contractions/minute) contractions as has been previously described in neonatal mice (231). The low-frequency contraction complexes that typically occurred at regular intervals (i.e. rhythmically) in control mice were abrogated by TTX (**Figure 2-2H**), indicating neuronal origin. The *Dlx1/2-/-* mice had many fewer low-frequency contraction complexes than controls (p=0.0055; **Figure 2-2H**) and none of the contraction complexes in *Dlx1/2-/-* mouse small bowel occurred in a rhythmic pattern (**Figure 2-2I**). This analysis confirmed that neurally-mediated motility patterns are abnormal in the small bowel of *Dlx1/2-/-* mice.

Unlike low-frequency contractions, high-frequency contractions were present and appeared similar in controls (*Dlx1/2+/+* and *Dlx1/2+/-*) and *Dlx1/2-/-* small intestine. These

contractions are probably mediated by interstitial cells of Cajal or smooth muscle cells since they are insensitive to TTX (231). We used Fourier transform analysis to determine frequency of this faster contraction pattern (**Figure 2-2J**) as previously described (231) and found no difference between control and *Dlx1/2-/-* mutant bowel (**Figure 2-2K**), consistent with an ENS-specific defect in these mice.

We next tested if small bowel in *Dlx1/2-/-* mice was tonically contracted or tonically dilated, problems that might suggest an imbalance in excitatory or inhibitory motor neuron signaling and could slow bowel intraluminal transit. Our analysis showed that *Dlx1/2-/-* bowel was neither more dilated nor more contracted than control bowel (**Figure 2-2L**). Baseline tortuosity (measured as length of pinned bowel divided by Euclidean distance from end to end in randomly-selected video frames) was also no different in *Dlx1/2-/-* bowel (**Figure 2-2M**). Control bowel became more contracted and tortuous on exposure to TTX (**Figure 2-2L** and **2-2M**), suggesting that neural activity is necessary for baseline bowel relaxation in P0 small intestine. *Dlx1/2-/-* bowel did not become significantly more contracted in the presence of TTX ($p=0.1423$) but became significantly more tortuous with TTX application ($p=0.0276$), consistent with a distinct pattern of neuromodulation in *Dlx1/2-/-* mutant bowel (**Figure 2-2L** and **2-2M**). Collectively, these *in vitro* and *in vivo* data suggest that bowel motility is abnormal in *Dlx1/2-/-* mice and that the dysmotility is due to defects in neuronal activity.

Dlx1 and *Dlx2* are not necessary for bowel colonization by ENCDC during fetal development

Because bowel motility was abnormal in *Dlx1/2-/-* mice, we tested the hypothesis that DLX1 and DLX2 influence colonization of the bowel by ENCDC during fetal development. We analyzed bowel at E12.5 when ENCDC have normally colonized the entire small intestine and half the colon. The extent of ENS precursor migration was assessed using an antibody to neuron-

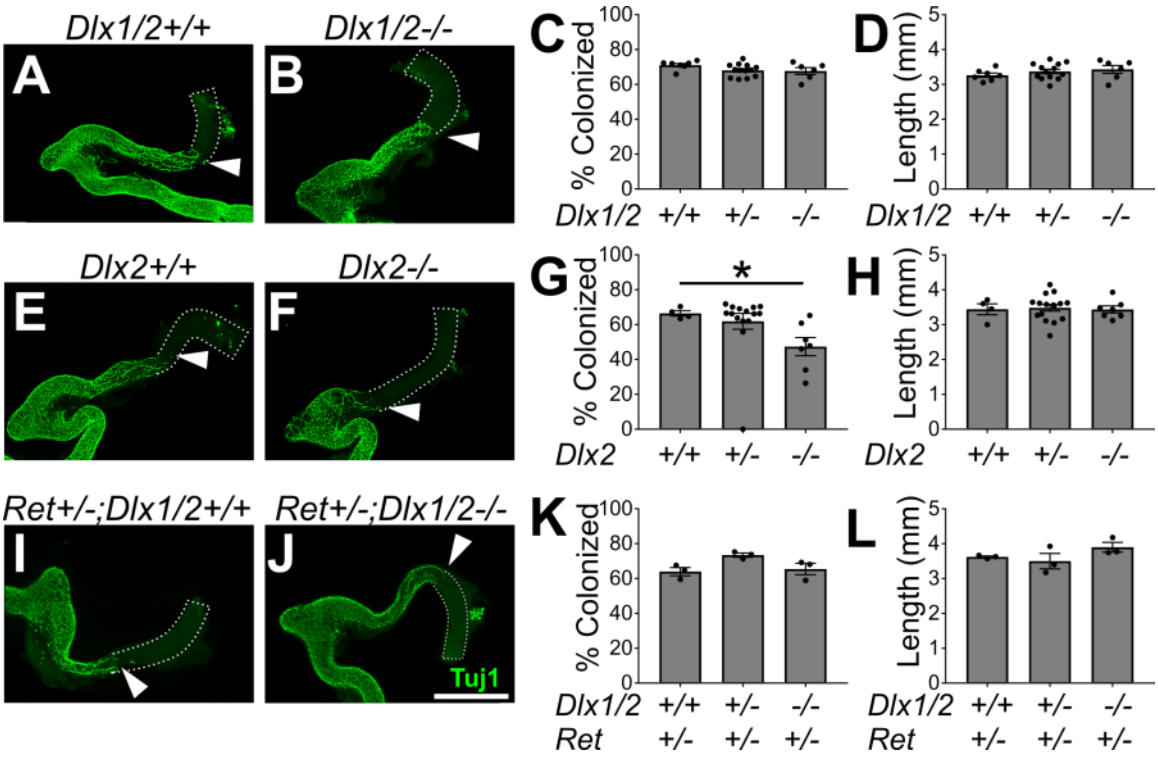

Figure 2-3: *Dlx1/2-/-*, *Dlx2-/-*, and *Ret+/-;Dlx1/2-/-* mice have normal bowel colonization rates by ENCDC or minimal defects at E12.5.
(A-B) Confocal Z-stacks of WT (A) and *Dlx1/2-/-* (B) E12.5 bowel stained with TuJ1 antibody that labels early and mature neurons (green). Maximum intensity projections are shown. White triangles mark distal-most TuJ1-positive neuron processes. Scale bar = 1 mm. (C-D) Percent hindgut colonized relative to total colon length (C; one-way ANOVA, n=7(+/+), n=13(+/-), n=6(-/-)) and colon length (D; one-way ANOVA, n=7(+/+), n=13(+/-), n=6(-/-)) was normal in *Dlx1/2-/-* mutants. (E-H) Representative WT (E) and *Dlx2-/-* (F) E12.5 bowel labeled with TuJ1 antibody. *Dlx2-/-* mice had a slight delay (66.5 ± 1.5% colonized (+/+) vs 47.4 ± 5.2% colonized (-/-)) in ENS migration of unknown functional significance (G; p =0.0499; Kruskal-Wallis test with Dunn's multiple comparisons test, n=4(+/+), n=15(+/-), n=7(-/-)) and normal colon length (H). (I-L) Representative *Ret+/-;Dlx1/2+/+* (I) and *Ret+/-;Dlx1/2-/-* (J) E12.5 bowel labeled with TuJ1 antibody. *Dlx1/2-/-* mice on a *Ret* heterozygous background had normal extent of bowel colonization (I; one-way ANOVA, n=3 per genotype) and normal colon length (L; one-way ANOVA, n=3 per genotype). Scale bar = 1 cm. *p<0.05.

specific class III β-tubulin (TuJ1) which is expressed at high levels in enteric neurons. By this criterion, E12.5 *Dlx1/2-/-* mice had normal colonization by ENCDC (**Figure 2-3A-C**). In contrast, *Dlx2-/-* mice had a small reduction in bowel colonization by ENCDC of dubious functional significance and marginal statistical significance (66.5 ± 1.5% colonized (+/+) vs 47.4 ± 5.2% colonized (-/-); p = 0.0499; **Figure 2-3E-G**). Because some gene defects are only

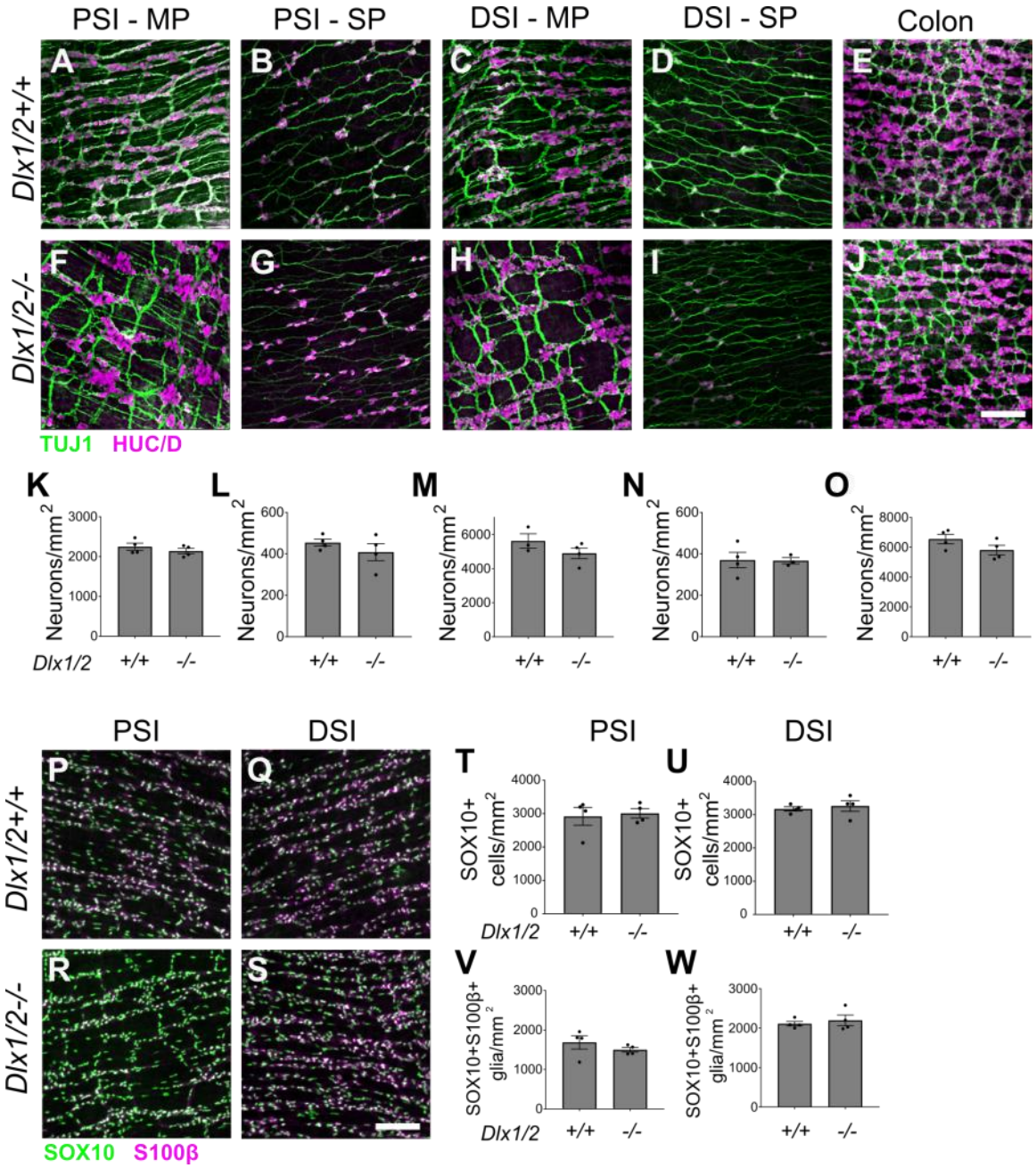

Figure 2-4: *Dlx1/2-/-* mice have normal density of neurons, SOX10+ cells, and glia at P0. (A-J) Representative images of *Dlx1/2+/+* and *Dlx1/2-/-* bowel immunostained for HuC/D (magenta) and TuJ1 (green). PSI=proximal small intestine, DSI=distal small intestine, MP=myenteric plexus, SP=submucosal plexus. (K-O) Quantification of neurons in (A-J) shows no difference between neuron number in control or mutant mice (Student's t-test; n=3-4 per condition). (P-S) Representative images of *Dlx1/2+/+* and *Dlx1/2-/-* bowel immunostained for S100β (magenta) and SOX10 (green). (T-W) *Dlx1/2-/-* mice had normal numbers of SOX10+ cells at P0 (Student's t-test; n=3-4 per condition; T-U) and normal numbers of SOX10+S100β+ glia at P0 (Student's t-test; n=3-4 per condition; V-W). Scale bar = 100 μm.

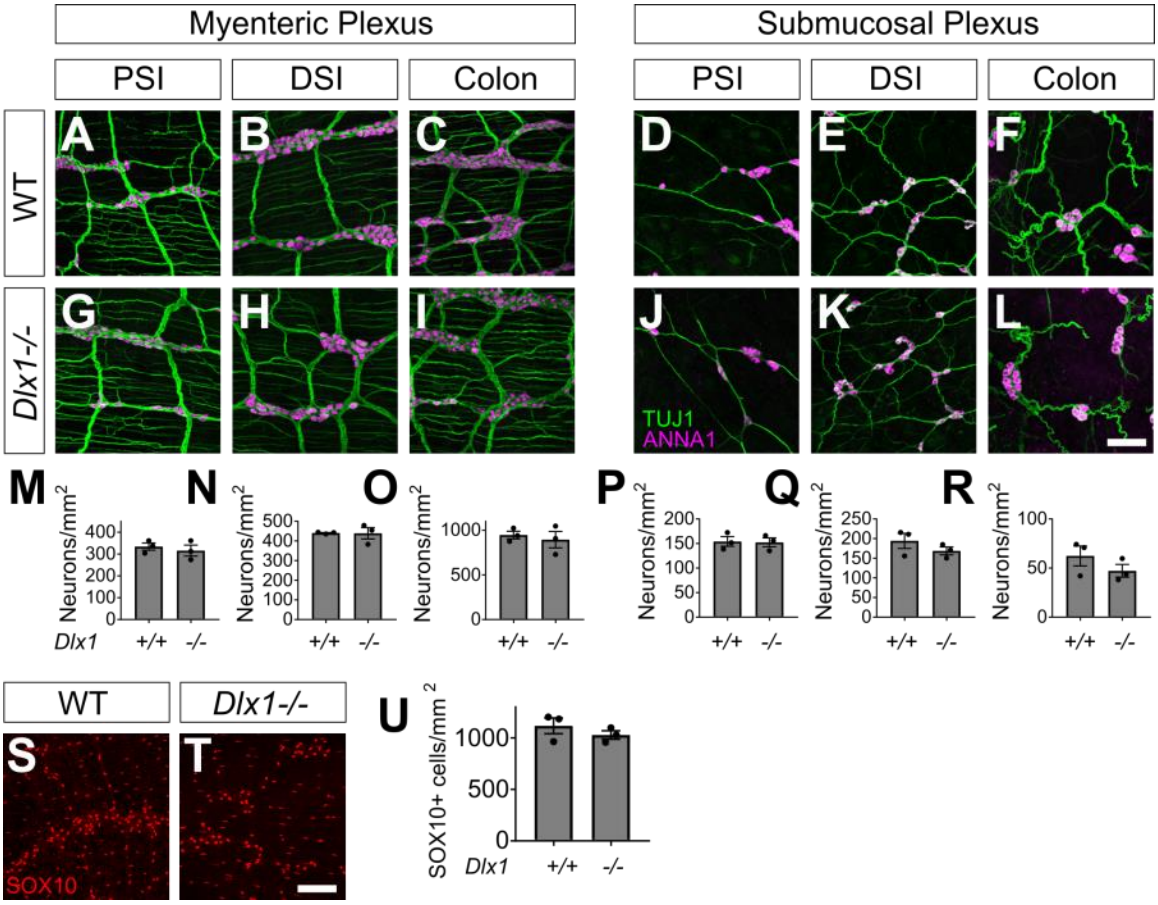

Figure 2-5: *Dlx1-/-* adults have normal neuron and glial numbers.
(A-L) Representative images of adult *Dlx1-/-* mouse proximal small intestine (PSI), distal small intestine (DSI), and colon immunostained using HuC/D (magenta) and TuJ1 (green) antibodies. Myenteric plexus (A-C, G-I) and submucosal plexus (D-F, J-L) are shown. (M-R) Neuron density was normal in *Dlx1-/-* mice for all bowel regions analyzed (Student's t-test; n=3 per condition). (S, T) Adult *Dlx1-/-* DSI was immunostained using an antibody against SOX10 which exclusively labels glia in adults (red). (U) Quantitative analysis of glial density shows no difference in glial cell density in distal small intestine of *Dlx1-/-* mice or WT mice (Student's t-test; n=3 per condition). Scale bar = 100 μm.

apparent with a sensitized genetic background (150), we next evaluated bowel colonization by *Dlx1/2-/-* ENCDC in the context of *Ret* heterozygosity. *Dlx1/2-/-;Ret+/-* mice on a mixed CD1 x C57Bl6/J background, had apparently normal colonization of the bowel by ENCDC (**Figure 2-3I-K**). Colon length was also normal in all mutant mice (**Figure 2-3D, H, L**). These observations suggest that the bowel dysmotility in *Dlx1/2-/-* mice is not due to defects in bowel colonization efficiency by ENCDC.

To determine if *Dlx1/2-/-* mice have major ENS structural defects causing dysmotility, we dissected mutant mice just after birth (P0) and stained bowel whole mounts with antibodies against the neuronal RNA-binding protein HuC/D (ANNA-1), neuron-specific class III β-tubulin (TuJ1), SOX10 (which is present in ENS precursors and mature glia), and the glia-specific marker S100β. There were no obvious differences in ENS organization or staining patterns between *Dlx1/2+/+* and *Dlx1/2-/-* mice. TuJ1 staining showed normal organization of nerve fibers. Quantitative analysis of HuC/D staining demonstrated normal neuron density in proximal small intestine (PSI), distal small intestine (DSI), and colon of P0 *Dlx1/2-/-* mice (**Figure 2-4A-O**). For small intestine, we assessed neuron density in both myenteric and submucosal plexus, but due to difficulty separating muscle from submucosa in neonatal mice, we were only able to assess total neuron density (myenteric plexus + submucosal plexus) in the colon. P0 *Dlx1/2-/-* mice also had normal SOX10+ cell density and SOX10+S100β+ glia density in bowel regions examined (**Figure 2-4P-W**).

Since neuron death occurs in subsets of CNS neurons in *Dlx1-/-* mice postnatally (214), we assessed neuron numbers in 10-week old *Dlx1-/-* mice, which lack cleft palate and survive to adulthood. We found no differences in neuron density in PSI, DSI, or colon in *Dlx1-/-* adults in either myenteric or submucosal plexus (**Figure 2-5A-R**). We also found no difference in SOX10+ glia and ENS precursors in the DSI of mature *Dlx1-/-* mice (**Figure 2-5S-U**).

No defects in ENS subtype ratios were detected in *Dlx1/2-/-* and *Dlx1-/-* mice

The ENS is home to over twenty neuron subtypes that perform distinct bowel functions (27). Because total neuron numbers are normal in *Dlx1/2-/-* mice, but bowel motility is abnormal, we hypothesized DLX1 and DLX2 might be required for the differentiation or survival of one or more neuron subtypes, leading to dysmotility in *Dlx1/2-/-* mice. To test this hypothesis, we stained P0 bowel with antibodies that distinguish many types of enteric neuron. We observed no

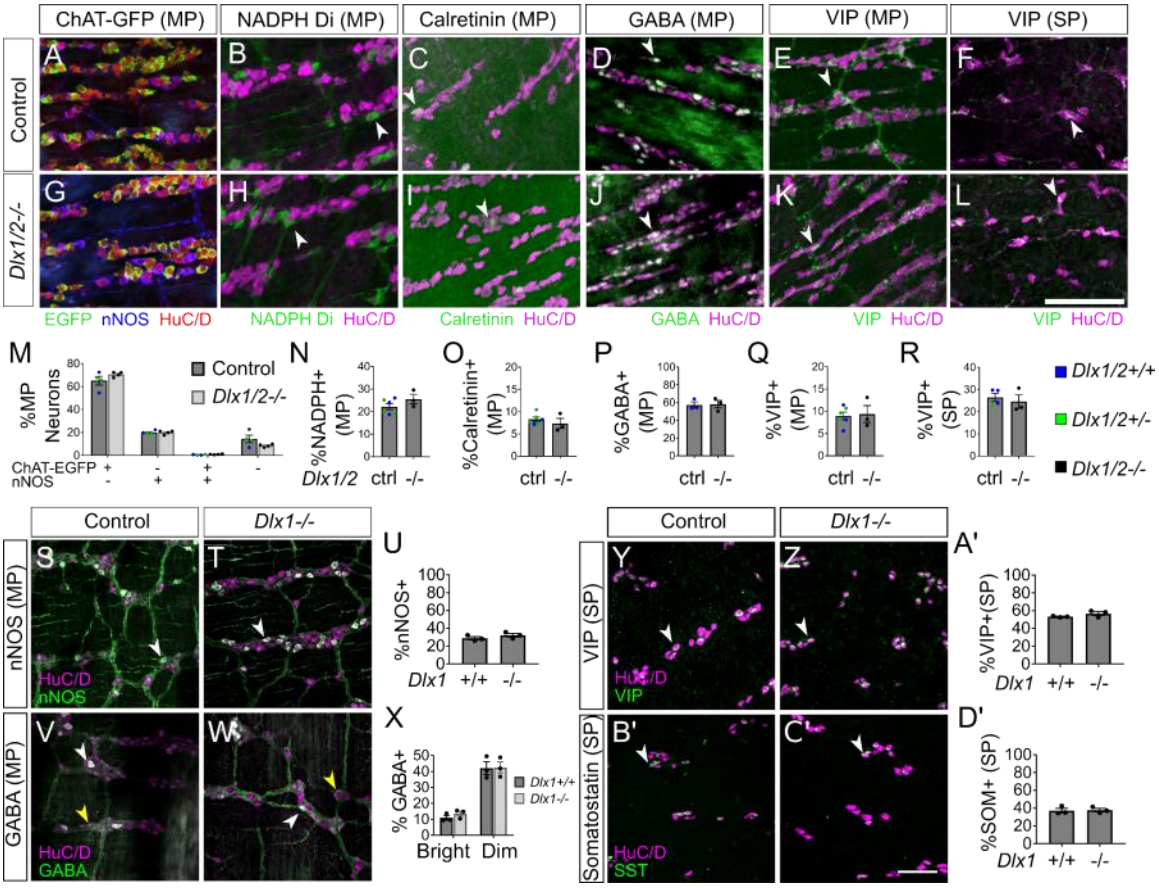

Figure 2-6: *Dlx1/2-/-* P0 and *Dlx1-/-* adult mice have normal ratios of neuron subtypes. (A-L) Representative images of HuC/D (red), nNOS (blue), and *ChAT*-GFP (green; A,G), HuC/D (magenta) and NADPH-diaphorase (green; B, H), HuC/D (magenta) and calretinin (green; C, I), HuC/D (magenta) and GABA (green; D, J), HuC/D (magenta) VIP (green; E-F, K-L) immunostaining in P0 control, P0 *Dlx1/2-/-*, and adult WT bowel. SP = submucosal plexus and MP = myenteric plexus. (M-R) We observed no difference in ratios of myenteric *ChAT-EGFP* or nNOS+ (M), myenteric NADPH+ (N), calretinin+ (O), GABA+ (P), VIP+ (Q) or submucosal VIP+ (R) neurons to total HuC/D+ neurons in *Dlx1/2-/-* mice compared to control mice. WT and *Dlx1/2+/-* were grouped as "control" and color coded *Dlx1/2+/+* (blue), *Dlx1/2+/-* (green) (Student's t-test, n=3-6 per condition). (S-T; V-W; Y-Z, B'-C') Representative images of HuC/D (magenta) and nNOS (green; S-T), HuC/D (magenta) and GABA (green; V-W), HuC/D (magenta) and VIP (green; Y-Z), and HuC/D (magenta) and somatostatin (green; B'-C') immunostaining in adult control and *Dlx1-/-* ENS. SP = submucosal plexus and MP = myenteric plexus. (U, X, A', D') We observed no difference in myenteric nNOS+ (U) or GABA+ (X) neurons, and no difference in submucosal VIP+ (A') or somatostatin+ (D') neurons in *Dlx1-/-* ENS (Student's t-test, n=3 per condition). Arrowheads indicate examples of neurons that were counted. For GABA-ergic neurons in *Dlx1-/-* adults, white arrowheads indicate brightly-positive GABA-ergic neurons, while yellow arrowheads indicate dimly-positive GABA-ergic neurons. Scale bar = 100 μm and applies to all images in the set.

differences in ratios of neurons expressing myenteric plexus neurotransmitter markers nitric oxide synthase (NOS), calretinin, γ-aminobutyric acid (GABA), or vasoactive intestinal peptide (VIP; **Figure 2-6A-E, G-K, M-Q**) or the submucosal plexus neurotransmitter VIP (**Figure 2-6F, L, R**). Since we lacked reliable antibodies for choline acetyl-transferase (ChAT), we bred and analyzed *Dlx1/2;ChAT-EGFP-L10a* mice but found no difference in EGFP+ neuron number (**Figure 2-6A, G, M; Supplementary Figure 2-2A-H**). One technical issue is that fluorescence intensity of immunohistochemical signals for certain neurotransmitters at P0 (substance P, tyrosine hydroxylase) was quite low (**Supplementary Figure 2-2I-L**). We suspect this reflects incomplete differentiation of these subtypes at P0, since immunostaining in adult mouse ENS was excellent for all antibodies used (**Supplementary Figure 2-2M-R**). Despite substantial effort, we were unable to identify neuron populations that were dramatically altered at an anatomic level to explain the severe intestinal dysmotility in neonatal *Dlx1/2-/-* mice.

In *Dlx1-/-* mice, we evaluated ENS in adult bowel since somatosensory cortex of the CNS has normal neuron numbers at birth, but postnatal apoptosis occurs in several cortical neuron subtypes, including GAD67+ (which catalyzes GABA synthesis from glutamate), NOS+, somatostatin+, and calretinin+ neurons (214). Taking advantage of postnatal survival in *Dlx1-/-* mice, we determined if similar age-dependent neuronal subtype loss occurs in the *Dlx1-/-* ENS by staining adult *Dlx1-/-* DSI with antibodies marking NOS, GABA, somatostatin, and VIP. Neuron subtype ratios were similar in WT and *Dlx1-/-* mice (**Figure 2-6S-D'**).

Dlx1/2-/- neurons did not exhibit obvious neurite differences in vitro

We next hypothesized that the functional defects in *Dlx1/2-/-* mutant bowel might be due to abnormal neurite growth, which is difficult to assess *in vivo* where neurites are closely intermingled. To test this hypothesis, we cultured ENCDCs from unselected E12.5 bowel in the presence of glial cell-line derived neurotrophic factor (GDNF) for two days and stained with TuJ1

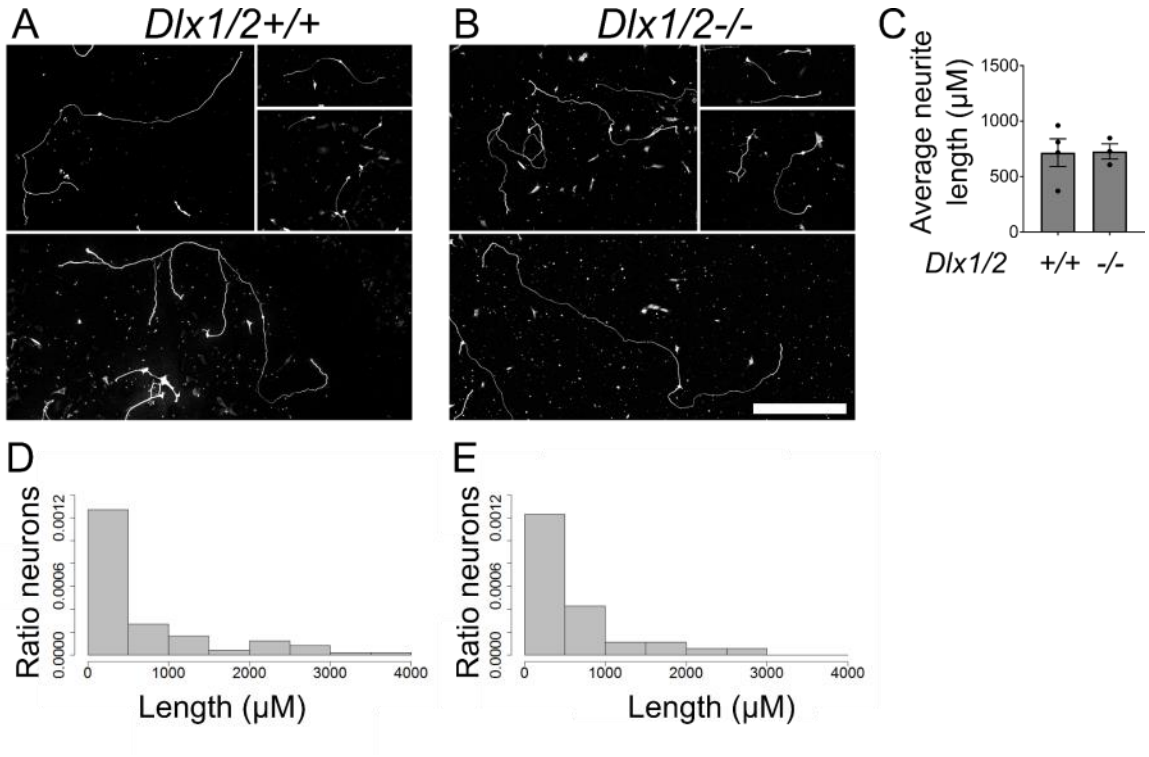

Figure 2-7: Cultured *Dlx1/2-/-* enteric neurons show no neurite length differences in vitro. (A-B) Representative images of cultured WT (A) and *Dlx1/2-/-* (B) neurons stained with TuJ1 antibody. (C) Quantification of total neurite length/total neuron number (Student's t-test, N > 400 nerve cell bodies, n = 4 embryos (+/+) and n=3 embryos (-/-)). (D-E) Histograms of total neurite length in single cells where neurites could be traced unambiguously (N = 96 (*Dlx1/2*+/+), N = 70 (*Dlx1/2-/-*)). Scale bar = 500 μm and applies to all images shown.

to label neurites. For this experiment, we used *Dlx1/2;ChAT-EGFP-L10a* mice on a mixed CD1xC57BL/6 background, because we initially hoped to use EGFP to distinguish ChAT+ and ChAT- neurons in culture; however, EGFP was not expressed at this young age. Consistent with the innate heterogeneity of the ENS, cultured neurons exhibited highly variable morphology (**Figure 2-7A-B**). Quantification of total neurite length per cell body revealed no differences between *Dlx1/2-/-* and WT neurons (**Figure 2-7C**; >400 cells traced). Histograms for total neurite length for individual traced cells were also similar for mutant and wild type neurons (**Figure 2-7D-E**).

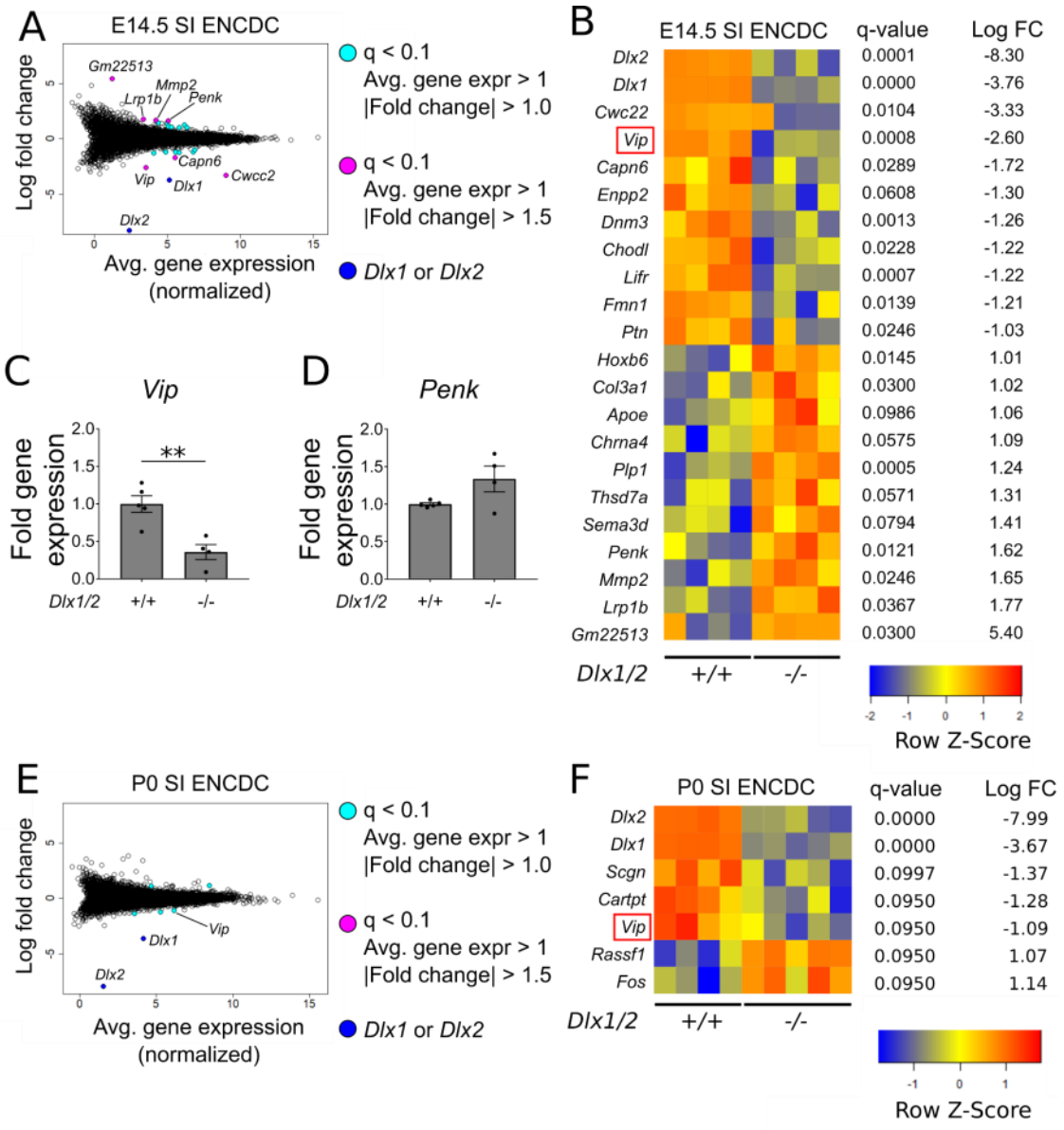

Figure 2-8: *Vip* levels are decreased in the developing ENS of *Dlx1/2-/-* mice at E14.5 and P0.

(A) Bland-Altman plot of differentially expressed genes in *Dlx1/2-/-* versus WT E14.5 FACS-sorted small bowel ENCDC after RNA-seq. (B) Heatmap of differentially-expressed genes shows 20 dysregulated genes in *Dlx1/2-/-* ENS at E14.5, in addition to *Dlx1* and *Dlx2* which were substantially decreased in mutant mice. (C-D) Quantitative RT-PCR was performed for *Vip* (C) and *Penk* (D) mRNA on independent samples to validate expression patterns for these neurotransmitters in E14.5 mouse ENS (*Vip*, p=0.0042, Student's t-test, n=5(+/+) and n=4(-/-); *Penk*, p=0.0634, Student's t-test, n=5(+/+) and n=4(-/-)). (E) Bland-Altman plot of differentially expressed genes in *Dlx1/2-/-* versus WT P0 FACS-sorted ENCDC after RNA-seq. (F) Heatmap of differentially-expressed genes shows 5 dysregulated genes in *Dlx1/2-/-* ENS at P0, in addition to *Dlx1* and *Dlx2*. **p<0.001

Vip is dysregulated in E14.5 and P0 *Dlx1/2-/-* ENCDC

Since our detailed anatomic analyses failed to reveal obvious structural problems of the ENS of *Dlx1/2-/-* mice, we next hypothesized that dysmotility in *Dlx1/2-/-* mice occurs due to altered gene expression not discernable at the level of ENS anatomy. We tested this hypothesis by RNA-seq of pooled ENCDC isolated from E14.5 and P0 bowel using fluorescence activated cell sorting (FACS). We chose these ages for theoretical and technical reasons. E14.5 was selected because *Dlx1* and *Dlx2* are expressed in murine ENS by E12.5 (202, 209), and we wanted to evaluate early effects of these mutations, rather than secondary effects that might occur as development proceeds. Furthermore, at E14.5 there are many ENCDC for analysis, and neuron subtype markers are starting to appear as the enteric neural network is established. We also analyzed P0 ENS to match our functional experiments, which were performed using neonatal bowel. For our E14.5 analysis, we bred *Dlx1/2* mice to an *Ednrb-L10A-GFP* reporter line which expresses a fluorescent protein in ENCDC at E14.5 (220) and performed RNA-seq on FACS-sorted ENCDC from E14.5 *Dlx1/2-/-;Ednrb-L10A-GFP*$^{Gfp/wt}$ (mutant) and *Dlx1/2+/+;Ednrb-L10A-GFP*$^{Gfp/wt}$ (WT) small intestine. To analyze P0 bowel, we bred *Dlx1/2* mice to a *Wnt1-Cre;R26R-Tdtomato* line and performed RNA-seq on FACS-sorted ENS from P0 *Dlx1/2-/-;Wnt1-Cre*$^{cre/wt}$*;R26R-Tdtomato+* (mutant) and *Dlx1/2+/+;Wnt1-Cre*$^{cre/wt}$*;R26R-Tdtomato+* (WT) small intestine.

We identified 22 dysregulated genes in *Dlx1/2-/-* E14.5 ENCDC using $q < 0.1$ as a statistical threshold after filtering out genes with low expression (average expression < 1) and fold change (|log fold change| < 1; **Figure 2-8A-B**). Remarkably, we observed ~84% reduction in mRNA levels for the ENS neurotransmitter vasoactive intestinal peptide (*Vip*) and a 3-fold increase in abundance of mRNA for the neurotransmitter proenkephalin (*Penk*) in small bowel ENCDC from *Dlx1/2-/-* mice compared to WT animals. We also observed changes in receptors (*Lifr*), extracellular matrix genes (*Mmp2, Col3a1*), cytoskeletal regulators (*Dnm3, Capn6, Fmn1*), neurite growth factors (*Ptn*), and glia-associated genes (*Plp1, Lrp1b*; **Figure 2-7B**). Since

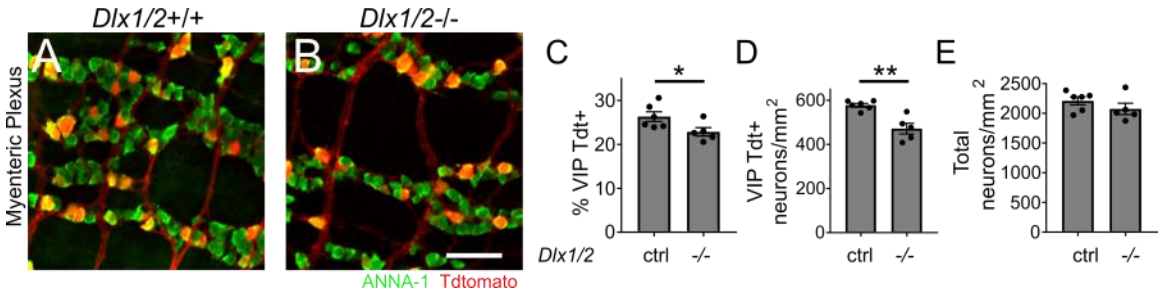

Figure 2-9: VIP+ neuron numbers are mildly decreased in *Dlx1/2-/-* myenteric plexus. (A-B) Myenteric plexus from *Dlx1/2*$^{wt/wt}$*;VIP-IRES-Cre*$^{Cre/wt}$*;R26R-TdTomato*+ control (A) and *Dlx1/2-/-;VIP-IRES-Cre*$^{Cre/wt}$*;R26R-TdTomato*+ mouse (B) stained with ANNA-1 antibody labeling HuC/D (green) reveals fewer TdTomato+ cells in mice lacking *Dlx1/2*. (C-D) Quantification of (A-B) shows a reduced proportion of TdTomato+ neurons in mice lacking *Dlx1* and *Dlx2* (C; p=0.047, n=6(ctrl) and n=5(-/-)) and reduced overall TdTomato+ neuron density (D; p=0.0017, n=6(ctrl) and n=5(-/-)). (E) Total neuron density was unchanged in *Dlx1/2* mutant mice (E; p=0.26, n=6(ctrl) and n=5(-/-)). Scale bar = 100 μM.

neurotransmitter dysregulation might most directly explain bowel dysmotility in *Dlx1/2-/-* mice, we attempted to validate altered levels of *Vip* and *Penk* mRNA using quantitative RT-PCR on an independently isolated set of E14.5 mutant and control samples (**Figure 2-8C-D**; see **Supplementary Figure 2-3** for standard curves). qRT-PCR analysis showed 3-fold reduction of *Vip* mRNA in E14.5 *Dlx1/2-/-* ENCDC compared to WT (1.0 ± 0.11 (+/+) vs 0.36 ± 0.10 (-/-), p = 0.004) and no statistical difference in *Penk* mRNA (1.0 ± 0.02 (+/+) vs 1.34 ± 0.17 (-/-), p = 0.063). Although we identified many fewer dysregulated genes at P0, our RNA-seq data suggest *Vip* may continue to be dysregulated in *Dlx1/2-/-* neonatal ENS (**Figure 2-8E-F**). These data support the hypothesis that bowel dysmotility in *Dlx1/2-/-* mice occurs as a result of gene dysregulation, instead of problems with neuron subtype loss or altered ENS morphogenesis.

Although we had previously investigated VIP expression in *Dlx1/2-/-* mice using an antibody, antibody expression was difficult to interpret since it preferentially labeled neurites instead of soma. To restrict VIP to the cytoplasm, we attempted colchicine treatment of myenteric plexus, but experienced neuron death after 6 hours despite oxygenated conditions. To more accurately quantify VIP-expressing neurons, we bred *Dlx1/2;Vip-IRES-Cre;R26R-TdTomato* mice which express a TdTomato reporter in cells expressing *Vip*. Quantification of TdTomato+

neurons in mid-small intestine showed a mild (13.3%) but statistically significant reduction in VIP+ cells in the myenteric plexus (**Figure 2-9A-D**). As before, we observed no difference in neuron density (**Figure 2-9E**).

2.5 DISCUSSION

Bowel motility disorders include life-threatening problems like Hirschsprung disease where the ENS is missing from distal bowel (57) and neuropathic CIPO where ENS is present, but dysfunctional (89). CIPO causes abdominal distension and bowel dysmotility that resembles the bowel motility problems in *Dlx1/2-/-* mice, but anatomic defects are often difficult to identify in people with CIPO. While it is possible that more careful analysis of ENS structure would identify defects in CIPO bowel, functional defects can also occur in the absence of pronounced anatomic abnormalities.

We chose to investigate bowel motility in *Dlx1* and *Dlx1/2* mutants because *Dlx1* and *Dlx2* are expressed in developing ENS at ages relevant for ENCDC migration, differentiation, and subtype specification, and because the original description of *Dlx2-/-* mice suggested they die from bowel dysmotility (202, 209, 215-217). We showed that neonatal *Dlx1/2-/-* mice have serious bowel function defects, including delayed gastric emptying and slow small bowel transit via an *in vivo* FITC-dextran assay. FITC-dextran was found in the stomachs of all *Dlx1/2-/-* mice tested, confirming that despite cleft palate, *Dlx1/2-/-* mutants were capable of swallowing and that stomach empties slowly. When we maintained bowel in an oxygenated organ bath and treated with TTX, which blocks nerve cell activity, we found *Dlx1/2-/-* bowels had severely reduced TTX-sensitive contraction patterns. Interpreting these findings is challenging because a complex interplay of excitatory and inhibitory neural input regulates bowel smooth muscle contraction and relaxation. A naïve interpretation is that neuron-mediated smooth muscle excitation (contraction) is defective in *Dlx1/2-/-* mice. Another possibility is that *Dlx1/2-/-* bowel has reduced smooth

muscle *inhibition* at baseline, leading to a mildly contracted phenotype approaching that of control bowel treated with TTX. Consistent with this hypothesis, *Dlx1/2-/-* bowel did not seem to contract significantly upon TTX treatment, unlike control bowel. Moreover, our bowel videos suggest that neurally-mediated "contraction complexes" actually consist of complex motor patterns, where the bowel first straightens (possibly reflecting longitudinal smooth muscle relaxation), then contracts rapidly, and finally returns to baseline tortuosity (Supplementary Video 1). TTX-treated bowel, which is highly contracted, never undergoes this pattern, and *Dlx1/2-/-* mouse bowel does so only rarely. Since *Dlx1/2-/-* mice had a normal pattern of TTX-insensitive (i.e. non-neuronal) contractions, and *Dlx1* and *Dlx2* are prominently expressed in developing ENS, we interpret these findings to mean that *Dlx1/2* mutations cause neuropathic CIPO-like disease in mice. We did not observe evidence of functional defects in *Dlx1-/-* mice.

Surprisingly, *Dlx1/2-/-* bowel had apparently normal ENS structure at birth, with normal neuron and glia density and ratios of enteric neuron subtypes. Although *Dlx2-/-* mice had a small ENCDC migration delay at E12.5, this may occur because of different strain backgrounds for *Dlx2-/-* (C57BL/6) and *Dlx1/2-/-* mice (CD1). It is unlikely this minimal transient migration delay impairs bowel function at P0. Since *Dlx1* and *Dlx2* have many possible transcriptional targets, we performed RNA-seq to determine which genes were dysregulated in *Dlx1/2-/-* ENCDCs. Unexpectedly, we identified a novel regulatory connection between *Dlx* genes and *Vip* expression, with *Dlx1/2-/-* ENCDCs exhibiting decreased *Vip* at two distinct developmental timepoints. Immunohistochemistry using a *Dlx1/2;Vip-IRES-Cre;R26R-TdTomato* reporter line suggests *Dlx1/2-/-* mice have a slight (~13%) reduction in numbers of VIP+ neurons, which seems unlikely to account for the >50% *Vip* decrease seen in our RNA-seq experiments. It is likely *Vip* expression within individual neurons is also reduced.

Our findings highlight several striking differences between the role of *Dlx1* and *Dlx2* in the ENS and their developmental functions in the brain. In CNS, *Dlx1* and *Dlx2* are required for

migration of multiple populations of inhibitory interneuron precursors from the ventral telencephalon into the neocortex and olfactory bulb (212, 213, 232). *Dlx2* also regulates expression of the transcription factor *Zfhx1b* in brain (218). *Zfhx1b* is critical for normal ENCDC migration, and in humans *ZFHX1B* mutations cause Mowat-Wilson syndrome (a genetic disorder characterized by intellectual disability, epilepsy, microcephaly, and Hirschsprung disease) (136, 150, 233). Given the large body of evidence implicating *Dlx1* and *Dlx2* in processes critical for neuron migration and differentiation, we anticipated serious defects in ENCDC migration in *Dlx1/2-/-* mutants. We were therefore surprised when *Dlx1/2-/-* bowel exhibited normal ENCDC migration at E12.5 and normal neuron density at P0.

In the CNS, *Dlx1* and *Dlx2* are also necessary for expression of glutamic acid decarboxylase 1 and 2 (*Gad1* and *Gad2*) enzymes that catalyze gamma-amino butyric acid (GABA) synthesis from glutamate (234, 235). GAD1 and GAD2 are also expressed in the ENS, where they are thought to constitute the primary GABA synthesis pathway (236). We therefore hypothesized GABA synthesis might be disrupted in *Dlx1/2-/-* ENS. Surprisingly, we found normal numbers of GABAergic neurons in *Dlx1/2-/-* ENS, and we did not observe significantly decreased *Gad1* or *Gad2* gene expression in *Dlx* mutant ENCDCs at E14.5 or P0. These findings suggest that unlike their CNS counterparts, ENS GABAergic neurons do not depend on *Dlx1* or *Dlx2* for *Gad1*, *Gad2* or GABA synthesis. We also note that loss of *Dlx1* causes apoptosis in subsets of CNS interneurons in 1-2-month-old mice (214), but *Dlx1* adult ENS showed no evidence of neuron subtype loss or decreased neuron density. These findings underscore highly distinct roles for *Dlx* genes in ENS neurons, compared to the CNS.

Although our RNA-seq studies identified several dysregulated genes in *Dlx1/2-/-* ENS that could explain defective bowel motility, *Vip* is an especially attractive candidate since VIP is a critical ENS neurotransmitter. In myenteric plexus, VIP is co-expressed with nitric oxide synthase and PACAP in inhibitory motor neurons. These neurons inhibit the multicellular motor syncytium

composed of smooth muscle cells (SMC), interstitial cells of Cajal (ICC), and platelet-derived growth factor receptor (PDGFR)α+ cells (106). VIP signaling to SMC occurs through G_s, cyclic AMP, and PKA, and leads to increased Ca^{2+} that causes membrane hyperpolarization via Ca^{2+}-activated K^+ channels, contributing to SMC relaxation (237). VIP also decreases Ca^{2+} transients in ICC, modulating the activity of Ca^{2+}-dependent chloride channels (CaCC) that regulate slow waves (33). In submucosal plexus, VIP+ secretomotor and vasodilator neurons influence epithelial secretion and blood flow, respectively. VIP regulation of secretion is well-described and mediated by *VIR1* receptors on crypt epithelial cells that increase cyclic AMP to activate the cystic fibrosis transmembrane regulator (CFTR) leading to secretion of Cl^-, Na^+, and water (48, 106). In addition, VIP acts on the neurons and glia within the ENS (238) and is an important modulator of gut immunity (239). Thus, there are many ways that altered VIP abundance might impact gut motility, epithelial function and immune system activity to impair *Dlx1/2-/-* mouse survival.

Dlx1/2-/- mice had a 53% reduction in *Vip* mRNA at P0 and an even larger reduction in *Vip* mRNA at E14.5 in ENCDCs (64% reduction by qPCR, 84% reduction by RNA-seq). The importance of VIP is highlighted by the observation that *Vip-/-* mice have severely delayed small intestine transit, impaired mucin production, smooth muscle thickening, shortened bowel, and die early due to GI stenosis (240). In contrast, *Vip+/-* mice are healthy enough to reproduce, but limited data exists about bowel motility in *Vip* heterozygotes. These observations are consistent with the hypothesis that reduced VIP levels in *Dlx1/2-/-* mice could contribute to bowel dysmotility, but it is not easy to determine if the level of VIP reduction detected in *Dlx1/2-/-* mice adequately explains the profound bowel motility defects in these animals. We found altered levels of many additional mRNA in the ENS of *Dlx1/2-/-* mice and expression changes in one or more of these genes might also contribute to bowel dysmotility.

Summary: Chronic intestinal pseudo-obstruction (CIPO) describes a poorly-understood constellation of diseases in which bowel motility is abnormal despite the presence of neurons throughout the bowel. Although neuron dysfunction accounts for many cases of CIPO, few causative genes have been identified (89, 106, 241). Our study provides a unique example of how bowel motility defects may occur in the absence of ENS structural defects, likely due to gene-level dysregulation. To our knowledge, few prior studies have performed such a comprehensive analysis of the neonatal ENS in mutant mice. There is a strong need to develop new tools to assess motility at young ages, since many ENS-relevant genes are also critical for palate development (178, 211, 217), kidney development (119, 120, 242), and other systems essential for life after birth. Our study is also the first to comprehensively investigate the role of DLX1 and DLX2 in gut motility, and the first to show a regulatory link between DLX1 and DLX2 and *Vip*. Remarkably, well-described functions for *Dlx1* and *Dlx2* in CNS like regulation of *Gad1* and *Gad2* to make GABA, control of cell migration, and effects on neurite growth do not appear to occur in the ENS. Furthermore, DLX2 was reported to be essential for CNS *Zfhx1b* expression, and mutations in *Zfhx1b* lead to almost complete loss of enteric neurons in mice, whereas bowel colonization by ENCDC proceeds normally in *Dlx1/2-/-* mice. Collectively these observations highlight how differently genes shared between ENS and CNS may function. Future studies in humans are important to determine if *Dlx* mutations are present in individuals with CIPO and to elucidate if *Dlx* genes control *Vip* expression in developing human ENS.

2.6 ACKNOWLEDGMENTS

The authors are grateful to Dr. Marina Avetisyan, Silvia Huerta-Lopez, Dr. Joel Bornstein, and Dr. John Grider for insightful comments and assistance during preparation of the manuscript. This work was supported by the Irma and Norman Braman Endowment (ROH), the Suzi and Scott Lustgarten Center Endowment (ROH), The Children's Hospital of Philadelphia

Research Institute (ROH), Children's Discovery Institute of Washington University and St. Louis Children's Hospital (grant no. MD-II2013-269) (ROH/JDD), NIH grants 5 F30 DK117546-02 (CMW), and RO1 DK087715 (ROH), March of Dimes 6-FY15-235 (ROH), and the Burroughs Wellcome Fund Clinical Scientist Award in Translational Research (grant no. 1008525) (ROH).

2.7 AUTHOR CONTRIBUTIONS

C.M.W. and R.O.H. designed experiments, analyzed results, and wrote the manuscript. C.M.W., J.P.G., H.L.M., and D.R.K. performed experiments. All authors edited the manuscript.

2.8 SUPPLEMENTARY MATERIALS

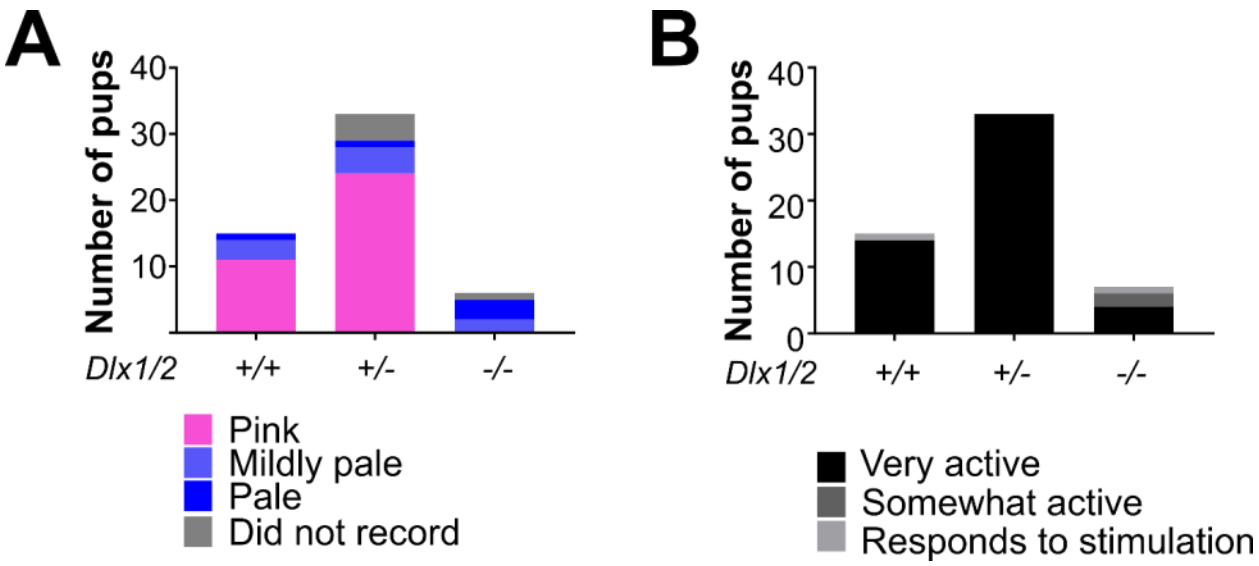

Supplementary Figure 2-1: Characteristics of *Dlx1/2-/-* mice given FITC-Dextran.

(A-B) A higher proportion of *Dlx1/2-/-* mice given FITC dextran were pale-appearing (A) and exhibited fewer spontaneous movements (B) compared to wild-type and heterozygous controls.

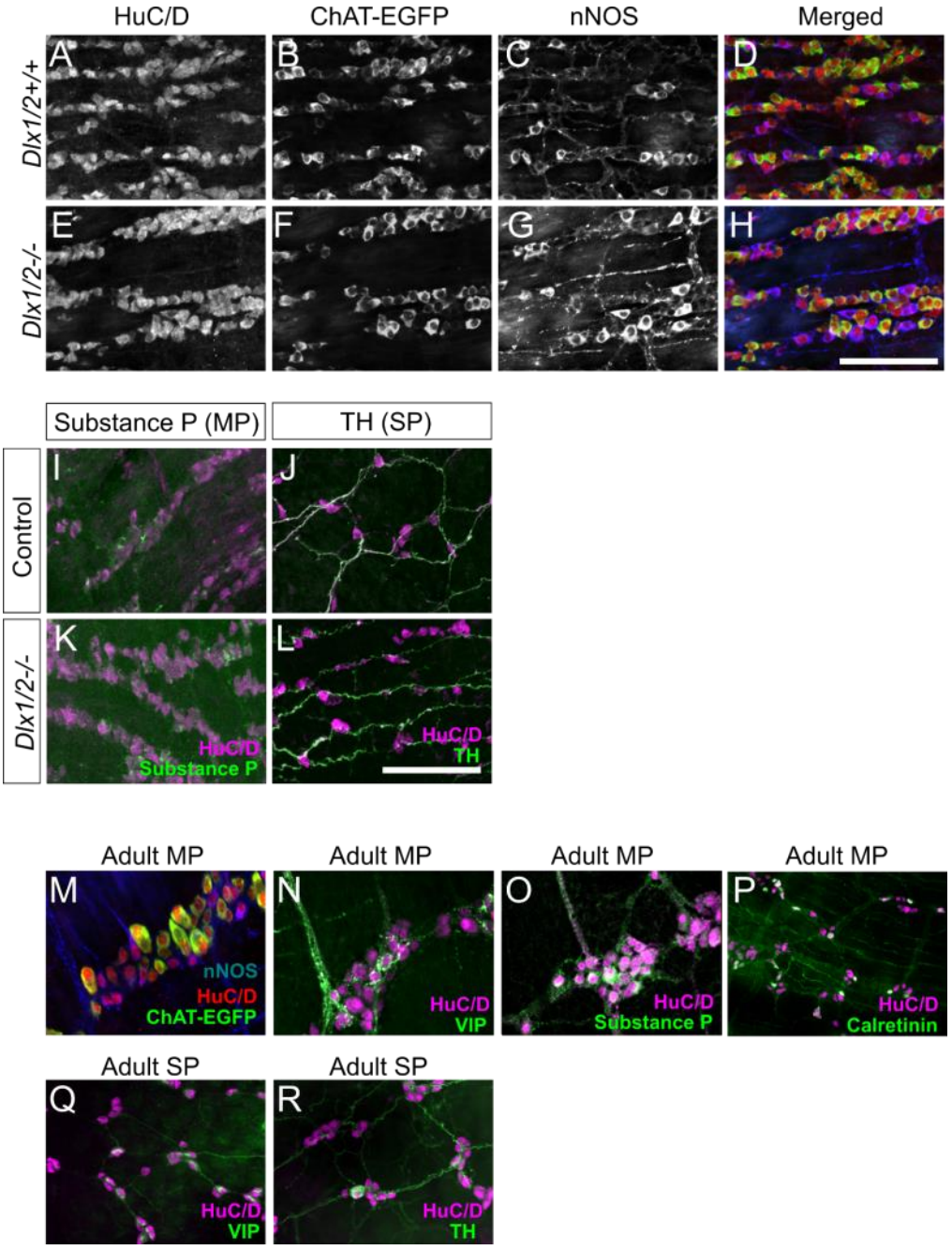

Supplementary Figure 2-2: Immunostaining positive controls

(A-H) Colorblind-friendly separation of channels for *Dlx1/2;ChAT-EGFP* images shown in Figure 6A (A-D) and Figure 6G (E-H). (I-L) Myenteric plexus (MP) substance P (I, K) and submucosal plexus (SP) tyrosine hydroxylase (TH; J, L) appeared normal in *Dlx1/2-/-* P0 small intestine, but we did not perform quantifications. (M-R) Positive control immunostaining in adult mouse small intestine for antibodies used in Figure 6. Scale bar = 100 μm.

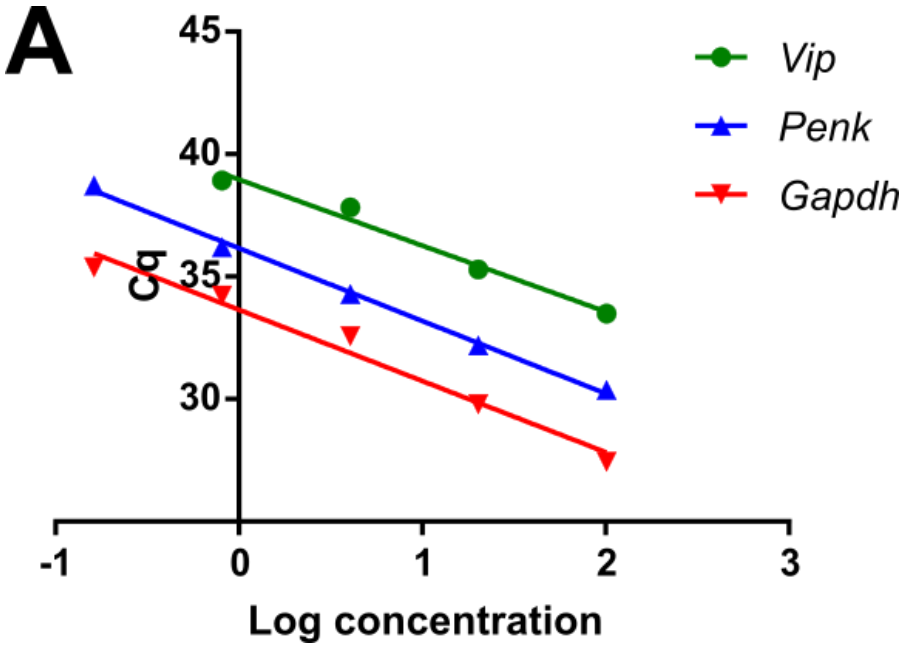

Supplementary Figure 2-3: qPCR curve for validation

(A) qPCR standard curve for validation of *Vip*, *Penk*, and *Gapdh*.

Supplementary Table 2-1: Genotyping primers

Primer name	**Sequence**	**Genotyping solution**
Dlx1/2 and *Dlx2* mutant F	5′ CTA CTC CGC CAA AAG CAG CTA CGA CC 3′	KAPA (Roche)
Dlx1/2 and *Dlx2* mutant R	5′ GCC AGC TCA TTC CTC CCA CTC ATG ATC 3′	KAPA
Dlx1/2 and *Dlx2* wild type F	5′ GCT GAT GGA TGA GCT CTA AGT ATG 3′	KAPA
Dlx1/2 and *Dlx2* wild type R	5′ ACG CAC CAT CTA CTC CAG TTT 3′	KAPA
Dlx1 wild type F	5′ AAC CCC TGT TCC GCT TAA ATT GGG TTC CTT C 3′	KAPA
Dlx1 wild type R	5′ GTG GCT GCT GAC CGA GTT GAC GTA GG 3′	KAPA
Cre wild type F	5′ GCA TTA CCG GTC GAT GCA ACG AGT GAT GAG 3′	KAPA
Cre wild type R	5′ GAG TGA ACG AAC CTG GTC GAA ATC AGT GCG 3′	KAPA
GFP mutant F	5′ GCA CGA CTT CTT CAA GTC CGC CAT GCC 3′	KAPA
GFP mutant R	5′ GCG GAT CTT GAA GTT CAC CTT GAT GCC 3′	KAPA
Tdtomato mutant F	5′ ACT ACT ACG TGG ACA CCA AGC TGG ACA TCA 3′	KAPA

Tdtomato mutant R	5′ GGC ATT AAA GCA GCG TAT CCA CAT AGC GTA 3′	KAPA
Tdtomato WT F	5′ GTT ATC AGT AAG GGA GCT GCA GTG GAG TAG 3′	GoTaq Green Master Mix (Promega, Madison, WI)
Tdtomato WT R	5′ CCG AAA ATC TGT GGG AAG TCT TGT CCC TCC 3′	GoTaq Green Master Mix

Supplementary Table 2-2: List of antibodies

Antibody	**Concentration**	**Catalog number**	**Source**
Rabbit anti-TuJ1	1:10,000	PRB-435P	Covance (Princeton, NJ); RRID:AB_10063850
Rabbit anti-nNOS	1:200	AB5380	Chemicon/Millipore (Burlington, MA); RRID:AB_91824
Rabbit anti-GABA	1:200	A2052	Sigma; RRID:AB_477652
Rat anti-Somatostatin	1:500	MAB354	Millipore; RRID:AB_2255365
Rabbit anti-Calretinin	1:5000	AB5054	Chemicon; RRID:AB_2068506
Rabbit anti-vasoactive intestinal peptide	1:300	20077	Immunostar (Hudson, WI); RRID:AB_572270

Sheep anti-tyrosine hydroxylase	1:500	AB152	Chemicon
ANNA-1 (HuC/D)	N/A	N/A	Kind gift from Dr. V. Lennon, Mayo Clinic
Rabbit anti-S100β	1:200	Ab52642	Abcam; RRID:AB_882426
Goat anti-Sox10	1:200	sc-17342	Santa Cruz (Dallas, TX); RRID:AB_2195374
Alexa Fluor goat anti-human 647	1:400	A21445	Life Technologies; RRID:AB_2535862
AlexaFluor donkey anti-rabbit 488	1:400	A21206	Life Technologies; RRID:AB_2535792
AlexaFluor donkey anti-rabbit 594	1:400	A21207	Life Technologies; RRID:AB_141637
AlexaFluor donkey anti-rabbit 647	1:400	A31573	Life Technologies; RRID:AB_2536183
AlexaFluor donkey anti-rat 488	1:400	A21208	Life Technologies; RRID:AB_141709
AlexaFluor donkey anti-goat 594	1:400	A11058	Life Technologies; RRID:AB_2534105
AlexaFluor donkey anti-sheep 594	1:400	A11016	Life Technologies; RRID:AB_10562537

Supplementary Table 2-3: qPCR primers

Primer name	**Sequence**	**Reference**
Vip Forward	5′ GCATGCTGATGGAGTTTTCA 3′	(243)
Vip Reverse	5′ GGCATCAGAGTGTCGTTTGA 3′	(243)
Penk Forward	5’ TTCAGCAGATCGGAGGAGTTG 3’	(244)
Penk Reverse	5’ AGAAGCGAACGGAGGAGAGAT 3’	(244)
Gapdh Forward	5’ AACTTTGGCATTGTGGAAGG 3’	(217)
Gapdh Reverse	5’ GTCTTCTGGGTGGCAGTGAT 3’	(217)

Supplementary video 1:

Video of *Dlx1/2-/-* (top) and control (bottom) bowel at baseline, at 8x speed. In control bowel (bottom), a neurally-mediated contraction complex involving pronounced bowel straightening occurs from 00:04-00:07.

Supplementary video 2:

Video of *Dlx1/2-/-* (top) and control (bottom) bowel after TTX treatment at 8x speed.

CHAPTER 3 : LOSS OF TBX3 IN MURINE NEURAL CREST REDUCES ENTERIC GLIA AND CAUSES CLEFT PALATE, BUT DOES NOT INFLUENCE HEART DEVELOPMENT OR BOWEL TRANSIT

This chapter has been published in *Developmental Biology* and reprinted here with permission. López SH, Avetisyan MA, **Wright CM**, Mesbah, K, Kelly RG, Moone AM, Heuckeroth RO. Loss of Tbx3 in murine neural crest reduces enteric glia and causes cleft palate, but does not influence heart development or bowel transit. *Dev Biol.* 2018 Dec 1;444 Suppl 1:S337-S351. doi: 10.1016/j.ydbio.2018.09.017. Copyright©2018 the authors

3.1 ABSTRACT

Transcription factors that coordinate migration, differentiation or proliferation of enteric nervous system (ENS) precursors are not well defined. To identify novel transcriptional regulators of ENS development, we performed microarray analysis at embryonic day (E) 17.5 and identified many genes that were enriched in the ENS compared to other bowel cells. We decided to investigate the T-box transcription factor Tbx3, which is prominently expressed in developing and mature ENS. Haploinsufficiency for TBX3 causes ulnar-mammary syndrome (UMS) in humans, a multi-organ system disorder. TBX3 also regulates several genes known to be important for ENS development. To test the hypothesis that Tbx3 is important for ENS development or function, we inactivated Tbx3 in all neural crest derivatives, including ENS progenitors using Wnt1-Cre and a floxed Tbx3 allele. *Tbx3 fl/fl; Wnt1-Cre* conditional mutant mice die shortly after birth with cleft palate and difficulty feeding. The ENS of mutants was well-organized with a normal density of enteric neurons and nerve fiber bundles, but small bowel glial cell density was reduced. Despite this, bowel motility appeared normal. Furthermore, although Tbx3 is expressed cardiac neural crest, *Tbx3 fl/fl; Wnt1-Cre* mice had structurally normal hearts. Thus, loss of Tbx3

within neural crest has selective effects on Tbx3-expressing neural crest derivatives.

3.2 INTRODUCTION

TBX3 is a transcription and splicing factor that belongs to the TBX2 subfamily of T-box transcription factors (245, 246). Despite sharing an evolutionarily conserved DNA binding domain of approximately 200 amino acids known as the T-box, all 20 known T-box transcription factors regulate different genes. Furthermore, TBX3-mediated regulation of target genes is context-specific, suggesting that association of TBX3 with different cofactors drives target specificity (245, 247, 248). In humans, point mutations within and outside of the conserved T-box domain of TBX3 cause ulnar-mammary syndrome (UMS). UMS is an autosomal dominant disorder that affects limb, tooth, hair, apocrine gland and genital development (249). TBX3 is also known to be abundantly expressed in the ENS (189, 215, 250), but roles for TBX3 in the ENS have not been previously defined.

The ENS is a complex nervous system in the bowel wall that controls motility, blood flow, and epithelial function. ENS defects can cause life-threatening medical problems like Hirschsprung disease or chronic intestinal pseudoobstruction, and our understanding of genes that regulate enteric nervous system (ENS) development remains incomplete (59, 134, 251-257). Several studies have shown ENS expression of *Tbx3* at E11-12, E14.5, E15-16, and E18-19 (189, 215, 250). Consistent with this, we profiled the transcriptome of the developing ENS at E17.5 by microarray and found abundant *Tbx3* transcripts. In other developmental contexts, TBX3 regulates several genes known to impact ENS development (258-262), increasing our interest in studying the role of TBX3 in the ENS.

The ENS is a neural crest derivative formed primarily from vagal neural-derived crest cells (NCCs) that migrate through fetal bowel, proliferate and then differentiate into diverse neuron and glia subtypes. Proliferation of progenitor cells, differentiation of mature neuronal

phenotypes, and formation of functional neuronal circuits continues after birth and into adulthood (263). *In vivo* studies of ENS function in *Tbx3* mutant mice were not previously possible because homozygous *Tbx3* -/- mice have heart malformations that cause prenatal death (264-266).

To further understand the role of *Tbx3* in ENS development, we generated conditional *Tbx3 fl/fl; Wnt1-Cre* mutant mice. In this mouse line, *Wnt1-Cre* induces DNA recombination to inactivate *Tbx3* in essentially all enteric nervous system precursors and their mature progeny (collectively called enteric neural crest-derived cells (ENCDC)) (266, 267). *Wnt1-Cre* also inactivates *Tbx3* in other neural crest-derived tissue including great vessels of the heart and craniofacial bones (268, 269). We found that *Tbx3 fl/fl; Wnt1-Cre* mice die within 24 hours of birth, but have normal enteric neuron density, bowel motility, and cardiac septation at birth. Interestingly, enteric glia density was reduced in small bowel of mutant mice. We also found that *Tbx3 fl/fl; Wnt1-Cre* mice have highly penetrant cleft palate and reduced levels of *Osr2* in the developing palate. OSR2 is a transcription factor that regulates many genes involved in palate mesenchyme development (270, 271), suggesting that reduced OSR2 may contribute to the cleft palate phenotype observed in *Tbx3 fl/fl; Wnt1-Cre* mutant mice.

3.3 MATERIALS AND METHODS

Animals and genotyping

Animal experiments were approved by the Institutional Animal Use and Care Committee at The Children's Hospital of Philadelphia Research Institute, the University of Utah, and by the Washington University School of Medicine Animal Studies Committee. All mice were maintained on mixed genetic backgrounds (*Wnt1-Cre* (C57BL/6J x CBA/J)F1), *Tbx3 floxed* (*Tbx3 fl/fl*) (Bl6/SV129). The *Tbx3 floxed* (*Tbx3 fl/fl*) conditional allele was generated as described (266). *Tbx3 fl/fl; Wnt1-Cre* and *EYFP; Wnt1-Cre* reporter mice animals were generated by breeding *Tbx3 flox/flox* mice or *Rosa26EYFP* reporter mice (*Gt(ROSA)26Sortm1(EYFP*) (272) (RRID:IMSR_JAX:006148) to *Tg(Wnt1cre)11Rth* (RRID:IMSR_JAX:003829) (273) mice (referred to as *Wnt1-Cre*). *Tbx3 fl/fl* and *Tbx3 fl/wt; Wnt1-Cre* males and females were then intercrossed to obtain *Tbx3 fl/wt*, *Tbx3 fl/wt; Wnt1-Cre*, or *Tbx3 fl/fl* (control genotypes) and the conditional knockout genotype, *Tbx3 fl/fl; Wnt1-Cre*. *tdTomato* reporter mice (*Gt(ROSA)26Sor*$^{tm9(CAG\text{-}tdTomato)Hze}$, stock #007909),were bred into *Tbx3;Wnt1-Cre* mice. The vaginal plug day was counted as embryonic day 0.5. Newborn P0 mice were euthanized by decapitation. Genotyping reactions for *Cre* recombinase-containing transgenes and *Rosa26EYFP* used previously described primers (61). The *Tbx3* wild-type and *Tbx3* floxed alleles were genotyped using primer pair Tbx3-F: 5’ GTG TGA GAC AGA GAA ATC AGT GG 3′ and Tbx3–R: 5′ CCA ACT GGT ATC TTG ATA AAC CTC 3′, producing a 320 bp band from the wild-type allele and a 480 bp band from the conditional allele (266).

Bone and cartilage staining

Simultaneous staining with alizarin red S and alcian blue was performed with minor modifications to a published protocol (274). P0 newborn mice were fixed in 95% ethanol for two hours, after which skin and organs were removed and fixation was continued in 95% ethanol for

one week. Samples stored in 4% paraformaldehyde for more than 72 hours were rinsed in milliQ water overnight before evisceration and post fixation in 95% ethanol. Samples were moved to acetone for two days and then stained for 3 days at 37 °C in 0.015% alcian blue (Sigma #A5268), 0.005% alizarin red S (Sigma #5533), 5% glacial acetic acid, and 70% ethanol. Samples were washed with water and rocked in a 1% KOH solution at room temperature until skeletons became visible after 48 h. Samples were then passed through a graded series of 20%/1% KOH, 50%/1% KOH, and 80% glycerol/1% KOH baths over the course of several weeks or until tissues cleared. Skeletal preparations were stored and photographed in 80% glycerol/1% KOH.

Whole-mount immunofluorescent staining

P0 bowel was harvested, flushed with PBS, pinned flat and fixed with 4% paraformaldehyde in phosphate-buffered saline (PBS) for 30 minutes at room temperature, and then incubated in blocking solution (5% normal donkey serum (Jackson ImmunoResearch #017-000-121) in 0.5% Triton-X 100 (PBS-T)) for 1 h at 25 °C. Samples were then incubated overnight at 4 °C in primary antibody diluted in 5% normal donkey serum in 0.5% PBS-T. Samples were washed 3 times with PBS for 5 minutes and incubated with secondary antibody at 25 °C for 20 minutes in PBS. Samples were mounted in 50% Glycerol in PBS.

Antibodies

Primary antibodies: ANNA–1 antiserum (a gift from Vanda Lennon, Mayo Clinic, RRID:AB_2313944, 1:2000), SOX10 (goat, RRID:AB_2195374, Santa Cruz Cat# SC-17342, 1:400), TuJ1 (rabbit, RRID:AB_10063850, Covance Research Products Inc Cat# PRB-435P-100,1:10,000), TBX3 (goat, RRID: AB_2240328, R&D Systems Cat #AF4509-SP, 1:100), and S100β (rabbit, RRID: AB_882426, Abcam Cat #AB52642, 1:200).

Secondary antibodies: donkey anti rabbit, goat anti-human, donkey anti-goat Alexa fluor-

488, -594, or -647 (Invitrogen, 1:400).

FITC dextran intestinal transit study

Bowel transit was determined by assessing the distribution of a FITC-conjugated dextran marker (70-kDa FITC-dextran; Sigma, Cat# 46945) in the bowel of control and *Tbx3 fl/fl; Wnt1-Cre* mice after feeding the non-absorbed fluorescent marker FITC-dextran as previously described (275). Pregnant dams were euthanized and mice were delivered at E19.5 by caesarian section to avoid having fed control and unfed mutant mice. All mice were fasted and kept on a warming pad for 1 h. Mice were then fed by mouth 7µL of a solution containing 50 mg FITC Dextran (70 kDa) per mL of 2% methylcellulose in water. Six hours later, mice were euthanized, and the bowel was divided into 8 segments (esophagus, stomach, small intestine 1-3, colon 1-3). Each bowel segment was opened and suspended in 100 µL of 1X phosphate buffered saline solution. Samples were vortexed for 15 seconds and centrifuged at 4000 rpm for 10 min, and fluorescent activity of the supernatant was measured using a fluorimeter (excitation 485 nm, emission at 525 nm). Bowel transit was analyzed using the intestinal "geometric center" of the distribution of dextran throughout the bowel and was calculated as described (276). For the geometric center calculation we included all bowel segments.

Fluorescence activated cell sorting (FACS) of cells from prenatal bowel

Prenatal bowel was dissected from reporter mouse strain (*Tbx3; Wnt-1Cre; TdTomato* or *Wnt1Cre-EYFP*) at E17.5 and digested in 0.5 mg/mL collagenase (Sigma Cat. #C-6885) and 0.5 mg/mL dispase (ThermoFisher Scientific, Cat. #17105-041) in PBS at 37 ºC for 30 minutes. Digested samples were triturated using a P1000 pipette and filtered through a 40 µm cell strainer (Fisher #352340). Dissociated cells were re-suspended in FACS buffer (10mM HEPES, 1mg/mL BSA, 1% penicillin and streptomycin in HBSS). Samples were sorted into DMEM on a Beckman Coulter MoFlo (Siteman Flow Cytometry Core at Washington University in St. Louis School of

Medicin) or a MoFlo Astrios EQ (Children's Hospital of Philadelphia Flow Cytometry Core Laboratory) then re-suspended in Buffer RLT (RNEasy Micro Kit Qiagen #74004 or RNeasy Mini Kit (Qiagen #74104) to proceed immediately with RNA isolation as per the manufacturer's instructions.

Microarray

Microarrays were performed using Affymetrix gene chips that contain probes for 28,000 mouse genes (GeneChip Mouse Gene 1.0 ST Array, performed at the Genome Technology Access Center, Washington University School of Medicine). N=3 chips for EYFP-positive samples, N=4 chips for EYFP-negative samples. Gene expression data was analyzed using the Partek Genomics Suite. Data across multiple arrays was normalized using Robust Multi-array Average (RMA) and ANOVA with correction for multiple comparisons was used to identify genes with > 2-fold higher expression in the EYFP-positive fraction (ENCDC) versus the EYFP-negative fraction (non-ENCDC) at a false discovery rate of 0.05. Genes were displayed using Bioconductor software and the Oligo package in R (277, 278).

Histological analysis

Heads and hearts were fixed in 4% paraformaldehyde, dehydrated and embedded in paraffin prior to sectioning at 6 μm (heads) or 10 μm (hearts). Sections were stained with hematoxylin and eosin using standard protocols.

EDU and TUNNEL staining

Four consecutive 6 μm sections from anterior and from posterior palate were taken from three embryos of each genotype at E13.5. Proliferation was measured using Click-iT® EdU Alexa Fluor® 488 Imaging Kit (Thermo Fisher Scientific #C10337). Percent of proliferative

(EdU+) positive cells was defined as the number of EdU positive nuclei to total number of nuclei as detected by Hoechst counterstain in the mesenchyme of the palatal shelf tip region (150μm from the tip of the palate).

qRT-PCR

Total RNA was isolated from FACS sorted bowel cells or microdissected palatal shelves at E13.5 using RNeasy Mini Kit (Qiagen #74104) or RNEasy Micro Kit Qiagen #74004 and reverse-transcribed using SuperScript II Reverse Transcriptase for cDNA synthesis (Invitrogen #18064014). qRT-PCR was performed on at least three biological replicates with three technical replicates per run using SsoFast™ EvaGreen® Supermix with Low ROX (Bio-Rad #1725211) and Bio-Rad Cycler CFX96. Primers are listed in Table 1.

Microscopy

Photographs of whole fetuses, skeletal preparations, and hearts were acquired on an Olympus SZ40 stereomicroscope. Images of fluorescent whole-mount bowel were acquired as multiple optical sections using a Zeiss LSM 710 confocal (Zen software). FIJI (NIH ImageJ) software was used to process images including only cropping, stitching, rotating, centering, and uniform adjustments of brightness, contrast and saturation. Confocal images show flattened Z-stacks.

Statistics

GraphPad Prism (version 7.03 for Windows, GraphPad Software, La Jolla California USA, www.graphpad.com) was used for statistical analysis via student's t-test. All studies include at least three biological replicates, unless otherwise noted in the text. Data are plotted with mean and positive standard error of the mean. A p-value < 0.05 was considered significant.

3.4 RESULTS

Tbx3 is enriched in enteric neural crest-derived cells (ENCDC) compared to other cells of E17.5 bowel

To identify novel genes that might regulate development of the ENS during late embryonic development, we used a microarray to compare gene expression in ENS and non-ENS cells of the E17.5 bowel. For this study, *Wnt1-Cre; Rosa26EYFP* reporter mice were employed for fluorescence-activated cell sorting to separate *EYFP* expressing ENCDC from other cells of the bowel wall. This is a commonly used mouse line that expresses *EYFP* in essentially all ENCDC (>99.9%), but not in other cells of the bowel wall (Lake et al., 2016). As expected, we identified many differentially expressed genes encoding transcription factors, as well as other proteins (**Figure 3-1**). Differential expression of many of these genes have been described and validated previously (215, 250), providing a high level of confidence in our results.

For this study, we decided to focus on *Tbx3*, as its transcripts are 7-fold more abundant in ENCDC compared to non-ENS cells of the bowel (p= 2.7E-7) (**Figure 3-1**). TBX3 protein was recently demonstrated to be expressed at high levels in most enteric neuron types at E18.5 and we previously demonstrated *Tbx3* mRNA in the region of the ENS at E14 (189, 215). Our primary hypothesis was that *Tbx3* would be essential for some aspect of ENS development or function.

Deletion of *Tbx3* in neural crest cells results in early postnatal death

To determine how loss of *Tbx3* impacts the ENS, we generated conditional mutant mice using the *Wnt1-Cre* mouse line to recombine *Tbx3* alleles in *Tbx3 fl/fl* mice. To ensure that CRE-mediated DNA recombination occurred as expected in the ENS, we confirmed loss of TBX3 protein and *Tbx3* mRNA by immunohistochemistry and qRT-PCR (**Supplemental Figure 3-1**). *Tbx3 fl/fl; Wnt1Cre* mice were born in normal Mendelian ratios at E19.5 and appeared healthy at birth with normal weight and no exterior anatomic defects (**Figure 3-2 A-B**). Initially, *Tbx3 fl/fl;*

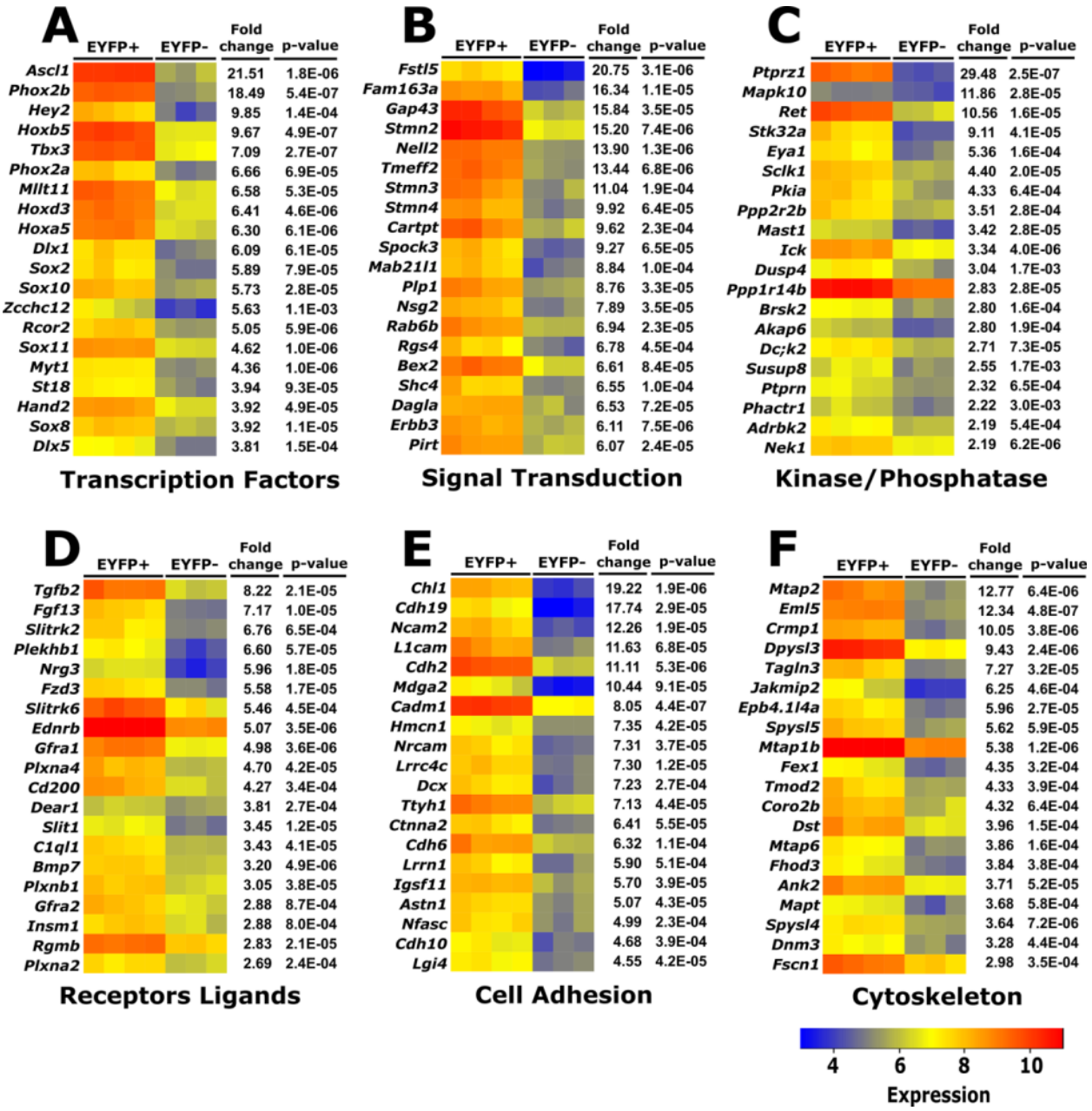

Figure 3-1: Differentially expressed genes in ENS vs. non-ENS cells at E17.5
(A-F) Genes differentially expressed in EYFP+ (ENS) vs. EYFP- (non-ENS) cells isolated from *Wnt1-Cre; Rosa26EYFP* reporter mice at E17.5. A full list of differentially expressed genes can be found in Supplementary Table 1.

Wnt1Cre mice were indistinguishable from littermates without cyanosis, respiratory distress or abnormal movements. However, by weaning at 21 days after birth (P21), there were no surviving *Tbx3 fl/fl; Wnt1Cre* mice (Chi^2-test, p=0.000895, N=66) and we never found *Tbx3 fl/fl; Wnt1-Cre*

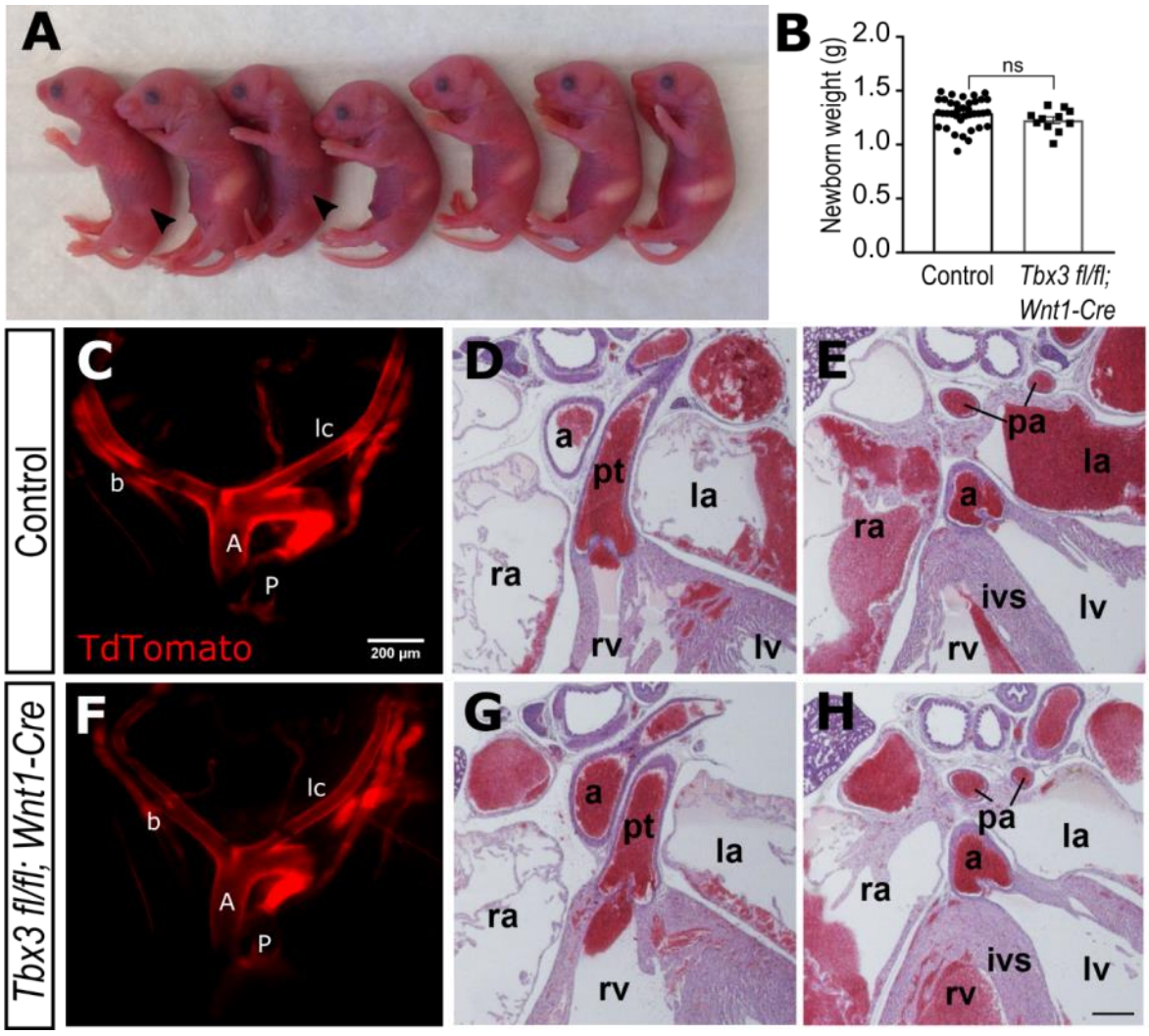

Figure 3-2: Early deletion of *Tbx3* in neural crest derived cells via *Wnt1-Cre* results in postnatal lethality.

(A) *Tbx3 fl/fl; Wnt1-Cre* mice were found in normal Mendelian ratios at P0 (Chi^2-test, p>0.05, n=79) and appear normal. Mutants can be distinguished from wild type littermates by the absence of a milk spot in the stomach (black arrowheads). (B) Average weight is normal after birth (p-value<0.05, N= 37 control, N=11 mutant). Error bar = SEM. (C,F) External anatomy of the great vessels and outflow tract visualized using a Tdtomato reporter in control and *Tbx3 fl/fl; Wnt1-Cre* newborn mice appears normal. A=aorta, p=pulmonary artery, b=brachiocephalic trunk, lc=left common carotid artery. Scale bar= 200µm. N= 3 of each genotype. (D-E,G-H) Histological sections through the region of the ventricular outlets of control (D-E) and *Tbx3 fl/fl;Wnt1-Cre* (G-H) E18.5 hearts showing normal connection of the pulmonary trunk with the right ventricle (D,G) and ascending aorta with the left ventricle (E, H). a=aorta, pt=pulmonary trunk, pa=pulmonary artery rv=right ventricle, lv=left ventricle, ra, right atrium, la, left atrium, ivs, interventricular septum. Scale bar= 200µm. Control N= 2, *Tbx3 fl/fl;Wnt1-Cre* N=6.

result from cardiac defects, renal failure, or because of nutritional deficiency due to inadequate

mice that survived longer than 24 hours. Death during the neonatal period can intake or intestinal dysfunction (279).

Heart structure is normal in *Tbx3 fl/fl; Wnt1Cre* mice

We evaluated heart anatomy because *Tbx3* is required for normal cardiac outflow tract and conduction system development (264-266, 280) and because *Wnt1-Cre* is active in cardiac neural crest cells required for outflow tract septation and proper smooth muscle cell investment of the great arteries. Furthermore, *Tbx3* is expressed in a subset of the *Wnt1-Cre*+ neural crest-derived cells. We analyzed the outflow tract and major arteries of the heart using a *tdTomato; Wnt1-Cre* reporter and did not detect gross morphologic differences in the outflow tract or great vessels of *Tbx3 fl/fl; Wnt1Cre* mice (Figure 2 C, F). Histological analysis of mutant fetal hearts revealed normal ventriculo-arterial connections and no ventricular septal defects (N=6; **Figure 3-2D-E, G-H**). This ruled out structural heart disease as a cause of neonatal mortality.

Feeding problems in *Tbx3 fl/fl; Wnt1-Cre* newborn mice are not due to ENS defects

Mutant mice could be distinguished from their wild-type littermates by the absence of milk spots, consistent with empty stomachs and an inability to feed normally (**Figure 3-2 A**). Serious ENS defects in conjunction with functional bowel obstruction can cause poor neonatal feeding in children. Since TBX3 is abundant in enteric neurons, we pursued analysis of ENS structure and function. The ENS forms primarily from vagal neural crest-derived cells (ENCDC) that colonize the developing bowel in a rostrocaudal direction from E9.5 to E13.5 (134). To determine if *Tbx3* is necessary for proper migration of ENCDC through the bowel, we stained E13.5 bowel with TuJ1 antibody, which binds neuron-specific class III β-tubulin. TuJ1 staining correlates well with the position of the most distal ENCDC in fetal bowel because neurons are generated as ENCDC colonize the bowel (113, 134). We found that the TuJ1-staining pattern was similar in *Tbx3 fl/fl;*

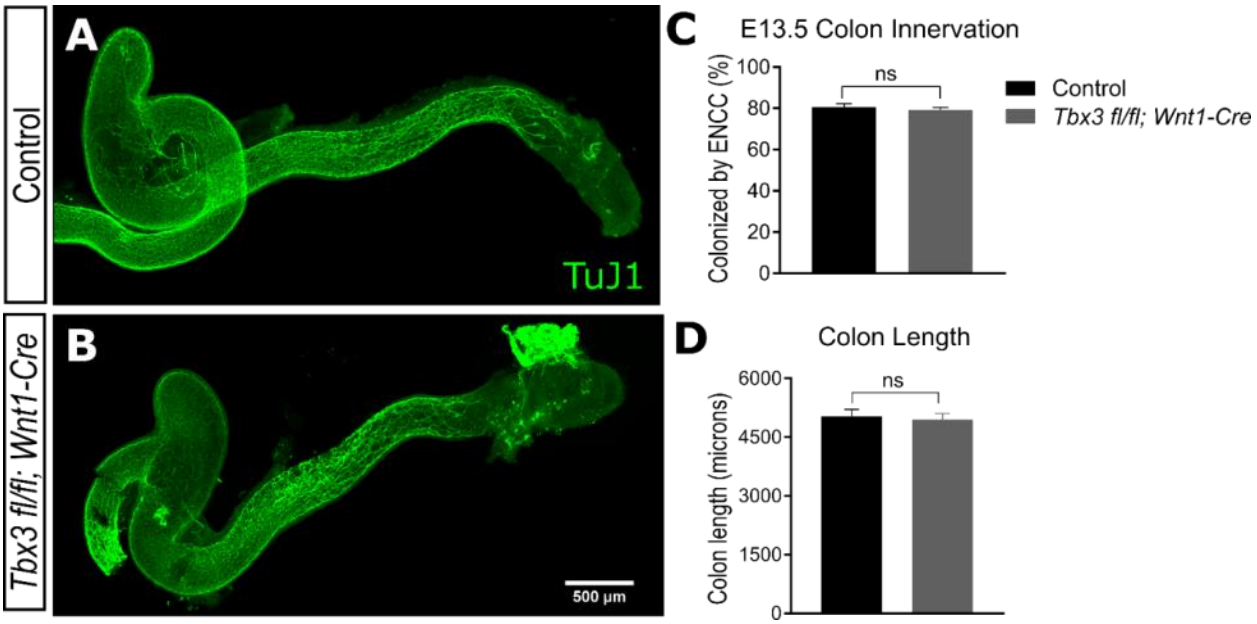

Figure 3-3: Enteric neural crest-derived precursors colonize the bowel normally in *Tbx3 fl/fl; Wnt1-Cre* mice at E13.5.
(A-B) At E 13.5 the colon is colonized by TuJ1+ ENCDC that have nearly completed their rostro-caudal migration from the vagal neural tube down to the distal colon in both *Tbx3 fl/fl; Wnt1-Cre mice* and control littermates. (C) Measurements of the percent of colon that is colonized by TuJ1+ fibers that accompany migrating ENCDC. (D) Mean absolute length of colon in *Tbx3 fl/fl; Wnt1-Cre* mice and control littermate is comparable. (Student's t-test, $p > 0.05$, N=7 control, N=4 mutant). Error bar = SEM. Scale bar = 500 µm. Scale bar in B also applies to A.

Wnt1Cre embryos and control littermates. Specifically, patterning of ENCDC and the extent of bowel colonization by TuJ1+ cells was equivalent (**Figure 3-3 A-C**). Colon length was also comparable in *Tbx3 fl/fl; Wnt1Cre* and control littermates (**Figure 3-3 D**). Because E13.5 is the stage at which ENCDC colonization of the bowel is nearly complete, these data provide convincing evidence that *Tbx3* expression within ENCDC is not needed for bowel colonization or for major aspects of ENS organization during morphogenesis.

To examine ENS structure at later stages, we stained newborn (P0) mouse bowel using ANNA-1 (anti-HuC/HuD) antibody to identify enteric neurons. We found a normal density of enteric neurons (**Figure 3-4 A-F, M, S-U**) in the small bowel and colon of *Tbx3 fl/fl; Wnt1-Cre* mice. We also found a normal density of SOX10+ cells in the proximal small intestine and colon of *Tbx3 fl/fl; Wnt1-Cre* mice (**Figure 3-4 A, C, D, F, M, V, X**), but there was a statistically

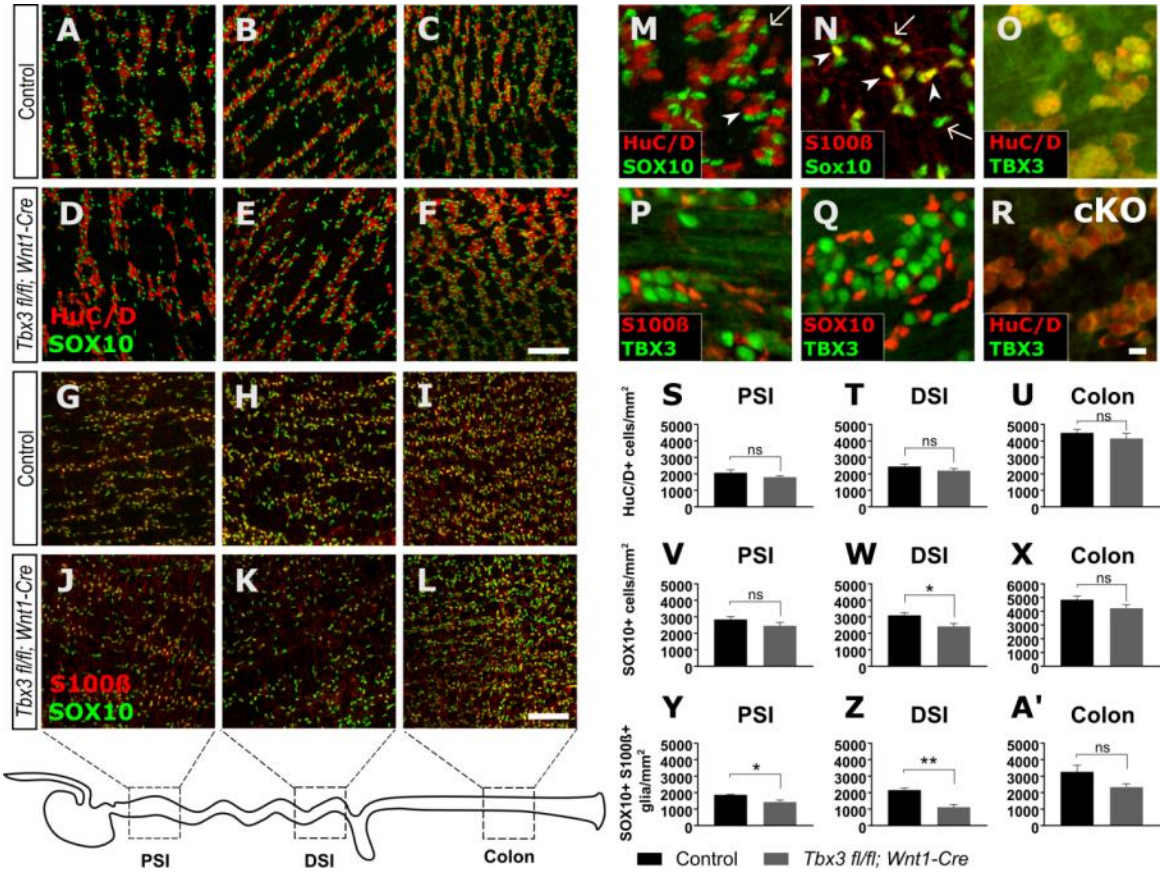

Figure 3-4: Normal density of neurons and glia are present in T*bx3 fl/fl; Wnt1-Cre* mice at P0.

(A-F) ANNA–1 (anti-HuC/HuD) staining (red) of enteric neurons and SOX10 staining of glia and precursor cells (green) reveals that *Tbx3 fl/fl; Wnt1-Cre* and their wild-type littermates have a comparably dense network of enteric neurons but fewer SOX10+ cells in distal small bowel at P0. Scale bar = 100 µm. Scale bar in F applies to A-E. (G-L) S100β (red) and SOX10 (green) staining reveals decreased numbers of SOX10+ S100β+ glia in *Tbx3 fl/fl; Wnt1-Cre* P0 mice compared to their control littermates. Scale bar = 100 µm. Scale bar in L applies to G-L. (M) Expanded view of B. White arrowhead indicates a HuC/D+ neuron; white arrow indicates a SOX10+ cell. (N) Expanded view of H. White arrowheads indicate SOX10+S100β+ cells (counted); white arrows indicate SOX10+ S100β- cells. (O-Q) TBX3 antibody (green) labels HuC/D+ neurons, but not S100β+ glia or SOX10+ cells in P0 myenteric plexus. (R) TBX3 antibody (green) does not label *Tbx3 fl/fl; Wnt1-Cre* myenteric plexus. cKO = conditional knockout. Scale bar = 10 µm. Scale bar in R applies to M-R. (S-U) Quantification of neuronal cell bodies (ANNA-1+) reveals normal numbers in the proximal small intestine, distal small intestine and the colon of *Tbx3 fl/fl; Wnt1-Cre* mice. (Student's t-test, p> 0.05). (V-W) Quantification of SOX10+ cells reveals normal numbers in the proximal small intestine and colon of *Tbx3 fl/fl; Wnt1-Cre* mice (Student's t-test, p> 0.05). A 22% reduction in SOX10+ cell density was statistically significant in the distal small intestine of *Tbx3 fl/fl; Wnt1-Cre* mice. (Student's t-test, p = 0.0316). (Y-A') Quantification of glia (SOX10+, S100β+ cells) reveals reduced glial density in proximal (24% reduction, Student's t-test, p = 0.020) and distal (48% reduction, Student's t-test, p = 0.007) small intestine of *Tbx3 fl/fl; Wnt1-Cre* mice. Glial density was not significantly different from control in colon of *Tbx3 fl/fl; Wnt1-Cre* mice (Student's t-test, p = 0.111). * $p \leq 0.05$, ** $p \leq 0.01$. n = at least 3 for each genotype. Error bar = SEM.

significant reduction (22%, p=0.032) in SOX10+ cell density in distal small intestine of unclear physiologic or functional significance (**Figure 3-4 B, E, W**). SOX10 is expressed in all ENS precursors during early development, but then becomes restricted to enteric glia. To assess more mature glia, we stained P0 bowel with antibodies to S100β and SOX10 (**Figure 3-4N**) and found significantly reduced glial cell density in proximal (24% reduction, $p < 0.05$; **Figure 3-4G, J, Y**) and distal (48% reduction, $p < 0.01$; **Figure 3-4H, K, Z**) small bowel. Mean S100β+ cell density was also reduced in colon of *Tbx3 fl/fl; Wnt1-Cre* mice, but this was not statistically significant (28% reduction, $p = 0.111$; **Figure 3-4I, L, A'**). These data indicate that TBX3 is dispensable for differentiation of ENCDC into enteric neurons, but may be important for gliogenesis in the ENS. To determine which cells express TBX3 protein during development, we labeled normal P0 distal small bowel using an antibody against TBX3. Given the glial phenotype we were surprised that TBX3 protein was in HuC/D+ neurons (**Figure 3-4O**), but not in SOX10+ cells (**Figure 3-4P**) or in S100β+ glia (**Figure 3-4Q**). Collectively these data suggest that TBX3 is required for maturation of enteric glia, but that the effect is likely to be non-cell autonomous.

Little is known about mechanisms that control enteric gliogenesis, but in many regions of the nervous system including the ENS, Notch signaling is be critical. In particular, Hedgehog pathway activation was reported to robustly induce the Notch ligand *Dll1* and the Notch signaling molecule *Hes1* to promote ENCDC proliferation and glial differentiation (171, 174). To determine if *Tbx3* mutants have reduced induction of *Dll1* and *Hes1* as a function of altered Hedgehog or Notch signaling, we performed quantitative PCR. ENCDC were FACS-isolated from E17.5 control and *Tbx3 fl/fl; Wnt1-Cre; TdTomato* distal small bowel. Levels of *Dll1* and *Hes1* mRNA were normal in ENCDC of *Tbx3* mutant bowel (**Figure 3-5A-B**). Together, these results suggest that gliogenesis defects in *Tbx3* bowel are mediated by a neuron-dependent, but *Dll1* and *Hes1*-independent pathway.

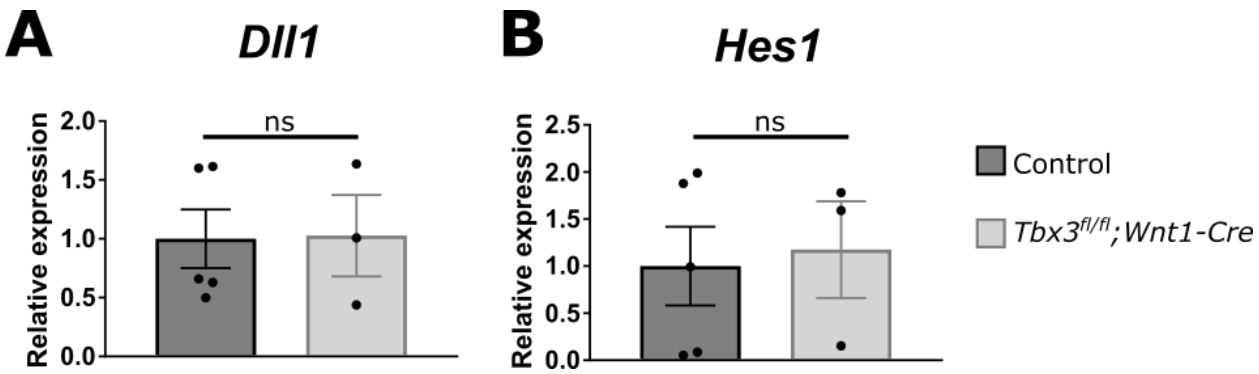

Figure 3-5: Notch pathway members *Dll1* and *Hes1* are expressed at normal levels in *Tbx3fl/fl; Wnt1-Cre* distal small intestine.
(A-B) Quantitative PCR was performed on ENCDC from E17.5 distal small intestine. Levels of Notch pathway members *Dll1* (Mann-Whitney Rank Sum Test, p = 1; n=5 control, 3 mutant) or *Hes1* (Student's t-test, p = 0.803; n=5 control, 3 mutant) were normal in the ENS of *Tbx3 fl/fl; Wnt1-Cre; Tdtomato* mice. Expression levels are relative to mean expression in *Tbx3* controls. Error bar = SEM.

Functional bowel motility appears normal in *Tbx3 fl/fl; Wnt1-Cre* newborn mice

Bowel dysmotility can be profound even without striking anatomic defects in the ENS (117). We therefore tested the hypothesis that ENS dysfunction and bowel dysmotility might underlie perinatal death in *Tbx3 fl/fl; Wnt1-Cre+* mice because TBX3 was absent from ENCDC. In support of this hypothesis, some *Tbx3 fl/fl; Wnt1-Cre* mice accumulated large amounts of air in the small bowel, a problem that can occur with serious bowel dysmotility (**Figure 3-6 A**). Although *Tbx3 fl/fl; Wnt1-Cre* mice were not spontaneously feeding (evidenced by no milk in their stomachs as compared to littermates), we used a previously established protocol (275, 276) to administer Fluorescein isothiocyanate (FITC) dextran to newborn mice by mouth. FITC dextran is poorly absorbed, so intraluminal FITC abundance is a good measure of transit through the bowel and should be abnormal if bowel motility is impaired. Unlike adult mice, where bowel motility moves FITC dextran through the small bowel and into the colon within 1-2 hours, bowel transit is much slower in P0 mice. To quantify transit through the bowel, we measured FITC dextran levels in sequential bowel regions six hours after oral administration. FITC dextran distribution was indistinguishable between *Tbx3 fl/fl; Wnt1-Cre* mice and control littermates

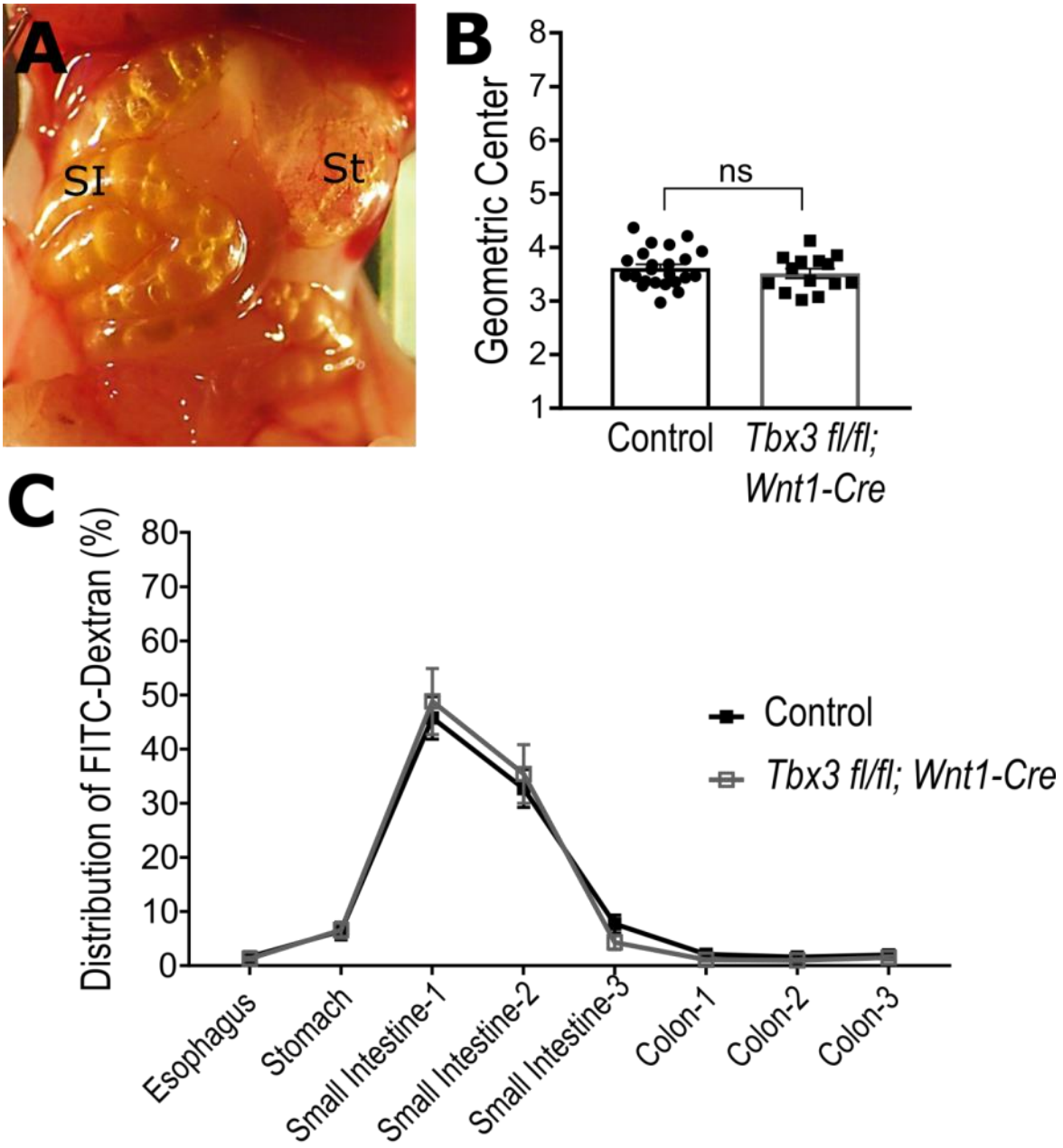

Figure 3-6: Fluorescein isothiocyanate (FITC) dextran transit after 6 hours is normal in *Tbx3 fl/fl; Wnt1-Cre* mice delivered by caesarian section.
(A) P0 *Tbx3 fl/fl; Wnt1-Cre* mice have air in the stomach (St) and throughout the proximal small intestine (SI). (B) One hour after delivery by caesarian section, neonatal mice were fed FITC-dextran and the distribution of FITC was assessed along 8 segments of bowel. FITC dextran was concentrated in the proximal small intestine in both *Tbx3 fl/fl; Wnt1-Cre* mice and control littermates. (Student's t-test, $p > 0.05$). N=23 control, N=14 mutant. Error bar = SEM. (C) The geometric center was calculated for each replicate and revealed no significant difference in FITC-dextran transit after 6 hours in *Tbx3 fl/fl; Wnt1-Cre* mice. (Student's t-test, $p > 0.05$). N=23 control, N=14 mutant. Error bar = SEM.

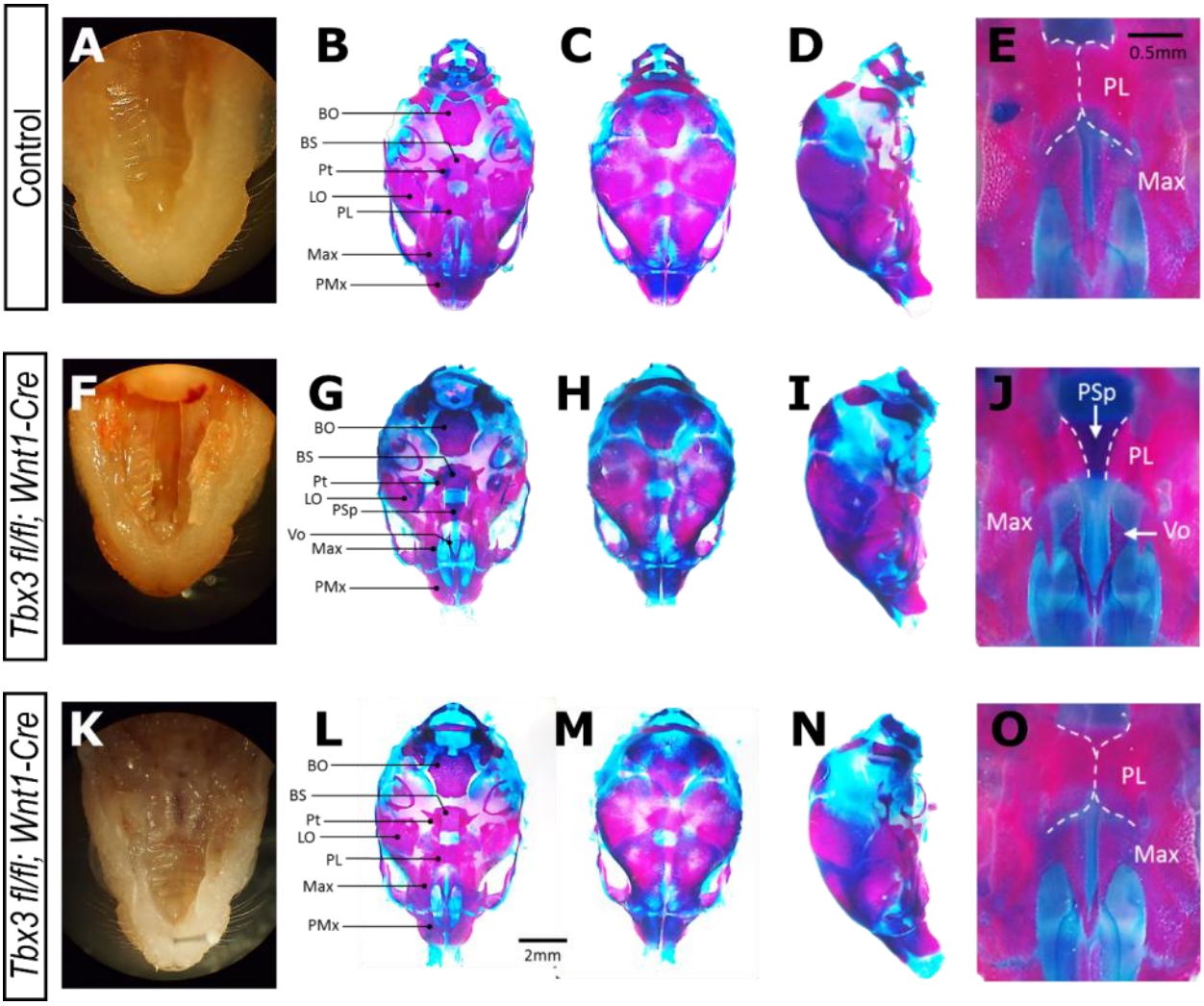

Figure 3-7: Cleft of the secondary palate in newborn *Tbx3 fl/fl; Wnt1-Cre* mice.
(A-E) Whole-mount and Alizarin Red (bone) and Alcian Blue (cartilage) simultaneous staining of newborn mice heads show that wild-type littermates have normal fused palates. Cranial and lateral views show normal skull anatomy and no other major craniofacial defects. Note that in (E) the vomer (Vo) and presphenoid (PSp) bones cannot be seen because they are underneath the maxilla (Max) and palatine (PL). N=10. (F-J) Most *Tbx3 fl/fl; Wnt1-Cre* mice have overt cleft palatal defects. Note that in (J) the vomer (Vo) and presphenoid (PSp) bones are exposed. N=7. (K-O) Two mutant animals were identified and revealed a normally fused palate. N=2. Abbreviations: BO, basioccipital; BS, basisphenoid; Pt, pterygoid; LO, lamina obturans; PMx, premaxilla

(**Figure 3-6 B-C**). These results indicate that the connectivity and function of the ENS at P0 is sufficient to coordinate normal bowel motility in the small intestines of *Tbx3 fl/fl; Wnt1-Cre* newborns. Further analysis of colon motility was not practical because of slow bowel transit in

neonatal mice and < 24 hour lifespan of the *Tbx3 fl/fl; Wnt1-Cre* animals. Nonetheless, these data provide clear evidence that *Tbx3 fl/fl; Wnt1-Cre* mice can swallow (since FITC-dextran was given orally) and that bowel motility or esophageal motility defects are unlikely to account for neonatal death or the absence of milk within the stomach. Observation of the neonates also did not reveal problems with motor function or coordination that should affect feeding.

TBX3 is required for palate development

Since defects in swallowing and bowel motility could not account for the abnormal accumulation of air and absence of milk spots in stomachs of *Tbx3 fl/fl; Wnt1-Cre* mice, we examined the palate of the mutants. Cleft palate causes serious feeding problems because the secondary palate is needed to generate negative pressure for suckling (279). We found that 96.5% (55/57) of *Tbx3 fl/fl; Wnt1-Cre* mice had a cleft secondary palate (**Figure 3-7**). Bone and cartilage staining with Alcian Blue and Alizarin Red confirmed and defined the secondary palate defect in *Tbx3 fl/fl; Wnt1-Cre* mice (**Figure 3-7 A-O**). Two of the *Tbx3 fl/fl; Wnt1-Cre* mice analyzed in this study had what appeared to be a normally fused palate (**Figure 3-7 K-O**), but this was early in the process of interbreeding *Tbx3 fl/fl* to *Wnt1-Cre* mice, suggesting strain background effects on penetrance. Abnormalities in other craniofacial structures were not observed in any *Tbx3 fl/fl; Wnt1-Cre* mice, suggesting that the failure of palatal shelf fusion is an intrinsic defect of the palatal shelf. Consistent with this hypothesis, *Wnt1* regulatory elements drive *Cre* expression in premigratory cranial neural crest cells that contribute to the palatal mesenchyme (Ito, 2003).

To better define this developmental defect, we compared palate development in *Tbx3 fl/fl; Wnt1-Cre* mice versus control littermates. Palatal shelf morphogenesis occurs by coordinated survival, proliferation, migration and differentiation of mesenchymal cells and their epithelial lining (281). We visualized palate development in paraffin sections from anterior and posterior palate between

E12.5 and E15.5 (**Figure 3-8**) in control and *Tbx3 fl/fl; Wnt1-Cre* mice.

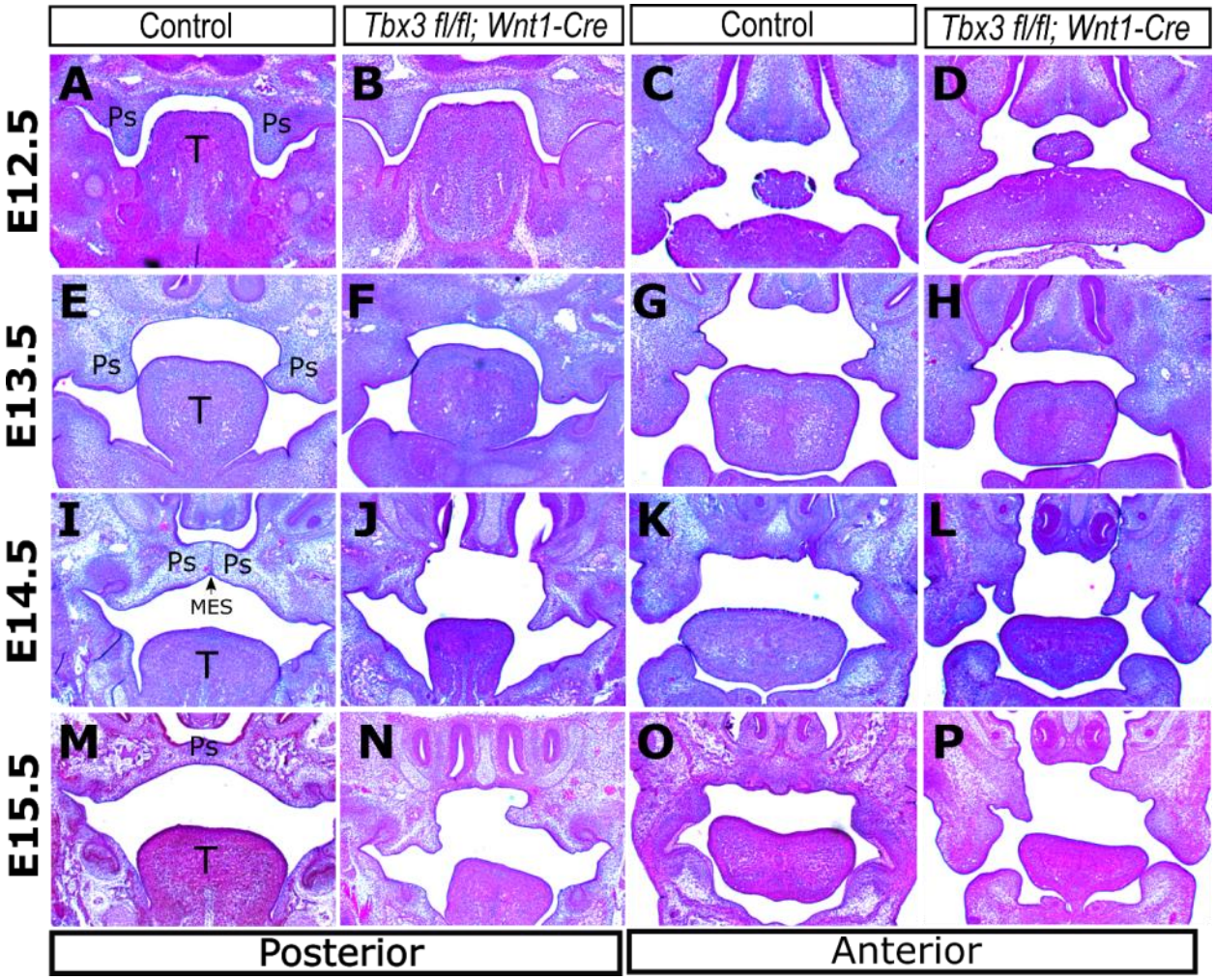

Figure 3-8: *Tbx3 fl/fl; Wnt1-Cre* mice present defects in palatal shelf elevation.
(A-P) Histological staining with hematoxylin and eosin in the anterior and posterior region of the secondary palate at key developmental stages show a delay in palatal shelf elevation at E14.5. N=3 of each genotype for each time point. Abbreviations: Ps, palatal shelf, T: tongue, MES: midline epithelial seam.

Beginning at E11.5 bilateral palatal shelves arise from the oral surface of the maxillary processes. Then in control mice (**Figure 3-8**), proliferation of epithelial and mesenchymal cells causes vertical downward growth of palatal shelves between E12 and E14 (**Figure 3-8 A, E**). By E14.5, the palatal shelves normally undergo elevation, a process defined by asynchronous reorientation into the horizontal position (**Figure 3-8 I**). Palatal shelves continue to grow horizontally above

the tongue until they meet and initiate fusion at a transient multilayered epithelium called the midline epithelial seam (MES) at E15 (**Figure 3-8 I**). By E15.5 the MES has disappeared and the palate has a single continuous mesenchymal layer lined by epithelial cells (**Figure 3-8 M**). Histological analysis at key developmental time points demonstrated a failure of palatal shelf elevation in *Tbx3 fl/fl; Wnt1Cre* mice (**Figure 3-8 J, L, N, P**). These results suggest that TBX3 is required in the palatal mesenchyme for normal development of the secondary palate.

The role of *Tbx3* in palatal shelf elevation

Although the prevailing model of palatal shelf elevation suggests that this process is independent of palatal shelf-growth (281, 282), some mouse models with delayed palatal shelf elevation have disturbed cell proliferation and apoptosis of mesenchymal cells in the developing palate (271, 283). To determine whether the defect of palatal shelf elevation observed in *Tbx3 fl/fl ; Wnt1Cre* mice was caused by changes in cell proliferation and apoptosis, we analyzed EdU incorporation into dividing palate mesenchymal cells and stained for active caspase-3 in E13.5 embryos, a time just prior to palatal shelf elevation. We found that *Tbx3 fl/fl; Wnt1Cre* mice had normal levels EdU incorporation in both the anterior and posterior region of palatal shelf mesenchyme (**Figure 3-9 A-F**) and very low levels of active capsase-3 in both control and mutant animals (**Figure 3-9 G-L**). These data suggest that defects in elevation of the palatal shelves of *Tbx3 fl/fl; Wnt1Cre* mice are not a consequence of altered cell proliferation or apoptosis at E13.5.

Molecular mechanisms of TBX3 in palatal shelf elevation

To understand the molecular mechanisms through which TBX3 regulates palatal shelf elevation, we analyzed gene expression in the palate of *Tbx3 fl/fl; Wnt1-Cre* and control mice at E13.5. Genes selected for analysis by qRT-PCR have known roles in palate morphogenesis or are known to interact with TBX3 in other contexts. For example, sonic hedgehog (SHH) binds the

receptor patched (PTC) to activate smoothened (SMO) and signals downstream via several of the GLI family transcription factors (281). Mice with inactivation of *Shh*, *Smo*, *Gli2* or *Gli3* have

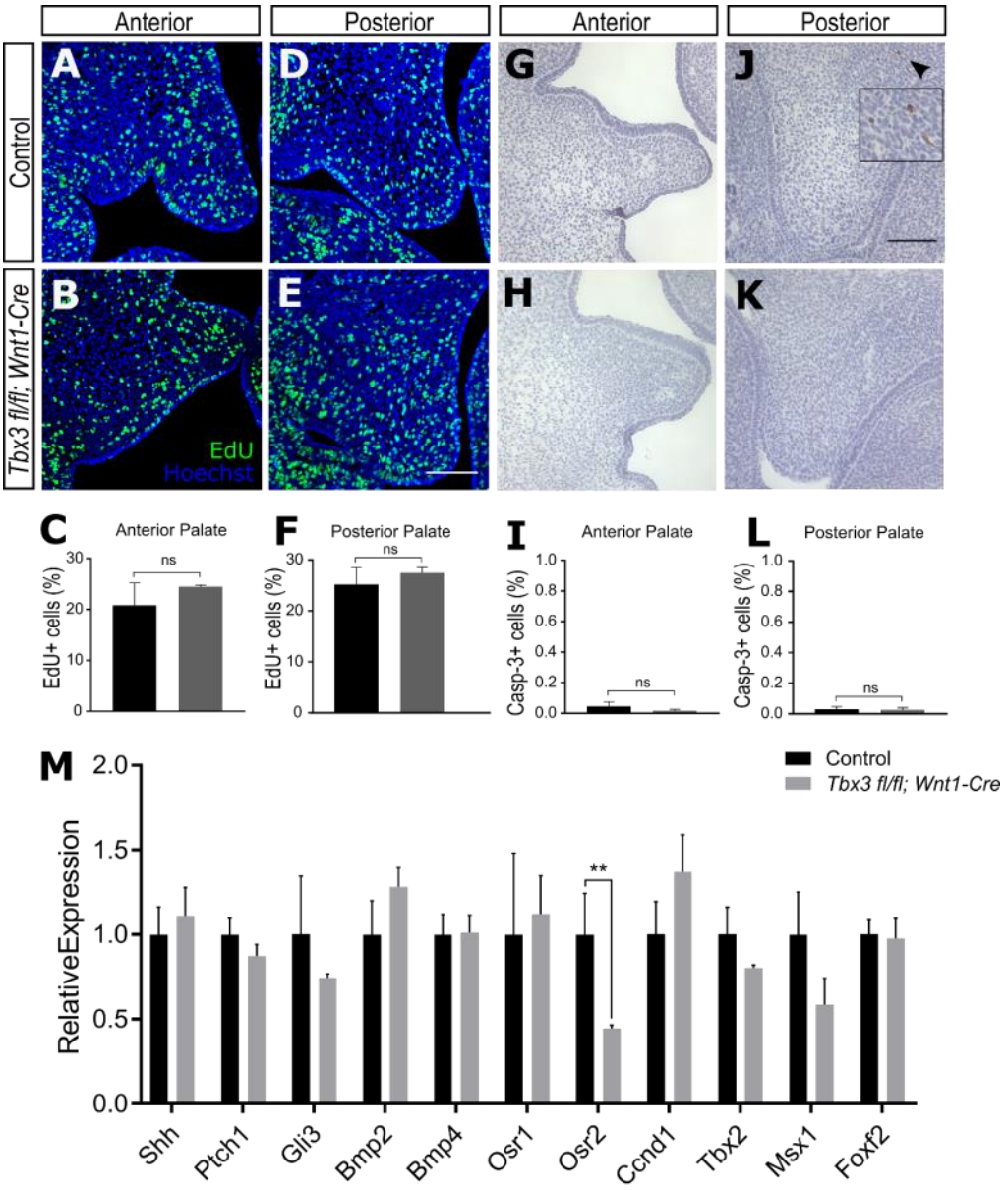

Figure 3-9: Molecular mechanisms of palatal shelf elevation.
(A-F) EdU incoorporation assay was used to identify proliferative cells at E13.5 in the palatal mesenchyme four hours after EdU injection. The ratio of EdU+ cells to total cells (Hoechst+) does not differ significantly in the anterior **(A-C)** or posterior **(D-F)** region of the palatal shelf in *Tbx3 fl/fl; Wnt1-Cre* mice. (Student's t-test, p> 0.05, N=3 of each genotype). **(G-L)** Immunostaining for cleaved caspase 3 was used to identify apoptotic cells at E13.5 in the palatal mesenchyme. The ratio of cleaved caspase3+ cells to total cells does not differ significantly in the anterior **(G-I)** or posterior **(J-L)** region of the palatal shelf in *Tbx3 fl/fl; Wnt1-Cre* mice. (Student's t-test, p> 0.05, N=3 of each genotype). **(M)** Quantitative RT-PCR analysis was performed to determine expression of genes known to regulate palate development. *Osr2* mRNA

levels were markedly reduced in *Tbx3*-deficient mice at E13.5 ($p = 0.0079$). Expression levels are relative to mean expression in *Tbx3* controls. Error bar = SEM. (N=5 of each genotype). Scale bar = 100 μm.

cleft palate defects (284-286) and TBX3 influences expression of SHH related genes during limb development (260). Similarly, TBX3 and BMP4 act in an autoregulatory loop to control mesenchymal proliferation in palatal shelves (287) and MSX1 is a target of BMP2 and BMP4 signaling critical for palate development (288). We therefore examined expression of each of these genes in E13.5 palatal shelves from *Tbx3 fl/fl; Wnt1-Cre* and control mice, but gene expression levels were equivalent (**Figure 3-9M**). We next evaluated *Tbx2* and *cyclin D1* (*Ccnd1*) mRNA levels because of reported partial functional redundancy between *Tbx2* and *Tbx3* in the palate (289); these mRNA were also of normal abundance in *Tbx3 fl/fl; Wnt1-Cre* mice. Finally, *Osr2-/-* mutant mice also have cleft palate and disturbed palatal shelf elevation (271). We found that *Osr2* mRNA levels were reduced by 55% ($p = 0.0079$) in E13.5 palatal mesenchyme (**Figure 3-9 M**) suggesting palate defects in *Tbx3 fl/fl; Wnt1-Cre* mice might result at least in part from reduced OSR2 in mutant mice.

3.5 DISCUSSION

The ENS forms from neural crest-derived precursors that colonize the bowel from E9.5 to E13.5 in mice. These cells differentiate into a wide array of neurons and glia that control most aspects of bowel function. Over the past two decades, many genes that control these early phases of ENS development have been identified, but much less is known about molecular and cellular mechanisms that guide differentiation of specific enteric neuron types, that support axon guidance and synaptogenesis, or that influence enteric glial development. In an attempt to identify genes that control these later developmental processes, we performed microarray analysis at E17.5 and identified numerous genes that are differentially expressed in the ENS versus other cells of the bowel wall. Many of these genes were previously identified and validated by our group and

others at E14 and E15.5 (189, 215, 250). Furthermore, our cell selection strategy robustly separates ENS from non-ENS cells at E17.5. Thus, many of the genes in **Figure 3-1** and **Supplementary Table 3-1** may be worthy of investigation as we strive to define mechanisms of ENS morphogenesis.

For this study, we investigated the role of *Tbx3*, a transcription factor that is highly expressed in developing ENS relative to other cells of the bowel. We demonstrated that *Wnt1-Cre* efficiently depleted TBX3 from ENCDC, as expected since prior studies show *Wnt1-Cre* induces almost complete recombination in the ENS lineage (267). We found that *Tbx3* is not required within ENCDCs for prenatal bowel colonization by ENS precursors, that *Tbx3 fl/fl; Wnt1-Cre* mice had a normal density of enteric neurons at P0, and that transit of FITC-dextran though the upper gastrointestinal tract occurred at a normal rate despite a reduced number of enteric glia. Nonetheless, *Tbx3 fl/fl ;Wnt1-Cre* mice die within 24 hours after birth with no milk in their stomachs. We attribute neonatal death to the highly penetrant cleft palate that occurred in >95% of *Tbx3 fl/fl; Wnt1-Cre* mice. The mechanistic link between the loss of *Tbx3* and cleft palate is unclear at this point: we found normal levels of many candidate genes in the palate of E13.5 *Tbx3* mutant mice. There was a significant reduction in *Osr2* mRNA levels and since *Osr2* null mutants have cleft palate (271), TBX3 may directly or indirectly regulate *Osr2* mRNA levels and contribute cleft palate in *Tbx3 fl/fl ; Wnt1-Cre* mice.

TBX3 in prenatal ENS and cardiac development

Our work and prior studies show that *Tbx3* mRNA and TBX3 protein are abundant in the developing ENS from E11 to E19 in mice and that TBX3 is present in the human ENS at week 10 of gestation, shortly after colonization of fetal bowel by ENCDC (189, 215, 250). Prior studies also show that TBX3 is co-expressed with many enteric neuron subtype markers including tyrosine hydroxylase, calcitonin gene related peptide, calbindin, neuronal nitric oxide synthase,

neuropeptide Y, serotonin and vasoactive intestinal peptide (189). Furthermore, in other cellular contexts TBX3 regulates many genes that are critical for ENS development, including Gli3, Bmp4, Shh, Hand2, and PTEN (81, 177, 178, 188, 258-262, 287, 289-293). Therefore, we hypothesized that loss of TBX3 within ENCDC would impact ENS development or function. Instead, we found that TBX3 is not required for efficient colonization of the bowel by ENCDC, that *Tbx3* mutant mice have normal neuron numbers, and that *Tbx3* loss within the ENS does not affect transit of FITC-dextran through neonatal bowel even though TBX3 is prominently expressed in enteric neurons at P0. Specifically, our functional studies suggest that P0 *Tbx3 fl/fl; Wnt1-Cre* mice can swallow liquids (although inefficiently with cleft palate), have normal gastric emptying and normal transit of luminal contents though the small bowel, but that they also have excess air swallowing due to cleft palate. Unfortunately, the *Tbx3 fl/fl; Wnt1-Cre* mice die as neonates, so we could not test colon motility or later aspects of ENS development or function. It remains possible that TBX3 has important roles after birth or that the closely related gene *Tbx2* compensates for the loss of *Tbx3* as has been shown in other contexts (294, 295).

Notably, we found that *Tbx3 fl/fl; Wnt1-Cre* mice have a marked reduction in S100β+ enteric glia in small bowel without a comparable loss of SOX10+ cells. Since SOX10 is expressed in uncommitted ENS precursors and in enteric glia, but S100β is only expressed in the more mature glial lineage, this finding suggests that TBX3 enhances enteric glial cell differentiation. Remarkably, we did not detect TBX3 protein in enteric glia, but only in enteric neurons. Collectively, these data suggest that TBX3 promotes maturation enteric glia in a non-cell autonomous manner. A potential mechanism for this finding would be altered Notch signaling, since Notch enhances enteric gliogenesis (171), but we did not detect changes in expression of the Notch ligand *Dll1* or the transcriptional effector *Hes1* that were previously implicated in ENS gliogenesis. Reduced glial numbers did not alter small bowel transit, but this was expected since even more complete glial loss does not affect this parameter (296).

Our studies of *Tbx3 fl/fl; Wnt1-Cre* mouse heart anatomy revealed no defects in cardiac outflow tract alignment or in the great vessels of the heart. This is in contrast to results from constitutive *Tbx3* deficient embryos which showed arterial pole alignment defects (264, 265, 280), suggesting that *Tbx3* acts primarily in non *Wnt1-Cre* lineage cells to regulate aspects of cardiac development.

Tbx3 is necessary for palatal shelf elevation

Development of the secondary palate from cranial ectoderm-derived epithelial cells and *Wnt1* expressing cranial neural crest-derived mesenchymal cells is mediated by a network of growth factors and transcription factors (297-299). Our observations show for the first time that palatal shelf elevation requires TBX3, but suggest that TBX3 effects on palatal shelf elevation are not due to changes in cell proliferation or apoptosis. These findings are consistent with the prevailing model of palatal shelf elevation as a process mediated by an internal mechanical force that drives the rapid and asynchronous reorientation of each palatal shelf independent of changes in cell number (282, 300).

Our work also complements previous studies of *Tbx3* in palate development (287, 289). For example, studies of wild-type palatal shelf explants isolated at E13.5 and cultured for 48 hours showed that BMP4 induces *Tbx3*, but TBX3 reduces *Bmp4* levels in mesenchyme, creating a negative feedback loop that influenced cell proliferation (287). In contrast, our *in vivo* data show that loss of TBX3 in palatal shelf mesenchyme did not alter *Bmp4* mRNA levels or mesenchymal proliferation at E13.5. It remains possible that interactions between TBX3 and BMP4 regulate cell proliferation at other stages in palate development, including during the initial vertical growth of palatal shelves or the horizontal growth that occurs after palatal shelf elevation. Alternatively, the apparently contradictory results between our work and prior studies of TBX3/BMP4 interaction may reflect differences in the timing of TBX3 manipulation or the

presence of factors *in vivo* that were missing from the published *in vitro* studies.

Our results in *Tbx3 fl/fl; Wnt1-Cre* mice are surprising considering that prior *in vivo* studies suggest a less important role for *Tbx3* in palate fusion than for the closely related gene *Tbx2*. *Tbx2-/-* mice have increased proliferation and apoptosis in palatal shelf mesenchyme and have partially penetrant cleft palate in two different mouse strains (289). Furthermore, Zirzow showed that while 38% of *Tbx2+/- Tbx3+/-* mice had a cleft secondary palate, the one *Tbx3* null that survived to E15.5 mouse had a partially fused palate at E15.5 suggesting palatal shelf growth and fusion occur normally, but may be delayed. While it is possible that these differences reflect global *Tbx3* loss versus *Wnt1-Cre* driven *Tbx3* loss, the NMRI background strain of the *Tbx3 -/-* mouse in prior studies (289) may be more resilient to cleft palate relative to the Bl6/SV129/FVB mixed background used in our studies. In support of this hypothesis, two *Tbx3 fl/fl; Wnt1-Cre* mice with a fused palate at P0 were discovered during our initial breeding between *Tbx3 fl/fl* and *Wnt1-Cre* lines. As our studies progressed, we were unable to identify additional *Tbx3 fl/fl; Wnt1-Cre* mice with a fused palate, consistent with the hypothesis that strain background affects penetrance of the mutant *Tbx3* cleft palate phenotype. Our finding that *Tbx3* loss can cause cleft palate independent of altered *Tbx2* gene expression argues against the fully redundant functional role of *Tbx3* and *Tbx2* in palatogenesis. Consistent with this hypothesis, *Tbx3* and *Tbx2* have previously been shown to have independent functions in heart (264-266, 280, 289, 301-303), limb (260, 266, 293) and other contexts (246, 304).

Osr2 **levels are reduced in the palate of** ***Tbx3fl/fl; Wnt1-Cre*** **mice**

Defining molecular mechanisms through which TBX3 impacts palate development is challenging given that TBX3 regulates the expression of many genes as well as mRNA splicing. Our approach was to evaluate mRNA levels for selected genes in microdissected E13.5 palate. We focused on genes that impact palate development and interact with TBX3. While our studies

were not comprehensive, we did discover reduced levels of *Osr2* mRNA in *Tbx3 fl/fl; Wnt-Cre* mouse palate compared to control littermates, but unchanged levels for many other genes. Similar to *Tbx3 fl/fl; Wnt1-Cre* mice, *Osr2-/-* mice have a delay or failure of palatal shelf elevation (271). *In situ* hybridization for *Tbx3* and *Osr2* suggests that they are co-expressed in palatal shelf mesenchyme (289) adding credence to the hypothesis that reduced *Osr2* contributes to cleft palate in *Tbx3 fl/fl; Wnt1-Cre* mice. TBX3 could directly regulate the expression of *Osr2* through DNA-binding interactions, or indirectly via RNA binding proteins and splicing factors that drive alternative splicing (245). Using published ChIP-Seq data from adult mouse heart, we noted a peak for TBX3 binding near the promoter sequence of *Osr2* (305) suggesting that TBX3 may directly regulate *Osr2* gene expression. How changes in *Tbx3* and *Osr2* regulate the internal mechanical forces needed to drive the rapid reorientation of the palatal shelves remains to be defined. It also remains likely that other TBX3 regulated genes are the critical for palatal development since *Osr2* heterozygous mice do not have cleft palate (271) and we found a roughly 50% reduction in *Osr2* mRNA in the palate of our *Tbx3 fl/fl; Wnt1-Cre* mice. Nonetheless, our data clearly show a role for TBX3 in normal palate morphogenesis.

Summary:

Our E17.5 microarray studies identify a large number of transcription factors, axon guidance molecules, cell adhesion proteins, signaling molecules, receptors and ligands that are enriched in the ENS or surrounding cells at late gestation. Our studies show that TBX3 is not needed for bowel colonization by ENCDC or for small bowel motility, but is important for enteric glial differentiation. TBX is also required for palatal shelf reorientation and fusion, in a mechanism that is independent of altered cell proliferation.

3.6 ACKNOWLEDGMENTS

We thank Dr. Meenakshi Rao for thoughtful comments and insight. We also thank Deepika Kothakapa and Beth Maguire for assistance with mouse colony management. We are grateful to Vanda Lennon for the human ANNA–1 serum. We also appreciate assistance and technical guidance of Florin Tuluc, Lily Wu, and Jennifer Murray at the Children's Hospital of Philadelphia Flow Cytometry Core and Daniel Martinez, Socrates Agrio, and Joon Jung from the Pathology Core Laboratory. This work was supported by: the Irma and Norman Braman Endowment (ROH), the Suzi and Scott Lustgarten Center Endowment (ROH): The Children's Hospital of Philadelphia Research Institute (ROH); Children's Discovery Institute of Washington University and St. Louis Children's Hospital (grant no. MD-II2013-269) (ROH); NIH grants RO1 DK087715 (ROH) and R01 HD046767 (AMM), March of Dimes 6-FY15-235 (ROH) and Basil O'Connor Award (AMM); the Burroughs Wellcome Fund Clinical Scientist Award in Translational Research (grant no. 1008525) (ROH); the NIH SPARC Program OT2OD023859. RK acknowledges support from the Fondation pour la Recherche Médicale (DEQ20150331717).

3.7 AUTHOR CONTRIBUTIONS

S.H.L., M.A, C.W., and R.O.H. designed experiments, analyzed results, and wrote the manuscript. K.M. and R.K. designed experiments and analyzed results. A.M. created the *Tbx3* mouse model, helped design experiments, analyzed results, and wrote sections of the manuscript. All authors edited the manuscript. S.H.L, M.A., C.W., and K.M. performed all the experiments.

3.8 SUPPLEMENTARY MATERIALS

Supplementary Table 3-1: Primers for qRT-PCR

Gene Symbol	Unigene Title		Sequences [a]
Bmp2	Bone Morphogenetic Protein 4		GCTTCTTAGACGGACTGCGG GCAACACTAGAAGACAGCGGGT

Bmp4	Bone Morphogenetic Protein 4		AGCCCGCTTCTGCAGGA AAAGGCTCAGAGAAGCTGCG
Ccnd1	Cyclin-D1		CTGGCCATGAACTACCTGGA GTCACACTTGATCACTCTGG
Dll1	Delta like canonical Notch ligand 1		CAACAAGAAGGCGGACTTTC CACTTGGTGTCACGTTTGCT
Foxf2	forkhead box F2		AGCATGTCTTCCTACTCGTTG TCTTTCCTGTCGCACACT
Gapdh	Glyceraldehyde-3-phosphate dehydrogenase		AACTTTGGCATTGTGGAAGG GTCTTCTGGGTGGCAGTGAT
Gli3			GCTCTTCAGCAAGTGGTTCC TTGCTGTCGGCTTAGGATCT
Hes1	Hes family BHLH transcription factor		ACACCGGACAAACCAAAGAC ATGCCGGGAGCTATCTTTCT
Msx1	Msh homeobox 1		AGTTCTCCAGCTCGCTCAGC GGAACCATATCTTCACCTGCGT
Osr1	odd-skipped-related 1		TGTAGCGTCTTGTGGACAGC GCGACCTTACACCTGTGACAT
Osr2	odd-skipped-related 1		TTGCTCATTCAGCAGAGGAC TCCCACACTCCTGACATTTG
Ptch1	Protein patched homolog 1		GGCAGGAGGAGTTGATTGTGG CATAGTCGTAGCCCCTGAAGTG
Shh	Sonic hedgehog		AAAGCTGACCCCTTTAGCCTA TTCGGAGTTTCTTGTGATCTTCC
Tbx2	T-box 2		TCCTGCTAATGGACATCGTG AGACATAGGTGCGGAAGGTG
Tbx3 Exon 1/2	T-box 3		TGAGGCCTCTGAAGACCATG TCAGCAGCTATAATGTCCATC
Tbx3 Exon 5/6	T-box 3		GGGACATCCAACCTCAAAGA CCGTAGTGGTGGAAATCTTG

[a] 5’ to 3’sequences; f = forward primer; r = reverse-strand primer

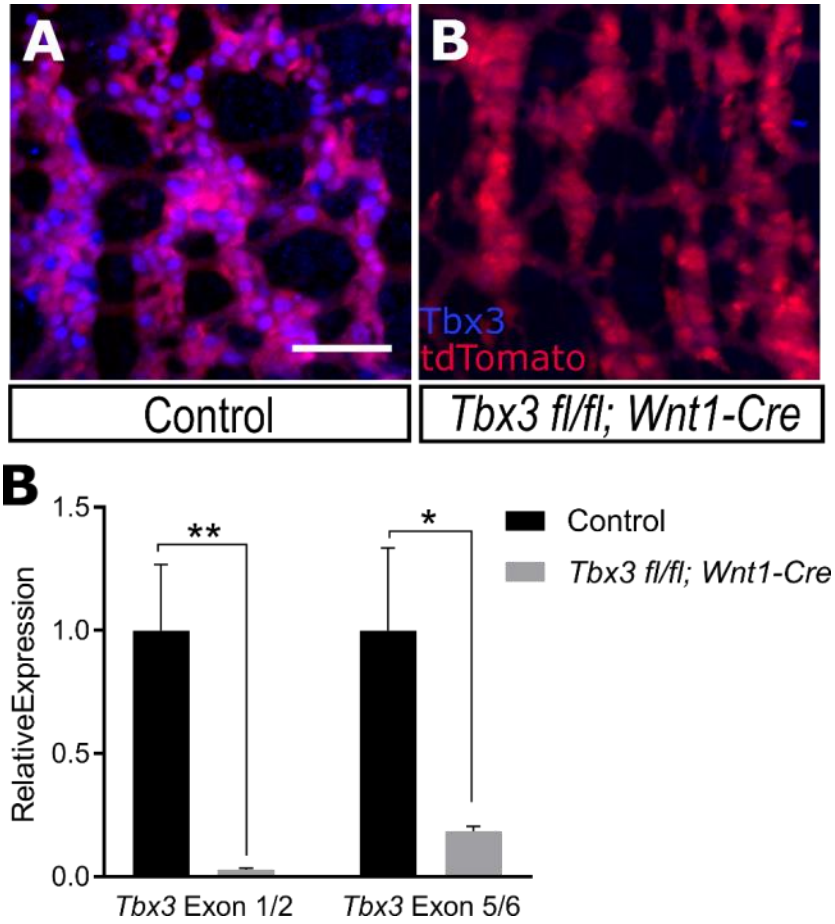

Supplementary Figure 3-1: Conditional loss of TBX3 in the enteric nervous system.
(A, B) P0 small intestine from *Tbx3 fl/fl; Wnt1-Cre; tdTomato* and control *Wnt1-Cre; tdTomato* mice. The tdTomato Cre reporter transgene is expressed in essentially all cells of the ENS. Immunohistochemistry readily identifies TBX3 protein in most enteric neurons of control mice, but TBX3 was not detected in the ENS of *Tbx3 fl/fl; Wnt1-Cre; tdTomato* mice. (C) Quantitative RT-PCR analysis was performed using RNA from cells of the ENS lineage isolated by FACS at E17.5 to verify efficient *Tbx3* recombination in the ENS. Expression of *Tbx3* was significantly reduced in ENS cells isolated from *Tbx3 fl/fl; Wnt1-Cre* mice. Expression levels are relative to mean expression in *Tbx3* controls. Error bar = SEM. N=5 of each genotype. Scale bar = 100 µm. Scale bar in A applies to B.

CHAPTER 4 : SINGLE-CELL AND SINGLE-NUCLEUS SEQUENCING OF MOUSE AND HUMAN ENTERIC NERVOUS SYSTEM REVEALS NUMEROUS SUBTYPE MARKERS

This manuscript is currently being prepared for publication. Authors: Christina M. Wright*, Sabine Schneider*, Kristen Edwards, Fernanda Mafra, Mike Gonzalez, Deepika R. Kothakapa, Silvia Huerta-Lopez, Tao Gao, Scott Gianino, Tricia Missall, Brian Davis, and Robert O. Heuckeroth. (2019)

*Co-first authors; contributed equally

4.1 - ABSTRACT

Single-cell sequencing of the enteric nervous system (ENS) poses unique challenges due to the scarcity of enteric neurons relative to other bowel cells and the thickness of the surrounding muscle layers. We sequenced 635 neuronal nuclei and 885 glial nuclei from adult mouse distal colon, and 707 neurons and neuron precursors from developing mouse bowel. We identified seven neuron subtypes and hundreds of differentially-expressed genes, including neurotransmitter receptors, ion channels, signaling pathway molecules, and transcription factors. In parallel, we developed a method for manually-dissecting myenteric plexus of human colon and sequenced 48 human neuronal nuclei, along with thousands of nuclei from smooth muscle cells, interstitial cells of Cajal, and muscularis macrophages. Many genes exhibited similar expression patterns across multiple datasets, and we validated protein expression of several transcription factors in mouse and human ENS. Excitingly, we found that mice in which the transcription factor *Tbx3* was conditionally deleted had decreased nNOS+ neurons at birth. We also demonstrated that the RET co-receptor *Gfra1* is expressed in select neuron classes and showed that the GFRA1 ligand GDNF

robustly induces calcium transients in subsets of neurons. These findings provide insight into gene expression in enteric neuron subtypes and serve as a valuable resource for future studies.

4.2 - INTRODUCTION

Hirschsprung disease (HSCR) is a rare but serious bowel motility disorder in which distal bowel lacks enteric neurons and glia that are normally clustered into ganglia. The aganglionic bowel tonically contracts and lacks propagating contractions leading to abdominal distention, intractable constipation, growth failure, abdominal pain, vomiting and death if untreated (57). Even after corrective surgery to bypass or resect aganglionic bowel, many children with HSCR suffer from persistent constipation and abdominal distension, or from diarrhea caused by Hirschsprung-associated enterocolitis (66-69). A prevailing hypothesis is that these persistent symptoms occur because enteric neurons in remaining bowel are abnormal. This hypothesis is supported by HSCR mouse models (70, 71) and by limited human data showing aberrant ratios of neurochemical markers in HSCR colon (73, 74). A longstanding goal is to determine which neuron subtypes are disrupted in HSCR, so that lost subsets of neurons might be replaced (i.e. by stem cell therapy (306)). Unfortunately, enteric neuron subtype composition in normal healthy bowel remains poorly understood, making it challenging to define what is abnormal in HSCR bowel, and we know very little about transcription factor networks governing enteric neuron subtype development, making it even more challenging to direct stem cell differentiation (111).

The enteric nervous system (ENS) is thought to contain over 20 distinct neuron classes that respond to sensory signals, induce smooth muscle relaxation or contraction, and modulate bowel epithelial secretion, vasodilation, and immune system function (27, 106). The mouse ENS consists of a myenteric plexus, located between the circular and longitudinal smooth muscle layers, and a submucosal plexus, located between circular smooth muscle and bowel mucosa. These enteric plexi are present throughout the small and large intestine, but there are substantial

regional differences in neuron and glial density, neuron subtype composition, and neuron function. The human ENS also contains a myenteric and submucosal plexus, along with additional smaller submucosal plexi that vary by bowel region (307). In both species, the myenteric plexus is thought to contain intrinsic primary afferent neurons (IPANs) that transduce sensory signals, excitatory and inhibitory motor neurons that contract and relax bowel smooth muscle respectively, and interneurons that project orally or anally (2), while submucosal plexus contains IPANs, along with neurons that control epithelial, vascular and immune cell function.

Our limited knowledge of enteric neuron subtypes stems from inadequate classification schemes that rely on morphology, electrophysiology, and antisera against a small number of neurochemical markers to define neuron populations (2, 308). Most initial enteric neuron classification studies were conducted in or extrapolated heavily from guinea pig (2, 4, 5, 27), and we know surprisingly little about enteric neuron subtypes in mouse, and even less about enteric neuron subtypes in humans. Existing enteric neuron classification schemes also provide limited information about ion channels, ligands, receptors, and transcription factors expressed in distinct neuron subsets, and only a few regulatory genes affecting ENS subtype specification have been identified (111, 178, 186, 189). Defining the transcriptomic landscape regulating enteric neuron subtype specification is especially important in colon, as we consider targeted stem cell replacement therapy for diseases like HSCR.

While single-cell sequencing provides an obvious approach to overcoming these difficulties, several features of the colon make single-cell sequencing especially challenging. First, for myenteric plexus, cells of interest are sandwiched between fibrous circular and longitudinal smooth muscle layers that are not easily dissociated. Furthermore, enteric neurons are a tiny fraction of total bowel cells, so even if methods were established for fluorescence-activated cell sorting (FACS), obtaining data from large numbers of enteric neurons remains challenging. These problems are amplified in human colon, which is millimeters thick and has a

substantially smaller neuron-to-total-cell ratio than mouse. Finally, the tedious and time consuming methods needed to isolate the ENS may lead to changes in gene expression that obscure normal subtype distinctions or may provide misleading data about undisturbed ENS cell phenotypes.

Here we use single nucleus RNA-sequencing data from 635 murine enteric neuron nuclei to robustly define seven subpopulations of neurons that differentially express many neurotransmitter receptors, ion channels, and signaling pathway proteins, including the RET co-receptor *Gfra1*. We also generated data from 48 human myenteric neurons. We validated restricted expression of many differentially-expressed genes and used calcium imaging to demonstrate that the GFRA1 ligand GDNF rapidly induced calcium transients in subsets of mouse enteric neuron subsets. We identified over 40 novel regulatory genes that were differentially expressed between subgroups. Many of these regulatory genes were also restricted to specific neuron subsets in the embryonic day 17.5 (E17.5) ENS, including the T-box transcription factor *Tbx3.* Based on our single nucleus RNA-seq data we discovered that conditional deletion of *Tbx3* from mouse ENS led to a striking reduction in one subpopulation of cholinergic myenteric neurons, a phenotype we missed in prior analyses of *Tbx3* mutant mice. Finally, by comparing mouse to human data we confirmed that *TBX3* and many other regulatory genes are differentially expressed in subsets of human colon neurons. These observations more completely define enteric neuron subtypes, and provide a basis for many avenues of additional investigation.

4.3 - METHODS

Animals

ChAT-EGFP-L10a mice (RRID:IMSR_JAX:030250; C57BL/6J) were a kind gift from Joseph Dougherty at Washington University School of Medicine in St. Louis. *Tbx3* mice on a

mixed background were a kind gift from Dr. Anne Moon (Aix-Marseille Univ, CNRS, IBDM, Marseille, France) and have been described previously (265). *Tg(Wnt1cre)11Rth* mice (referred to as *Wnt1-Cre*; RRID:IMSR_JAX:003829), *B6;129S6-Gt(ROSA)26Sortm1(CAG-tdTomato*,-EGFP*)Ees/J* mice (referred to as $ROSA^{nT\text{-}nG}$; RRID:IMSR_JAX:023035), *B6;129S-Gt(ROSA)26Sortm1.1Ksvo/J* mice (referred to as *R26R-H2b-mCherry*; RRID:IMSR_JAX:023139), *B6(Cg)-Etv1tm1.1(cre/ERT2)Zjh/J* mice (referred to as *Etv1-CreERT2* mice; RRID:IMSR_JAX:013048), *Slc17a6tm2(cre)Lowl/J* mice (referred to as *Vglut2-IRES-Cre* mice; RRID:IMSR_JAX:016963), *B6;129S-Nos1tm1.1(cre/ERT2)Zjh/J* mice (referred to as *Nnos-CreERT2*; RRID:IMSR_JAX:014541), and Gt(ROSA)26Sortm9(CAGtdTomato)Hze mice (referred to as *R26R-TdTomato*; RRID:IMSR_JAX:007909) were obtained from The Jackson Laboratory (Bar Harbor, ME). *Wnt1-Cre* mice on a mixed C57BL/6J x CBA/J)F1 background were bred into *R26R-H2b-mCherry* mice on a mixed 129S4/SvJaeSor x C57BL/6J background and maintained on a mixed C57BL/6J x 129S4/SvJaeSor x CBA/J)F1 background. *Etv1-CreERT2* mice were bred to *R26R-TdTomato* mice and *ChAT-EGFP-L10a* mice to generate *Etv1-CreERT2;R26R-TdTomato;ChAT-EGFP-L10a* mice on a C57BL/6J background. *Vglut2-IRES-Cre* mice on a C57BL/6;FVB;129S6 background were bred to *R26R-TdTomato* on a C57BL/6J background and maintained on a mixed C57BL/6;FVB;129S6 background. *nNOS-CreERT2* mice were crossed with *R26R-TdTomato* mice and *ChAT-EGFP-L10a* mice to generate *ChAT-EGFP-L10a; nNOS-CreERT2; R26R-TdTomato* mice and maintained on a C57BL/6 background. *Wnt1-Cre;Tbx3* mice were generated by crossing *Wnt1-Cre* mice to *Tbx3* mice and were maintained on a mixed background. *E2a-Cre* mice (RRID:IMSR_JAX:003724) were crossed with mice containing a floxed-*STOP-GCaMP6s* sequence in the *Rosa26* locus (Ai96 mice; RRID:IMSR_JAX:028866) to generate mice that express GCaMP (a genetically encoded calcium indicator) in all cells. Genotyping was performed using previously published and novel

primers (Supplementary Table 1) and by Transnetyx (Cordova, TN). Vaginal plug day was considered E0.5.

Human colon

Colon tissue was acquired with the Institutional Review Board approval from Perelman School of Medicine at University of Pennsylvania (IRB #804376). The received tissue was de-identified, providing limited clinical data. Resected colons were maintained at ambient temperature until arrival in pathology, where they were transferred to ice-cold dPBS (1-4 hours after resection). Pathologists selected regions of colon without gross abnormalities, and colon specimens were transferred to the laboratory in dPBS on ice.

Tamoxifen treatment

Tamoxifen (10 mg/mL) was prepared by combining tamoxifen with 200 uL ethanol and 1800 uL sunflower seed oil, followed by alternately vortexing and incubation in a 37º water bath until dissolved. The E15.5 dam was injected with 200mg/kg tamoxifen and dissected at E17.5. *Etv1-Cre^{ERT2};R26R-TdTomato* mice were injected with 75 mg/kg tamoxifen at age 44 and dissected at age 47 days.

Preparing young adult mouse colon tissue for nuclei isolation

Wnt1-Cre$^{Cre/wt}$;R26R-H2b-mCherry+ 47-52-day-old mice were euthanized with 5% CO_2. Colon was removed, flushed with cold, sterile dPBS using a 20 mL syringe to remove luminal contents, and placed in cold, sterile dPBS. Colon was carefully cut along the mesentery, pinned mucosal side down on dishes treated with Sylgard Elastomer 184 (Dow Corning, Midland, MI). The muscularis was carefully peeled from the mucosa and placed in cold O.C.T. compound

(Fisher, Hampton, NH; Cat# 23-730-571) in a biopsy specimen crymold (VWR, Radnor, PA; Cat# 4565), frozen in methylbutane on dry ice, and stored at -80°C.

Preparing adult human colon for nuclei isolation

Using insect pins (Fine Science Tools, Cat# 26002-20), bowels were maximally stretched and pinned serosa side up on 30 mm dishes treated with Sylgard 184 (Dow Corning, Midland, MI). The tissue was incubated in a solution that was 9 parts room temperature, oxygenated Krebs-Ringers solution (118 mM NaCl, 4.6 mM KCl, 2.5 mM $CaCl_2$, 1.2 mM $MgSO_4$, 1 mM NaH_2PO_4, 11 mM D-(+)-Glucose, 25 mM $NaHCO_3$, pH 7.4), and 1 part room temperature 4-Di-2-Asp (Abcam, Cambridge, U.K, Cat# ab145266) in sterile dPBS. After 10 minutes, tissue was transferred to cold oxygenated Krebs-Ringers solution and placed under a SteREO Discovery.V20 fluorescent dissecting scope (ZEISS, Oberkochen, Germany) with a 488 nm filter. Fluorescent ENS was carefully dissected from muscularis by peeling away longitudinal muscle strips with Dumont #5 forceps (Fine Science Tools, Cat# 11251-30), placed in cold O.C.T. compound (Fisher, Hampton, NH; Cat# 23-730-571) in a biopsy specimen crymold (VWR, Radnor, PA; Cat# 4565), frozen in methylbutane on dry ice, and stored at -80°C.

RNA extraction for RIN assessment prior to sequencing

One to three days before sequencing, frozen samples were sectioned on a Microm HM 505 E Cryostat (GMI, Ramsey, MN; 100 µM sections, -20°C) and placed in Eppendorf tubes at -80°C for storage. For each prospective bowel, RNA was extracted from several (1-5) 100 µM sections using the Qiagen RNeasy Plus Micro kit (Qiagen, Hilden, Germany; Cat# 74034) combined with Qiagen's RNase Free DNase Set (Qiagen, Cat# 79254). Samples were run on an Agilent Bioanalyzer, and tissue was used if RNA Integrity Number (RIN) was > 7.0.

Nuclei isolation and sorting

To isolate nuclei, sections from bowels that met the RIN cutoff were placed in ice-cold lysis buffer (10mM Tris HCl pH 7.5, 10 mM NaCl, 3 mM $MgCl_2$, 0.005% Nonidet P40 Substitute; Life Technologies, Cat# AM9010, Sigma Aldrich, Cat# 74385), chopped rapidly with a large iridectomy scissors for 1 minute, then transferred to a pre-cooled Dounce homogenizer (VWR, Cat# 357538) on ice, homogenized with 15 strokes of the loose pestle and 40 strokes of the tight pestle, and filtered through a MACS SmartStrainer (Miltenyi Biotec, Cat# 130-098-458). Nuclei were centrifuged (590G, 8 min, 4C) and resuspended in staining buffer (1x PBS, 1% w/v Ultrapure BSA, 0.2 U/mL Protector RNase inhibitor; Life Technologies, Cat#AM2618 and Sigma Aldrich, Cat# 3335399001). Hoescht 33342, Trihydrochloride Trihydrate (ThermoFisher Scientific, Cat# H3570) was added to a final concentration of 2.5 µg/mL, and sample was filtered through a FlowMi strainer (VWR, Cat# H13680-0040) and FACS-sorted on a MoFlo Astrios into 5 µL staining buffer using a 70 micron nozzle, to isolate Hoescht+mCherry+ nuclei (mouse) or Hoescht+ nuclei (human).

Whole cell isolation from E17.5 mice

A pregnant E17.5 dam carrying *nNOS-Cre-ERT2;ChAT-L10A-EGFP;R26R-TdTomato* pups was sacked via cervical dislocation. Pups (2x TdTomato+, 3x GFP+) were rapidly dissected on ice. Bowels were placed into oxygenated HBSS, snipped into pieces using insulin needles (Beckton Dickerson, Cat# 08290-3284-18), and dissociated at 37°C for 40 minutes in Liberase (Sigma-Aldrich, Cat# 5401135001) supplemented with DNase I (0.02 U/µL, Roche, Basel, Switzerland; Cat# 04716728001), $MgCl_2$ (6 mM) and $CaCl_2$ (1 mM) in HBSS with repeated P1000 trituration. Dissociated cells were passed 2-3x through 200 µM filters, pelleted at 170g for 3 minutes in 10% FBS in Iscove's DMEM, resuspended in FACS buffer (0.04% w/v BSA in

HBSS), filtered again, sorted on a BD FACSJazz into 300 uL FACS buffer, and submitted for sequencing.

Library generation, sequencing, and data processing

Libraries were generated using the Chromium Single Cell 3' RNA-seq kit (10X Genomics, Pleasanton, CA) and sequenced on an Illumina HiSeq 2500. The Cell Ranger pipeline (10x Genomics) was used to convert BCL files into FASTQ files, perform STAR alignment, filtering, and UMI counting, and generate gene-barcode matrices. The Cell Ranger Aggr pipeline was used to aggregate multiple samples, normalize outputs, and re-compute gene-barcode matrices on the combined data.

Analysis of single-nucleus sequencing data

Using Seurat (309, 310), gene-barcode matrices were imported into R, filtered to remove low-expressors or doublets (nGene=200-5000) and mitochondrial contaminants (percent mitochondria <0.1%), normalized, scaled to regress out UMI and percent mitochondria. Cells were clustered using the most statistically significant principle components. Although we endeavored to follow guidelines for principle component selection laid out on the Seurat website, we found taking all of the statistically significant principle components resulted in difficult-to-interpret clustering, possibly due to batch effects in our dataset, and that the first ~11 components were usually sufficient to cluster our data in a biologically meaningful way. When reclustering was performed on subsets of data (i.e., to filter out contaminants), subsetted data was rescaled and reclustered using the same method described above, minus the normalization step. To identify genes that were differentially-expressed between clusters, clusters were compared one at a time to all other cells in the dataset using a Wilcoxon Rank Sum test with Bonferroni multiple testing correction (Seurat's FindAllMarkers command). A cutoff of at least 10% of cells in a group with

gene expression >0 was required for genes to be tested. Heatmaps (**Figures 4-1, 4-2, 4-4**) were generated by taking the mean of the log-normalized data scaled by Seurat for cells within each cluster. Except for the top of **Figure 4-4A**, only genes that were differentially expressed between neuronal clusters are shown. Hierarchical clustering (**Figure 4-8C**) was performed using the complete linkage method.

Preparing P0 small intestine for whole mount immunochemistry

P0 mice were decapitated and bowel was removed and placed in cold PBS, opened along the mesenteric border, and pinned serosal side up onto Sylgard® 184 Silicone Elastomer (Dow Corning, Midland, MI). Bowel was fixed for 20-30 minutes in 4% Paraformaldehyde at room temperature and the muscle layer of the small intestine was very carefully dissected away from the mucosa and submucosa. Gut was equilibrated in 50% glycerol/50% PBS (30 minutes, RT or overnight at 4ºC) and stored at -20°C until staining.

Preparing mouse distal colon for whole mount immunochemistry

Adult mice were euthanized (CO_2, 5 minutes) and cervically dislocated. Colon was flushed with cold PBS, opened along the mesenteric border, and pinned serosal side up onto Sylgard-treated dishes. To separate myenteric and submucosal plexus, the muscle layer was peeled away from the mucosa and submucosa. To enhance future immunostaining, the muscle layer was stretched to the maximum capacity using stainless steel insect pins. Tissue was fixed with 4% paraformaldehyde (20-30 minutes, RT) and transferred to cold PBS. After fixation, gut was equilibrated in 50% glycerol/50% PBS (30 minutes, RT) and stored at -20°C until staining.

Immunofluorescent staining of mouse whole mount

Bowel pieces stored at -20ºC in 50% glycerol 50% PBS was rinsed in PBS. Samples were blocked for 2 hours in PBS + 0.5% Triton X-100 (PBST) with 5% Normal Donkey Serum (NDS; Jackson Immuno Research Laboratory, West Grove, PA). Samples were incubated in primary antibody (**Supplementary Table 4-2**) with gentle rocking at 4°C for 2 days except for ANNA-1 which was incubated overnight at 4°C. Tissues were washed 3 x 5 minutes each in PBST and incubated in secondary antibody (**Supplementary Table 4-2**) with gentle rocking (1 hour, RT). After three 5-minute washes in PBS, samples were mounted serosal side up on glass slides in 50% glycerol/50% PBS.

Preparing mouse human colon for whole mount immunochemistry

Human colon was pinned serosa side up on Sylgard® 184 Silicone Elastomer-treated plates in ice-cold PBS using insect pins. Tissue was maximally stretched during pinning to make colon as thin as possible. Pinned tissue was fixed overnight at 4ºC in 4% paraformaldehyde, washed in dPBS, and stored at 4ºC in 50% PBS/50% glycerol/0.05% sodium azide until staining.

Immunofluorescent staining of human colon whole mount

Human tissue stored at 4ºC was cut into 1cm x 1cm (or smaller) pieces, washed (PBS, 3x5 minutes, room temperature), incubated in 100% methanol for 1 hour on ice, treated with Dent's bleach (1 mL 30% hydrogen peroxide, 1 mL dimethylsulfoxide, 4 mL 100% methanol (311) for 2 hours at room temperature, washed (PBS, 3x5 minutes, room temperature), and blocked (500-1000 µL PBS with 4% normal donkey serum, 0.5% Triton X-100) in 2 mL Eppendorf tubes at RT on a rotator (Cole-Parmer). After blocking, tissue was incubated for 14 days in 500 µL blocking solution containing primary antibodies (**Supplementary Table 4-2**) on a shaker (37ºC, 40-100 rpm, New Brunswick Scientific I24 Incubator Shaker Series). Tissue was washed on a gentle rocker at room temperature for 1 day (3 washes, 2 hours/wash, plus an

additional overnight wash). Tissue was incubated in secondary antibodies (1:400 in 500 µL PBS, 0.5% Triton X-100 on the shaker, 40-100 rpm) for 3 days at 37ºC. Tissue was washed on a gentle rocker at room temperature for 1 day (3 washes, 2 hours/wash, plus an additional overnight wash), and dehydrated in a methanol series (50%, 70%, 80%, 95%, 100%x3, for 30 minutes each). Tissue was placed in Murray's clear (2:1 benzyl benzoate:benzyl alcohol (312) with gentle rocking at room temperature until translucent (usually ~30min - 1hour). Transparent colon was mounted on glass slides in Murray's clear and imaged within 1 day.

Microscopy

Images were acquired with a Zeiss LSM 710 confocal microscope and Zeiss Zen software. Confocal images show either single optical projections or maximum intensity projections, as indicated in figure legend. Fiji (NIH) and Photoshop (Adobe, San Jose, CA) were used to crop and uniformly color adjust images.

Quantifications

Quantifications were performed using Fiji's CellCounter module (NIH) on at least 5 randomly-selected 20x fields per sample. Where possible, quantifications were performed using investigators blinded to genotype or condition.

RNA extraction and RT-PCR of *Pou3f3* mice

E14.5 and E17.5 dams were euthanized with CO_2, and pups were removed from the mother. For each litter, all TdTomato+ small intestines and colons were combined to increase cell count. Small intestines and colons were dissected in ice-cold dPBS, transferred to HBSS, separated, divided into small pieces using insulin needles (Beckton Dickerson, Cat# 08290-3284-18), and dissociated for 30 minutes at 37°C in Liberase (Sigma-Aldrich, Cat# 5401135001)

supplemented with DNase I (Roche, Basel, Switzerland; Cat# 04716728001), $MgCl_2$ (6 mM) and $CaCl_2$ (1 mM) in HBSS with P1000 trituration. Cells were filtered, washed with Iscove's DMEM (Corning Cellgro, Cat# 10-016-CM), and resuspended in FACS buffer (10mM HEPES, 1mg/mL BSA, 1% penicillin and streptomycin in HBSS). Fluorescent TdTomato+ cells were sorted on a BD FACSJazz and collected in Iscove's DMEM with 10% FBS. Cells were spun down at 600xg, resuspended in Buffer RLT plus, and RNA was isolated using the Qiagen RNeasy Plus Micro Kit (Qiagen, Hilden, Germany; Cat# 74034) with DNase treatment (Qiagen, Cat# 79254).

RNA integrity and concentrations were measured on a 2100 Agilent Bioanalyzer using an RNA 6000 Pico Kit (Agilent, Santa Clara, CA). All samples used had RIN ≥ 7. cDNA was generated using Superscript II RNase H- (Invitrogen, Cat# 18064022). RT-PCR was performed using KAPA mixture (KAPA biosystems) and previously-described primers (**Supplementary Table 4-2**). Three replicates were run for all experiments.

Calcium live imaging studies

Colons from 3 female *E2a-GCaMP6* mice aged 12 weeks were removed, cut open longitudinally and pinned (mucosa facing down) in a Sylgard-lined dish, superfused with carbogenated (95% O2, 5% CO2) artificial cerebrospinal fluid (ACSF) maintained at 35-37ºC. ACSF, containing (in mM): 117.9 NaCl, 4.7 KCL, 25 NaHCO3, 1.3 NaH2PO4, 1.2 MgSO4-7H2O, 2.5 CaCl2, 11.1 D-glucose, 2 sodium butyrate, 20 sodium acetate, was prepared on the day of the experiment. Nifedipine (1μM, Sigma), an L-type calcium channel blocker, was added to ACSF to improve stability for analysis of calcium imaging data. GCaMP signals in myenteric neurons were imaged with an upright DM6000FS Leica fluorescent microscope (Leica, Buffalo Grove, IL) and EMCCD camera (Photometrics; Roper Scientific, Tuscon, AZ) using a 40X objective lens, and images were collected with Metamorph software (Molecular Devices, San Jose, CA) at 10 or 40Hz sampling rate for spontaneous or evoked activity, respectively. To

examine evoked activity, concentric electrodes were placed on the colon 5mm oral and anal to the imaging field and electrical pulses (100μs pulse at 20Hz for 1sec) delivered to the colon during image acquisition. A pulse duration of 100μs was chosen because it is too short to directly elicit muscle fiber contractions, but reliably induces neuronal action potential firing, and 20Hz was used because this frequency consistently activates the largest proportion of myenteric neurons per ganglion (313). For each field, spontaneous activity was imaged for 2 minutes, and 30-s movies were collected with responses to oral and anal stimulation (order of presentation was randomized). Recombinant rat GDNF (Cat. #512-GF, R&D Systems, Minneapolis, MN) in ACSF was first directly applied to the dish containing colon tissue while imaging responses of myenteric neurons. Then GDNF was continuously superfused with circulating ACSF for a total of 10 minutes while taking intermittent movies of myenteric neurons. After 10 minutes of GDNF exposure, responses to oral and anal stimulation were re-imaged.

Analysis of live imaging studies

Image files collected in Metamorph (Molecular Devices, Downington, PA) were exported to ImageJ (NIH). The amplitude of GCaMP signals was analyzed and quantified as previously described (314) by calculating ΔF/F0 [% = ((F − F0)/F0) x 100], where F is the peak fluorescence signal and F0 is the mean fluorescence signal at baseline; ΔF/F0 of 4SD > than baseline was considered a response. Tissue movement, which is directly correlated to changes in muscle tension (313), in response to stimuli was determined using a Template-Matching plugin in ImageJ, which quantifies movement along the x- and y-axis, representing the circular and longitudinal muscle, respectively. Time-lapse color-coded images were also created in ImageJ, where each pixel is designated a color based on when it reached maximum F in a movie, thus giving both spatial and temporal information in a still image.

Study approval

All mouse experiments were performed in accordance with the Children's Hospital of Philadelphia Institutional Animal Care and Use Committee (IACUC), except for experiments in *E2a-Cre* mice, which were performed in accordance with the Institutional Animal Care and Use Committee at the University of Pittsburgh. Colon tissue was acquired with the Institutional Review Board approval from Perelman School of Medicine at University of Pennsylvania (IRB #804376).

Statistics

We used Prism 7.03 (GraphPad Software, San Diego, CA) and SigmaPlot 11.0 (Systat Software, Chicago, IL) for statistical analysis. A two-sided Student's t-test or Mann-Whitney Rank Sum Test (MWRST) was used when comparing two groups. When comparing multiple groups, a one-way ANOVA with *post hoc* multiple comparisons tests (Tukey) was used unless assumptions were not met, in which case we used a Kruskal-Wallis test with Dunn's *post hoc* multiple comparisons test. A cutoff of $p < 0.05$ was considered significant. Data represent mean ± standard error of the mean (SEM).

4.4 – RESULTS

RNA sequencing single nuclei from mouse distal colon defines enteric neuron subpopulations

Our primary objective was to define populations of adult distal colon myenteric neurons based on a robust assessment of gene expression at a single cell level. We attempted several methods for isolating intact whole enteric neurons and glia from distal colon (**Supplementary Table 4-1**) using *Wnt1-Cre$^{Cre/wt}$;R26R-EYFP* or *Wnt1-Cre$^{Cre/wt}$;R26R-Tdtomato* mice that express EYFP or tdTomato respectively in enteric neurons and glia. Despite many attempts with diverse proteases, disruption methods, and dissociation times, we could not reliably prepare healthy intact whole single neurons from the distal colon of adult mice. We were also concerned that enzymatically dissociating ENS from adult colon at elevated temperatures might alter gene expression due to neurite disruption and cell damage. We therefore decided to perform RNA-seq on isolated neuronal nuclei instead of using intact neurons from distal mouse colon, since nuclear isolation could be performed at lower temperature (315-319). Initial attempts to separate ENS nuclei for other bowel wall cells using *Wnt1-Cre$^{Cre/wt}$; ROSA^{nT-nG}* that express nucleus targeted EGFP after CRE-mediated DNA recombination were unsuccessful. Although EGFP localized to ENS nuclei in whole mount preparations of *Wnt1-Cre$^{Cre/wt}$; ROSA^{nT-nG}* mouse colon, few EGFP+ nuclei were recovered by flow cytometry. We suspect the EGFP-NLS fluorophore leaked out of nuclei during our isolation steps.

Ultimately, we analyzed ENS from muscle layers of 47-52-day-old *Wnt1-Cre$^{Cre/wt}$; R26R-LSL-H2B-mCherry* mice that express mCherry fused to histone H2B in all enteric neurons and glia. Since histones bind DNA, we reasoned this fluorophore would be less likely to leak out of nuclei than EGFP-NLS. In whole mount preparations, mCherry was robustly expressed in all enteric neuron and glial nuclei of 45-55 day old mice (**Supplementary Figure 4-1A-D**). To isolate nuclei, we devised a novel method of peeling the muscle layer, flash-freezing our tissue in

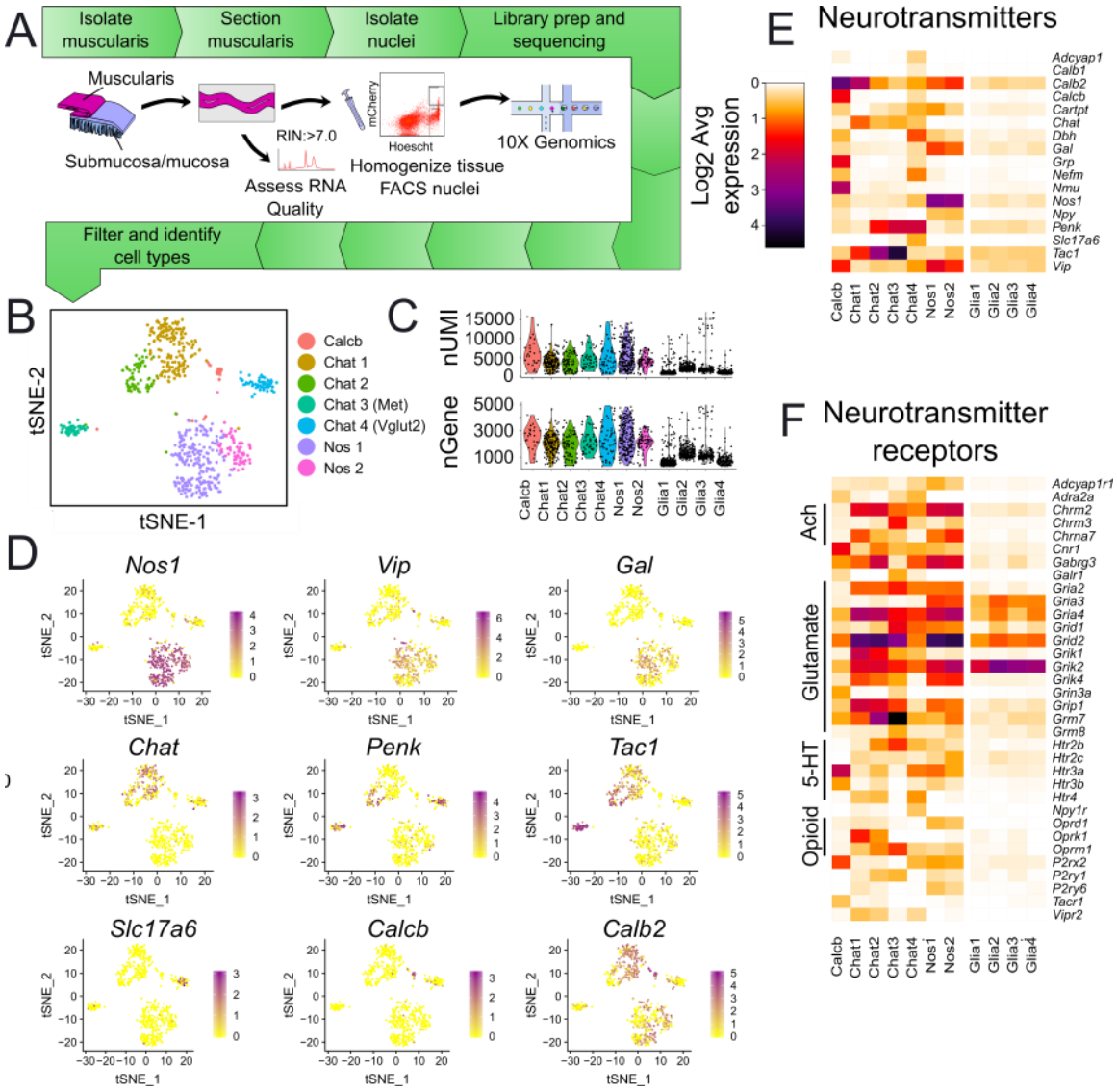

Figure 4-1: Single cell sequencing of mouse colon enteric neurons reveals multiple subsets of neurons and glia.

(A) Plan for single-nucleus sequencing of mouse distal colon. Distal colon muscularis from *Wnt1-Cre*$^{Cre/wt}$*;H2B-mCherry* mice was carefully peeled away from the mucosa, frozen in OCT, and sectioned on a cryostat. RNA was isolated and RNA quality was assessed. Tissue with RIN > 8 was Dounce homogenized, flow-sorted to isolate mCherry+ Hoescht+ nuclei, and submitted for sequencing by 10x Genomics. (B) T-SNE plot of mouse enteric neurons. (C) Neuron subgroups had an average of 4,629 UMI and 2,217 detected genes, while glia subgroups had an average of 1,780 UMI and 1,069 genes detected. (D) Representative feature plots of selected neurotransmitter genes reveals distinct expression patterns in different neuron subclasses. (E-F) Neurotransmitter (E) and neurotransmitter receptor (F) expression across distinct neuron subclasses. Glia subclasses are shown for reference.

Optimal Cutting Temperature (O.C.T.) Compound, cryosectioning at -20° C, and Dounce

homogenizing sections (**Figure 4-1A**). The additional cryosectioning step was crucial for disrupting muscle fibers and improving nuclei yield. Using this method, we successfully isolated and sequenced 1,662 mCherry+ nuclei from myenteric plexus (**Figure 4-1B**). Since average read depth was low, we included intronic reads in our analysis, giving us an average of 1,902 unique molecular identifiers (UMI) and 1,224 genes identified per cell.

Using the 10x Genomics and Seurat data analysis pipelines (309, 310), we identified 12 groups, including 4 glia populations (defined by *Plp1* and *Sox10* expression), 4 neuronal populations (which expressed *Elavl4*), and several smaller groups (6.5% total cells) that we think are non-ENS contaminants based on high levels of *Pdgfra* (PDGFRα+ cells), *Kit* (ICCs), and *Actg2* (smooth muscle cells; **Supplementary Figure 4-2**). To refine our analyses, we re-clustered just the neuronal groups (**Figure 4-1B**) and identified 6 neuron clusters (635 neurons total). Two groups expressed *Nos1, Vip,* and *Gal* (Nos 1 and Nos 2) consistent with known inhibitory motor neuron populations in other bowel regions (4). Two other groups expressed choline acetyl-transferase (*Chat*), Substance P *(Tac1),* and Proenkephalin (*Penk)* (Chat 1) or *Chat* and *Tac1* without *Penk* (Chat 2) suggesting that they are excitatory motor neurons. One group was heterogeneous, with some cells expressing *Chat, Penk,* and *Slc17a6* (encoding vesicular glutamate transporter (Vglut2)), while other cells expressed Gastrin releasing peptide (*Grp*), Neuromedin U (*Nmu*), and Calcitonin Related Polypeptide Beta (*Calcb*). We manually divided these neurons into two separate groups (*Chat/Penk/Vglut2,* a.k.a. Chat 4; and *Calcb/Grp/Nmu*, a.k.a Calcb) based on t-SNE clustering. Finally, the last group of cells expressed the HGF receptor *Met*, along with *Chat* and *Tac1* (*Chat/Tac1/Met*, a.k.a Chat 3; **Figure 4-1D, E**). Median UMI and gene counts were much higher for neurons than for glia (Neurons: 3,942 UMI and 2,152 genes; Glia: 1,289 UMI, 928 genes; **Figure 4-1C**). Many neurotransmitters (**Figure 4-1E; Supplementary Figure 4-3A**) and neurotransmitter receptors (**Figure 4-1F; Supplementary Figure 4-3B**) were differentially expressed between neuron subgroups, including receptors for

acetylcholine, glutamate, serotonin, opioids, and purines. Mean expression in glia is shown for comparison.

Single-nucleus sequencing reveals distinct expression patterns for *Gfra1* and *Gfra2* in mouse distal colon.

In addition to neurotransmitters and their receptors, we identified many additional classes of genes that were differentially expressed in myenteric neuron subpopulations including ion channels (**Figure 4-2A; Supplementary Figure 4-4A**) and cell signaling molecules (**Figure 4-2B; Supplementary Figure 4-4B**). Some of these genes are known to be involved in axon guidance (netrin and netrin receptors, semaphorins and plexins, ephrins and ephrin receptors, robos and slits), survival (BDNF, FGF, GDNF, HGF pathway members), and cell-cell adhesion (contactins, neurexins) in other parts of the nervous system. We were particularly intrigued by *Gfra1* and *Gfra2* expression patterns. *Gfra1* mRNA levels were high in *Nos/Vip/Gal* neurons and glia and low in other neuron subgroups, while *Gfra2* was low in *Nos/Vip/Gal* neurons and high in glia and some *Chat* subgroups (**Figure 4-3A**). GFRA1 and GFRA2 are co-receptors for the receptor tyrosine kinase RET and transduce signaling from glial cell-line derived neurotrophic factor (GDNF) and Neurturin, respectively. The *Gfra2* data are consistent with previous observations that GFRA2 localizes primarily to substance P+ nerve fibers and glia in mouse small bowel (127). Furthermore, GFRA2 KO mice have fewer substance P-containing nerve fibers and ganglion cells in the ENS, and mice missing the preferred GFRA2 ligand Neurturin have a 40% reduction in acetylcholinesterase stained nerve fibers in bowel muscle layers (127, 128). *Gfra1* data were more surprising, since postnatal elimination of GFRA1 did not appear to lead to enteric neuron loss (125). Instead GDNF is released in the ascending arm of the peristaltic reflex and appears to strengthen muscle contractions, the opposite of what might be expected if GDNF/GFRA1 signaling activated *Nos/Vip/Gal* neurons that are thought to be primarily

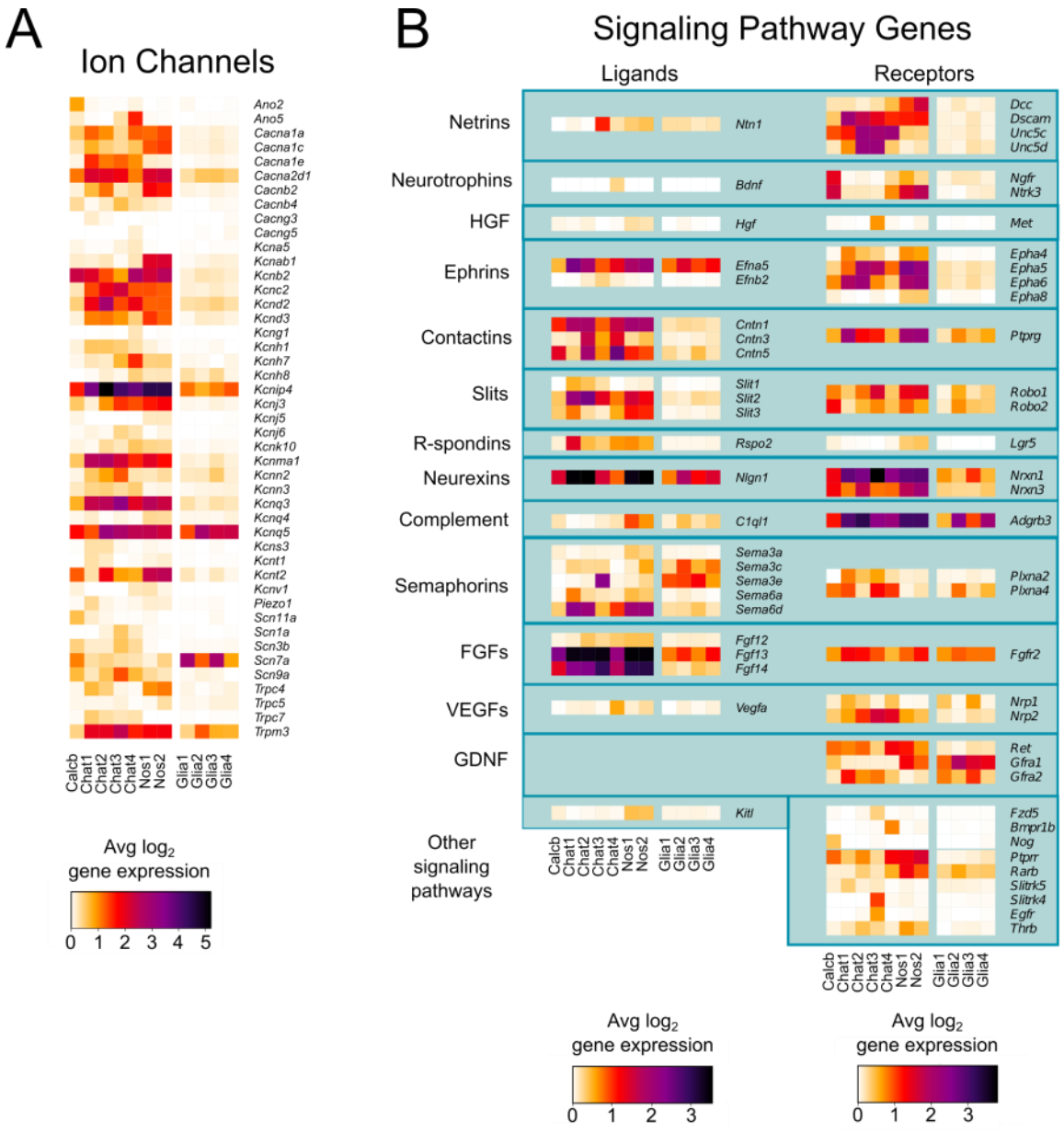

Figure 4-2: Differential expression of many receptors, ligands, and ion channels in distal colon.

(A) Average gene expression for ion channels with differential patterns of gene expression between neuron classes. (B) Average gene expression for selected ligands (left) and receptors (right) that were differentially expressed between different neuron subclasses.

inhibitory motor neurons (320). To test the validity of *Gfra1* single nucleus expression data, we therefore immunostained distal colon of mice expressing GFP from the *Gfra1* promotor (*Gfrα1*$^{Gfp/wt}$ reporter mice). We found GFP protein in 88.9 ± 1.8% of NOS+ neurons and 8.8 ±

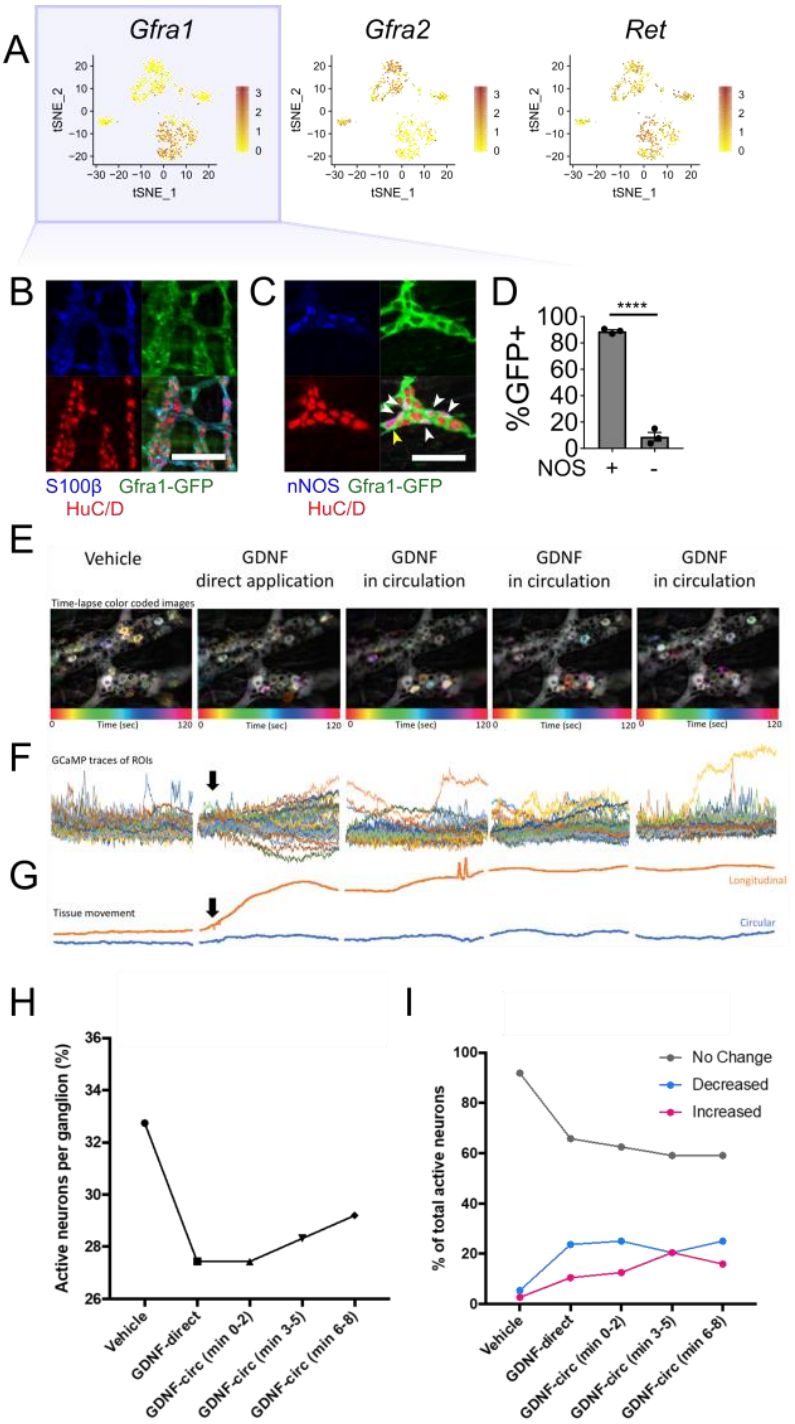

Figure 4-3: Gfra1 and Gfra2 are expressed in different neuron populations in adult distal colon.

(A) Feature plots suggest *Gfra1* is predominantly expressed in *Nos1/Vip/Gal*-expressing neurons, while *Gfra2* is predominantly expressed in the neuron populations that also express *Chat*. *Ret* appears to be expressed in almost all populations of neurons except the *Chat 3 (Met)* group. (B) Whole mount immunohistochemistry of *Gfra1*$^{Gfp/wt}$ distal colon showing colocalization of GFP (green) with most S100b+ (blue) glia and a subset of HuC/D+(red) neurons. (C) Whole mount

immunohistochemistry of *Gfra1*$^{Gfp/wt}$ distal colon showing colocalization of GFP (green) with most nNOS+ (blue) neurons. White arrowheads indicate GFP+, nNOS+ neurons, while yellow arrowhead indicates a nNOS+ neuron that was GFP-. (D) Quantification of (C) reveals that the percent of nNOS+ neurons that are GFP+ greatly exceeds the percent of nNOS- neurons that are GFP+, consistent with what our single-cell sequencing data predicts ($p<0.0001$, n=3(*Gfra1*$^{Gfp/wt}$), 88.9 ± 1.% GFP+/NOS+ neurons, and 8.8 ± 5.7% of GFP+/NOS- neurons). (E-F) Application of GDNF to the plexus of a mouse expressing GCAMP elicits changes in neuron firing patterns. Color represents time of peak fluorescence signal. (G) Longitudinal muscle tone, but not circular muscle tone, changed in response to GDNF application. (H) Quantification suggests a decrease in average neuronal activity immediately after bath-application of GDNF. (I) A subset of neurons show decreased activity after application of GDNF, while another subset of neurons shows increased activity. Scale bar = 100 microns. ****$p<0.0001$

5.7% of NOS-negative neurons (**Figure 4-3C-D**). GFP also colocalized with the glial marker S100β (**Figure 4-3B**), consistent with our sequencing data.

To explore the acute functional effects of GDNF on myenteric neurons in more detail, we decided to use calcium imaging. *E2a-Cre;ROSA-GCaMP6* mouse colon was pinned, flattened and imaged in a continuously-superperfused, carboxygenated artificial cerebrospinal fluid (ACSF). These mice express the calcium indicator GCaMP6 in all cells, permitting us to examine how calcium fluxes are impacted by acute application of GDNF. Neurons were imaged intermittently for 10 minutes before and after GDNF addition to the organ bath (**Figure 4-3E**), GCaMP signals were analyzed and quantified by calculating $\Delta F/F_0$ (**Figure 4-3F**). Changes in muscle tone were assessed by quantifying tissue movement in the x (circular muscle) or y (longitudinal muscle) direction. GDNF addition acutely induced movement in longitudinal smooth muscle but not circular muscle (**Figure 4-3G**). GDNF also slightly decreased the percentage of active neurons per ganglion (**Figure 4-3H**). Interestingly, however, GDNF application increased activity in one population of neurons, decreased activity in a second neuronal population, and had no effect on calcium transients in a third neuron group (**Figure 4-3I**). To test the hypothesis that these changes in activity correlate with specific neuron subtypes, we will repeat this experiment in *nNOS-CreERT2*$^{Cre/wt}$*;ROSA-GCaMP6* mice, which should express GCaMP6 exclusively in nNOS+ neurons.

Single-nucleus sequencing suggests a combinatorial code of transcription factors controlling neuron subtype specification in mouse distal colon.

To better understand neuronal subtype specification in myenteric plexus, we next examined transcription factor and splicing factor ('regulatory genes') abundance in enteric neuron subpopulations. We started with genes known to affect the ENS. Interestingly, *Ascl1*, *Hand2*, and *Sox6* were not statistically differentially expressed in adult myenteric neuron subtypes even though mutations in these genes alter subtype ratios. In contrast, *Tbx3*, *Tlx2*, and *Zeb2* (also known as *Zfhx1b* or *Sip1*) were differentially expressed in subpopulations of colon myenteric neurons (**Figure 4-4A; Supplementary Figure 4-5**). These three genes impact ENS glial differentiation (*Tbx3*), region-specific neuron density (*Tlx2*), and migration of ENS precursors into the bowel (*Zeb2*), but roles in enteric neuron subtype specification have not yet been identified (136, 155, 175, 190, 191). We found many other transcription factors with distinct expression patterns across neuron subgroups, including *Etv1*, *Casz1*, *Bnc2*, and *Zfhx3*, but the role of these genes in the ENS is not yet known. Consistent with data from other nervous system regions (321), few transcription factors were expressed in only one neuron subpopulation, suggesting that combinatorial codes may regulate neuron subtype identity in the ENS (**Figure 4-4A; Supplementary Figure 5**).

We were particularly interested in genes that distinguished two broad, mostly non-overlapping classes of neurons: ChAT+ neurons (which comprise excitatory motor neurons, intrinsic primary afferent neurons, and some interneuron populations) and NOS+ neurons (which comprise inhibitory motor neurons and possibly a small subset of interneurons). Consistent with our single nucleus RNA sequencing data, immunohistochemistry demonstrated preferential expression of TBX3 protein in *ChAT-EGFP*- neurons (which are mostly nNOS+) and preferential expression of SATB1, RBFOX1, and PBX3 proteins in *ChAT-EGFP*+ neurons (which are mostly nNOS-) (**Figure 4-4B-F; I-L**). This *ChAT-EGFP-L10A* mouse line has strong EGFP expression

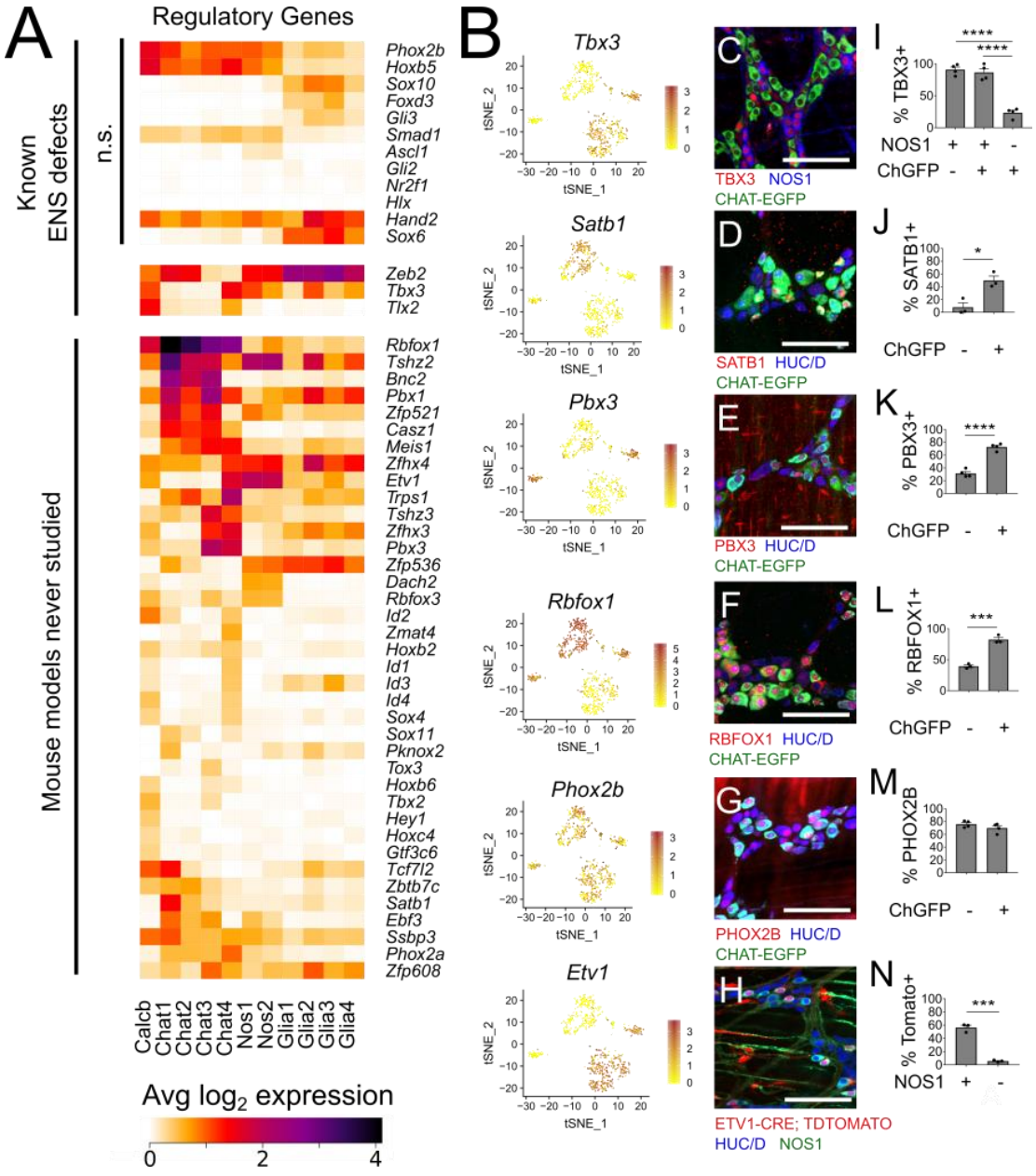

Figure 4-4: Regulatory genes are expressed in distinct ENS subsets.
(A) Transcription and splice factors associated with known roles in ENS developmental processes (top), and regulatory genes (transcription factors and splicing factors) newly-identified in the ENS in this study (bottom). n.s. = not significantly differentially expressed between neuron clusters. (B) Feature plots of select genes, colored by expression level. Color key represents log-$_2$(normalized gene expression). (C-G) Whole-mount immunohistochemistry of select regulatory genes in young adult *ChAT-EGFP-L10A* distal colon reveals gene localization in neuron subsets. (H) Whole mount immunohistochemistry in distal colon from a tamoxifen-treated *Etv1-Cre^{Ert2};R26R-TdTomato* mouse reveals TdTomato fluorescence in many nNOS+ neurons, as well as some non-neuronal cells (presumed to be ICC). (I-M) Quantification of immunohistochemistry reveals preferential expression of TBX3 in neurons expressing nNOS (I, $p<0.0001$, n=3, ANOVA with Tukey's post-hoc test) and preferential expression of SATB1 (J, $p=0.013$, n=3, Student's t-

test), PBX3 (K, p<0.0001, n=3, Student's t-test), and RBFOX1 (L, p=0.0006, n=3, Student's t-test) in EGFP+ neurons. Consistent with single-cell data, PHOX2B seemed to be expressed equally in both ChAT-EGFP+ and ChAT-EGFP- cells (M, p=0.2193, n=4, Student's t-test) ChGFP = ChAT-EGFP. (N) Quantification of (H) showed 56.37±3.64% of nNOS+ neurons are TdTomato+, while only 5.59±0.88% of nNOS- neurons are TdTomato+ (p=0.0002, n=3, Student's t-test). Scale bar = 100 microns. *p<0.05, **p<0.01, ***p<0.001, ****p<0.0001

in ChAT antibody immunoreactive neurons, and appears to be a reliable reporter for these ChAT+ cells. In addition, we confirmed relatively uniform expression of PHOX2B protein in both *ChAT-EGFP*+ and *ChAT-EGFP*- neurons (**Figure 4-4G, M**). We also quantified TdTomato expression using colons from *Etv1-CreERT2*$^{Cre/wt}$*;R26R-TdTomato* reporter mice treated with high dose tamoxifen. These mice should express TdTomato in cells with high *Etv1* expression. Over half (56.37±3.64%) of nNOS+ neurons expressed TdTomato, while only 5.59±0.88% of nNOS- cells expressed TdTomato, consistent with our single nucleus sequencing data (**Figure 4-4H, N**).

E17.5 mouse enteric neuron subtypes express similar transcription factors to adult distal colon enteric neurons

To identify transcription factors differentially expressed in developing ChAT+ and nNOS+ enteric neurons, we performed single-cell RNA-seq on E17.5 lineage-marked enteric neurons and precursors. We sequenced bowels from *ChAT-L10a-EGFP* $^{wt/wt}$*; nNos-CreERT2*$^{Cre/wt}$*;TdTomato*+ and *ChAT-L10a-EGFP* $^{Gfp/?}$*; nNos-CreERT2*$^{wt/wt}$*;TdTomato*+ E17.5 embryos (from the same litter) to get cells that constitutively express *L10a-EGFP* in ChAT+ neurons and that produce TdTomato in *nNOS*-lineage marked neurons after tamoxifen treatment. Mice were tamoxifen-treated at E15.5, two days before cell isolation (**Figure 4-5A**). We used whole bowel because distal colon alone produced too few cells to sequence at this age. We obtained single-cell RNA-seq data from 922 cells with a median of 15,374 UMI and 4,060 genes per cell. Of these, 707 cells were neurons or neuron precursors based on expression of *Elavl4* and

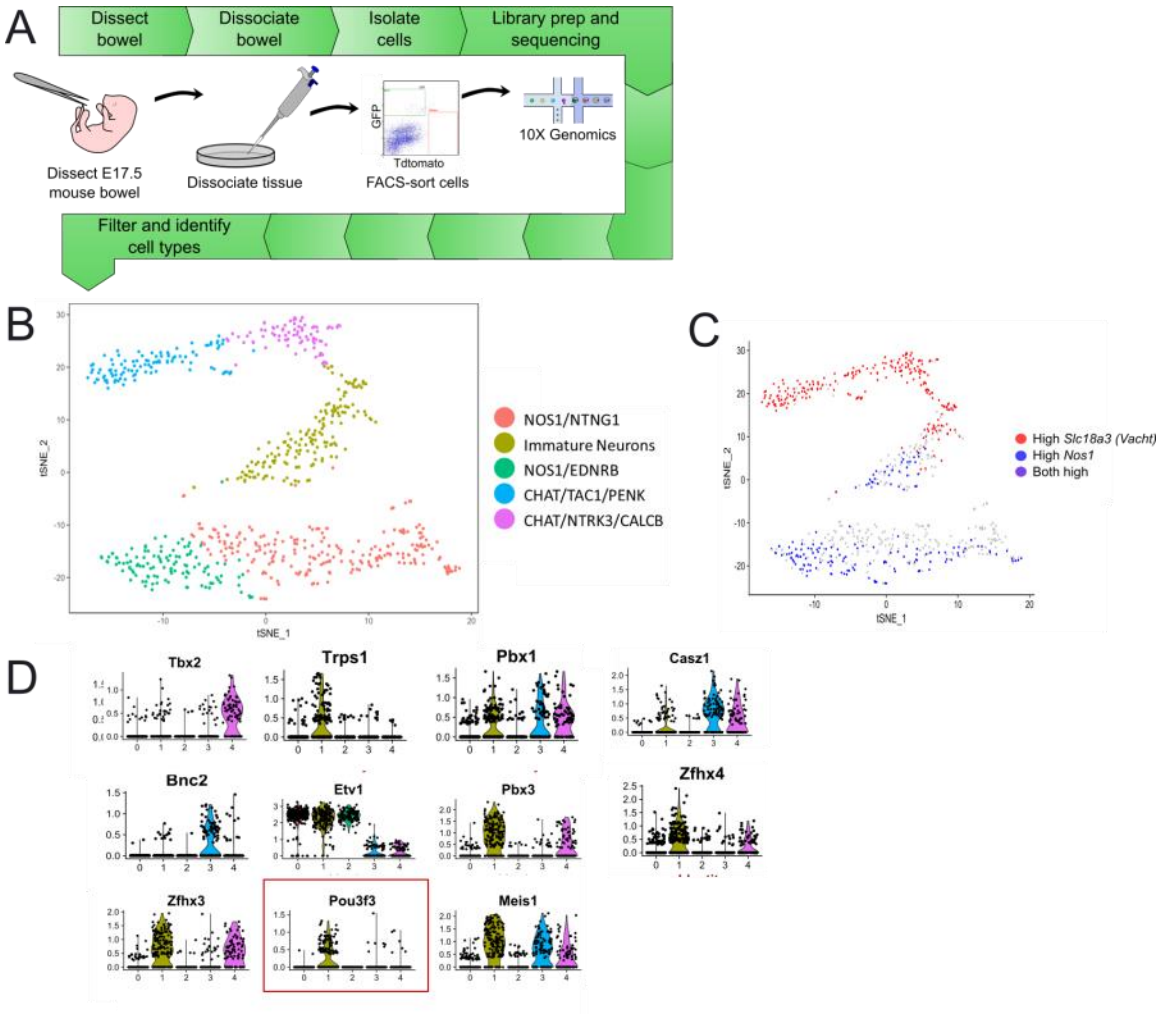

Figure 4-5: Single-cell sequencing of E17.5 ChAT-EGFP+ and nNos-CreERT2$^{Cre/wt}$;R26R-TdTomato+ neurons reveals many regulatory genes also found in adult distal colon.
(A) Plan for single-cell sequencing of E17.5 whole cells. Bowels from tamoxifen-treated E17.5 pups were dissected, chopped into tiny pieces, treated with Liberase®, flow-sorted, and single cell RNA-seq was performed with the10x genomics sequencing platform. (B-C) T-SNE plot reveals multiple neuron subpopulations including one group believed to be immature neurons, two groups expressing *Nos1*, and two groups expressing the cholinergic marker vesicular acetylcholine transporter (*Slc18a3/Vacht)*, presumed to be ChAT+ neurons. (C) Expression of *Nos1* (blue), *Slc18a3* (red), and both (purple). (D) Many regulatory genes expressed in adult distal colon were also expressed in subsets of E17.5 neurons. We also identified expression of *Pou3f3* in the immature neuron subset (red square).

Uchl1. Re-clustering using only neurons resulted in 5 groups: 1) *Nos1*+ and Netrin G1+ (*Nos1/Ntng1*), 2) *Nos1*+ and *Ednrb*+ (*Nos1/Ednrb*), 3) *Chat*+, *Tac1*+, and *Penk*+ (*Chat/Tac1/Penk*), 4) *Chat*+, *Ntrk3*+, and *Calcb*+ (*Chat/Ntrk3/Calcb*), and 5) a mixed population

of cells we hypothesize are predominantly immature neurons based on gene ontology (GO) term analysis (**Figure 4-5B**). Although surprisingly few *Chat* transcripts were detected, the vesicular acetylcholine transporter *Slc18a3* was detected at high levels in many cells and was used as a proxy for *Chat* expression (**Figure 4-5C**). Many of the same regulatory genes detected in adult mouse distal colon were also detected in subsets of neurons in E17.5 whole bowel, including *Casz1, Bnc2, Etv1, Pbx3, Zfhx4, Zfhx3, Meis1, Tbx2,* and *Trps1* (**Figure 4-5D**), suggesting that these genes may be relevant for neuron subtype specification.

Conditional deletion of *Tbx3* reduces nNOS+ neurons

To determine if differentially-expressed transcription factors impact neuron subtype specification or maintenance, we decided to first examine ENS in *Tbx3* and *Etv1* mutant mice. *Tbx3* and *Etv1* are strongly expressed in distinct neuron subgroups at E17.5 and in adults. To study *Tbx3*, we bred to generate *Wnt1-Cre;Tbx3*$^{fl/fl}$*;R26R-Tdtomato* mice that have CRE-dependent inactivation of *Tbx3* and CRE-dependent activation of *TdTomato* expression. We also bred *Etv1-CreERT2* mice that have CreERT2 knocked into the *Etv1* gene locus to *Chat-EGFP-L10A* that have fluorescent ChAT+ enteric neurons. Immunohistochemical analysis of P0 small intestine demonstrated a striking (~30%) decrease in the proportion of NOS+ neurons in mice conditionally lacking *Tbx3* (*Wnt1-Cre*$^{cre/wt}$*;Tbx3*$^{fl/fl}$*;R26R-Tdtomato* mice compared to non-homozygous controls **Figure 4-6A-C**) despite normal total neuron density as we previously reported (**Figure 4-6D**) (175). In contrast we did not find statistically significant differences in NOS+ or ChAT-EGFP+ neuron density in homozygous P0 *Etv1-Cre-ERT2* mutant mice (**Figure 4-6E-G**).

***Pou3f3* is expressed in colon but not small intestine**

We noted that a subset of E17.5 cells expressed the POU domain transcription factor

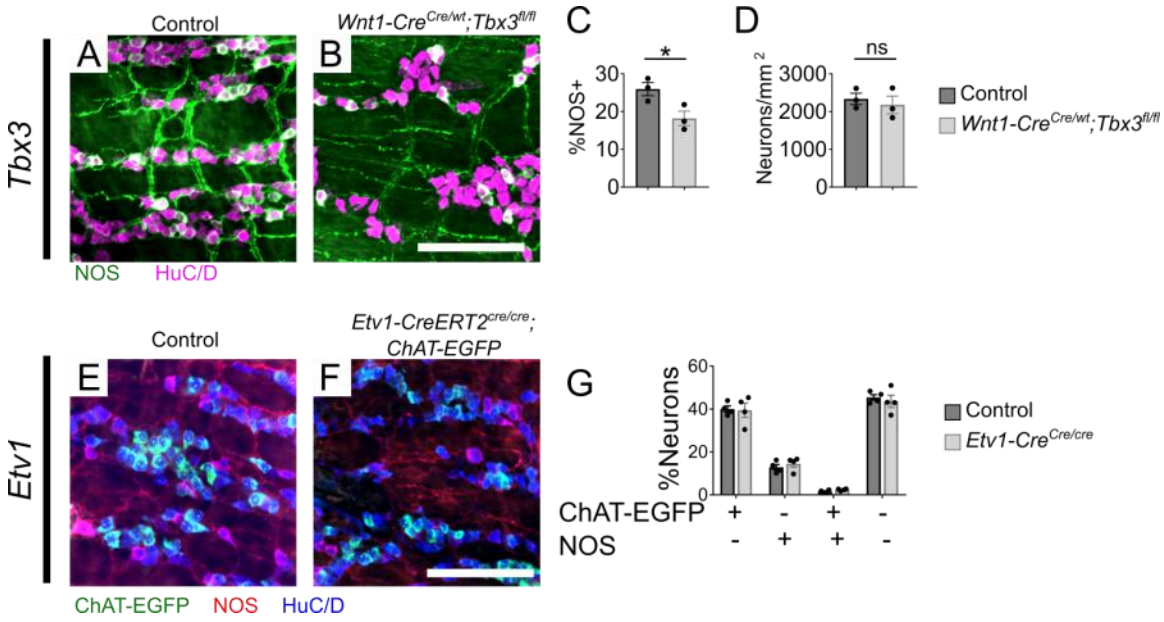

Figure 4-6: *Tbx3* conditional knockout mice have fewer nNOS+ myenteric neurons, while nNOS+ and ChAT-EGFP+ neuron numbers are normal in mice missing *Etv1*.
(A-B) Maximum-intensity projections of confocal z-stacks suggests nNOS+ (green) cells are sparser in *Tbx3* mutant P0 small intestine relative to total HuC/D neurons (magenta). (C-D) Quantification reveals a 30% reduction in the proportion of nNOS+ neurons in *Wnt1-Cre*$^{Cre/wt}$*;Tbx3*$^{fl/fl}$ P0 small intestine (C; p=0.041, n=3(ctrl), n=3 (*Wnt1-Cre*$^{Cre/wt}$*;Tbx3*$^{fl/fl}$)), despite apparently normal total neuron density (D; p=0.601, n=3(ctrl), n=3(*Wnt1-Cre*$^{Cre/wt}$*;Tbx3*$^{fl/fl}$)). (E-F) Maximum-intensity projections of confocal z-stacks in P0 control (E) and *Etv1-CreERT2*$^{Cre/Cre}$ mice (F) bred into a *Chat-EGFP-L10A* reporter were immunostained for EGFP (green), nNOS (red), and HuC/D (blue) (G). Quantification of the proportion of neurons that expressed ChAT, nNOS, both, or neither showed no difference in any of these broad subclasses of neuron (G; p =0.797, two-way ANOVA, n=4(control), n=4(*Etv1-CreERT2*$^{Cre/Cre}$)). Scale bar=100 µM. *p<0.05

Pou3f3 (a.k.a. *Brn1*) that is important for CNS development (322) and that these cells were primarily in the E17.5 immature neuron subgroup. To validate this observation, we immunostained mouse small bowel and colon at multiple ages (E12.5, E14.5, E17.5, adult) using a HuC/D antibody and two POU3F3 antibodies. We found robust pan-neuronal POU3F3 expression in colon enteric neurons, but no small intestine POU3F3+ enteric neurons at E12.5 – E17.5 mouse (**Figure 4-7A-J**). In adult mice, POU3F3 was present in colonic neurons of both myenteric and submucosal plexus (**Figure 4-7K-V**), but not expressed in small bowel ENS. At E17.5 we identified a transition in distal ileum, near the ileocecal junction from POU3F3 negative to POU3F3+ enteric neurons (**Figure 4-7W**). Both POU3F3 antibodies had similar expression

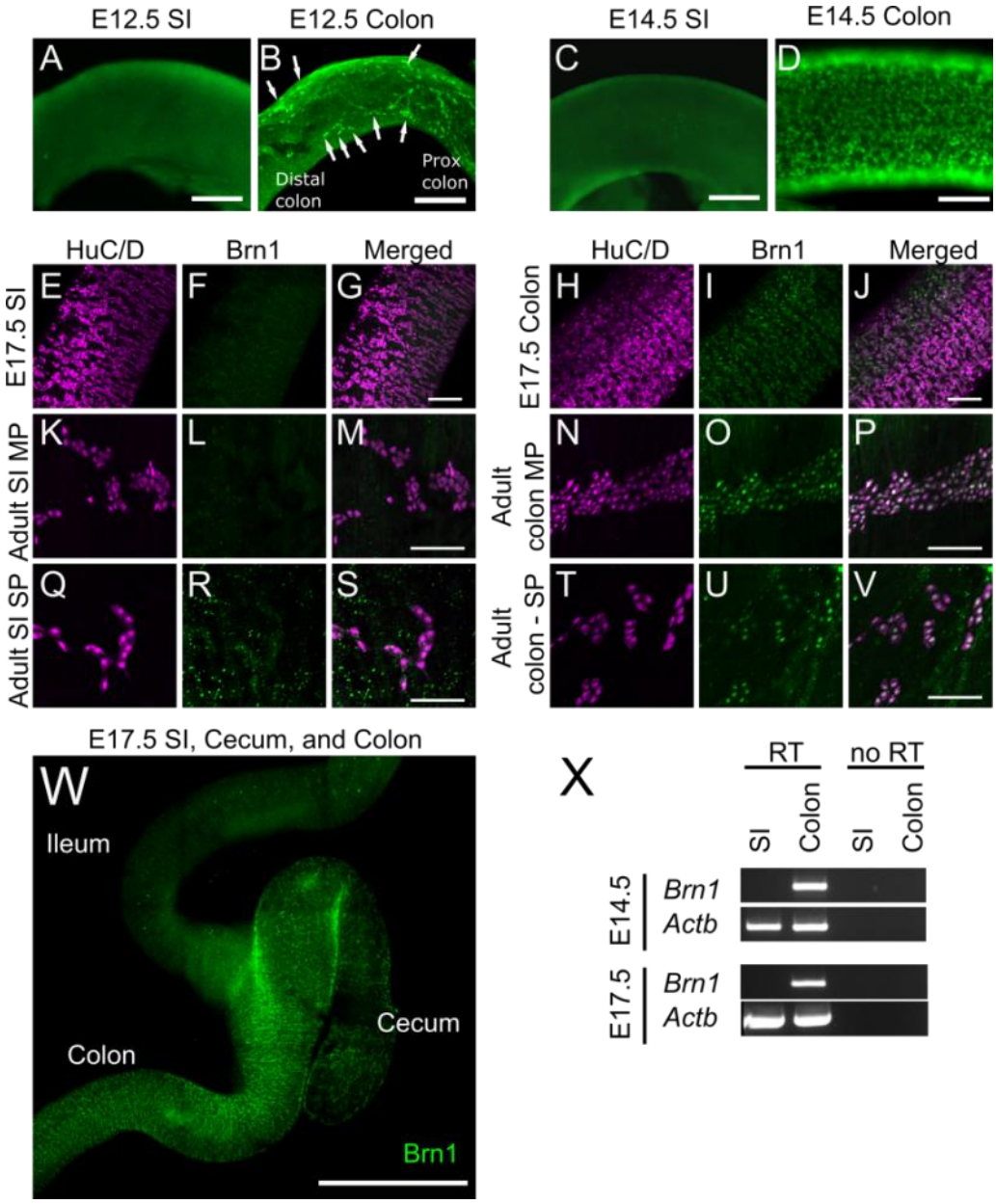

Figure 4-7: Brn1 is expressed in mouse colon but not small intestine.
(A-V) Whole mount immunohistochemistry confirms that Brn1 immunoreactivity (green) is not detected in most of the small bowel at E12.5 (A), E14.5 (C), E17.5 (F), or in adulthood (L, R). Brn1 immunoreactivity is easily detected in proximal colon (B) at E12.5 (arrows) and throughout the colon at E14.5 (D), E17.5 (I), and in adulthood (O, U). At E17.5 and in adulthood, colonic Brn1 co-localizes with the enteric neuron marker HuC/D (H, N, T). SP = submucosal plexus, MP = myenteric plexus. (W) Flattened, stitched confocal Z-stack showing Brn1 expression in E17.5 ileum, cecum, and colon. Brn1 is barely visible in ileum but is expressed in cecum and colon. (X) Representative RT-PCR for Brn1 from FACS-sorted Tdtomato+ ENCDCs confirms Brn1 expression in colon but not SI at E14.5, E17.5, and in adult ENS. RT-PCR was performed on 3 replicates for each age. Scale bar = 100 µM (A, C -V), 200 µM (B), and 1 mm (W).

patterns, suggesting specific antibody staining.

To further confirm regional differences in *Pou3f3* expression, we FACS-sorted TdTomato+ cells from E14.5 and E17.5 *Wnt1-Cre;R26R-TdTomato* mice that express TdTomato in all enteric neurons, glia, and precursor cells of small intestine and colon. Consistent with immunohistochemistry, RT-PCR revealed *Pou3f3* expression in colon, but not small intestine (**Figure 4-7X**). To our knowledge, this is the first example of a transcription factor with region-specific transcription within the colon.

Single nucleus sequencing of adult human myenteric plexus

To extend this work to human ENS, we performed single nucleus RNA-seq on micro-dissected cells from the region of the colon myenteric plexus. This work posed many challenges that were not encountered with mouse studies. The most significant problem is that human enteric neurons comprise an extremely small fraction of total bowel cells (<1/10,000 cells in the myenteric layers) and isolating ENS remains challenging. To identify human ENS, we stained live colon tissue with 4-Di-2-Asp (**Supplementary Figure 4-6**), a non-toxic dye taken up by mitochondria in presynaptic nerve terminals. We then micro-dissected myenteric plexus to enrich for cell populations that control bowel motility. After dissociation of "myenteric plexus" whole cell RNA-seq yielded data from many cell types , but few-to-no neurons, suggesting adult human enteric neurons were too fragile for this procedure or that our micro-dissection was not cleanly isolating myenteric plexus (**Supplementary Figure 4-7**). We also attempted to use flow cytometry to isolate single neuronal nuclei for RNA-sequencing. In the CNS, neuronal nuclei have been successfully isolated using the neuron-specific antibody NeuN (319). Unfortunately, NeuN immunoreactivity was faint in human ENS, and despite many attempts, we did not observe an obvious population of NeuN+ nuclei after flow sorting. We next tried using an antibody against PHOX2B to flow sort human ENS cell. Although this antibody yields intense nuclear

staining of human ENS via immunohistochemistry, when we sequenced a population supposedly enriched for PHOX2B+ nuclei, we still identified almost no neurons (**Supplementary Figure 4-8**). We suspect flow sorting enteric neuron nuclei was unsuccessful because of neurons are scarce in human bowel and because antibodies may leak from nuclei during the isolation process.

Ultimately, we obtained RNA-seq data from a limited number of human colon neuronal nuclei by micro-dissecting myenteric plexus labeled with 4-Di-2-Asp. This approach dramatically enriched for the ENS, but dissection was imperfect and isolated "plexus" included muscle and other nearby cells that control bowel motility. After freezing in optimal cutting temperature (OCT), sectioned on a cryostat generating 100 µM slices, Dounce homogenized to isolate nuclei, labeled the nuclei with Hoescht, and flow sorted to separate single nuclei from cell debris. All isolated nuclei were sequenced using the 10x Genomics platform (**Figure 4-8A**), yielding data from 20,167 nuclei from 16 adult colon samples (sample characteristics in **Supplementary Table 4-4**) with an average of 1,455 UMI and 894 genes per nucleus (**Supplementary Table 4-5**). In addition to neurons, we identified nuclei from smooth muscle cells, interstitial cells of Cajal (ICC), PDGFRα+ cells, enteric glia, muscularis macrophages, vascular endothelial cells, and several unknown cell populations (**Figure 4-8B; Supplementary Figure 4-9**). One subgroup of nuclei (Unknown 3) was an unfamiliar cell type, predominantly from a single patient that we suspect may reflect the patient's pathology (rectal cancer). Otherwise, there were no obvious batch effects specific to different samples or when comparing right versus sigmoid colon (**Supplementary Figure 4-10**). Our dataset, therefore contains substantial information about gene expression is all of the cell types in bowel muscle that impact motility.

One small cluster of 48 cells on our t-SNE plot appeared to be strongly positive for neuronal genes like *ELAVL4*, *SNAP25*, and *UCHL1* (**Supplementary Figure 4-11A-C**). Scattered cells in other groups of the t-SNE plot also expressed *ELAVL4*, *SNAP25*, and other neuronal markers. To determine the identity of the *ELAVL4+/SNAP25+/UCHL1+* cells that did

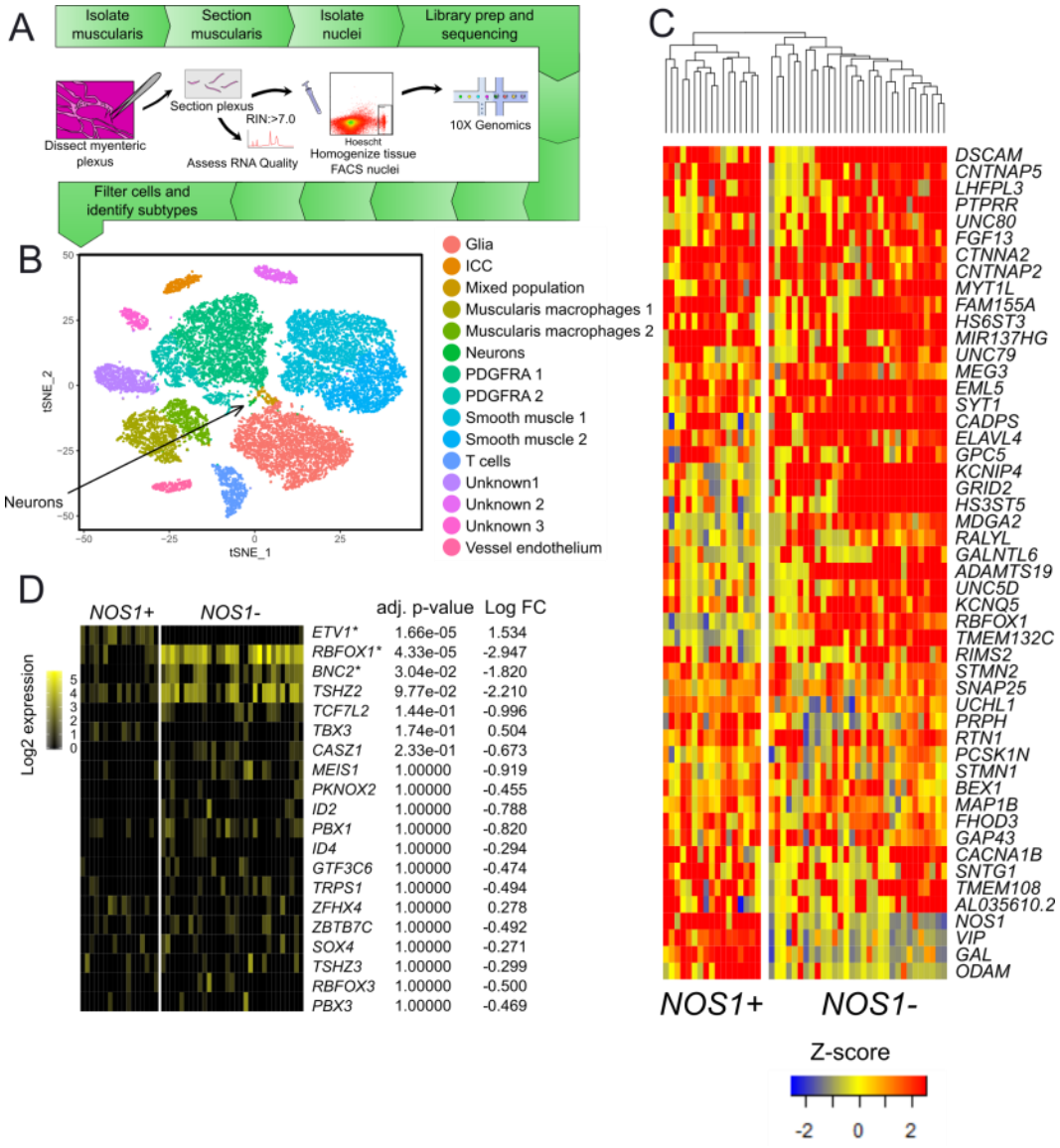

Figure 4-8: Single-nucleus sequencing of dissected human myenteric plexus reveals *NOS1/VIP/GAL*+ and *NOS1/VIP/GAL*- neuron subsets.
(A) Plan for single-nucleus sequencing of adult human colon myenteric plexus. Plexus and surrounding cells were micro-dissected in 4-Di-2-Asp, frozen in OCT, sectioned on a cryostat, Dounce homogenized and flow sorted for nuclei isolation. (B) T-SNE plot of 20,167 nuclei showing multiple cell types including glia, ICC, muscularis macrophages, *Pdgfrα*+ cells, smooth muscle cells, T cells, blood vessel endothelial cells, and several unknown groups. Neurons comprise one small cluster (~48 cells). (C) Heatmap showing the top 50 differentially expressed genes that distinguish neurons from other cells in our dataset (i.e. the 50 genes with highest fold change). Hierarchical clustering based on these genes suggests that neurons fall into 2 subgroups: one that is largely *NOS1/VIP/GAL*+ (17 neurons), and another that is largely *NOS1/VIP/GAL*- (31 neurons). (D) Transcription and splicing factors identified in mouse colon that were expressed in >10% of human myenteric neurons. *RBFOX1*, *ETV1*, and *BNC2* were differentially expressed between *NOS1/VIP/GAL*+ and *NOS1/VIP/GAL*- human neurons (Wilcoxin rank-sum test with Bonferroni correction).

not cleanly cluster together, we filtered our dataset to include only cells expressing either *ELAVL4*, *SNAP25*, or *UCHL1* and re-clustered. We saw 7 subgroups that we believe are doublets containing neuronal and non-neuronal nuclei based on co-expression of genes like *ACTG2, PLP1, KIT*. One subgroup appears to be pure single neuron data based on high expression of other neuronal markers like *SYT1* and *DSCAM* and the absence of markers for other well-defined cell populations (**Supplementary Figure 4-12**). The group of pure neurons contains 48 nuclei and maps back into the expected location on our original t-SNE plot.

Although 48 neurons was too few to cluster using PCA-based methods, we wondered if we could still draw conclusions about NOS and ChAT neuron classes from this small dataset. Intriguingly, when we performed hierarchical clustering (Euclidean, complete-linkage) on the neurons using the top 50 markers that distinguished these cells from other cells in our dataset, we saw two distinct clusters emerge. One cluster expressed *NOS1*/*VIP/GAL+*, while the other was mostly *NOS1*/*VIP/GAL* negative. To our surprise, we detected no *CHAT* or *SLC18A3* (*VAChT*) transcripts in the *NOS1/VIP/GAL-* neuron subgroup, although this may have been due to read depth limitations.

We asked if any of the regulatory genes that were differentially expressed between *NOS1+* and *NOS1-* neurons in mouse were also differentially expressed in our human neurons. After multiple testing correction on a list of 41 genes, we found differential expression in three genes: *RBFOX1*, *BNC2*, and *ETV1* (**Figure 4-8D**). The expression patterns of these three genes match that of our mouse data (i.e. *ETV1* is highly expressed in *NOS1+* neurons, and *RBFOX1* and *BNC2* are highly expressed in *NOS1-* neurons. We suspect other regulatory genes exhibit distinct expression patterns but that read depth and cell number are too low to show this currently.

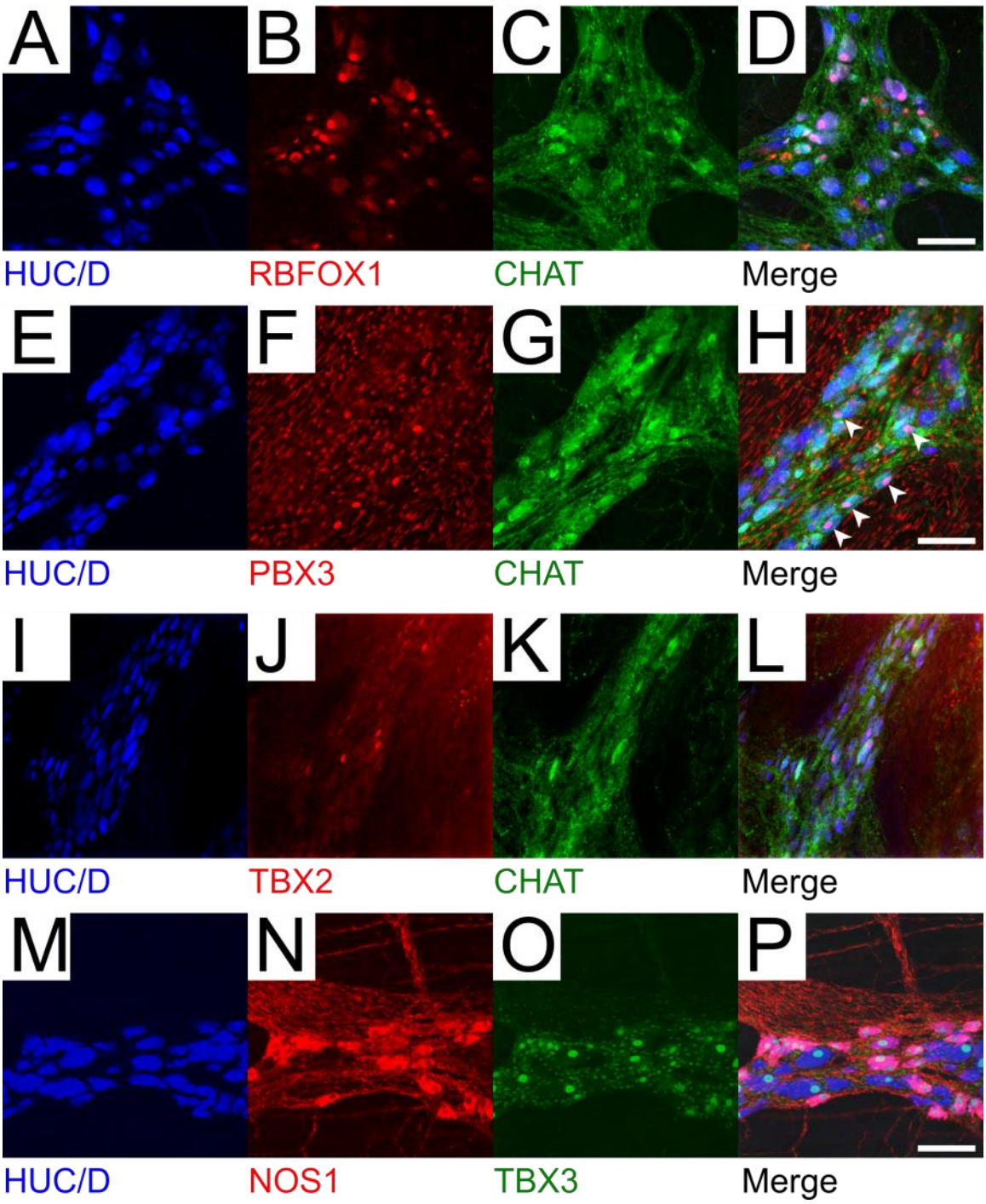

Figure 4-9: Many regulatory genes identified in mouse also label subsets of human enteric neurons.
(A-T) Maximum intensity projections of confocal Z-stacks in adult human ENS. RBFOX1 (A-D), PBX3 (E-H), TBX2 (I-L), and TBX3 (M-P) are present in subsets of neurons. White arrowheads indicate nuclear transcription factor staining. Scale bar = 100 microns.

Transcription factor expression in adult human ENS

Using previously-described clearing techniques developed in our laboratory, we stained adult human colon with the same antibodies used in mouse (**Figure 4-9**). Some antibodies which stained mouse did not stain human colon (e.g. SATB1), but we observed robust staining from most antibodies, including RBFOX1 (**Figure 4-9A-D**), PBX3 (**Figure 4-9E-H**), TBX2 (**Figure 4-9M-P**), and TBX3 (**Figure 4-9Q-T**). Staining patterns for these antibodies appears consistent with their expression in mouse distal colon (i.e. most RBFOX1+, PBX3+, and TBX2+ cells are CHAT+, while most TBX3+ cells are NOS+). Quantifications are in progress.

4.5 - DISCUSSION

Life-threatening bowel motility disorders like Hirschsprung disease, chronic intestinal pseudo-obstruction syndrome, achalasia, and diabetic gastroparesis (73, 74, 89, 94) remain challenging to treat and difficult to diagnose. One exciting possibility is that stem cell-based therapy might allow regeneration and repair for the defective ENS in these disorders (323-326), but optimal approaches for preparing stem cells or directing these cells toward specific enteric neuron lineages are not yet established. Furthermore, enteric neuron subtypes remain incompletely defined, and this makes it difficult to determine which cell types are defective or missing in individuals with bowel motility disorders. To enhance our ability to define cellular mechanisms that cause dysmotility, and to facilitate directed stem cell differentiation, we need much more information about signaling pathways and transcriptional regulators driving neuronal subtype differentiation and maintenance. To fill this knowledge gap, we used single-nucleus and single-cell transcriptomics to identify a vast array of neurotransmitters, receptors, ion channels, signaling molecules, and regulatory genes that define different neuron subclasses in mouse ENS at two ages. Using unbiased clustering, we identified seven distinct neuron subtypes in mouse distal colon. These neuron subtypes differentially express signaling molecules that in other

systems are involved in axon pathfinding, cell-cell adhesion, and survival. We clarified adult neuron subtypes that express *Ret* and its co-receptors, *Gfra1* and *Gfra2* and used calcium imaging to demonstrate that GDNF acutely modifies activity in a subset of adult enteric neurons.

Similar to what has been described for other regions of the nervous system, enteric neuron express what appears to be a combinatorial code of transcription factors that define subtypes. All transcription factors evaluated immunohistochemically had expression patterns similar to what was predicted by our sequencing data. To support the hypothesis that these transcription factors guide neuronal subtype maturation, we conditionally deleted *Tbx3*, a transcription factor with high expression in nNOS+ neurons. The *Tbx3* mutants had a striking decrease in nNOS+ neuron density, confirming the importance of at least one of these regulatory genes for subtype differentiation or survival. We also discovered that the transcription factor *Pou3f3* is expressed in all colon enteric neurons, but was completely absent in small intestine. To our knowledge, this is the first transcription factor with colon-specific expression that has ever been identified in the ENS.

To complement murine data, we analyzed single-nucleus RNA-sequencing data from 48 human enteric neurons, including 17 *NOS1*+ and 31 *NOS1*- neurons. Using a curated list of regulatory genes derived from our mouse dataset, we found differential expression of *RBFOX1*, *BNC2*, and *ETV1* in subsets of human enteric neurons. We hypothesize that other subtype-specific genes from our mouse dataset may be conserved in human enteric neuron subtypes, but we did not have the statistical power or sequencing depth in human single-nucleus RNA-seq data to confirm this hypothesis. We began to test this hypothesis for a limited set of additional genes by immunostaining human bowel for TBX2, PBX3, and TBX3 using a state-of-the-art clearing technique we recently developed. We confirmed that TBX3, PBX3, and TBX2 protein are present in subsets of human enteric neurons as predicted by mouse data, even though these genes were not statistically significantly differentially expressed in our relatively small human dataset.

We expect these data will serve as a resource for ENS biologists interested in many aspects of ENS function and will facilitate cellular reprogramming for stem cell therapy needed to regenerate damaged or missing ENS circuitry. Our human data, in addition to providing insights about gene expression within the ENS, illustrates the extensive array of cell types that interface with the myenteric plexus, including ICCs, smooth muscle cells, PDGFRα+ cells, muscularis macrophages, and vascular endothelial cells. Although an extensive discussion of these other cell types is beyond the scope of this paper, we hope this data will also provide a resource for investigators studying the interacting partners of the ENS.

Integrating our data with what is known about ENS subtypes

It is tempting to try to integrate our mouse distal colon data with what is known about ENS subtypes. Unfortunately, this has proved surprisingly challenging, as mouse distal colon has not been neurochemically characterized. Guinea pig distal colon myenteric plexus, which is probably similar in composition, is supposed to contain inhibitory and excitatory motor neurons, intrinsic primary afferent neurons, three groups of ascending interneurons and four types of descending interneurons (27). Most interneuron subgroups are expected to occur at low (1-5%) frequency, and our mouse distal colon dataset may have too few cells to separate these rarer subgroups reliably.

We believe our *Nos1*-expressing subgroups (Nos 1 and Nos 2 in Figure 1) are inhibitory motor neurons, based on their co-expression of *Vip* (vasoactive intestinal peptide), *Gal* (galanin), and *Npy* (neuropeptide Y). This neurotransmitter pattern is fairly consistent in defining inhibitory motor neurons throughout the ENS (4, 27) and these neurons are common (~25% of neurons in mouse small intestine). Likewise, we hypothesize that at least one, and possibly both, of our two largest Chat groups (Chat 1 and Chat 2, which express *Chat/Penk/Tac1* and *Chat/Tac1* respectively), are excitatory motor neurons. This hypothesis is based on several observations: 1)

excitatory motor neurons in guinea pig distal colon contain ChAT+, TK, and enkephalin 2) excitatory motor neurons make up ~35% of myenteric neurons, and 3) *Satb1* expression is highest in these two populations, and most *Satb1*-containing neurons were small (consistent with reports that excitatory motor neurons have small cell bodies) (4).

One interesting observation is that a population of neurons in distal colon expresses the hepatocyte growth factor receptor *Met*, but not *Ret* (Chat 3). Our lab previously reported MET expressions in RET- CGRP+ intrinsic primary afferent neurons (IPANs) in mouse small intestine (327). Oddly, almost none of the *Met*+ neurons in our distal colon data express CGRP (*Calcb*). Instead, *Calcb* is expressed by a small subgroup of neurons expressing *Nmu* and *Grp*, but not *Chat* (Calcb group). At the moment, it is impossible to determine if one, both, or neither of these groups comprise IPANs. This example highlights the difficulties extrapolating from other bowel regions and species and emphasizes the need for further neurochemical characterization in mouse distal colon.

We were surprised by the minimal expression of calbindin (*Calb1*) and the extensive expression of calretinin (*Calb2*) in our adult mouse data. One study in mouse distal colon suggested calbindin and calretinin were present in ~30% and ~42% of neurons, respectively (328). Low read depth potentially accounts for the apparently low calbindin expression in our single-nucleus sequencing data, but it is unclear why the expression of calretinin appears so much higher in our dataset than has previously been reported. It is possible gene expression does not always translate to protein expression, or that in some neurons, calretinin is expressed at such low levels it is hard to detect with immunohistochemistry.

Role for GDNF-Gfra1-Ret signaling in mature bowel

Expression of *Gfra1* is critical for ENS development and for enteric neuron survival in colon through E18.5, but *Gfra1* gene deletion two weeks or more after birth does not have

deleterious effects (125). In rat colon, past studies showed that GDNF induced increases in substance P release and ascending contraction (320). Our data suggest GDNF application to adult colon leads to changes in neural activity patterns, including increased activity of one group of neurons and decreased activity of another. Further experiments are needed to determine the neurochemical coding of these neuron subsets.

Regulatory gene deletions in mouse models: *Tbx3* and *Etv1*

We identified a decreased proportion of nNOS+ neurons in P0 *Wnt1-Cre;Tbx3*$^{fl/fl}$ ENS, which was surprising given our prior research showing normal neuron density in P0 *Wnt1-Cre;Tbx3*$^{fl/fl}$ mutant mice (175). It is unclear if *Tbx3* mutants have increased proportions of other subtypes that compensate for the nNOS+ neuron loss (i.e. neurons are preferentially choosing a non-nNOS+ lineage), or if would-be nNOS+ neurons are appropriately lineage-restricted but not expressing the correct markers (i.e. *Tbx3* is necessary for maintaining expression of nNOS effector genes). Preliminary data (not shown) indicates that nNOS+ neuron number is normal after conditional *Tbx3* deletion in adulthood, suggesting *Tbx3* is probably not needed for maintaining a nNOS neuron identity.

The effect of reduced nNOS+ neurons on bowel function in *Tbx3* mutant mice is also unclear. Our laboratory previously reported normal small bowel transit *Tbx3 fl/fl; Wnt1-Cre* mice, but the FITC-dextran assay we used lacks spatial resolution to detect a minor delay in transit (175), no *in vitro* contractility studies were performed and we could not evaluate adult mice since these mutant mice die as neonates with cleft palate.

The lack of ChAT/nNOS neuron subtype imbalances in *Etv1-CreERT2*$^{Cre/Cre}$ mice was disappointing, particularly given that *ETV1* was detected as highly expressed in mouse and human NOS1+ neurons. Since this particular mouse model lacks certain other features expected in *Etv1* deletion mutants, we are currently evaluating if these mice truly have deletion of the *Etv1*

gene (329). Of course, ETV1 might be critical for nNOS+ neuron functions other than cell survival, like regulating axon pathfinding, synaptic connectivity, receptor or transmitter expression, and these functions would not have been uncovered by our studies.

Other regulatory genes

We noted differential expression of many other transcription factors in our dataset, both at E17.5 and in adult enteric neurons. Some of these genes were expressed at E17.5 in more immature neuron precursors, defined by the expression of GO terms indicative of neuron immaturity. Transcription factors play many roles in neuronal development, including spatial and temporal compartmentalization, cell type specification, terminal and post-mitotic differentiation, and the maintenance of subroutines defining subtype identity (330). Based on their timing of expression, we expect some of these genes play roles as terminal selectors involved in the establishment and maintenance of subtype identity. Others could play multiple roles (111). We were especially intrigued by the observation that *Zeb2* was differentially expressed in subsets of neurons. Mutations in *Zeb2* cause Mowat-Wilson syndrome, a complex neurocristopathy that includes HSCR. Interestingly, children with HSCR and Mowat-Wilson syndrome have much worse outcomes after pull-through surgery than children with isolated HSCR, and children with *Zeb2* mutations who do not have HSCR have a high incidence of chronic constipation (153, 154). It is tempting to speculate that *Zeb2* plays roles in aspects of development other than neuron migration, such as subtype specification and differentiation. *Zfhx3* is another interesting differentially-expressed gene identified in our dataset. *Zfhx3* has been implicated in neuronal differentiation in other systems, and variants of *Zfhx3* have been associated with HSCR (331). It will be important to study these and other transcription factor mutants *in vivo* in order to better understand their roles in ENS development.

The observation that *Brn1 (Pou3f3)* is limited to colon enteric neurons is also exciting, as no spatial transcriptional selectors have previously been identified in the ENS. Interestingly, in CNS, *Brn1* and a closely related gene *Brn2* seem to regulate positional control of post-migratory L2/3 neurons by inhibiting expression of retinoic acid related orphan receptor beta (332). *Brn1* has many other roles in neurogenesis, including activation of the Notch ligand Delta (333). An ENS phenotype in *Brn1-/-* mice has not been reported, but these mice die within 24 hours of birth due to renal failure, and it is possible the bowel was never examined (192). Again, it will be important to do a careful analysis of the ENS of *Brn1* mutant mice.

Challenges associated with sequencing enteric neurons in humans

Single-cell sequencing of human ENS poses significant challenges, and acquiring a comprehensive body of human enteric neuron sequencing data will likely be the next major frontier in ENS biology. Although our single-nucleus sequencing method was designed to enrich for neurons by specifically dissecting myenteric plexus, our data surprisingly had very few neurons, and we generated data from *79 times* as many glia as neurons. In contrast, our recent quantitative analysis of glia to neuron ratio in human colon by immunohistochemistry indicated a ~3:1 ratio. While we may have underestimated glia in immunohistochemical studies by focusing on myenteric ganglia, the enormously high glia:neuron ratio in our single nucleus RNA-seq dataset suggests the possibility that human neuronal nuclei are especially sensitive to Dounce homogenization compared to glial nuclei. This might occur because neuronal nuclei are much larger than glial nuclei and may be more susceptible to damage (neuronal nuclear diameter ~10-15 µM; glial nuclear diameter ~5 µM). Human neuronal nuclei may be slightly larger than mouse (~7-12 µM) enteric neuron nuclei, which might explain why we were more successful collecting single neuronal nuclei RNA-seq data in mouse than in humans using a similar strategy to isolate nuclei. Clearly, more human enteric neuron single cell sequencing data are needed to

fully define neuron subtypes, but our new data substantially advance knowledge about gene expression ENS subpopulations, leading to many new testable hypotheses. These data should facilitate stem cell biology needed for regenerative medicine and enhance our ability to make molecular diagnoses in people with chronic intestinal pseudo-obstruction where etiology remains largely undefined.

4.6 - ACKNOWLEDGMENTS

We wish to thank Dr. Emma Furth, Dr. Federico Valdivieso, Dr. Ali Naji, Caitlin Feltcher, Andrew Kromer, Lauren Schmucker, and Jennifer Finan for help coordinating tissue acquisition. Funding for the work comes from the Irma and Norman Braman Endowment, The Children's Hospital of Philadelphia Research Institute, the Suzi and Scott Lustgarten Center Endowment, NIH grants 5 F30 DK117546-02 (CMW), and RO1 DK087715 (ROH), March of Dimes 6-FY15-235 (ROH), the Burroughs Wellcome Fund Clinical Scientist Award in Translational Research (grant no. 1008525) (ROH), and from NIH SPARC Program OT2OD023859 (Marthe Howard PI, Robert Heuckeroth co-I).

4.7 - AUTHOR CONTRIBUTIONS

C.M.W., S.S., K.E., B.D., and R.O.H. designed experiments, analyzed results, and wrote the manuscript. C.M.W., S.S., F.M., K.E., D.K., M.G., S.H., and T.G. performed experiments.

4.8 - SUPPLEMENTARY MATERIAL

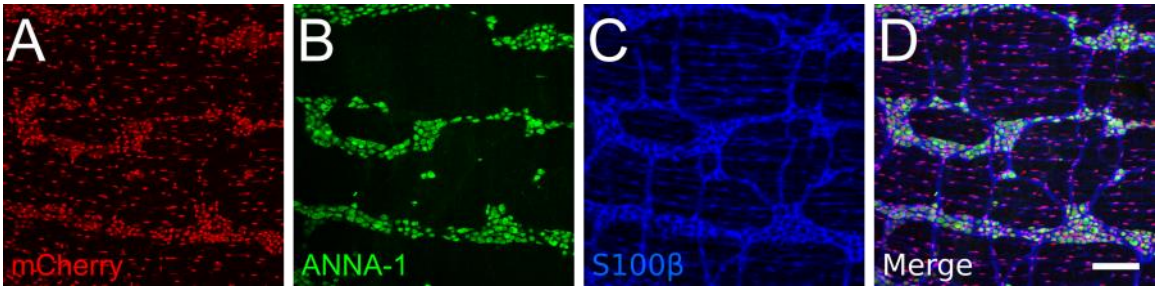

Supplementary Figure 4-1: Wnt1-Cre; H2B-mcherry mice show robust mCherry expression in colon nuclei of myenteric neurons and glia at ~50 days.
H2B-mCherry fluorescence (red) in *Wnt1-cre*$^{cre/wt}$*; R26R-H2B-mCherry*$^{ch/wt}$ mice colocalizes with ANNA-1+ neurons (green) and S100β+ glia (blue) in the ENS (A-D).

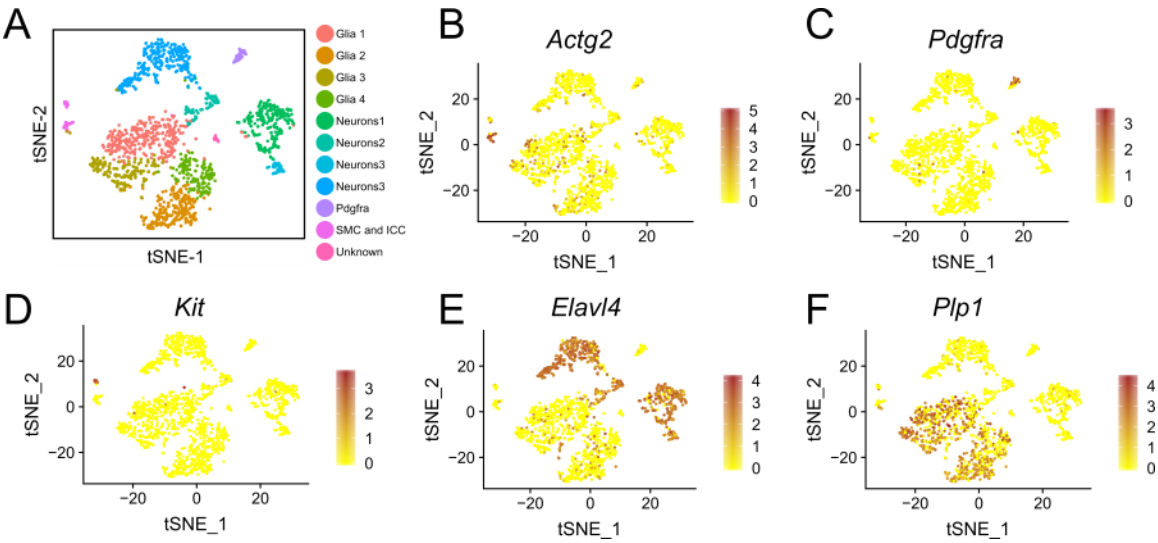

Supplementary Figure 4-2: T-SNE of all cell groups reveals *Pdgfrα*+ cells, SMCs, ICC, neurons, and glia 47-52-day old mouse distal colon.
(A) T-SNE plot of all cell groups from distal colon of *Wnt1-cre*$^{cre/wt}$*; R26R-H2B-mCherry*$^{ch/wt}$ reveals multiple cell types. (B-F) Feature plots of *Actg2* (B), *Pdgfrα* (C), *Kit* (D), *Elavl4* (E), and *Plpl1* (F) indicate the locations of SMC, Pdgfrα+ cells, ICC, neuron, and glial cell groups.

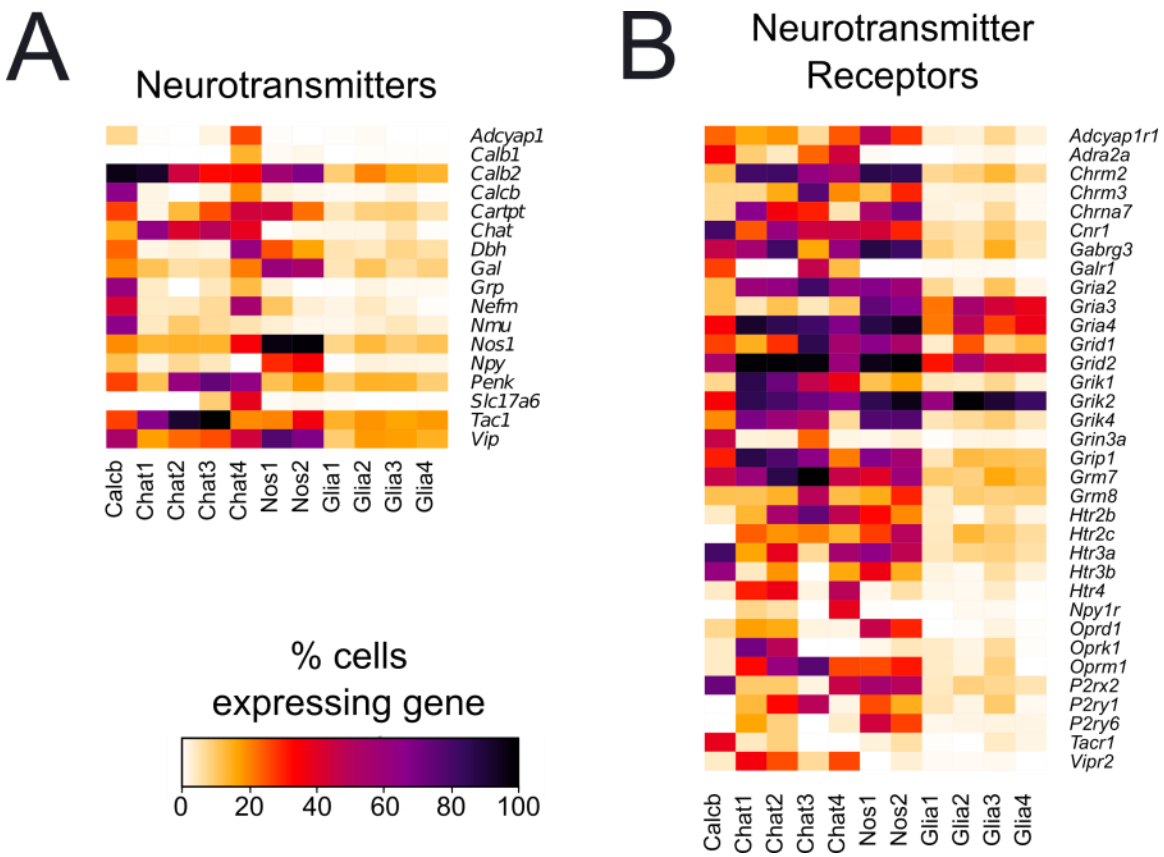

Supplementary Figure 4-3: Proportion of cells with expression greater than 0.
(A-B) Proportion of cells per group with expression values>0 for neurotransmitters (A) and neurotransmitter receptors (B). Color bar applies to both panels.

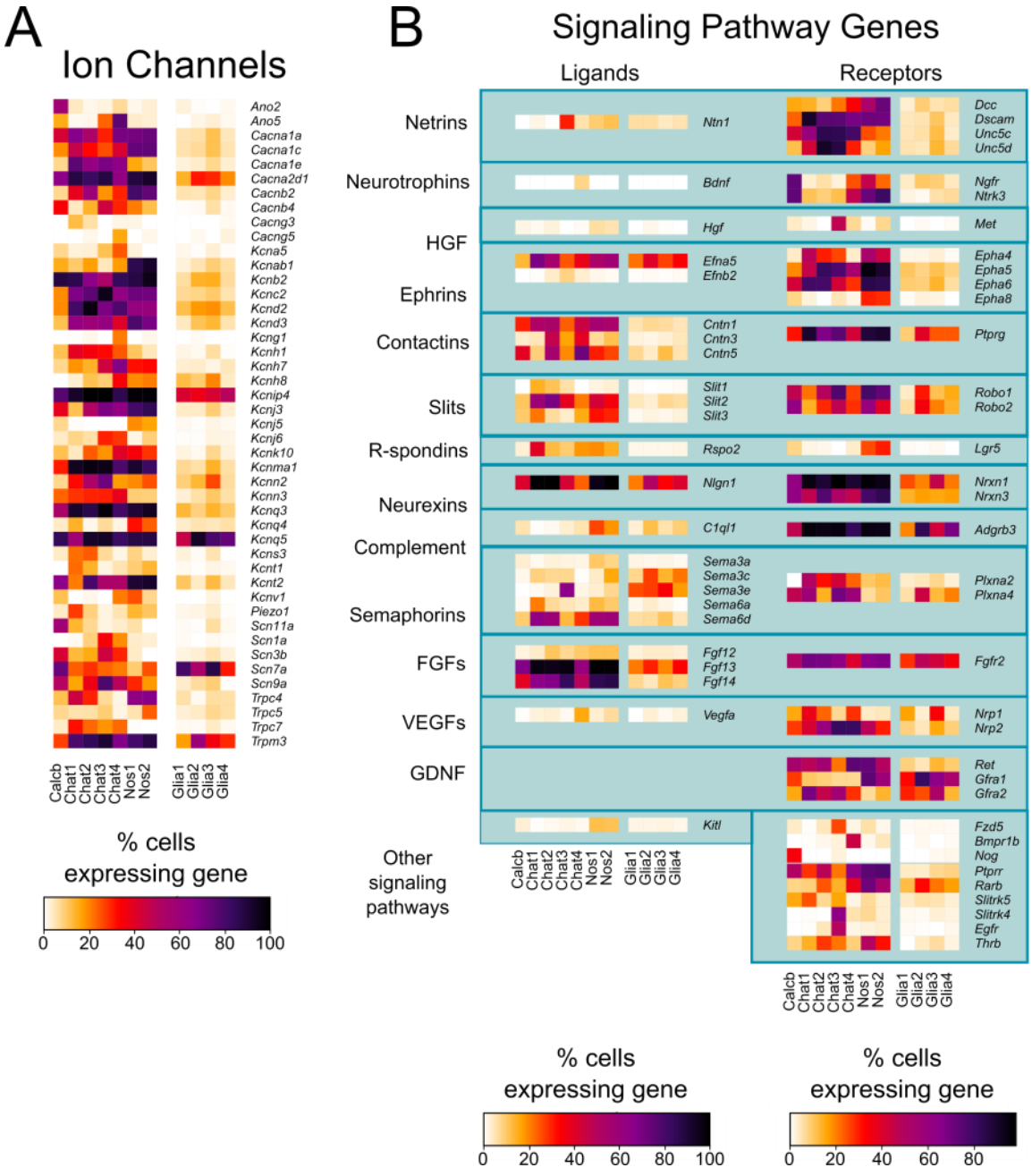

Supplementary Figure 4-4: Proportion of cells with expression greater than 0.
(A-B) Proportion of cells per group with expression values>0 for ion channels (A), ligands, and receptors (B).

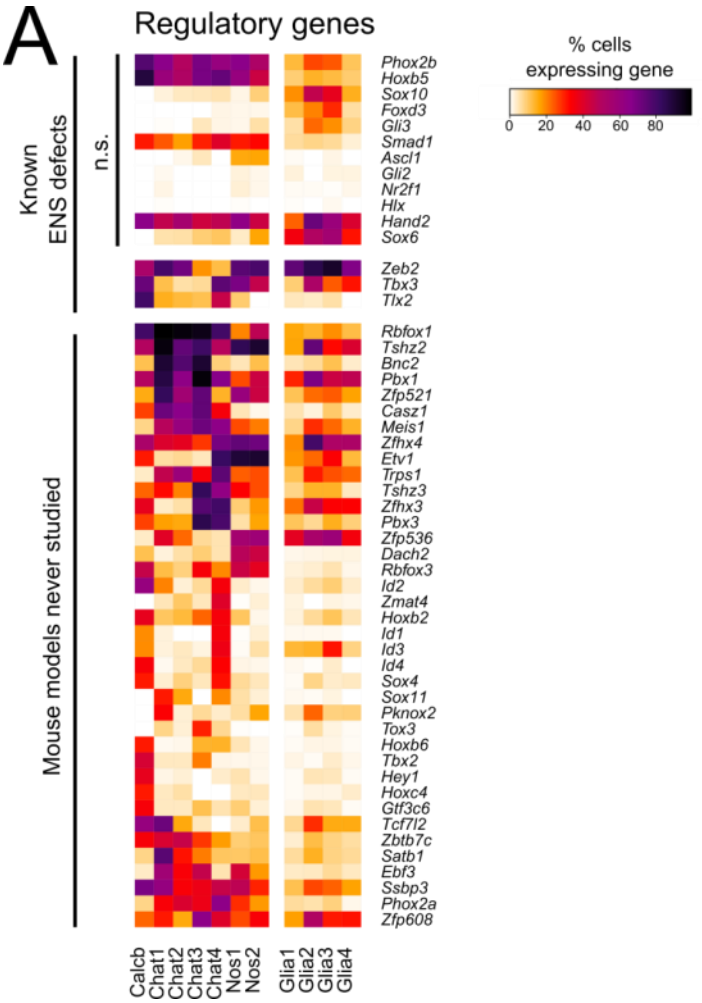

Supplementary Figure 4-5: Proportion of cells with expression greater than 0.
(A) Proportion of cells per group with expression values>0 for regulatory genes.

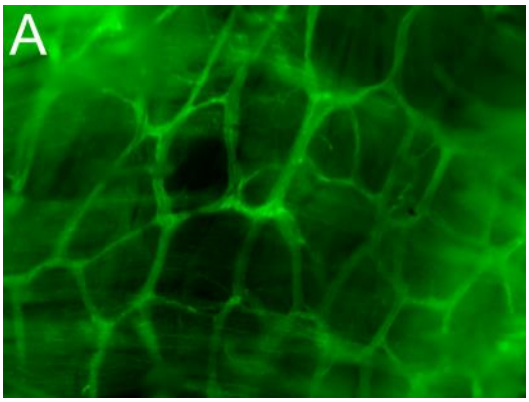

Supplementary Figure 4-6: Microdissection using 4-Di-2-Asp.
(A) Human myenteric plexus after incubation with 4-Di-2-Asp, with muscle layers partially peeled away.

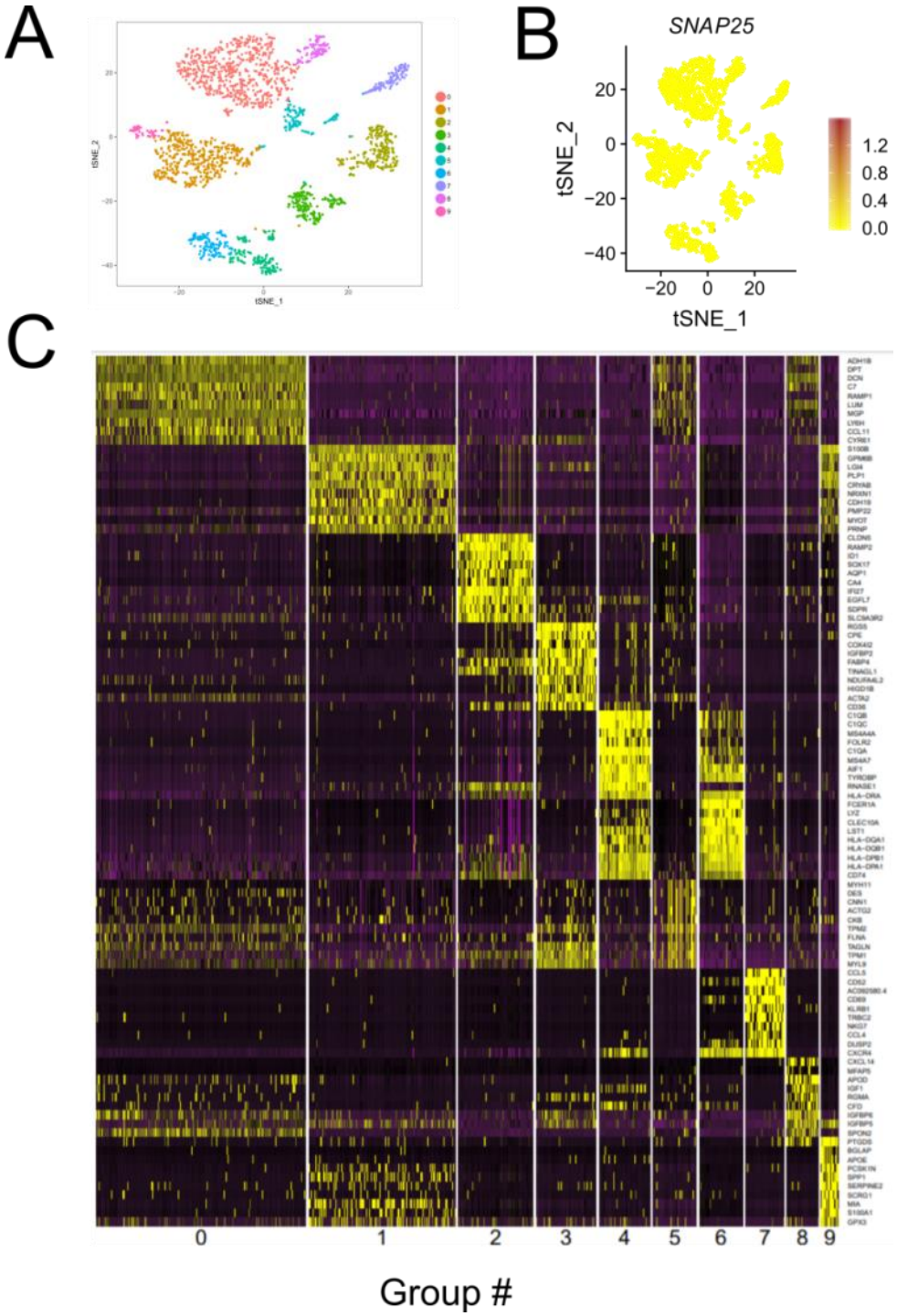

Supplementary Figure 4-7: Single-cell sequencing from whole cells micro-dissected from human colon myenteric plexus region using 4-Di-2-Asp.
(A) T-SNE plot shows multiple clusters of cells, but (B) no groups express neuronal markers *SNAP25* or *ELAVL4* (not shown because 0 cells in dataset expressed *ELAVL4*) suggesting intact neurons did not survive our isolation process. (C) Top highly differentially-expressed genes in different subgroups suggests that subgroups are mostly immune cells, smooth muscle cells, and glia.

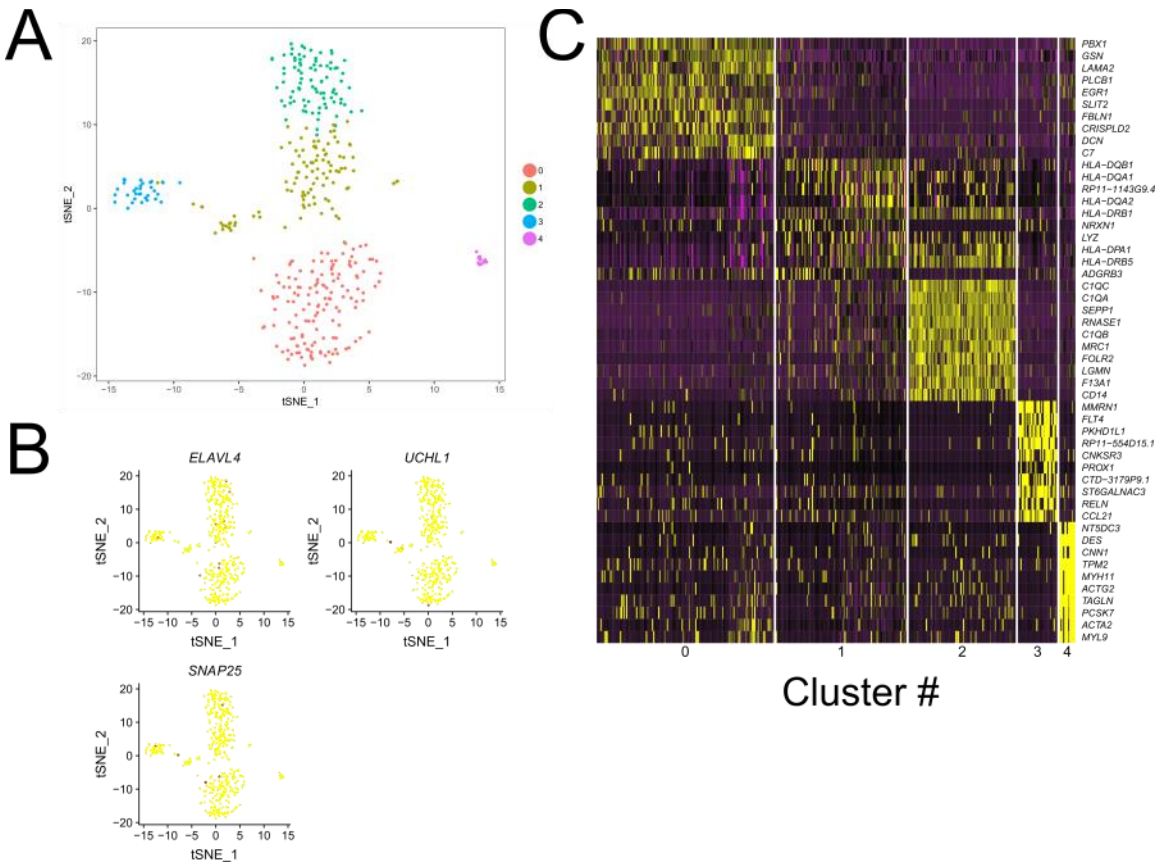

Supplementary Figure 4-8: Single-nucleus sequencing from adult human nuclei after flow sorting dissociated muscle layers using antibody against PHOX2B.
(A) T-SNE plot shows multiple clusters of cells, but (B) no groups contain the neuronal markers *ELAVL4*, *UCHL1*, or *SNAP25*. (C) Top highly differentially-expressed genes in different subgroups suggests that subgroups are mostly immune cells and smooth muscle cells.

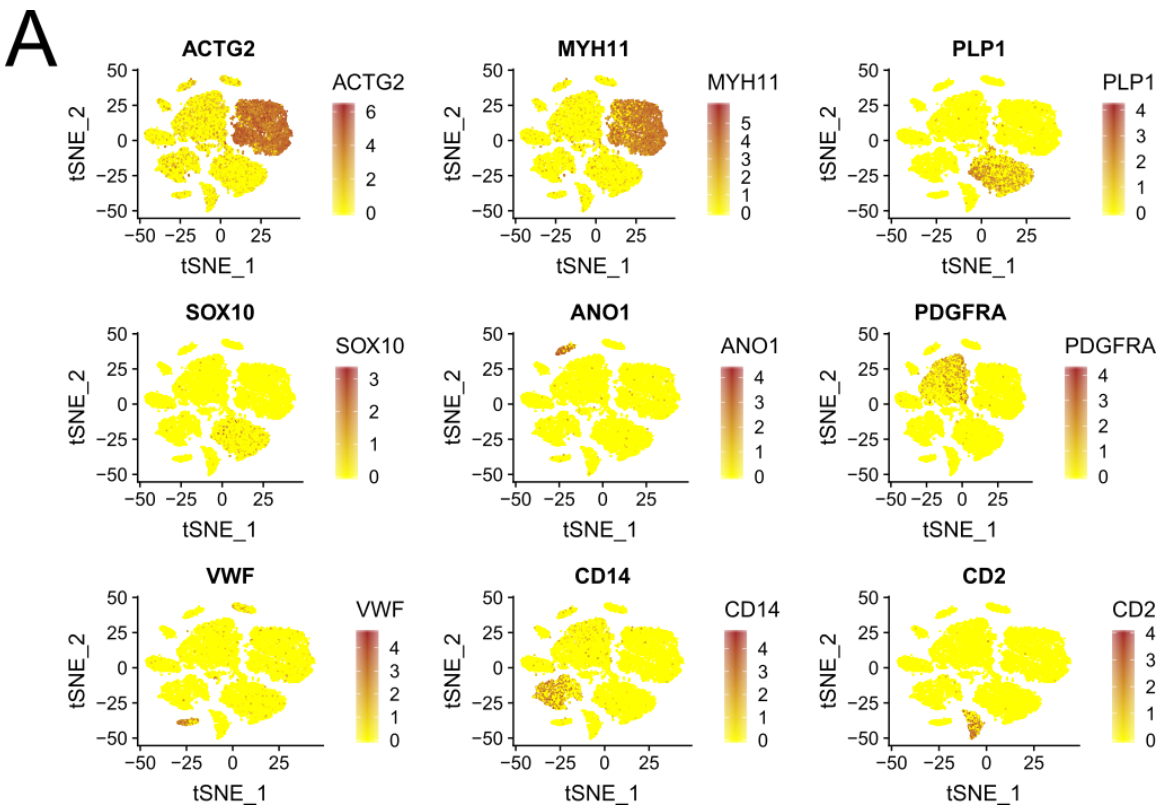

Supplementary Figure 4-9: Single-nucleus sequencing of >20,000 human nuclei reveals SMC, ICC, PDGFRA, blood vessel, muscularis macrophages, and glial cell markers. (A) Feature plots showing genes expressed highly in adult human smooth muscle (*ACTG2*, *MYH11*), glial cells (*PLP1*, *SOX10*), ICC (*ANO1*), PDGFRA+ cells (*PDGFRA*), vessel endothelial cells (*VWF*), muscularis macrophages (*CD14*), and T cells (*CD2*).

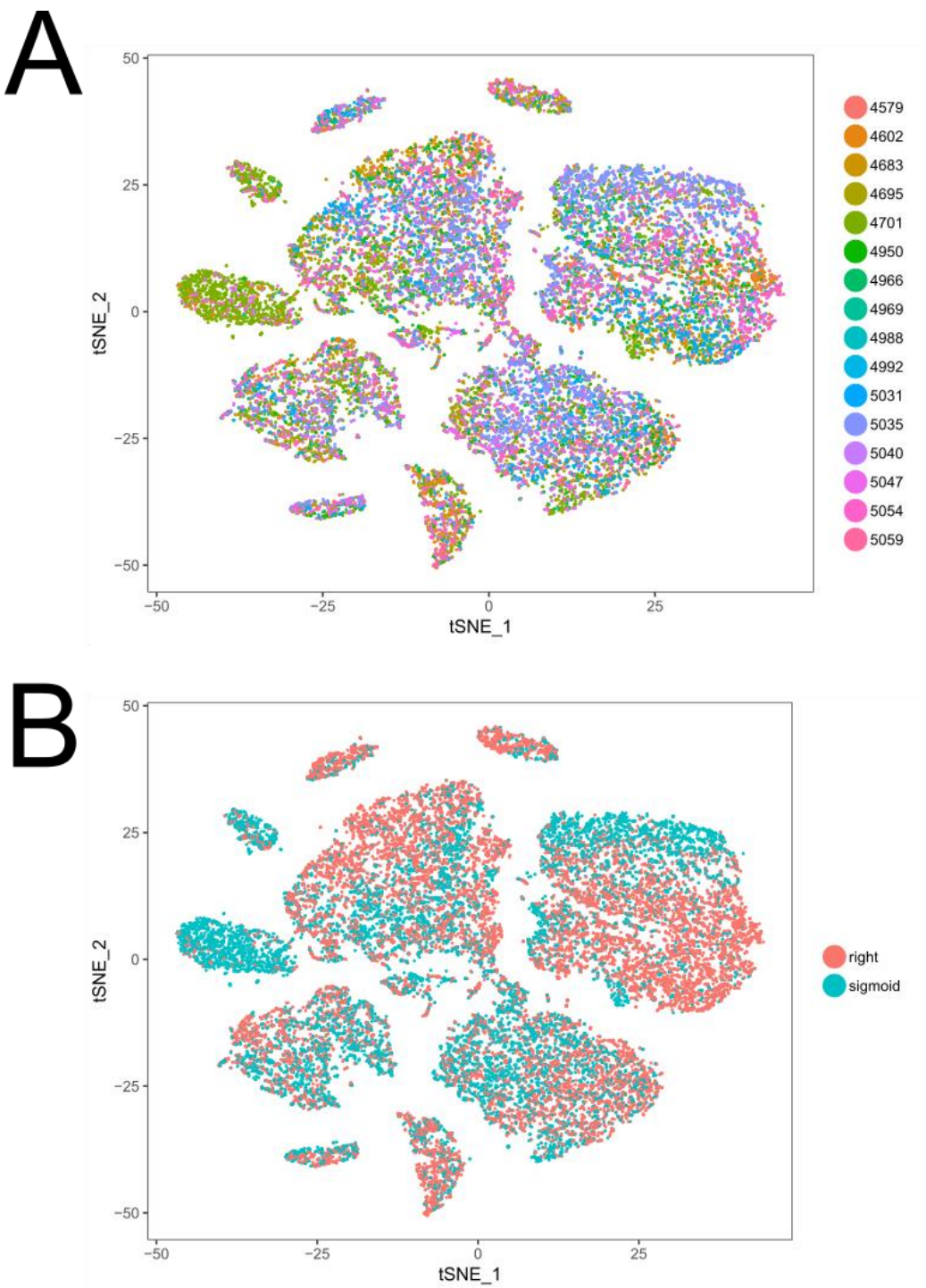

Supplementary Figure 4-10: T-SNE plots of >20,000 human nuclei colored by sample number or colon region.

(A-B) T-SNE plots of human nuclei colored by sample number (A) or colon location (right versus sigmoid; B). Cells from right and sigmoid colon largely form the same t-SNE clusters. One cluster of cells found almost exclusively only in sigmoid colon was from a subject with cancer and expressed cells that were highly KIT+ but formed a distinct cluster from ICC.

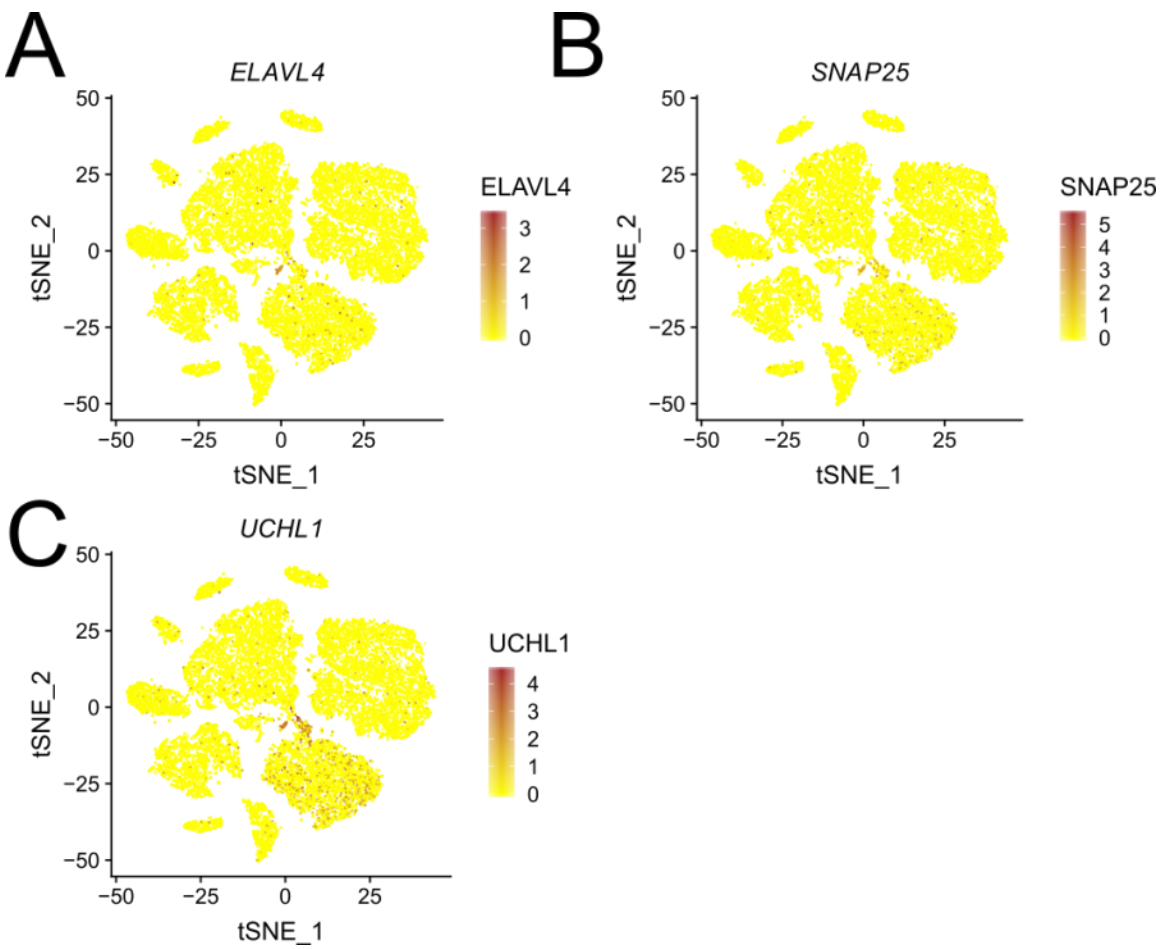

Supplementary Figure 4-11: Single-nucleus sequencing of >20,000 nuclei from human myenteric plexus and surrounding cells reveals a small population of neurons.
(A-C) Feature plots showing location of *ELAVL4* (A), *SNAP25* (B), and *UCHL1* (C) expression suggest that a small population of neurons expressing all three is present in this dataset, but most of the 20,000 nuclei are not *ELAVL4*, *SNAP25*, or *UCHL1*-positive.

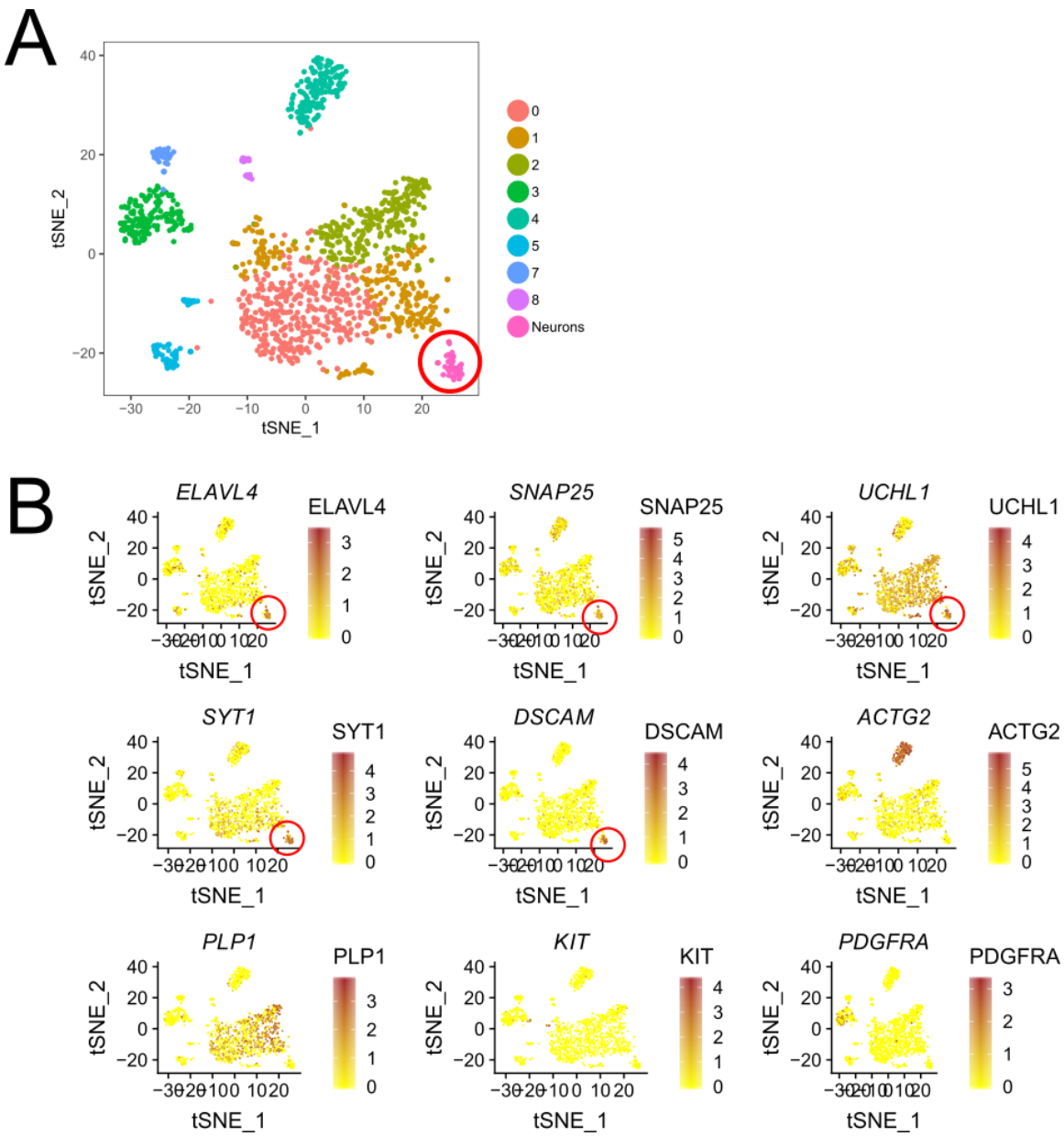

Supplementary Figure 4-12: T-SNE plot of all human nuclei expressing *ELAVL4, UCHL1,* or *SNAP25.*

(A) T-SNE plot of all human nuclei expressing *ELAVL4*, *UCHL1*, or *SNAP25* (inclusive or) reveals many populations that may be doublets because they cluster with nuclei expressing non-neuronal cell markers. For this manuscript, we only describe in detail expression data for the tight cluster of cells we believe are neurons based on high expression of *ELAVL4*, *SNAP25*, *UCHL1*, *SYT1*, and *DSCAM* (highlighted with red circle) (B) Feature plots of neuronal markers (*ELAVL4*, *SNAP25*, *UCHL1*, *SYT1*, and *DSCAM*), SMC markers (*ACTG2*), glial cell markers (*PLP1*), ICC markers (*KIT*), and PDGFRA+ cell markers (*PDGFRA*) suggest that other populations are not neurons.

Supplementary Table 4-1: Methods used to isolate cells or nuclei for RNA-seq.

Genotype	Whole cells, or nuclei?	Description
Wnt1-Cre;R26R-EGFP	Cells	The EGFP signal in *Wnt1-Cre;R26R-EGFP* animals is too weak to flow sort effectively given the high degree of background in the 488 channel.
Wnt1-Cre;R26R-tdTomato	Cells	The localization of tdTomato to neurites in our *Wnt1-Cre;R26R-Tdtomato* line is problematic, since we desire clean separation of single cells. Sorting myenteric plexus from this mouse line often results in messy preps with neurites attached to tdTomato- cells. We tried dissociating with different proteases (cold active protease, dispase and collagenase), different incubation times (15 minutes, 30 minutes), multiple methods of trituration (pipette-based, needle-based), and different bowel layers, with little improvement in outcome
Wnt1-Cre;ROSA$^{NT\text{-}NG}$	Nuclei	*Wnt1-Cre;Rosa$^{NT\text{-}NG}$* mice had tdTomato in their nuclei at baseline; with CRE-induced recombination, they accumulated GFP in their nuclei instead or tdTomato. Unfortunately, these mice lost fluorescent signal during the nuclear homogenization procedure. We hypothesize that membrane damage associated with homogenization led to diffusion of GFP and loss of signal.
Wnt1-Cre;Rosa26 LSL H2B mCherry	Nuclei	Successful and used to generate data in **Figures 4-1** through **4-4.**
Wild type	Nuclei	We attempted to use directly-conjugated NeuN antibody to isolate mouse ENS nuclei with flow sorting, since some nuclei in mouse stain with this NeuN antibody by immunohistochemistry. We were unsuccessful.

Supplementary Table 4-2: List of antibodies

Antibody	Concentration	Catalog number	Source
Rabbit anti-nNOS	1:200	AB5380	Chemicon/Millipore (Burlington, MA); RRID:AB_91824
ANNA-1 (HuC/D)	N/A	N/A	Kind gift from Dr. V. Lennon, Mayo Clinic
Goat anti-Tbx3	1:100	AF4509-SP	R&D Systems, RRID:AB_2240328
Goat anti-Phox2b	1:100	AF4940-SP	R&D Systems, RRID:AB_10889846
Rabbit anti-Satb1	1:100	ab109122	Abcam, RRID:AB_10862207
Chicken anti-GFP	1:500	#GFP-1020	Aves Labs, RRID:AB_10000240
Rabbit anti-S100β	1:200	Ab52642	Abcam; RRID:AB_882426
Rabbit anti-Pbx3	1:100	12571-1-AP	Proteintech Group; RRID:AB_2160469
Rabbit anti-Tbx2	1:100	22346-1-AP	Proteintech Group
Rabbit anti-POU3F3	1:100	HPA067151	Sigma-Aldrich, RRID:AB_2685790
Rabbit anti-RBFOX1	1:100	HPA040809	Sigma-Aldrich, RRID:AB_10796228
Guinea pig anti-vGluT2	1:200	135 404	Synaptic Systems
Goat anti-Brn1	1:100		Santa Cruz; no longer sold
Alexa Fluor goat anti-human 647	1:400	A21445	Life Technologies; RRID:AB_2535862
AlexaFluor donkey anti-rabbit 488	1:400	A21206	Life Technologies; RRID:AB_2535792
AlexaFluor donkey anti-rabbit 594	1:400	A21207	Life Technologies; RRID:AB_141637
AlexaFluor donkey anti-rabbit 647	1:400	A31573	Life Technologies; RRID:AB_2536183
AlexaFluor donkey anti-goat 594	1:400	A11058	Life Technologies; RRID:AB_2534105
AlexaFluor goat anti-chicken 488	1:400	A11039	Life Technologies; RRID:AB_142924
AlexaFluor donkey anti-goat 647	1:400	A21447	Life Technologies; RRID:AB_141844
AlexaFluor donkey anti-goat 488	1:400	A11055	Life Technologies; RRID:AB_2534102
AlexaFluor goat anti-rabbit 488	1:400	A31556	Life Technologies; RRID:AB_221605

Supplementary Table 4-3: RT-PCR Primers

Gene	Primer Sequence	Band size	Genotyping solution	Reference
Brn1 (mouse)	5'-CAACAGCCACGACCCTCACT-3' 5'-CAGAACCAGACCCGCACGAC-3'	450 bp	KAPA (Roche)	(334)
Brn1 (human)	5'-TTGGCGCTGGGCACACTCTA-3' 5'-CCTTGACGCTCACCTCGATAG-3'	223 bp	KAPA	(335)
Actb (mouse)	5'-GAGAGGGAAATCGTGCGTGAC-3' 5'-AGCTCAGTAACAGTCCGCCTA-3'	534 bp	KAPA	(171)

Supplementary Table 4-4: Characteristics of colon resection samples

Sample ID	Age	Sex	History	Colon region	RNA Integrity #: Plexus	RNA Integrity #: Surrounding muscle
4579	54	M	Cecal polyp	Right colon	7.6	7.9
4602	75	M	Hx of cecal lesion	Right colon	7.5	6.9
4683	38	M	Goblet cell carcinoma	Right colon	7.9	8
4695	77	F	Colonic mass	Right colon	7.4	7.4
4701	78	M	Rectal cancer	Sigmoid colon	8.2	6.3
4950	78	M	Bowel obstruction	Sigmoid colon	6.50, 6.90, and 7.10 (3 pieces)	7.6
4969	83	M	Adenocarcinoma	Right colon	6.5	7.90, 5.80 (2 pieces)
4966	71	F	Bowel obstruction	Right colon	7.2	8.1, 7.9 (2 pieces)
4988	65	F	Colon polyp	Right colon	5.20 and 2.90 (RNA conc. v low)*	7.5 and 7.4 (2 pieces)
4992	47	M	Rectal carcinoma	Sigmoid colon	4.4 (RNA conc v. low)*	7.1
5031	70	M	Colon polyp	Right colon	7.8	7.4 and 7.2
5035	24	M	Volvulus	Sigmoid colon	8	6.6 and 7.2
5040	44	M	Colonic mass	Right colon	7.7	7.5 and 7.8
5047	65	M	Rectal adenocarcinoma	Sigmoid colon	6.6	7.4
5054	36	F	Bowel adhesions	Right colon	7.6	7.20 and 7.70
5059	59	F	Adenocarcinoma	Right colon	7.2	7.50 and 6.40

Supplementary Table 4-5: UMI and gene counts from colon resection samples.

Sample ID	Cells or nuclei loaded (predicted from FACS)	# of Cells	Ratio to cells loaded	Avg UMI count with intronic reads mapped	Avg gene count with intronic reads mapped
4579	4000	680	0.17	2,474	1,559
4602	6900	2,316	0.3356522	2,004	1,268
4683	6300	2,081	0.3303175	1,397	876
4695	4000	833	0.20825	1,487	974
4701	12300	4,414	0.3588618	1,296	780
4950	5200	1,237	0.2378846	1,415	910
4969	5300	653	0.1232075	1,262	1,262
4966	2100	432	0.2057143	1,856	1,193
4988	1200	237	0.1975	2,354	1554
4992	673	60	0.089153	3,939	2336
5031	5200	1728	0.3323077	1,538	967
5035	7100	2524	0.355493	1,886	1119
5040	2300	755	0.3282609	1,941	1212
5047	5000	957	0.1914	1,701	1013
5054	3100	1219	0.3932258	2,071	1216
5059	1200	338	0.2816667	2470	1474

CHAPTER 5 : DOWN SYNDROME MOUSE MODELS HAVE AN ABNORMAL ENTERIC NERVOUS SYSTEM

This chapter has been published in *JCI Insight* and reprinted here with permission: Schill, EM*, **Wright CM***, Jamil A, LaCombe JM, Roper RJ, Heuckeroth RO. Down syndrome mouse models have an abnormal enteric nervous system. *JCI Insight.* 2019 Apr 18;5. pii: 124510. doi: 10.1172/jci.insight.124510. Copyright©2019 the authors

* Co-first authors; contributed equally

5.1 ABSTRACT

Children with trisomy 21 (Down syndrome [DS]) have a 130-fold increased incidence of Hirschsprung Disease (HSCR), a developmental defect where the enteric nervous system (ENS) is missing from distal bowel (i.e., distal bowel is aganglionic). Treatment for HSCR is surgical resection of aganglionic bowel, but many children have bowel problems after surgery. Post-surgical problems like enterocolitis and soiling are especially common in children with DS. To determine how trisomy 21 affects ENS development, we evaluated the ENS in two DS mouse models, Ts65Dn and Tc1. These mice are trisomic for many chromosome 21 homologous genes, including *Dscam* and *Dyrk1a*, which are hypothesized to contribute to HSCR risk. Ts65Dn and Tc1 mice have normal ENS precursor migration at E12.5 and almost normal myenteric plexus structure as adults. However, Ts65Dn and Tc1 mice have markedly reduced submucosal plexus neuron density throughout the bowel. Surprisingly, the submucosal neuron defect in Ts65Dn mice is not due to excess *Dscam* or *Dyrk1a*, since normalizing copy number for these genes does not rescue the defect. These findings suggest the possibility that the high frequency of bowel

problems in children with DS and HSCR may occur because of additional unrecognized problems with ENS structure.

5.2 INTRODUCTION

Children with Down syndrome (DS, trisomy 21) have high rates of congenital heart disease, central nervous system dysfunction (i.e., behavioral and emotional problems, Alzheimer's disease, seizures), vision problems, hearing loss, infections, hypothyroidism, leukemia, poor muscle tone, atlantoaxial dysplasia (an upper spine defect), dental problems, and gastrointestinal disease (duodenal atresia, anal atresia, celiac disease and Hirschsprung disease) (336). Even without serious bowel disease, children with DS commonly have chronic constipation or diarrhea (87, 88). One major challenge is defining which genes on human chromosome 21 (Hsa21) cause each disease manifestation and what structural and functional problems underlie symptoms. Here we examine how trisomy affects enteric nervous system (ENS) development and bowel function using two DS mouse models.

The ENS is a complex network of neurons and glia that autonomously controls most aspects of bowel function (106, 134, 337). Abnormal ENS development can be life-threatening, especially when the ENS is missing from distal bowel, a problem called Hirschsprung disease (HSCR). The ENS is derived from diverse cell sources. Most ENS precursors are enteric neural crest derived cells (ENCDC) originating from somite levels 3-7. These ENCDC invade the foregut by mouse embryonic day 9.5 (E9.5), proliferate, and migrate distally to fully colonize developing bowel by E14.5. Additional ENCDC in esophagus and stomach are derived from somite levels 1-2, while sacral neural crest and pelvic Schwann cell-derivatives contribute to ENS in descending colon and rectum (107, 108). Recent papers suggest cells of endodermal origin also contribute to the ENS (109) and that there is continuous ENS replacement during postnatal life (115). Independent of cell origin, initial longitudinal colonization of the bowel by ENCDC occurs in the region of future myenteric plexus. After longitudinal migration is complete, a subset of ENS precursors migrates inward toward the lumen to form the submucosal plexus, in a process called radial migration (124, 337, 338). These inner submucosal plexus and outer myenteric

plexus cells comprise the ENS and work together to regulate fluid secretion, blood flow, and motility needed for survival.

HSCR occurs in 1 in 5000 live births (64), but strikingly, HSCR incidence is about 1 in 40 in children with DS (86, 339). The primary problem in HSCR is that migrating ENCDC fail to completely colonize distal bowel, leaving a region of aganglionic bowel that tonically contracts and does not have normal propulsive motility, leading to functional obstruction. Diverse HSCR symptoms and data from animal models suggest additional ENS defects may occur in children with HSCR (57, 71, 340, 341). Standard HSCR treatment is surgical resection of aganglionic bowel and re-anastomosis of ENS-containing proximal bowel to near the anal verge. While this "pull-through" surgery is life-saving, many children experience problems after surgery including enterocolitis, constipation, and fecal incontinence (64, 65). These problems are especially common in children with DS (85, 342). We suspect some post-surgical problems result from subtle defects in ENS structure or function, including altered neuron number, connectivity, and differentiation, but methods to identify these defects in human bowel are not well established. The higher prevalence of HSCR in children with DS has also not been explained, although it is likely due to overexpression of one or more Hsa21 genes.

One longstanding hypothesis is that overexpression of *Down Syndrome Cell Adhesion Molecule (DSCAM)* explains increased HSCR risk in people with DS (77). Consistent with this hypothesis, *DSCAM* is one of ~160 genes in the HSCR-associated critical region in individuals with rare partial trisomy 21 (78). Furthermore, *DSCAM* mRNA is present in migrating ENS precursors (75), and recent genetic studies identified selected *DSCAM* SNPs at increased frequency in individuals with HSCR (76, 77). Additionally, DSCAM is a receptor for netrin (343, 344), a protein that attracts ENCDC to submucosal plexus (338). Despite these suggestive data, *DSCAM* function in ENS development has not been evaluated.

Another HSCR critical region-associated gene identified in partial trisomy is Dual-specificity tyrosine phosphorylation-regulated kinase, *DYRK1A* (78). DYRK1A is expressed in adult human colon ganglia (Human Protein Atlas) (345) and *Dyrk1a* is transcribed in mouse ENS precursors (GenePaint) (216). DYRK1A phosphorylates and activates GLI1 (79), an important Hedgehog pathway protein whose overexpression is implicated in some human HSCR cases (80, 81). In brain, *DYRK1A* overexpression lengthened G1, leading to fewer cell divisions and cortical neuron deficits persisting into adulthood (82-84). However, the role of *DYRK1A* in ENS development has not been explored.

To examine how trisomy predisposes to HSCR and other ENS defects, we studied two commonly used mouse trisomy 21 models, Ts65Dn and Tc1. Neither model perfectly recapitulates DS since human chromosome 21 has mouse orthologs on parts of mouse chromosomes (Mmu) 16 (28 Mb), 17 (1.5 Mb), and 10 (3 Mb). Ts65Dn (B6EiC3Sn a/A-Ts(17<16>)65Dn/J), the most commonly studied mouse DS model (346), has a freely segregating chromosome that includes the distal end of Mmu16 attached to the centromeric end of Mmu17 (including ~25 protein coding Mmu17 genes). Ts65Dn mice are trisomic for ~55% of protein-coding Hsa21 orthologous genes (347), including HSCR risk candidate genes *Dscam* and *Dyrk1a* (78). The resulting partial trisomy has been used to model many molecular, anatomic, and behavioral aspects of DS in mice, but an ENS phenotype in this model has not been reported (346, 348-354). Ts65Dn mice might be a particularly good HSCR model since they have three copies of almost all genes identified in the HSCR critical region in humans (78). Another DS mouse model is the B6129S-Tc(HSA21)1TybEmcf/J line known as Tc1 (355, 356). This transchromosomal model has most of human chromosome 21 integrated into its genetic material, including the HSCR critical region containing *DSCAM* and *DYRK1A*. This model has limitations including mosaicism of the human chromosome (with retention of Hsa21 in as few as 49% of cells for some organs (355)), interspecies gene differences, duplications, deletions, and structural

rearrangements (356). Because Ts65Dn and Tc1 have three copies of some, but not all of the same genes, comparing outcomes in these models allows refinement of gene regions that lead to DS-associated bowel phenotypes (78).

Here we show that Ts65Dn and Tc1 mice have neurons throughout the bowel including in distal colon, and that longitudinal migration of ENCDCs during development is normal. However, adult trisomic Ts65Dn mice have reduced neuron density in distal colon, and both Ts65Dn and Tc1 mice have marked submucosal plexus hypoganglionosis. Reduced submucosal neuron density is not accompanied by altered neuron subtype ratios and the defect is not corrected by normalizing gene copy number for *Dscam* or *Dyrk1a* in Ts65Dn trisomic mice. Although small bowel motility in Ts65Dn and Tc1 mice is normal, colon motility and stooling patterns in Ts65Dn trisomic mice are abnormal, consistent with enteric neuron defects. These results suggest that genes present in triplicate in two mouse models for DS are important for submucosal plexus formation and for bowel function. Our results challenge the longstanding hypothesis that *Dscam* is important for ENS precursor migration down developing bowel and may provide insight into the increased incidence of post-surgical problems in children with DS and HSCR.

5.3 MATERIALS AND METHODS

Animals

Dscam mice on a C57BL/6J background were from Dr. Robert Burgess at The Jackson Laboratory (Stock Number 008000). The B6EiC3Sn *a*/*A*-Ts(17^{16})65Dn/J (referred to as Ts65Dn) mice were from Jackson Laboratory (Stock Number 001924). Male Ts65Dn mice are subfertile, and Ts65Dn females breed poorly. Unless otherwise stated, all Ts65Dn mice were maintained on the same recombinant inbred background as at The Jackson Laboratory (B6EiC3Sn). Trisomic mice with two copies of *Dscam* were generated by breeding *Dscam*+/- males (C57BL/6J) to trisomic Ts65Dn females (B6EiC3Sn). These mice were maintained by strictly breeding brothers

and sisters for 3-4 generations and analyzing offspring from each generation. Some Euploid, *Dscam*+/+ and Ts65Dn, *Dscam*+/+/+ mice on this mixed B6EiC3Sn x C57BL/6J background were used in functional studies. *Dyrk1a* mice were originally generated by Dr. Mariona Arbones (357). Ts65Dn mice with two copies of *Dyrk1a* (Ts65Dn, *Dyrk1a*+/+/-) were generated by breeding *Dyrk1a*+/- males to Ts65Dn females. These mice were maintained on a ~50% C57BL/6J and ~50% C3H/HeJ background as described (358). The B6129S-Tc(HSA21)1TybEmcf/J (referred to as Tc1) were from Jackson Laboratory (Stock Number 010801) and maintained on a C57BL/6 X 129S8/SvEv background by breeding Tc1 females to euploid males. *Ret*+/- mice on a C57BL/6J background have been previously described (221). Ts65Dn, *Ret*+/+/- mice were generated by breeding Ts65Dn females (B6EiC3Sn) to *Ret*+/- males (C57BL/6J).

Adult myenteric and submucosal plexus whole mount bowel preparations

Whole gut from adult mice (80-120 days old) was processed as described (359). Briefly, bowel was rinsed in cold phosphate-buffered saline (PBS). Entire colon and 5 cm mid-small intestine were opened along the mesenteric border and pinned flat onto Sylgard® 184 Silicone Elastomer (Dow Corning). Flattened gut was fixed (4% paraformaldehyde, 30 minutes, room temperature), and muscle layers were separated from submucosa by careful dissection. Samples were cut into 1 cm pieces and stored in 50% glycerol/50% PBS (-20ºC) until staining. For villus analysis, muscle layers were not separated from submucosa. Thin (~1 mm) cross-sectional pieces of bowel containing multiple villi were cut with a scissors prior to staining. Mid-small intestine, mid-colon, and distal colon were used for all described analysis unless noted.

Submucosal plexus analysis at P1

P1 mice were injected intraperitoneally with EdU (12.5 µg/g; Click-iT® EdU Alexa Fluor® 488 Imaging Kit, Thermo Fisher Scientific, #C10337) and maintained on a far infrared warming pad (Kent Scientific; DCT-20) at 30 °C. After 4 hours, mid-small bowel was dissected, pinned flat and fixed (4% paraformaldehyde). Muscle was dissected off submucosa and tissue was stored in 50% glycerol/50% PBS (-20°C) until staining.

Immunohistochemistry and enzymatic staining

Adult bowel stored in glycerol was washed twice in PBS and blocked (room temperature (RT), one hour or 4°C overnight) in Tris-Buffered Saline/0.1% Triton X-100 (TBST) or PBS/0.1% Triton X-100 (PBST) containing 5% Normal Donkey Serum (Jackson ImmunoResearch Laboratory). Primary antibody incubations were 4°C overnight. Antibody details are in Supplementary Table 1. Tissues were washed 3X in TBST or PBST and incubated in secondary antibody (one hour, RT). NADPH-diaphorase staining was performed as described (223). Briefly, Nitro Blue Tetrazolium (NBT; Roche) and NADPH (Sigma) were dissolved in PBS with 0.2% Triton-X. Samples were incubated for 15-30 minutes at 37°C to develop blue color. After PBS washes, samples were stained with antibodies as described above. Samples were mounted on glass slides in 50% glycerol/50% PBS. For P1 analyses, all above steps were followed except submucosa was pinned flat on Sylgard®-treated 48-well plates during staining to maximize antibody exposure. EDU labeling was performed using the Click-iT® EdU Alexa Fluor 488® Imaging Kit (Thermo Fisher Scientific, #C10337).

Quantitative analysis of whole gut samples

For E12.5 mice, we measured total colon length from tip of cecum to end of colon and also position of most distal TuJ1+ nerve fiber as previously described (61). Neuron density, glial cell density, and neuronal subtype analyses were performed by counting all stained cells in 10

randomly selected 20x fields from each sample. All counting was done by observers blinded to genotype.

Midgut slice explant culture

E12.5 mouse small bowel was cut into 300-500 μM slices, plated on fibronectin-coated (250 μg/mL; Life Technologies) plastic or glass Lab-Tek Permanox chamber slides (ThermoFisher) and incubated in OptiMem (Life Technologies) supplemented with 2 mM L-glutamine (Life Technologies), 100 IU/mL penicillin, 100 μg/mL streptomycin (Life Technologies). GDNF (100 ng/mL final concentration) was added to cultures four hours after plating. Sixteen hours after GDNF addition, cultures were fixed (4% paraformaldehyde, RT, 20 minutes) and immunostained with RET antibody (Neuromics), phalloidin (to highlight F-actin) and 4',6-Diamidino-2-Phenylindole, Dihydrochloride (DAPI). Distance between farthest-migrating ENCDC and gut slice edges were measured for eight slices per chamber well.

Small bowel transit assay

Adult mice fasted overnight were gavage-fed 100 μL FITC-Dextran (10 mg/mL, Molecular Weight 70,000 (Sigma, #46945)) dissolved in 2% methylcellulose (Sigma, #274429) in water. After 1 hour (Tc1) or 2 hours (Ts65Dn), bowel was removed and divided into 10 segments for small bowel, 2 segments for cecum, and 3 segments for colon. Each bowel segment was placed in 400 μL PBS, vortexed 15 seconds, and spun 10 minutes (4000 RCF) to pellet tissue and debris. 100 μL supernatant was analyzed using a 96-well plate reader (Turner Biosystems Modulus II Microplate Multimode Reader). A weighted geometric mean was calculated as (segment number x FITC fluorescence) / total FITC fluorescence, as described (360).

Microscopy

Images were acquired using Zeiss Axio Imager.A2, Axio Observer.A1, or LSM 710 microscopes, and Zeiss Zen software. ImageJ was used for image processing, which was limited to stitching multiple fields, rotating, cropping, and uniform color adjustments. Confocal images show single optical projections or maximum intensity projections.

Colonic bead expulsion assay

Adult mice were anesthetized with isoflurane for 1.5 minutes. A glass bead (3 mm, Sigma #Z143928) lubricated with sunflower seed oil (Sigma S5007) was inserted 2 cm into colon using a custom-made 3 mm rounded glass rod. Mice were placed in empty cages and time to bead expulsion was recorded. Assay was repeated three times per mouse with >48 hours between procedures. Tc1 and controls were food-deprived overnight prior to testing, but Ts65Dn and controls were not food-deprived before testing.

Bowel motility in vitro

Colons from adult Ts65Dn and euploid littermates were rapidly and immediately placed in warmed (37°C), oxygenated (95% O_2 and 5% CO_2) physiological saline (Krebs-Ringers Solution; 118 mM NaCl, 4.6 mM KCl, 2.5 mM $CaCl_2$, 1.2 mM $MgSO_4$, 1 mM NaH_2PO_4, 25 mM $NaHCO_3$, 11 mM D-Glucose, pH 7.4). Intestinal contents were emptied by gently flushing bowel with physiological saline using a needle attached to a 20 mL syringe. Distal-most centimeter of bowel was removed and fixed (4% paraformaldehyde) for immunohistochemistry. Remaining colon was maintained in a continually-perfused physiological saline organ bath (Hugo Sachs Elektronik Harvard Apparatus D-79232) with a flow rate of 9 mL/min. The colon was cannulated and intraluminal pressure was maintained using a liquid reservoir connected to the proximal colon raised to 2 cm above the fluid level in the organ bath. The outflow tube from the colon ended at 1 cm above the fluid level in the organ bath to induce continuous flow of Krebs-Ringer

solution through the bowel. Cannulation in this manner reliably elicits CMMCs in adult mouse colon. After a 15 minute equilibration, video was recorded for 1 hour.

Video Imaging

Videos were captured using an E-PM1 Olympus digital video camera mounted on a dissecting microscope (15 frames per second, 1,920x1,080 pixel resolution). Gut was well-illuminated to accentuate contrast with the darker background. Videos were converted from MTS to WMV format using Windows Movie Maker. Spatiotemporal maps were generated using MATLAB (MathWorks) code we generated. The MATLAB code is freely available on GitHub. Briefly, a video frame was thresholded to distinguish gut from background. This thresholded image was used to measure bowel width at each point along the bowel length, generating a one-dimensional array of widths. This process was repeated for relevant video frames (relevance was determined by desired sampling frequency) to generate a two-dimensional spatiotemporal map. CMMCs (defined as contractions that extend at least half the length of the spatiotemporal map) were quantified by a trained investigator blinded to condition.

Stool collection

Animals were placed in individual bedding-free cages with free access to food and water (361). One hour later, fecal pellets were collected, weighed to determine “wet” weight and placed on a 100^{o}C heat block in open tubes overnight to dry. Pellets were then weighed to determine “dry” weight and stool water content was computed as (wet weight - dry weight)/wet weight.

Statistics

SigmaPlot 11.0 (Systat Software) and Prism 7.03 (GraphPad Software) were used for statistical analyses. When comparing two groups, a two-sided Student's t-test was used unless

assumptions were not met, in which case a Mann-Whitney Rank Sum Test (MWRST) was used. Multi-group analyses were performed using one-way ANOVA with *post hoc* multiple-comparisons tests (Tukey). Data represent mean ± standard error of the mean (SEM). A cutoff of $p<0.05$ was considered significant. All experiments used at least three biological replicates. All quantifications were performed by investigators blinded to condition.

Study approval

All animal experiments were approved by the Children's Hospital of Philadelphia Institutional Animal Care and Use Committee (IACUC).

5.4 RESULTS

Ts65Dn and Tc1 have normal-appearing mid-gestation ENS

Because human DS increases HSCR risk 130-fold, we hypothesized ENS in Ts65Dn and Tc1 mice might be abnormal. Aganglionosis, however, would be uncommon in a mouse completely recapitulating human DS, since only about 1 in 40 children with DS has HSCR (86). Unsurprisingly (since aganglionosis is fatal), adult Ts65Dn and Tc1 trisomic mice analyzed all had neurons in distal colon (Ts65Dn: n=6, Tc1: n=7). We also did not detect statistically significant death by weaning when many mice with HSCR-like disease tend to die (43.75% Ts65Dn, p=0.4786, Chi^2 test, n=36 (euploid) and n=28 (Ts65Dn); 42.7% Tc1, p=0.106, Chi^2 test, n=71 (euploid) and n=53 (Tc1)) (129, 156), although larger cohorts of Ts65Dn and Tc1 mice have shown significant reductions of trisomic offspring (355, 362). To determine if trisomy slows ENCDC migration through fetal bowel or reduces neuron density, we stained embryonic day 12.5 (E12.5) hindgut with TuJ1, an antibody against neuron specific beta-3 tubulin (**Figure 5-1A-D**). We found the extent of bowel colonization by ENCDC was normal compared to age- and strain-

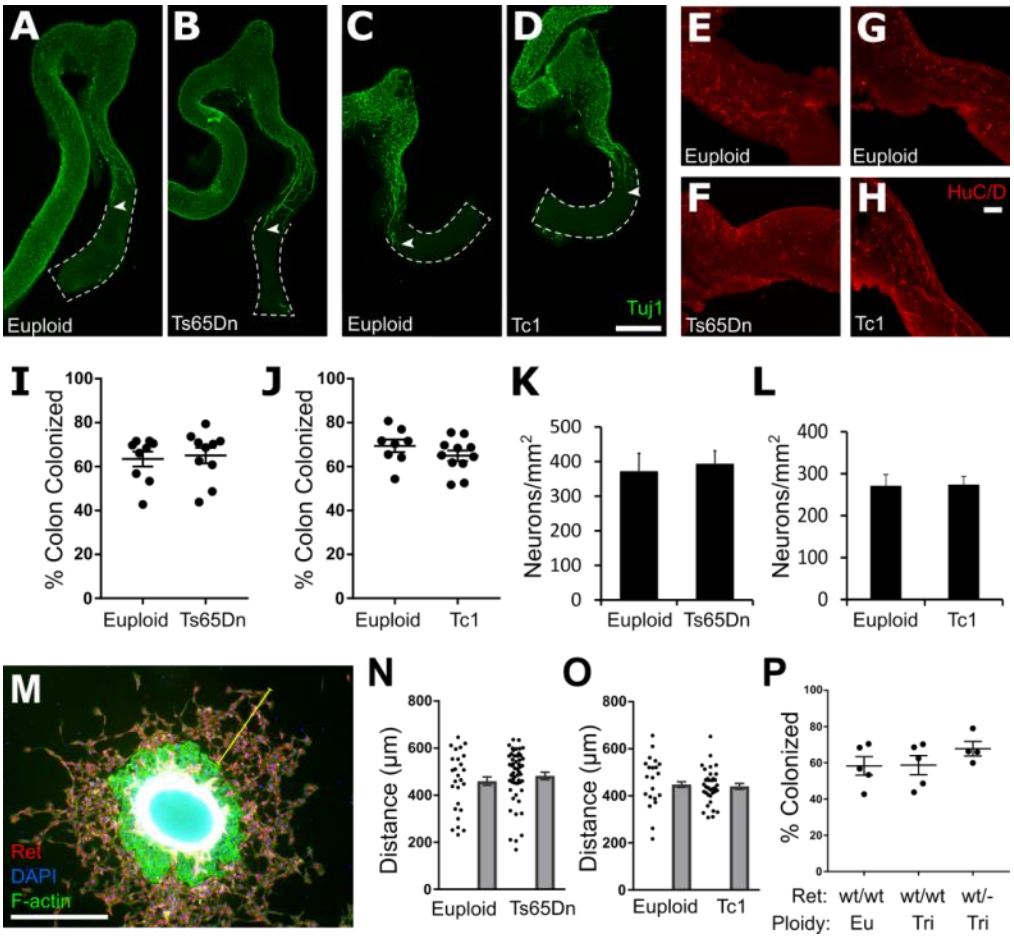

Figure 5-1: Tc1 and Ts65Dn mice have normal bowel colonization by ENS precursors at E12.5.

(A-D) Ts65Dn and Tc1 euploid and trisomic E12.5 colon and distal small bowel were stained using Tuj1 antibody that marks early and mature neurons. Maximum intensity projections of confocal Z-stacks are shown. White arrowheads indicate position of most caudal TuJ1 immunoreactive neuronal process (green); scale bar = 500 µm. (E-H) High-resolution images show HuC/D+ cell bodies (red) in hindgut in Ts65Dn (E, F) and Tc1 (G, H) lineage mice. Scale bar = 100 µm. (I, J) Percent colon colonized by ENCDC relative to total colon length for Ts65Dn (I; p = 0.653, Mann-Whitney Rank Sum Test (MWRST), n=9 (wt) and 10 (Ts65Dn)) and Tc1 (J; p = 0.24, t-test, n=9 (wt) and 11 (Tc1)) mice. (K, L) Mean HuC/D+ neuron density in most distal 500 µm of colonized bowel for Ts65Dn (K, p=0.76; t-test, n=3 (wt), n=7 (Ts65Dn)) and Tc1 (L, p=0.94, t-test, n=7(wt), n=8 (Tc1)) mice. (M-O) Small bowel slices from E12.5 Ts65Dn and Tc1 mice were plated on fibronectin-treated chamber slides. GDNF was added 4 hours later. After an additional sixteen hours in GDNF-containing media, slices were fixed and distance from the farthest-migrated ENCDC to the slice edge (yellow line) was measured and averaged over four quadrants. (M) Representative image from slice culture after staining for RET (to identify ENCDC, red), phalloidin (which stains F-actin, green) and DAPI (nuclear stain, blue). (N, O) Ts65Dn (N, p=0.436, MWRST, n=26 (euploid) and 52 (Ts65Dn)) and Tc1 (O, p=0.385, t-test, n=21 (euploid) and 35 (Tc1)) animals had similar ENCDC migration distance to euploid animals. (P) *Ret* heterozygosity did not affect migration of Ts65Dn ENCDC (p=0.38, ANOVA, n=5 (Euploid, *Ret*+/+), n=5 (Ts65Dn, *Ret*+/+), and n=4 (Ts65Dn, *Ret*+/-)).

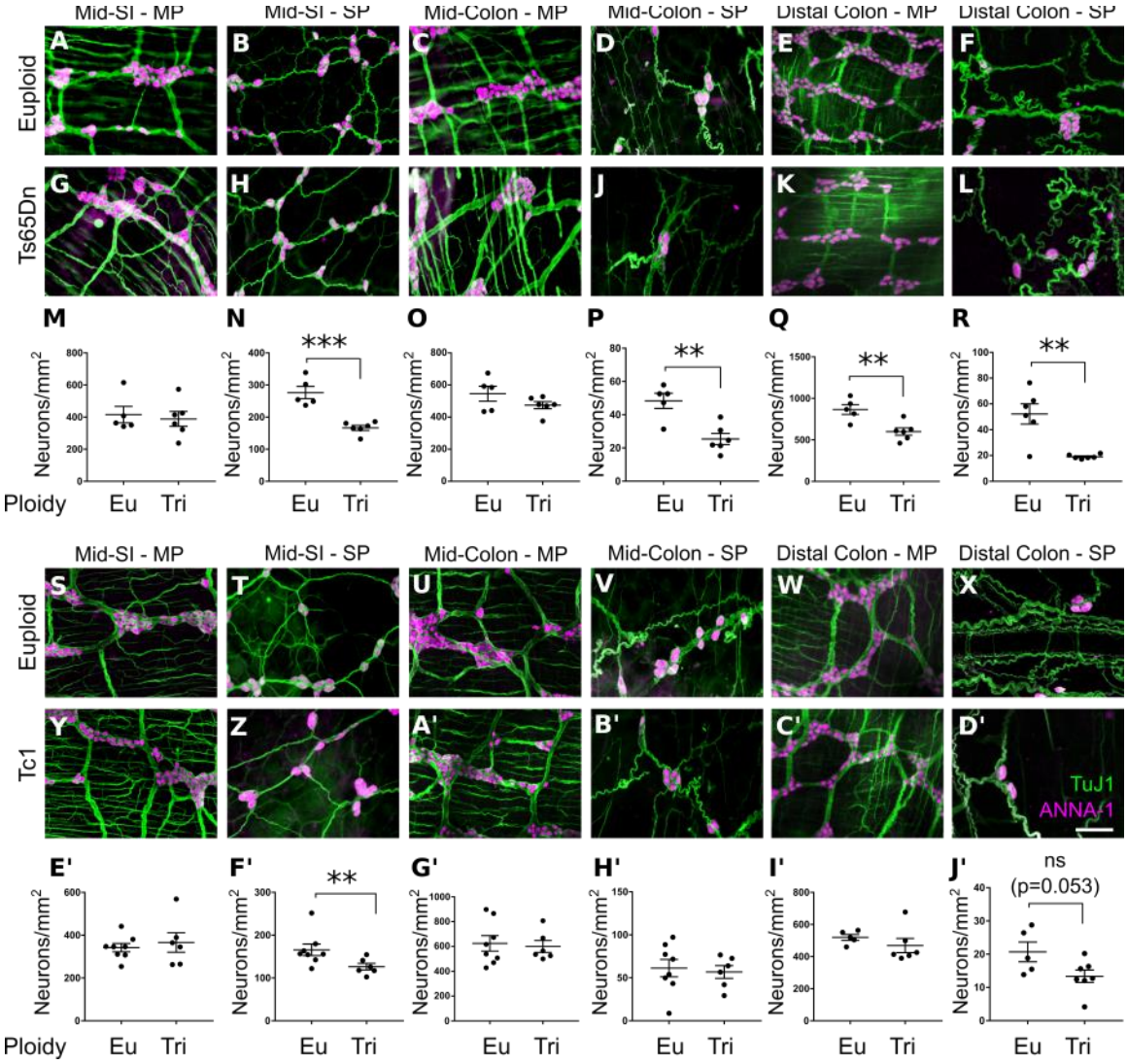

Figure 5-2: Tc1 and Ts65Dn mice have hypoganglionosis, especially in submucosal plexus. (A-L) Ts65Dn and (S-D') Tc1 trisomic and euploid myenteric and submucosal plexus were stained with TuJ1+ (green) and HuC/D+ (magenta) antibodies. (A, C, E, G, I, K, S, U, W, Y, A', C') Myenteric plexus (MP). (B, D, F, H, J, L, T, V, X, Z, B', D') Submucosal plexus (SP). (M-R) Quantitative analysis of neuron density for euploid and Ts65Dn mice (see also Table 1). (E'-J') Quantitative analysis of neuron density for euploid and Tc1 mice (see also Table 1). Scale bar = 100 μm. *p<0.05, **p<0.01, ***p<0.001.

matched littermate controls (**Figure 5-1I-J**). Specifically, the entire small bowel and ~65% of colon were colonized by ENCDC in each mouse strain. TuJ1+ and HuC/D+ enteric neurons were also present at normal density at the migration wavefront (i.e., most distal 500 μm of colon with neurons) in E12.5 Ts65Dn and Tc1 mice (**Figure 5-1E-H, K-L**). As an alternative approach to

evaluate ENCDC migration, we cultured E12.5 midgut slices overnight on fibronectin-coated dishes (**Figure 5-1M**). ENS precursors migrated from gut slices in response to the RET ligand glial cell-derived neurotrophic factor (GDNF). Consistent with in vivo data, the distance ENCDC migrated from gut slices was normal in Ts65Dn and Tc1 mice (**Figure 5-1N-O**). Finally, to more closely recapitulate human HSCR where inactivating *RET* receptor tyrosine kinase risk alleles are common (339, 363), we analyzed Ts65Dn; *Ret*+/- mice, but also found normal bowel colonization by ENCDC at E12.5 (**Figure 5-1P**). Collectively these data suggest that extent of colonization of fetal bowel by ENCDC and efficiency of ENCDC migration in vitro are normal in Ts65Dn and Tc1 mice.

Ts65Dn and Tc1 trisomic mice have reduced submucosal plexus neuron density

The ENS is complex, with many cell types in the myenteric and submucosal plexus (5). To evaluate Ts65Dn and Tc1 ENS in more detail, whole mount preparations from 80-120-day bowel were stained with TuJ1 and HuC/D antibodies (**Figure 5-2A-L** and **S-D'**). Quantitative analysis showed normal density of myenteric neurons in small bowel and mid-colon of Ts65Dn and Tc1 mice (**Figure 5-2M, O, E', G'**). Intriguingly, myenteric plexus neuron density was reduced in distal colon of Ts65Dn, but not Tc1, adult mice (**Figure 5-2Q** and **I'; Table 5-1**).

In contrast to myenteric plexus, submucosal neuron density was markedly reduced in many bowel regions of Ts65Dn animals including small bowel, mid-colon, and distal colon (**Figure 5-2N, P, R; Table 5-1**). Tc1 mice also had reduced submucosal neuron density in small bowel (**Figure 5-2F'; Table 5-1**) and the mean distal colon submucosal neuron density was reduced 35%, but with p=0.053 compared to controls (**Figure 5-2J', Table 5-1**). In contrast, submucosal neuron density was normal in mid-colon (**Figure 5-2H'**) of Tc1 mice. Neuron density also differed between euploid control animals of different stains, consistent with prior reports that ENS structure and bowel motility are strain-dependent (364). These data suggest

Table 5-1: Quantitative neuron density data.

	Cell density (cells/mm^2)		% Change	*p* value	Test
Ts65Dn	**Euploid**	**Trisomy**			
Small intestine myenteric plexus	415.4 ± 51.15	388.5 ± 46.32	- 6.5%	0.7049	t-test
Small intestine submucosal plexus	276.2 ± 19.18	166.4 ± 7.78	- 39.8%	0.0003	t-test
Mid colon myenteric plexus	545.5 ± 46.58	474.5 ± 22.01	- 13.0%	0.1777	t-test
Mid colon submucosal plexus	48.32 ± 4.58	25.37 ± 3.336	- 47.5%	0.0025	t-test
Distal colon myenteric plexus	866 ± 58.85	599.9 ± 44.69	- 30.7%	0.0052	t-test
Distal colon submucosal plexus	52.21 ± 7.86	19.06 ± 0.68	- 63.5%	0.0018	t-test
Tc1	**Euploid**	**Trisomy**			
Small intestine myenteric plexus	341.6 ± 19.54	365.9 ± 45.83	+ 7.1%	0.6006	t-test
Small intestine submucosal plexus	165.6 ± 13.60	126.4 ± 7.60	- 23.7%	0.0093	MWRST
Mid colon myenteric plexus	624.6 ± 62.5	600.2± 47.84	- 3.9%	0.7759	t-test
Mid colon submucosal plexus	61.29 ± 10.06	56.79 ± 7.45	- 7.3%	0.7419	t-test
Distal colon myenteric plexus	519.5 ± 18.27	468.8 ± 44.56	- 9.8%	0.3544	t-test
Distal colon submucosal plexus	20.67 ± 2.964	13.36 ± 1.88	- 35%	0.0533	t-test

partial trisomy mimicking human DS causes submucosal plexus hypoganglionosis in mice. Because Ts65Dn have a more dramatic ENS phenotype than Tc1 mice, and since Tc1 have mosaicism, our further analyses focused primarily on Ts65Dn.

Multiple submucosal neuron subtypes are reduced in Ts65Dn trisomic mice

The ENS has diverse neuron subtypes with various functions (5) including smooth muscle contraction and relaxation, regulation of fluid secretion, and vasodilation. Reduced submucosal neuron density might reflect loss of single submucosal neuron subpopulations or reductions in many neuron types. To determine if specific neuron subtypes are absent in Ts65Dn submucosal plexus, whole mount adult small bowel preparations were stained with antibodies to HuC/D, vasoactive intestinal peptide (VIP), somatostatin (SST), and tyrosine hydroxylase (TH). This permits analysis of VIP/TH secretomotor neurons (that also express neuropeptide Y and calretinin), VIP vasodilator neurons (that also express neuropeptide Y and calretinin), SST secretomotor neurons (that also express choline acetyl-transferase (ChAT), calcitonin gene related peptide, and calretinin), and neurons with unknown targets (that express ChAT alone, or

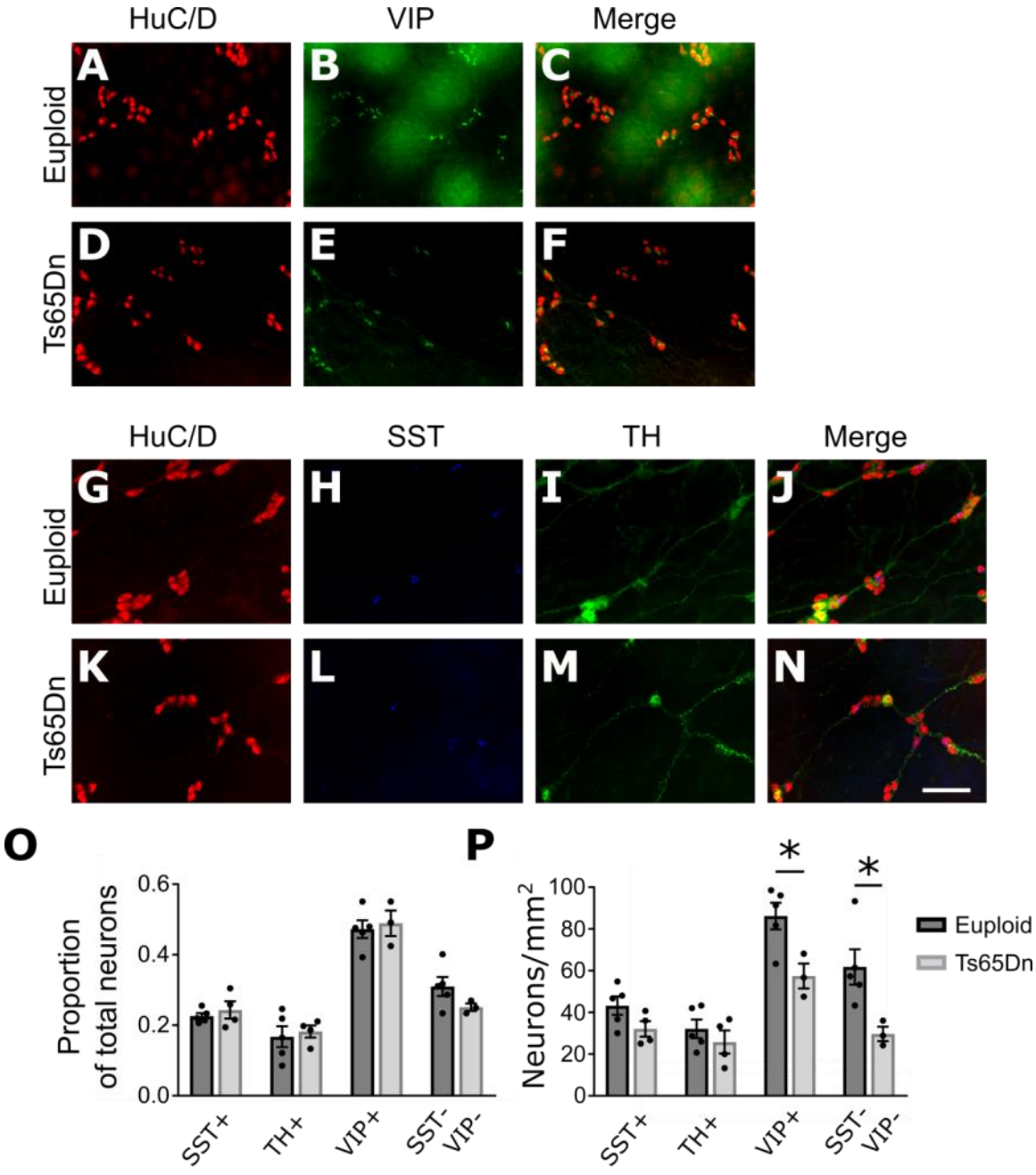

Figure 5-3: Analysis of subtypes of submucosal neurons in Ts65Dn adult mice.
(A-N) Euploid and Ts65Dn adult submucosal plexus from small bowel was stained for HuC/D (red) and VIP (green) (A-F) or HuC/D (red), SST (cyan), and TH (green) (G-N). Scale bar = 100 µm. (O) Proportion of neuron subtypes relative to total HuC/D+ cells (SST: p=0.477, t-test, n=5 (euploid) and n=4 (Ts65Dn); TH: p=0.905, MWRST, n=5 (euploid) and n=3 (Ts65Dn); VIP: p=0.712, t-test, n=5 (euploid) and n=3 (Ts65Dn); SST-VIP-: p=0.164, t-test, n=5 (euploid) and n=3 (Ts65Dn)). Note that TH+ neurons are a subset of VIP+ neurons. (P) Absolute neuron density per mm^2 for neuron subtypes (SST: p=0.104, t-test, n=5 (euploid) and n=4 (Ts65Dn); TH: p=0.40, t-test, n=5 (euploid) and n=3 (Ts65Dn); VIP: p=0.024, t-test, n=5 (euploid) and n=3 (Ts65Dn); SST-VIP-: p=0.032, t-test, n=5 (euploid) and n=3 (Ts65Dn)). *p<0.05.

neither ChAT nor VIP; hereafter referred to as SST-VIP-neurons) (11). Quantitative analysis showed the percentage of SST+, TH+, VIP+ and SST-VIP- neurons compared to total neurons (HuC/D+) was statistically equivalent in euploid and Ts65Dn mice (**Figure 5-3A-O**). This suggests all submucosal neuron populations were reduced in Ts65Dn animals. However, analysis of neurons per unit area showed statistically significant reductions only for VIP (33% reduced; p=0.024) and SST-VIP- (52% reduced; p = 0.032) submucosal neurons, suggesting a greater loss of these neuron subtypes (**Figure 5-3P**).

Since subtype alterations may occur without neuron loss, we additionally examined two major neuron subclasses in myenteric plexus of adult Ts65Dn mice. We found a normal density of small bowel excitatory (calretinin+) and inhibitory (nitric oxide synthase+) motor neurons (**Figure 5-4A-J**). Density of SOX10+ glia within adult small bowel myenteric layers was also normal (**Figure 5-4K-M**).

To assess if Ts65Dn mice have altered villus innervation, we immunostained villi from mid-small intestine using TuJ1 to label neurites and counted nerve fibers bisecting a line at mid-villus height (**Figure 5-5A-B**). Neurite numbers were equal in euploid and Ts65Dn mice (**Figure 5-5C**) despite ~40% reductions in submucosal neuron density in this region.

Reduced submucosal plexus neuron density in Ts65Dn mice is not explained by altered ENCDC proliferation, apoptosis or glial lineage commitment

To define cellular mechanisms that could reduce submucosal neuron density in Ts65Dn mice, we examined postnatal day 1 (P1) small bowel because submucosal plexus is not fully populated in mice prior to birth and many submucosal neuron precursors exit the cell cycle at P1 (110, 365). At this age, TuJ1 antibody stains neurons and committed neuronal precursors, while SOX10 is expressed in enteric glia and uncommitted neuron/glia precursors. Analysis of submucosal plexus showed TuJ1+ cells were already less abundant in Ts65Dn mice by P1

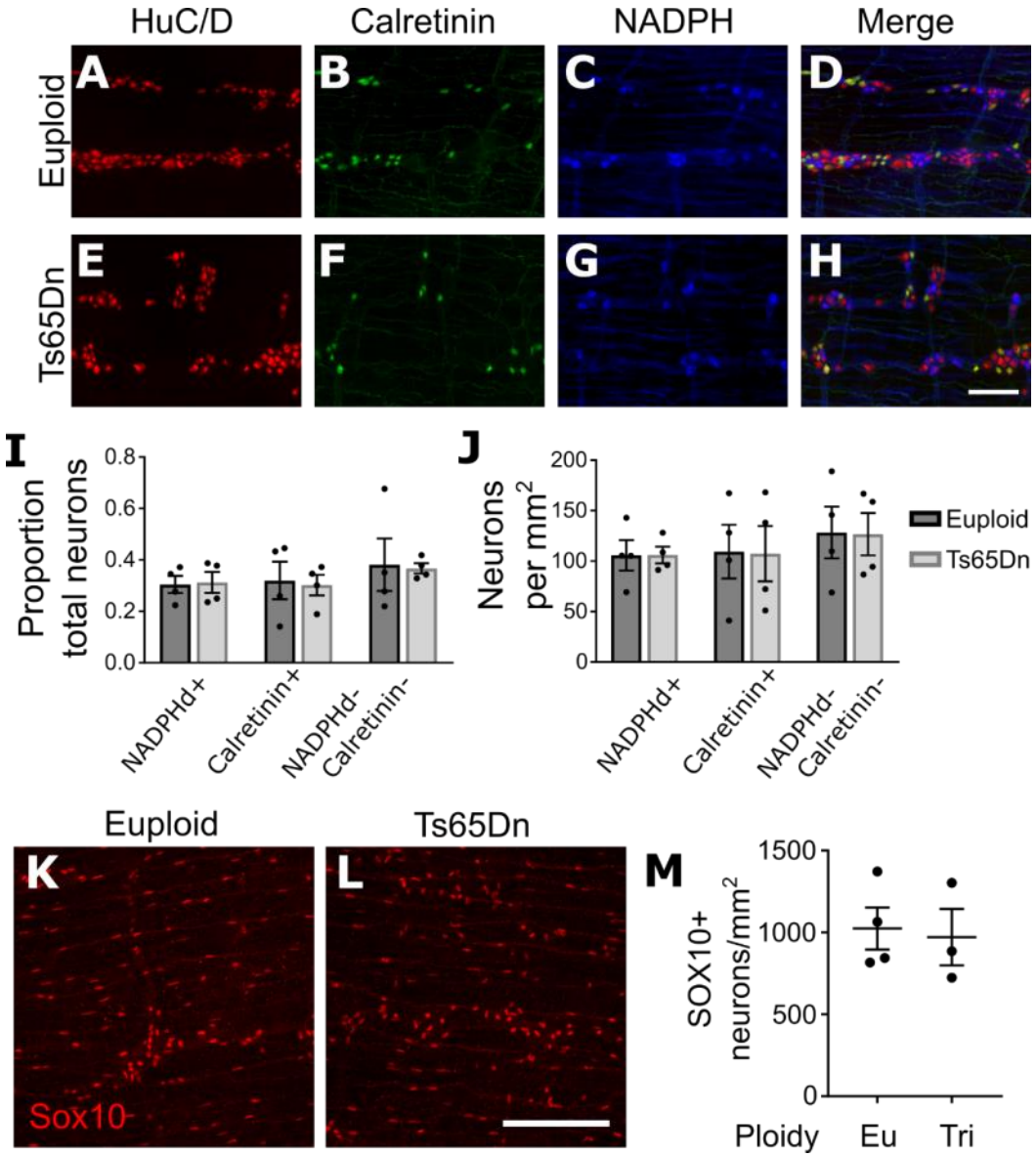

Figure 5-4: Density of NADPH-diaphorase+ neurons, calretinin+ neurons, and SOX10+ glia are normal in Ts65Dn adult small bowel.

Ts65Dn adult trisomic myenteric plexus from small bowel was stained with antibodies against HuC/D (A, E) and calretinin (B, F), and also stained using NADPH diaphorase histochemistry, which was pseudocolored blue to merge with fluorescent images (C,G). Merged images (D, H) show NADPHd+, calretinin+, and NADPHd-/calretinin- neurons. (I) Ts65Dn mice had normal ratios of specific neuron subtypes to total neurons (NADPH: p=0.881, t-test, n=4 (euploid) and n=4 (Ts65Dn); calretinin: p=0.839, t-test, n=4 (euploid) and n=4 (Ts65Dn); NADPHd-/calretinin-: p=0.898, t-test, n=4 (euploid) and n=4 (Ts65Dn)) and (J) absolute neuron density (NADPH: p=0.986, t-test, n=4 (euploid) and n=4 (Ts65Dn); calretinin: p=0.960, t-test, n=4 (euploid) and n=4 (Ts65Dn); NADPHd-/calretinin-: p=0.961, t-test, n=4 (euploid) and n=4 (Ts65Dn)). (K-L) Adult myenteric plexus from euploid and Ts65Dn mid-small intestine was stained with anti-SOX10 antibody and imaged using confocal z-stacks. Maximum intensity projections are shown. (M) Ts65Dn and euploid animals did not differ in numbers of myenteric SOX10+ glia (p=0.980, t-test, n=4 (euploid) and n=3 (Ts65Dn)). Scale bar = 100 μM.

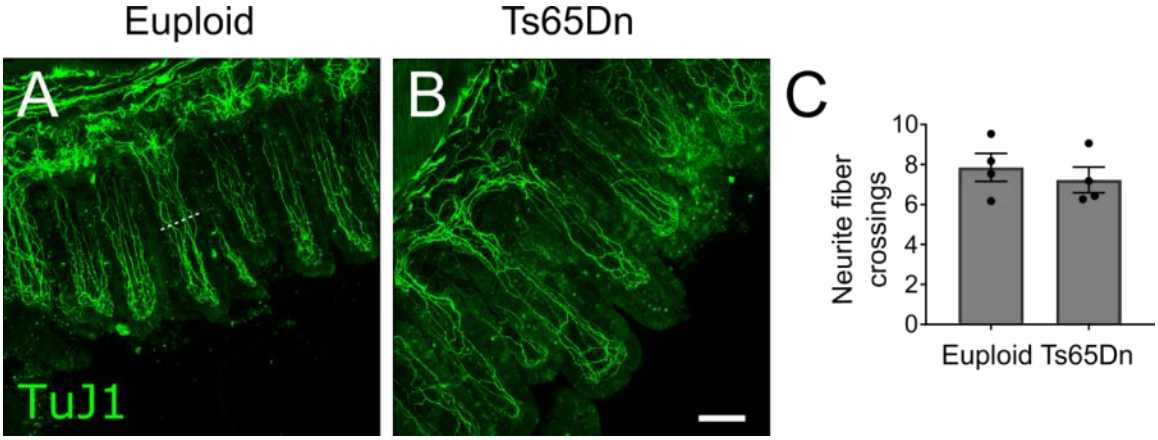

Figure 5-5: Neurite density within villi is normal in trisomic mice.
(A-B) Representative Z-projections of TuJ1+ nerve fibers in mid-small bowel villi from euploid (A) and Ts65Dn (B) mice. (C) Quantification of villus neurite fiber crossings shows no difference between euploid and Ts65Dn mice (p=0.5366, t-test, n=4(euploid) and n=4(Ts65Dn)). White dotted line in (A) represents example location where intersecting fibers were counted. Scale bar = 100 µM.

(**Figure 5-6 A-D**). In contrast, 5-ethynyl-2-deoxyuridine (EdU) staining showed normal proliferation rates for TuJ1+ and SOX10+ submucosal plexus cells (**Figure 5-6A-C, E, F**). Ki67 antibody, which labels proliferating cells in all cell cycle phases, also showed normal percentages of cycling TuJ1+ and SOX10+ cells in P1 Ts65Dn submucosal plexus (**Figure 5-6G-I, K, L**). Collectively these data suggest reduced precursor proliferation is unlikely to account for reduced submucosal neuron density in Ts65Dn mice. To evaluate cell death, we stained P1 submucosa for activated caspase-3 and TuJ1+, but only found rare TuJ1+ caspase-3+ cells in euploid or trisomic mice (**Figure 5-7A-D**). This suggests increased cell death is unlikely to explain reduced submucosal neuron density in Ts65Dn ENS. We also did not find evidence that ENCDC were selectively converted to enteric glia. Density of mature glial lineage cells (defined as SOX10+ Ki67-) was the same in Ts65Dn trisomic and WT submucosal plexus at P1 (**Figure 5-6G-J**) and in adults (SOX10+ cells; **Figure 5-7E-H**). Interestingly, although the percentage of SOX10+ cells that were EdU+ (**Figure 5-6F**) or Ki67+ (**Figure 5-6L**) was normal in Ts65Dn mice, the density of SOX10+ Ki67+ cells was slightly (17%) reduced in P1 trisomic mouse submucosal plexus (**Figure 5-6J**). A reduced density of cycling cells without a change in percentage of

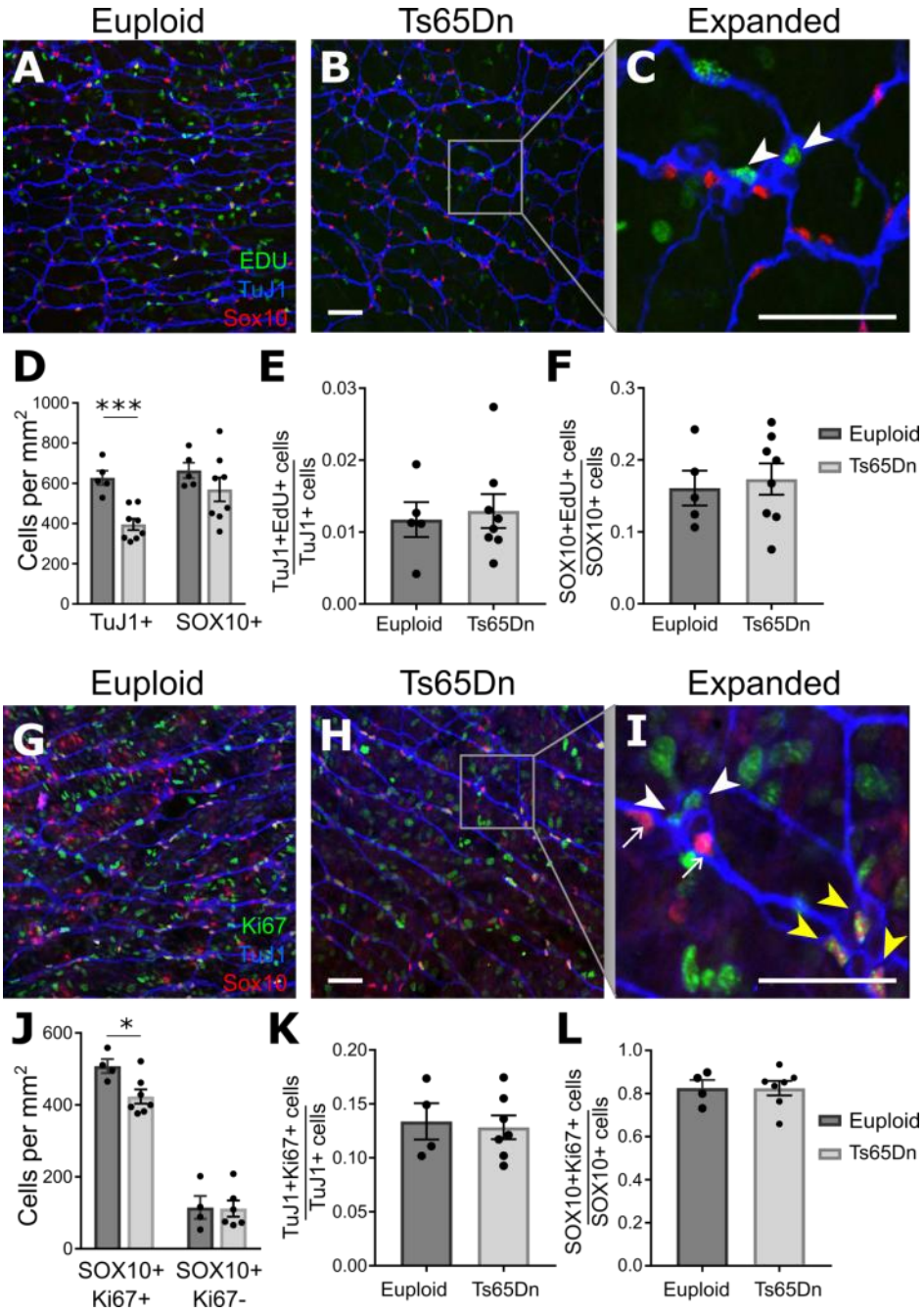

Figure 5-6: Neuronal and glial precursor proliferation were normal in Ts65Dn mice.
(A-B, G-H) Euploid and Ts65Dn P1 submucosal plexus from small bowel was labeled with EdU ClickIT® chemistry (green) plus antibodies to SOX10 (red), TuJ1 (blue) antibodies (A-B) or with antibodies to Ki67 (green), SOX10 (red), and TuJ1 (blue) (G-H). In higher magnification images (C and I), white arrowheads indicate TuJ1+EdU+ (C) or TuJ1+Ki67+ (I) neuron precursors. Yellow arrowheads indicate SOX10+Ki67+ cells (I). Small white arrows indicate SOX10+Ki67- glia (I). (D) TuJ1+ cell density was significantly reduced in P1 Ts65Dn submucosal plexus ($p<0.001$, t-test, n=5 (euploid) and n=8 (Ts65Dn)), while SOX10+ cell density was not significantly reduced in Ts65Dn animals ($p=0.267$, t-test; n=5 (euploid) and n=8 (Ts65Dn)). (E, F) Proportion TuJ1+EdU+ precursors relative to total TuJ1+ neurons (E), and proportion

SOX10+EdU+cells relative to total SOX10+ cells (F), was unchanged in P1 Ts65Dn submucosal plexus (TuJ1+EdU+ proportion: p=0.747, t-test, n=5 (euploid) and n=8 (Ts65Dn); SOX10+EdU+ proportion: p=0.719, t-test; n=5 (euploid) and n=8 (Ts65Dn)). (J) P1 Ts65Dn mice had reduced SOX10+Ki67+ cell density, but normal SOX10+Ki67- cell density (SOX10+;Ki67+: p=0.0214, t-test, n=4 (euploid) and n=7 (Ts65Dn); SOX10+Ki67-: p=0.748, t-test, n=4 (euploid), n=4 (Ts65Dn)). (K, L) Proportion TuJ1+Ki67+ precursors relative to total TuJ1+ neurons (K), and proportion SOX10+Ki67+ cells relative to total SOX10+ cells (L), was unchanged in P1 Ts65Dn submucosal plexus (TuJ1+Ki67+ proportion: p= 0.782, t-test, n=4 (euploid) and n=7 (Ts65Dn); SOX10+Ki67+ proportion: p=0.992, t-test; n=4 (euploid) and n=7 (Ts65Dn)). All scale bars are 50 μm. All images are confocal z-stacks. *p<0.05, **p<0.01, ***p<0.001.

cycling cells suggests fewer precursors recently migrated from outer bowel wall to submucosal plexus, but we have not found a direct way to test this.

Trisomy alters bowel motility and stooling patterns

To determine if trisomic mice have abnormal bowel motility, we assessed small bowel transit by gavage-feeding adult Ts65Dn and Tc1 mice fluorescein isothiocyanate (FITC)-dextran (327). FITC-dextran in each bowel segment was measured 2 hours (Ts65Dn) or 1 hour (Tc1) after gavage (**Figure 5-8A-B**). Geometric mean for FITC-dextran transit through the bowel showed no difference between euploid and trisomic mice (**Figure 5-8C-D**) suggesting normal small bowel motility. We also evaluated colon motility by bead expulsion assay (327) (**Figure 5-8E, F**). For this and subsequent functional experiments, Ts65Dn mice were on a mixed genetic background (B6EiC3Sn x C57BL/6J). Although mean bead expulsion time in Ts65Dn animals was longer than in euploid animals, this did not reach statistical significance (**Figure 5-8E**). One data point was identified as a clear outlier (red) using Grubb's and ROUT outlier tests. In this animal, which was tested three times, expulsion times were 99 seconds, 1758 seconds, and 91 seconds, suggesting colon injury on the second testing day. When this data point is excluded, the p-value is statistically significant (p=0.0117) suggesting slower colonic bead expulsion in Ts65Dn compared to euploid mice. In contrast, Tc1 and control mice had similar colonic bead expulsion times (**Figure 5-8F**).

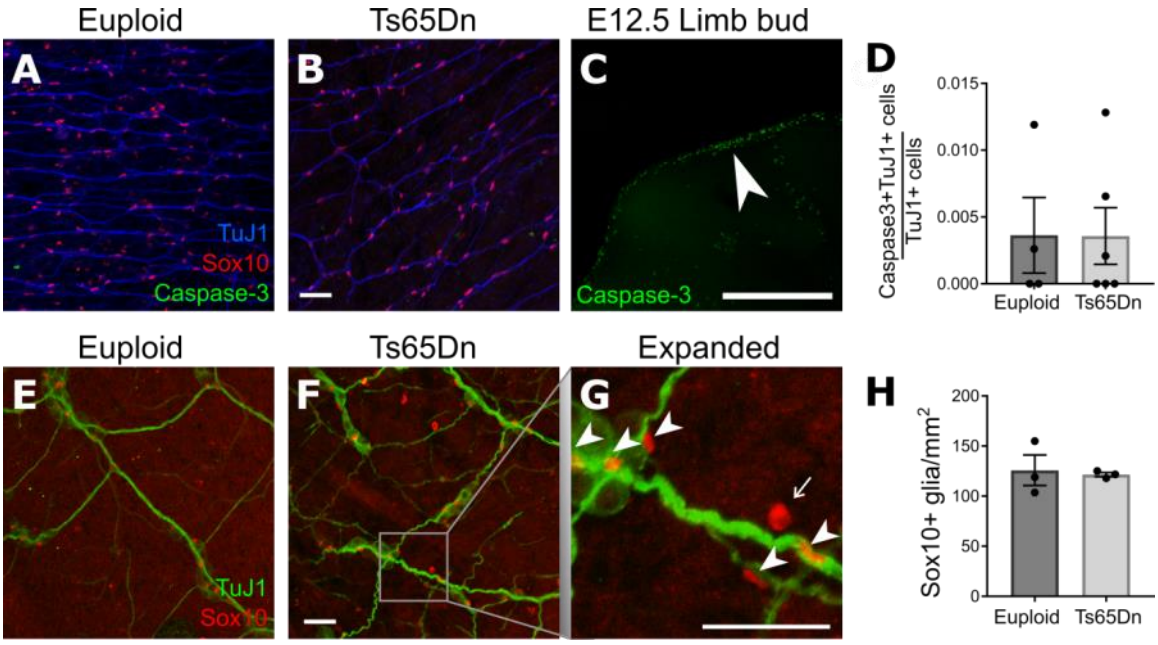

Figure 5-7: Apoptosis and glial number were normal in Ts65Dn submucosal plexus. (A-B) P1 bowel stained with antibody to cleaved caspase-3 (green) had few immunoreactive cells. (C) E12.5 mouse proximal limb was used as a positive control for cleaved caspase-3 antibody staining to ensure apoptotic cells were readily detected by the antibody. White arrowhead indicates densest region of apoptotic cells. (D) Quantitative analysis of cleaved caspase-3 data (p=1.0, MWRST, n=4 (euploid) and n=6 (Ts65Dn)). (E-F) Adult small intestine showing SOX10+ mature glia (red) in proximity to TuJ1+ (green) neuron processes. In expanded image (G), arrowheads indicate SOX10+ glia; arrows indicate autofluorescent blood cells, which were not counted. (H) Quantitative analysis of SOX10+ mature glia in adult submucosal plexus (p=0.59, t-test, n=3 (euploid) and n=3 (Ts65Dn)). All scale bars are 50 µm except for (C), which is 500 µm. All images are confocal z-stacks.

To further characterize colon motility, we generated spatiotemporal maps from Ts65Dn colons maintained in a warmed, oxygenated organ bath with 2 cm height of Krebs-Ringers solution generating intraluminal pressure. Ts65Dn colons exhibited neurally-mediated colonic migrating motor complexes (CMMCs) that propagated down the bowel in a rostro-caudal direction (**Figure 5-8G-H, Supplemental Videos 5-1** and **5-2**). The average frequency of CMMCs over an hour was similar for euploid and Ts65Dn mice (**Figure 5-8I**; p= 0.30, Mann-Whitney Rank Sum Test (MWRST), n=8 (euploid) and n=7 (trisomy)). Collectively these data suggest Ts65Dn mice have normal small bowel transit of luminal contents, but reduced colon motility in vivo (based on FITC-dextran and colonic bead expulsion tests). However, Ts65Dn

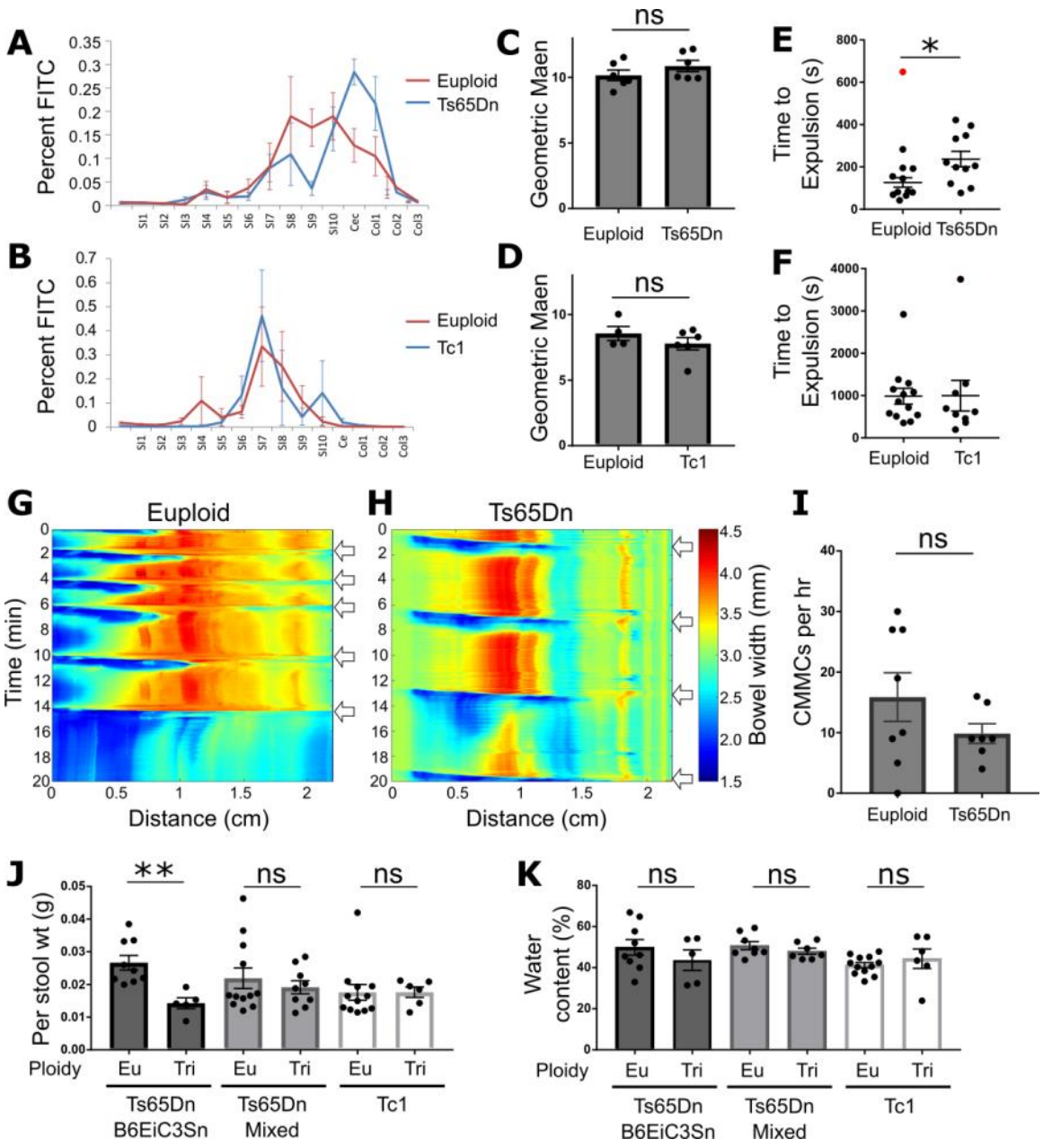

Figure 5-8: Ts65Dn mice have altered bowel motility and stooling patterns.
(A-D) Proximal bowel transit was measured by quantifying FITC dextran in bowel segments after gavage. There was no difference between each segment's FITC content (A-B; t-tests with Holm-Sidak multiple comparisons correction) or between geometric means of trisomic and euploid mice (Ts65Dn: C, p=0.255, t-test, n=6 (euploid) and 6 (Ts65Dn); Tc1: D, p=0.311, t-test, n=6 (euploid) and 4 (Ts65Dn)). (E-F) Colon transit, measured by inserting a glass bead into distal colon and timing expulsion, was no different with all data points included (E, p=0.0595, MWRST; n=12 (euploid) and n=11 (Ts65Dn)), but was significantly increased in Ts65Dn when one outlier (red; ROUT and Grubb's Outlier tests) was removed (E, p=0.0117; t-test; n=11 (euploid) and n=11 (Ts65Dn)). No difference in colonic bead expulsion time occurred in Tc1 mice (F, p= 0.26; MWRST; n=13 (euploid) and n=9 (Tc1)) even when one outlier (ROUT analysis, red) was removed (p = 0.08). (G-H) Representative kymographs plotting bowel width as a function of time

and bowel distance for euploid (G) and Ts65Dn (H) colon maintained at 2 cm pressure in an oxygenated organ bath. (I) CMMC (white arrows) frequency in Ts65Dn mice was not significantly different from euploid littermates (p= 0.30, MWRST, n=8 (euploid) and n=7 (Ts65Dn)). (J) Per stool weight was significantly larger in Ts65Dn mice on a B6EiC3Sn background (G, p=0.003, t-test, n=9 (euploid) and n=5 (Ts65Dn)), but normal for Ts65Dn mice on a mixed (B6EiC3Sn x C57BL/6J) background (p=0.749, MWRST, n=12 (euploid) and n=9 (Ts65Dn)) or Tc1 mice (p=0.482, MWRST, n=12 (euploid) and n=6 (Ts65Dn)). (K) Stool water content was normal for all strains tested (B6EiC3Sn: p=0.346, t-test, n=9 (euploid) and n=5 (Ts65Dn); mixed background: p=0.297, t-test, n=8 (euploid) and n=7 (Ts65Dn); Tc1: p=0.526, MWRST, n=12 (euploid) and n=6 (Ts65Dn)). *p<0.05, **p<0.01.

colon generates normal patterns of contractility in vitro suggesting there are not gross disturbances in colon ENS circuitry.

Since submucosal plexus regulates bowel water and electrolyte secretion (41, 366), we assessed stool mass and water content in trisomic and euploid mice. Stool was collected for an hour. Wet weight per stool pellet was reduced in Ts65Dn mice on a B6EiC3Sn background (p=0.003), but was normal for Ts65Dn mice on a mixed (B6EiC3Sn x C57BL/6) background (**Figure 5-8J**). Per stool weight was normal in Tc1 mice (**Figure 5-8J**). Both Ts65Dn and Tc1 mice had normal stool water content (**Figure 5-8K**). These data suggest trisomy may affect stool volume, but only in Ts65Dn mice on specific genetic backgrounds.

Ts65Dn submucosal plexus defects are not due to excess *Dscam* or *Dyrk1a*

Defining molecular mechanisms that reduce submucosal neurons in trisomic animals is not trivial. Ts65Dn mice have three copies of part of Mmu16. Tc1 mice are mosaic for an extra human chromosome that contains most Hsa21 genes. Since Ts65Dn and Tc1 both have reduced submucosal neurons, we hypothesize that critical regulators of submucosal neuron number must be encoded in shared trisomic genes. Unfortunately, over sixty genes are shared in Ts65Dn and Tc1 trisomic regions. We decided to test the hypothesis that excess *DSCAM* or *DYRK1A* causes submucosal neuron hypoganglionosis in trisomic mice for the following reasons. *DSCAM* and *DYRK1A* are encoded in a critical region on Hsa21 thought to increase HSCR risk (**Figure 5-9A**).

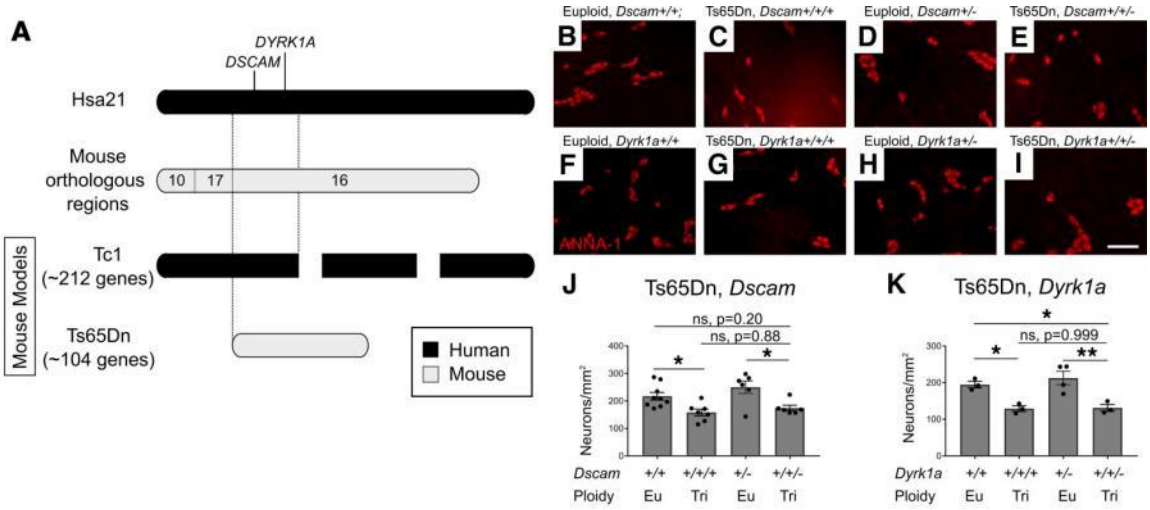

Figure 5-9: Normalizing *Dscam* or *Dyrk1a* gene copy number in Ts65Dn mice does not correct the submucosal plexus hypoganglionosis.
(A) Map of Ts65Dn and Tc1 trisomic regions. (B-E) Submucosal plexus of adult Euploid, *Dscam*+/+, Ts65Dn, *Dscam*+/+/+, Euploid, *Dscam*+/-, and Ts65Dn, *Dscam*+/+/- and (F-I) Euploid, *Dyrk1a*+/+, Ts65Dn, *Dyrk1a* +/+/+, Euploid, *Dyrk1a* +/-, and Ts65Dn, *Dyrk1a* +/+/- mice stained for HuC/D (red). (J, K) Quantification of neuron density from images like B-I indicates normalizing copy number for *Dscam* and *Dyrk1a* did not prevent distal colon hypoganglionosis (p=0.0.2008 Euploid, *Dscam*+/+ versus Ts65Dn, *Dscam*+/+/-, and p=0.884 Ts65Dn, *Dscam*+/+/+ versus Ts65Dn, *Dscam*+/+/-, ANOVA with post-hoc Tukey test, n=9 (Euploid, *Dscam*+/+), n=7 (Ts65Dn, *Dscam*+/+/+), n=6 (Euploid, *Dscam*+/-), and n=6 (Ts65Dn, *Dscam*+/+/-)) or *DYRK1A* (p=0.048 Euploid, *Dyrk1a*+/+ vs Ts65Dn, *Dyrk1a*+/+/-, and p=0.999 Ts65Dn, *Dyrk1a*+/+/- versus Ts65Dn, *Dyrk1a*+/+/+, ANOVA with post-hoc Tukey test, n=4 (Euploid, *Dyrk1a*+/+), n=3 (Ts65Dn, *Dyrk1a*+/+/+), n=3(Euploid, *Dyrk1a*+/-), and n=3 (Ts65Dn, *Dyrk1a*+/+/-)). Scale bar is 100 µm.

DSCAM is a netrin receptor, and netrin attracts ENS precursors to submucosal plexus during radial migration (338, 343, 344). DYRK1A regulates neuronal precursor cell cycle, and DYRK1A overexpression impairs CNS neuron precursor proliferation (82). To determine if excess DSCAM or DYRK1A causes submucosal neuron hypoganglionosis, we normalized copy number in Ts65Dn by breeding Ts65Dn females to *Dscam*+/- or *Dyrk1a*+/- males. Offspring from Ts65Dn × *Dscam*+/- were on a mixed (C57BL/6J x B6EiC3Sn) background, while offspring from Ts65Dn × *Dyrk1a*+/- were on a ~50% C3H/HeJ and ~50% C57BL/6J background. Quantitative HuC/D immunohistochemistry (**Figure 5-9B-K**) showed submucosal neuron density remained low in trisomic Ts65Dn mice that had only two copies of either *Dscam* or *Dyrk1a* (i.e.

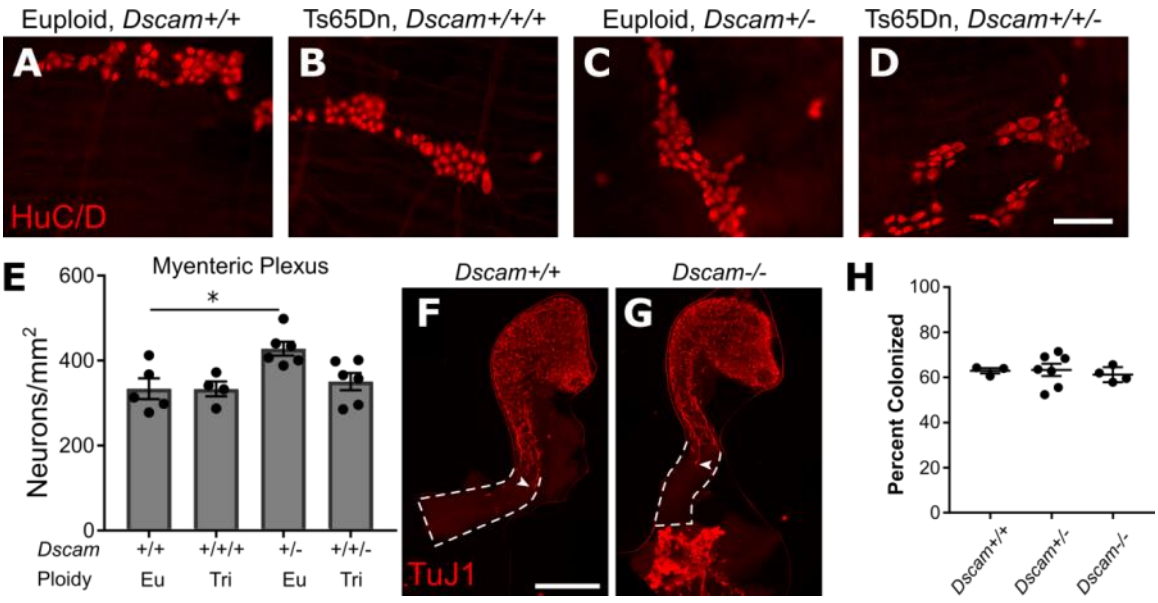

Figure 5-10: Adult Dscam heterozygous mice have increased myenteric plexus neuron density, but normal bowel colonization rate by ENCDC.
(A-D) HuC/D staining of adult small bowel myenteric plexus in adult Euploid, *Dscam*+/+, Ts65Dn, *Dscam*+/+/+, Euploid, *Dscam*+/-, and Ts65Dn, *Dscam*+/+/- mice. Scale bar is 100 µm. (E) Quantification of neurons reveals increased myenteric plexus density in mice with one copy of *Dscam* (p=0.0169 Euploid, *Dscam*+/+ versus Euploid, *Dscam*+/-, ANOVA with post-hoc Tukey test, n=5(Euploid, *Dscam*+/+), n=4 (Ts65Dn, *Dscam*+/+/+), n=6 (Euploid, *Dscam*+/-), and n=6 (Ts65Dn, *Dscam*+/+/-)). (F-G) TuJ1-stained large bowel of E12.5 *Dscam*+/+ and *Dscam*-/- mice. Scale bar is 500 µm. (H) Quantification of proportion of colonized colon in E12.5 mice with 2, 1, or 0 copies of *DSCAM* (p=0.838, ANOVA, n=3(*Dscam*+/+), n=7(*Dscam*+/-), n=4(*Dscam*-/-)).

not statistically different from mice with three copies of *Dscam* or *Dyrk1a*). This suggests normalizing *Dscam* and *Dyrk1a* copy number is insufficient to rescue submucosal plexus defects in Ts65Dn animals.

Unexpectedly, mice with only one *Dscam* (Euploid, *Dscam*+/-) copy had significantly *increased* myenteric plexus neuron density compared to wild type euploid animals (**Figure 5-10A-E**). Although this might occur if fewer ENCDC migrated from myenteric to submucosal regions in Euploid, *Dscam*+/- mice, submucosal neuron density is not reduced compared to Euploid, *Dscam*+/+ mice (**Figure 5-10J**). Since numerous studies suggest *DSCAM* may be a risk allele for HSCR, we also investigated rostrocaudal colonization of developing bowel in *Dscam*-/- mice, but found normal extent of colonization at E12.5 (**Figure 5-10F-H**). These data suggest

Dscam heterozygosity increases neuronal density in the MP, but *Dscam* copy number alone has minimal, if any, effect on longitudinal or radial ENCDC migration in developing bowel.

5.5 DISCUSSION

ENS structure and function in Trisomy 21: clues from mouse models

Surgical resection of distal aganglionic bowel has been the gold-standard treatment for HSCR for seventy years (367, 368), but >30% of people with HSCR have problems after surgery (64, 65). Intriguingly, meta-analysis of 16,497 people with HSCR showed that children with DS and HSCR have considerably worse post-operative outcomes than children with HSCR alone, including higher rates of enterocolitis and soiling (86). These long-standing observations are not mechanistically understood. One possibility is that trisomy 21 not only increases HSCR risk, but also causes other changes in ENS structure and function. Consistent with this hypothesis, even without HSCR, people with DS have a high incidence of unexplained severe chronic constipation (between 19-56%) and chronic diarrhea (19%) (87, 88). We recognize DS increases risk of other gastrointestinal problems (e.g. duodenal stenosis and imperforate anus) (369, 370), but our data support the hypothesis that ENS defects in addition to HSCR may contribute to bowel symptoms in people with DS.

Using two established DS mouse models (Ts65Dn and Tc1), we demonstrated normal rates of bowel colonization by ENCDC during fetal development, but reduced submucosal neuron density in adult mice. Ts65Dn mice also had reduced myenteric neuron density in distal colon, but myenteric neuron density was normal in more mildly-affected Tc1 mice. Interestingly, neurite fiber projections into villi appear normal in Ts65Dn small bowel, suggesting increased neurite length or branching from each innervating neuron as fewer cells compete for available trophic factors. The difference between Ts65Dn and Tc1 phenotypes may be due to Hsa21 mosaicism in Tc1 mice (355), incompatibility between mouse and human transcription factors on Hsa21, or

differences in gene expression between Ts65Dn and Tc1 mice. We focused mechanistic studies on Ts65Dn because they had more severe ENS defects.

We next asked if reduced neuron density reflected loss of specific neuron subpopulations, but found reduced density of multiple neuron subtypes, suggesting the problem precedes neuron subtype specification. We did not detect altered proliferation or cell death to account for the reduced neuron numbers. We also did not find increased glia that might reflect preferential precursor differentiation into glia at the expense of neuronal differentiation. We hypothesize reduced submucosal neuron density occurs because of reduced ENCDC migration from outer bowel wall to the submucosal plexus, but have not found a method to directly test this hypothesis.

In conjunction with anatomic defects, Ts65Dn mice had prolonged colonic bead expulsion times. Interestingly, individual stool pellet weights in the B6EiC3Sn strain were also reduced in Ts65Dn mice, but as we generated a mixed B6EiC3Sn x C57BL/6J background that bred more efficiently, weight per stool pellet normalized, consistent with the observation that strain background affects other DS phenotypes (371, 372).

Although the detected bowel motility problems did not cause life-threatening disease, these studies show for the first time that two DS mouse models have reduced enteric neuron density and that Ts65Dn mice have colonic dysfunction. Our findings are intriguing, leading us to speculate that bowel problems in children with DS could reflect ENS abnormalities even in the absence of HSCR. Further research using human tissue will be needed to test this hypothesis. Given low HSCR frequencies in children with DS (i.e., 2.6%), we were not surprised that Ts65Dn and Tc1 mice studied had enteric neurons throughout the bowel and that extent of bowel colonization was normal at E12.5. Because many children with DS and HSCR have reduced RET levels (e.g. *RET* hypomorphic T allele (rs2435357 SNP)) (339), we generated Ts65Dn, *Ret* +/- mice, but these animals also had normal ENCDC bowel colonization at E12.5, a sensitive time for detecting delayed ENS precursor migration. Additional work could be done to determine if

Ts65Dn or Tc1 increase penetrance of HSCR-like disease in mice with other predisposing mutations, but this may require analysis of hundreds of animals given low HSCR penetrance in people with DS.

Trisomic *Dscam* or *Dyrk1a* alone does not explain submucosal plexus defects in Ts65Dn mice

Reduced submucosal neuron density in Ts65Dn animals is interesting because mechanisms controlling radial migration of ENCDC from myenteric to submucosal plexus layers are poorly understood. Data suggest sonic hedgehog (SHH), GDNF and Netrin-1 all impact radial migration. SHH appears to repel ENCDC since SHH is produced in gut epithelium and SHH-deficient mice have ectopic enteric neurons too close to the epithelial lining. In contrast, GDNF signaling via RET and GDNF receptor alpha 1 (GFRA1) promotes ENCDC migration toward submucosal plexus as suggested by the observation that conditional deletion of *Gfra1* or *Ret* at E13.5 dramatically reduces submucosal neuron density. ENCDC cell death does not account for this phenotype (124). Instead, GDNF appears to attract ENCDC and GDNF expression shifts from outer gut mesenchyme to the submucosal side of the circular muscle layer late in embryonic development. This makes it plausible that GDNF could attract ENCDC to submucosal plexus (124). Netrin-1 also attracts ENCDC to submucosal plexus by binding deleted in colon cancer (DCC). Mice lacking DCC have no submucosal ganglia at P0 (338). While these data implicate SHH, GDNF and netrin-1 signaling in radial migration, it remains unclear how trisomy 21 might influence submucosal neuron number. One hypothesis is that overexpression of a gene in the trisomic region of Ts65Dn or Tc1 alters GDNF, netrin-1 or SHH signaling to reduce submucosal neuron number, but these signaling pathways are complicated and there are many ways that they could be altered. Intriguingly, trisomy has been linked to SHH signaling deficits in neuronal

precursors in Ts65Dn mice (373-375), but increased SHH signaling would presumably be needed to reduce submucosal neuron number.

To test the role of specific genes in the ENS phenotype of Ts65Dn mice, we focused initially on *Dscam* because DSCAM is a receptor for netrin-1, and prior studies suggested *DSCAM* overexpression may increase HSCR risk (61, 75-78). In the central nervous system, DSCAM mediates spinal commissural axon turning in response to netrin-1 (343) and DSCAM patterns the retina via self-repulsion. DSCAM can increase or decrease adhesion between cells depending on context (376, 377) making it likely DSCAM abundance would affect ENS development, as DSCAM is expressed in ENCDCs at ages critical for ENS precursor migration and differentiation (75). These findings led us to hypothesize that three copies of *Dscam* in Ts65Dn might reduce submucosal neuron number. Surprisingly, normalizing *Dscam* copy number by generating Ts65Dn, *Dscam*+/+/- mice did not prevent submucosal plexus hypoganglionosis. Furthermore, *Dscam* heterozygosity did not alter submucosal neuron number, and loss of *Dscam* did not alter bowel colonization by ENCDC in euploid mice. Intriguingly, Euploid, *Dscam*+/- adult mice had elevated myenteric neuron density compared to WT, but the significance of this mild neuron density increase is uncertain. Increased myenteric neuron number might be linked to the observation that loss of *DSCAM* increases neuron proliferation in the medulla (378), but mechanisms underlying this observation are not known. Collectively, our findings raise questions about whether DSCAM has important roles in ENS precursor migration as previously hypothesized (77).

We also tested the hypothesis that excess DYRK1A causes submucosal hypoganglionosis in Ts65Dn mice. *DYRK1A* is part of the HSCR-associated critical region on Hsa21 and encodes a tyrosine kinase with diverse functions. In mouse neocortex, DYRK1A induces premature neuronal differentiation through effects on Cyclin D1 (379). If DYRK1A excess also induced premature differentiation of ENCDC, hypoganglionosis would be expected. However, restoring

normal *Dyrk1a* copy number did not prevent submucosal plexus hypoganglionosis in otherwise trisomic Ts65Dn mice, and *Dyrk1a* haploinsufficiency did not alter submucosal neuron density in euploid mice.

Collectively, these data show that two mouse DS models, one partial trisomy and one transchromosomal, have submucosal plexus hypoganglionosis, but critical genes causing this problem remain uncertain. Identifying key genes is challenging because Ts65Dn and Tc1 mice share ~68 triplicated genes. Several additional candidates are found in three copies in Ts65Dn and Tc1 mice include *Bace2*, *Chaf1b*, *Fam3b*, and *Pcp4* (78). Triplication of these genes were reported in three children with HSCR and partial trisomy 21 (374). *BACE2* is especially interesting because variants are linked to HSCR, knockdown or inhibition of BACE2 rescued migration defects in human embryonic stem cell-derived ENS precursors (380), and some BACE2 variants prevent enteric neuron apoptosis (381). Other encoded proteins influence migration of non-ENCDC cell types, but do not have known ENS roles. Submucosal plexus hypoganglionosis in Ts65Dn and Tc1 mice might also be due to cooperative effects of multiple simultaneously overexpressed genes. For example, in *Drosophila*, COL6A2 and DSCAM exert synergistic effects on cardiac development. Overexpression of both COL6A2 and DSCAM causes atrial septal defects that do not occur with overexpression of the individual genes (382). This complexity underscores the difficulties in defining mechanisms in polygenic diseases like DS and HSCR.

HSCR, hypoganglionosis, and DS

It is unclear why we did not observe aganglionic bowel in Ts65Dn or Tc1 mouse models. Perhaps we would have found mice with short segment aganglionosis if we had evaluated hundreds of animals, since humans with DS only have 2.6% HSCR occurrence rates (130-fold increased risk). Nonetheless, our data clearly show that Ts65Dn mice have reduced distal bowel

ENS density and reduced submucosal neuron density. Additional genetic or non-genetic risks may be needed to cause aganglionosis. Interestingly, trisomy 16 mice do not survive past birth, and a subset have complete colonic aganglionosis over short regions (383, 384). Trisomy 16 mice have three copies of some genes homologous to Hsa21, but also have extra copies of genes homologous to other human chromosome regions, so they only partially mimic human DS. It is possible additional HSCR risk alleles relevant to human DS are present in trisomy 16 compared to Tc1 or Ts65Dn mice and increased expression of more than one gene impacts distal bowel ENS morphogenesis. An alternative is that mouse strain background influences severity of ENS defects in these models (as is well known for other mouse HSCR models (385)). If this is true, shared trisomic genes could underlie HSCR risk, causing hypoganglionosis in Tc1 and Ts65Dn mice, but more severe reductions in neuron number (i.e., aganglionosis) in trisomy 16 animals. Adding complexity, mouse and human chromosomes are not completely syntenic. For example, postulated HSCR risk genes *COL6A1* and *COL6A2* encode collagen on Hsa21 and excess collagen slows ENCDC migration (156), but mouse homologues are on Mmu10 (156) and are not triplicated in Ts65Dn or trisomy 16 mice (386). These issues leave many avenues for future investigation to define why children with DS have increased HSCR risk and more frequent and severe bowel problems even after HSCR surgery.

Summary: Our new work defines a model where additional DS candidate genes can be tested for their effect on ENS development using heterozygous inactivating mutations in combination with Ts65Dn trisomy to determine if increased copy number causes distal bowel hypoganglionosis. Our studies also provide a new hypothesis to explain why some people with DS experience severe functional bowel defects without bowel aganglionosis. Future studies should explore ENS structure and function in human DS, an area in need of additional research. Unfortunately, normal values for submucosal neuron density are not established in humans and reported myenteric

neuron density values vary >20-fold (387). Furthermore, effects of age and bowel region on neuron density are not known, so defining how DS affects ENS structure in humans will require extensive systematic effort, mapping colon location, employing quantitative 3-dimensional imaging, and comparing bowel resected during HSCR surgery in children with and without DS.

5.6 ACKNOWLEDGMENTS

The authors thank Beth Maguire for mouse colony management assistance. We are grateful to Robert Burgess for providing *Dscam* mice and verifying strain background, to Mariona Arbonés for sharing *Dyrk1a* mice, and to Vanda Lennon for human ANNA-1 serum. We also thank Dr. Benjamin Wilkins and Amanda Lemke for insightful comments and assistance during manuscript preparation. This work was supported by the Irma and Norman Braman Endowment (ROH), the Suzi and Scott Lustgarten Center Endowment (ROH), The Children's Hospital of Philadelphia Research Institute (ROH), Children's Discovery Institute of Washington University and St. Louis Children's Hospital (grant no. MD-II2013-269) (ROH), NIH grants RO1 DK087715 (ROH), March of Dimes 6-FY15-235 (ROH), and the Burroughs Wellcome Fund Clinical Scientist Award in Translational Research (grant no. 1008525) (ROH). The Ts65Dn, *Dyrk1a*+/- animals were generated through support from the Indiana Clinical and Translational Sciences Institute and funded in part by Grant Number UL1TR001108 from the National Institutes of Health, National Center for Advancing Translational Sciences, Clinical and Translational Sciences Award (RJR).

5.7 AUTHOR CONTRIBUTIONS

E.M.S, C.M.W, and R.O.H. designed experiments, analyzed results, and wrote the manuscript. E.M.S., C.M.W and A.J. performed experiments. R.J.R. and J.M.L. bred Ts65Dn,

Dyrk1A mice, harvested their bowels, and provided thoughtful advice about study design and data interpretation. All authors edited the manuscript.

CHAPTER 6 : CONCLUSIONS AND FUTURE DIRECTIONS

Children with CIPO can have serious neuropathic bowel motility problems despite an abundance of enteric neurons throughout the bowel. Abnormal motility in these children may occur due to defective enteric neuron differentiation, wiring, subtype specification, or neurotransmitter expression leading to defective neuron function. Similar defects in enteric neuron function may explain why children with HSCR often experience bowel motility problems despite surgery. To understand these diseases requires a thorough grasp of the genetics underpinning enteric neuron development, differentiation, and subtype specification.

This thesis offers many examples of how genetic perturbations can impact subsets of neurons and also influence motility. We describe a novel submucosal hypoganglionosis phenotype in mouse models of Down syndrome, which offers insights into why children with Down syndrome may be at increased risk for bowel motility problems. We also describe mouse gene deletion models for three transcription factors that are highly expressed in developing ENS. *Dlx1/2-/-* mice had serious bowel motility problems at birth including absent neurally-mediated contraction complexes, and decreased expression of *Vip*. *Tbx3* conditional deletion mutants had decreased numbers of SOX10+ cells, glia, and nNOS+ neurons. Although these findings provide novel insights into the function of these transcription factors, many more regulatory genes remain to be characterized. Indeed, using single-cell and single-nucleus sequencing, we identified over 40 transcription factors that could be involved in ENS subtype specification, including some with known roles in other aspects of ENS development. I discuss these findings, and future directions, in more detail below.

Interestingly, most of the genetic defects described in this thesis resulted in subtle structural defects. The ENS was not completely missing, and if a hospital pathologist looked at tissue sections from any of these mouse models, they might describe the ENS as "normal."

Despite the subtlety of the structural phenotypes, some of these defects resulted in serious functional issues in our mouse models. This underscores a problem with how clinicians think about and diagnose neurogenic bowel motility problems. As we begin to better understand diseases like HSCR and CIPO, we need to find new ways of defining ENS pathology in patients, such as through improved ENS imaging modalities (Chapter 8).

6.1 - Down Syndrome and ENS abnormalities

In Chapter 5, we showed that mouse models of Down Syndrome have submucosal plexus defects, and Ts65Dn mice have decreased neuron density in distal colon and abnormal colon motility. These findings offer an explanation for why children with comorbid Down Syndrome and HSCR might have more serious disease than children with HSCR, and they also may explain why individuals with Down Syndrome are more likely to have functional issues like chronic constipation.

Although our study ruled out triplication of *Dyrk1a* and *Dscam* as causing hypoganglionosis in Ts65Dn and Tc1 mice, we did not identify the gene(s) responsible for decreased submucosal plexus density. Since over sixty genes are shared between Tc1 and Ts65Dn trisomic regions, this task is nontrivial and would involve systematically normalizing the copy number of every single gene on the Ts65Dn chromosome that is expressed in the bowel. As a first step, we should evaluate the ENS of Ts1Rhr mice, which are trisomic for only 33 of the genes triplicated in Ts65Dn mice (388), and could reduce this gene list by half. We also still do not know which genes cause individuals with Down syndrome to be at increased risk for HSCR. This problem is difficult to solve given that none of the mice we examined had HSCR, and HSCR only occurs in 2.6% of individuals with Down syndrome. We may have to rely on additional studies in patients with rare partial trisomies and HSCR to further hone in on a genetic locus (78).

DSCAM has been identified as a risk locus for HSCR (76, 77). We were therefore surprised to see normal ENS precursor migration in mice lacking *Dscam* at E12.5. It is possible that even though migration is normal at E12.5, distal colon colonization at older ages is abnormal in *Dscam-/-* mice. We need to more thoroughly characterize P0 *Dscam-/-* mouse ENS, particularly distal colon, using quantitative approaches. We should also examine glia and submucosal plexus neurons in these animals since DSCAM is a receptor for netrin, which is involved in targeting enteric neuron precursor cells to the submucosal plexus. The ENS of *Dyrk1a-/-* mice should also be more thoroughly characterized using quantitative and functional approaches. We recently received correspondence from a clinical geneticist suggesting that *Dyrk1a* mutations may be associated with constipation in children. Motility problems associated with *Dyrk1a* have not been described in the literature, but if such a link exists, it would be interesting to study since there are many small molecules targeting DYRK1A (389, 390).

6.2 - *Dlx1/2* and ENS functional defects

Mice lacking *Dlx1* and *Dlx2* have serious bowel function defects at P0 and significant reductions in *Vip* gene expression at E14.5 and P0. They also exhibited a mild (~13%) reduction in proportion of VIP+ neurons at P0, but this decrease was too small to account for the difference in gene expression. Although we hypothesize that decreased *Vip* might be enough to cause the functional defect seen in *Dlx1/2-/-* mutants, we cannot rule out potential contributions from other dysregulated genes. Mice lacking VIP have bowel function defects, but unfortunately, ENS function in VIP haploinsufficient mice has not been examined (240). In the future, we should determine if P0 *Vip+/-* bowel has contractility defects similar to *Dlx1/2-/-* bowel. A more definitive test would be to perform contractility experiments on a rescue mouse expressing *Vip* off the *Dlx1/2* locus. Luciferase assays could also confirm if *Dlx1* and/or *Dlx2* bind directly to the *Vip* promoter, or if deleting *Dlx* genes decreases *Vip* through an indirect pathway.

It is possible VIP plays an important role in ENS connectivity during development and the functional defect in *Dlx1/2-/-* mice is due to a wiring defect. Absence of serotonin leads to altered neuron subtype development (19), and blocking nerve firing with tetrodotoxin during ENS development leads to changes in subtype specification (194). Thus, it is reasonable to hypothesize that the absence of a neurotransmitter could lead to developmental problems as neural circuits are established. We might be able to answer this question using low-dose tamoxifen treatment of different *[Neurotransmitter]-CreERT2;Dlx1/2* lines to trace the projections of single neurons, or by quantifying neurotransmitter-containing vesicles in different regions. However, these strategies would be extremely labor-intensive and may not provide definitive answers.

Another interesting piece of the *Dlx* story is that ENS precursor migration in *Dlx2-/-* mice is slightly impaired, but we did not see this defect in *Dlx1/2-/-* mice. We hypothesize this difference is due to differences in strain background, since we received *Dlx2* and *Dlx1/2* mice on a C57Bl6/J and CD1 background, respectively. Given that at least two papers have now shown increased severity of ENS precursor migration defects on a C57Bl6/J background (385, 391), *Dlx1/2* mice should be bred onto a C57Bl6/J background and re-evaluated for precursor migration defects. We should also determine if the *Dlx1/2-/-* functional defect is due to synergistic interactions between *Dlx1* and *Dlx2*. Functional redundancy between *Dlx1* and *Dlx2* is well-described in CNS (213) and it will be important to determine if this is a feature in ENS as well.

6.3 - *Tbx3*, gliogenesis, and neuron subtype specification

The work presented here points toward TBX3 as a possible regulator of gliogenesis or glia cell maintenance and NOS1 neuron development and/or maintenance. This research leaves open many intriguing mechanistic questions about TBX3's role in gliogenesis and neuron subtype specification. A critical next step will be identifying genes regulated by TBX3, but this is complicated by the fact that TBX3 might regulate different genes in different ENS cell

populations. For example, TBX3 might regulate *Sox10* or *Gli1* expression in glia, and *Nos1* expression in Nos neurons. To overcome this problem, single cell sequencing could be performed and novel bioinformatic techniques such as ClusterMap (392) could be used to compare subtypes and gene expression levels between controls and *Wnt1-Cre*$^{cre/wt}$*;Tbx3*$^{fl/fl}$*;R26R-Tdtomato* mutants. Alternatively, bulk RNA-seq using subtype-specific Cre lines, or chromatin immuno-precipitation sequencing are promising options.

6.4 - Transcription factor expression and subtype specification

When this thesis was started, only three transcription factors with roles in enteric neuron subtype development had been described. Today, that number has increased to six. Although this 2-fold increase is progress, many transcription factors involved in ENS subtype specification remain to be characterized. Excitingly, we have generated an extensive body of mouse transcriptomics data containing over forty transcription factors differentially-expressed in subsets of neurons. Many of these genes likely play roles in subtype specification, but determining which genes are necessary and/or sufficient for generating neuron subtypes will be a major challenge. It is likely no single transcription factor is sufficient for establishing a particular subtype, but instead, combinatorial expression of multiple transcription factors is required. Stem cell experiments could provide the flexibility to overexpress multiple transcription factors in combination. If our main goal is stem cell regenerative therapy, combinatorial overexpression experiments similar to the Yamanaka approach would be an excellent strategy (393). However, if our goal is also to understand the role of the genes *in vivo* and how loss of these genes could impact bowel function in patients (i.e. if the genes are *necessary*), mouse models may be a better choice. Screening the ENS of ~40 different mouse mutants for neuron subtype defects would be ideal, but this is costly and difficult to implement. A more realistic approach will involve carefully selecting additional genes to study in individual mouse models. The zinc finger protein

Basonuclin 2 (*Bnc2*) and ETS family member *Etv1* are ideal candidates since they are also expressed highly in human ENS. *Bnc2* is expressed in nNOS- neurons in all three of our datasets. In mouse, *Bnc2* is also expressed in submucosa, muscularis, and serosa in large and small intestine (394). Due to this widespread expression, it would be valuable to generate and study ENS-specific conditional deletion *Bnc2* mutants. *Etv1* is another gene that should be studied as an ENS-specific conditional deletion, since in addition to *Nos1*+ neurons, *Etv1* is highly expressed in ICC (395). The castor zinc finger *Casz1* is another interesting gene with an existing mouse model that we are currently examining for ENS defects. Although it did not reach statistical significance after multiple testing correction in our human dataset, it is significantly elevated in ChAT+ neurons in mouse at E17.5 and in adult colon. In retinal ganglion cells, *Casz1* levels slowly increase during development, and *Casz1* overexpression in retinal progenitor cells promotes mid- and late-born neuronal fates (396). *Casz1* expression is also necessary for long-term survival of rod photoreceptors (397). It is possible *Casz1* plays similar roles in subsets of ENS neurons.

The splicing regulator *Rbfox1* has also emerged as a gene of interest. *Rbfox1* is one of the most highly-expressed genes in all nNOS- neuron populations in both mouse and human colon. In the CNS, this gene is required to establish the connectivity of SST+ and parvalbumin+ cortical interneurons (398). A conditional deletion *Rbfox1* mouse exists, and we are currently breeding it with *Wnt1-Cre* mice to generate ENS-specific conditional *Rbfox1* deletion mutants.

Finally, we have already mentioned that *Zeb2* (*Zfhx1b*) should be studied more carefully in mouse models, given that heterozygous mutations in this gene cause Mowat-Wilson syndrome and that *Zeb2* continues to be expressed in subsets of enteric neurons into adulthood. As a first step, adult *Zeb2* heterozygote ENS should be carefully examined for neuron and glial deficiencies and subtype defects. Conditional deletion of *Zeb2* at timepoints relevant for neuron subtype specification should also be performed to study subtype defects. This could be done by breeding

floxed *Zeb2* mice (399) to *Ret-Cre-ERT2* transgenic mice which express CreERT2 in most neurons, to generate *Ret-Cre-ERT2*$^{Cre/wt}$;*Zeb2*$^{fl/fl}$ mice. Pregnant dams could be tamoxifen-treated at E15.5, and pups delivered via C-section to circumvent tamoxifen-induced parturition problems.

6.5 - Single-cell sequencing and neuron subtype classification

Published enteric neuron subtype classifications are grossly incomplete and have extrapolated heavily between species and gut regions. Our mouse data provide an excellent starting point for classifying myenteric neuron subtypes in colon, but we are probably missing several rare populations. To resolve rarer subtypes, we need to sequence more neurons. A binomial model calculator provided by the Satija lab suggests that if our rarest subtype is 1% of total neurons, we need ~4,000 cells to have 95% confidence in getting at least 25 cells of that type (https://satijalab.org/howmanycells). This is over four times as many neurons as our current dataset provides, which may explain why the number of cell types resolved in our dataset is lower than expected.

Once we have a more complete set of data, the next task will be correlating different neuron clusters to their function in the ENS. One strategy is to identify markers for rare cell populations, such as Vglut2, and use these markers to sparsely label individual neurons. Sparse labeling could be accomplished using low-dose tamoxifen treatment of Cre-ERT2 reporter lines, or by filling individual cells with biocytin. It would then be possible to trace neuron projections and predict their function. We expect IPANS to interface with enterochromaffin cells in the epithelium. Interneurons might project within the plane of the myenteric plexus or might project from the myenteric to the submucosal plexus (or vice versa). Smooth muscle motor neurons should project into the longitudinal or circular smooth muscle. It is possible we will discover that the current classification scheme (IPAN, interneuron, motor neuron) is an oversimplification, and neuron classes serve multiple roles. Multiple populations of neurons in the ENS are already

known to be mechanosensing (23), consistent with neurons in the ENS being capable of assuming multiple roles.

6.6 - Improving methods for single-cell sequencing of human ENS

We also need better methods for sequencing human ENS so we can better classify neuron subtypes in humans. A major limitation of our human colon sequencing was the starting quality of human tissue. Per normal hospital protocol, the human tissue in our experiments was transported from surgery to pathology at room temperature and was not maintained in dPBS or other containing liquid during transport. Sometimes tissue was not placed in cold dPBS until 2 or 3 hours after it was removed during surgery. This delay may have led to alterations in early immediate gene expression, neuron death, and lower RNA yield. Another limitation to our study was that colon tissue was removed from individuals with colon pathology, including cancer, obstruction, and adhesions. We only used tissue that in-house pathologists deemed "normal" and we excluded inflammatory bowel syndrome and diverticulitis from our study after discovering T cell infiltrates in the myenteric plexus of some of our samples on H&E staining. However, it remains unclear if the bowel we were sequencing was truly "normal," particularly since cancer is often an inflammatory state.

A possible solution to the problem listed above is to sequence colon from deceased organ donors. The Heuckeroth lab recently began receiving deceased donor tissue. Although we have not yet sequenced this tissue, we have immunostained pieces and seen vast improvements in staining quality. To maximize tissue viability, colon is immediately placed on ice in Belzer UW® Cold Storage Solution. This solution is the gold standard for organ preservation during transplant, and contains several features that preserve tissue quality including: 1) a high potassium, low sodium concentration that mimics an intracellular environment, 2) a hydroxyethyl starch to reduce interstitial edema, 3) lactobionate and raffinose in place of glucose to prevent cell

swelling, and 4) allopurinol and glutathione to scavenge oxygen free radicals and minimize oxidative stress (400). Colon is transported to the lab on ice, with luminal contents stapled inside. Since the lumen contains higher concentrations of RNases, keeping muscularis layers separate from lumen may improve RNA quality and read depth.

Independent of tissue quality, we also need to increase the relative ratio of neurons that are sequenced. More precise dissection methods that better isolate the myenteric plexus are being developed by some of our collaborators and show promising results. Gentler dissociation methods are probably also needed, given that human enteric neurons seem particularly susceptible to damage. As sequencing becomes cheaper, it may become possible to sequence more cells for less money (and thus, profile rarer subtypes).

Once we have a reliable method for sequencing human ENS, it will be important to gain a more complete view of the human ENS transcriptome by choosing regions to sequence. Most ENS single-cell sequencing efforts, including ours, have thus far ignored the submucosal plexus in favor of obtaining data from the more densely-populated myenteric plexus (401). However, sequencing data from submucosal plexus should also be obtained from mouse, and if possible, human as well. Although less relevant for HSCR, small intestine is often affected in CIPO, and small intestine ENS data should be obtained. Finally, sequencing embryonic human ENS would give a more complete picture of human ENS developmental processes that could aid regenerative medicine efforts, but this is likely not possible in U.S. laboratories.

6.7 - Using sequence data to understand human disease

Over the last two decades, a wealth of whole exome sequencing data has been collected from children with HSCR, CIPO, and other motility disorders. In many cases, the cause of the motility problem remains unclear. A critical next step will be to systematically compare genes identified through single-cell sequencing studies to the deletions, mutations, and variants

identified in patients, in order to generate hypotheses and better understand disease. Gene variants should be studied in the laboratory using mouse models or stem cells differentiated into enteric neurons. Single gene mutagenesis in stem cells using TALENS or CRISPR-CAS9 offers an elegant method to compare nearly genetically identical stem cell lines and has been used with great success in stem-cell-derived ENS experiments (402). Such studies may lead to the development of personalized, targeted therapies. For instance, individuals with mutations known to decrease excitatory ChAT+ neuron density may benefit from motility agents like pyridostigmine (403), which impairs acetylcholine breakdown at the synaptic cleft. In contrast, someone with an *increased* density of excitatory ChAT+ neurons may find pyridostigmine unhelpful or even harmful. Testing prospective therapies on stem cell and mouse models of gene mutations may help guide treatment.

6.8 - Human colon single-nucleus sequencing data: insight into ENS interacting partners

In addition to neuropathic causes, CIPO can be caused by defects in smooth muscle cells (404, 405), ICCs (406-408), and potentially PDGFRA+ cells. To our knowledge, the human single-nucleus sequencing data presented in Chapter 4 is the first dataset describing the transcriptome of colon SMCs, ICCs, and PDGFRA+ cells in humans. We should compare this data to recently-published bulk-RNA-seq data from mouse SMCs, ICCs, and PDGFRA+ cells (409-411) to identify transcriptional regulators and other genes involved in differentiation. SMCs have proven especially difficult to culture (412), but if we could find a way to grow these cells reliably *in vitro*, it might help us better model myopathic CIPO caused by *MYH11* or *ACTG2* mutations.

Muscularis macrophages are also present in the human colon single-nucleus sequencing data set. They are transcriptionally distinct from the more widely studied lamina propria macrophages (413), and they are increasingly believed to mediate inflammation-induced motility

problems like postoperative ileus, gastroparesis, and intestinal ischemia-reperfusion injury (414). Our human data may provide new insight into ways to modulate this cell type and treat these disorders.

6.9 - Summary:

We are at an incredibly exciting juncture in the field of ENS biology. Recent advances in transcriptomics are revolutionizing our understanding of the enteric nervous system, and we are discovering new genes faster than we can evaluate their functional roles. Although we do not yet have enough data to cleanly resolve all human enteric neuron subtypes, it is likely that this data will become available in the next five years. The challenge of the future will be deciding how to allocate resources to study these newfound genes, and how best to use this information to aid patient care.

CHAPTER 7 : APPENDIX A: UNEXPECTED ROLES FOR THE SECOND BRAIN: ENTERIC NERVOUS SYSTEM AS A MASTER REGULATOR OF BOWEL FUNCTION.

This chapter has been published in Annual Review of Physiology and reprinted here with permission. Sabine Schneider,* Christina M. Wright,* and Robert O. Heuckeroth. Unexpected roles for the second brain: enteric nervous system as a master regulator of bowel function. Annu Rev Physiol. 2019 Feb 10;81:235-259. doi: 10.1146/annurev-physiol-021317-121515.
Copyright©2019 the authors.

*Co-first authors; contributed equally

7.1 - ABSTRACT

At the most fundamental level, the bowel facilitates absorption of small molecules, regulates fluid and electrolyte flux, and eliminates waste. To successfully coordinate this complex array of functions, the bowel relies on the enteric nervous system (ENS), an intricate network of more than 500 million neurons and supporting glia that are organized into distinct layers or plexi within the bowel wall. Neuron and glial diversity, as well as neurotransmitter and receptor expression in the ENS, resembles that of the central nervous system. The most carefully studied ENS functions include control of bowel motility, epithelial secretion, and blood flow, but the ENS also interacts with enteroendocrine cells, influences epithelial proliferation and repair, modulates the intestinal immune system, and mediates extrinsic nerve input. Here, we review the many different cell types that communicate with the ENS, integrating data about ENS function into a broader view of human health and disease. In particular, we focus on exciting new literature highlighting relationships between the ENS and its lesser-known interacting partners.

7.2 - INTRODUCTION

Digesting nutrients that fuel our survival requires complex integration of many bowel functions and all must run smoothly to maintain a normal quality of life. Food must be broken into small particles and chemically digested for nutrient absorption. Indigestible components must efficiently pass through the gastrointestinal tract for elimination, while fluid and electrolyte balance is maintained. All of these processes occur in the setting of a complex microbiome that aids nutrient absorption, but can trigger inflammation and even infection should the system go awry. The intestine could not coordinate these functions without the enteric nervous system (ENS), a complex network of neurons and glia that reside in the bowel wall and send nerve fibers throughout the bowel. Like an orchestra conductor, the ENS is a critical regulator of many processes described above and interacts with an astounding array of cell types to facilitate bowel function.

The ENS is distributed all the way along the bowel in two layers called the myenteric and submucosal plexus (1). Each plexus is comprised of diverse enteric neuron and glial cell types that interact closely with each other and with other intestinal cells. Myenteric plexus cells cluster into ganglia between the outer longitudinal and inner circular smooth muscle of the bowel. Myenteric neurons provide the majority of direct innervation to the bowel's motor apparatus and the final output controlling bowel relaxation and contraction. Myenteric neurons interact closely with the tissue-resident macrophages (muscularis macrophages) that influence motility. Submucosal plexus ganglia reside between muscle and epithelium, where they regulate epithelial secretion and local blood flow. Neurons in both plexi respond to input from mucosal enteroendocrine cells and the autonomic nervous system. The ENS also interacts with immune and epithelial cells to promote barrier function that protects the bowel from pathogens in the gut lumen. Enteric neurons are currently classified by function, axon number, direction of axonal projections, synaptic connectivity, neurotransmitters, receptors, and electrophysiologic signatures.

Approximately 20 enteric neuron subtypes and four glial subtypes have been characterized thus far, but a wealth of single cell sequencing data is expected to redefine enteric neuron and glial subtypes in the next few years. Many excellent recent reviews detail known ENS circuitry, cell types, transmitters and functions (2, 415-417) Instead of duplicating those efforts, our goal is to show how the ENS interacts with non-ENS cell types and the implications of these interactions for human disease.

To facilitate communication, enteric neurons extend an elaborate network of neurites with associated glia. These ENS components contact almost all bowel cells including muscle, epithelial cells, pacemaker cells (called the interstitial cells of Cajal, (ICC)), blood vessels and immune cells. Enteric neurons synapse on each other, but also release neurotransmitters from varicosities along neurites to regulate smooth muscle cell (SMC) and ICC activity. The ICC act as pacemakers since they have intrinsic slow waves of depolarization and hyperpolarization (29).

The contractile force for bowel motility is provided by SMC, which must coordinate activity to mix luminal contents or move undigested food toward the distal bowel for eventual elimination (30). To contract smooth muscle, myenteric plexus excitatory motor neurons project their axons predominantly orally. In contrast, inhibitory motor neurons project axons distally and cause smooth muscle relaxation. Simultaneous activation of excitatory and inhibitory motor neurons in a bowel region causes proximal bowel contraction and distal relaxation, a pattern called peristalsis that is frequently observed in the small intestine.

Additional enteric neuron types control epithelial secretion (secretomotor neurons), epithelial secretion and blood vessel dilation (secretomotor/vasodilator neurons), epithelial proliferation, or innervate enteroendocrine cells and lymphoid follicles. Enteric neurons also send intestinofugal fibers to pancreas, gallbladder, prevertebral sympathetic ganglia, and the central nervous system (CNS) (2). Finally, although the ENS can control many aspects of bowel function autonomously, *in vivo* ENS activity is modulated by luminal contents (nutrients and microbes),

muscularis macrophages, parasympathetic neurons, sympathetic innervation from the celiac, superior and inferior mesenteric ganglia, and hormonal signals (e.g., adrenaline, thyroid hormone, corticotrophin releasing hormone, oxytocin). Many of these extrinsic signals are influenced by CNS activity, explaining how emotional responses like anxiety and fear can alter bowel function. The remainder of this article will explore cell types that interact with the ENS, integrating basic science with human disease to explore how ENS function and dysfunction impact human health.

7.2 - The ENS interfaces with the SIP syncytium to regulate motility

ENS interactions with SMC, ICC, and PDGFRα+ cells are critical for bowel motility. Many excellent manuscripts describe these interactions in detail (29, 30, 418), so here we highlight a few important interactions and recent developments.

Gap junctions connect **S**MC, **I**CC, and fibroblast-like **P**DGFRα+ cells into a multicellular syncytium commonly called the "SIP syncytium", whose name derives from the first letter of each cell type (**Figure 7-1A**) (29). The SIP syncytium receives input from excitatory and inhibitory motor neurons whose cell bodies reside within the myenteric plexus. Although SMC were once considered the main targets of excitatory and inhibitory ENS motor neurons, neural input onto ICC and PDGFRα+ cells is likely also critical for mediating smooth muscle contractility and for generating complex motility patterns necessary for life.

There are at least five types of ICC in the bowel: ICC-MY, located between the circular and longitudinal muscle layers, ICC-IM, located within the circular muscle layer in colon and stomach, ICC-DMP, between the inner and outer parts of the circular muscle layer of the small intestine, ICC-SM, on the submucosal surface of the circular muscle layer of colon, and ICC-SS, in the subserosal layer (**Figure 7-1B**). ICC-MY and ICC-SM, the "pacemaker" cells of the bowel, generate rhythmic electrical slow waves of depolarization and hyperpolarization that propagate passively to SMC via gap junctions and synchronize SMC contraction. This baseline electrical

rhythm is present even when the ENS is absent. ICC-IM and ICC-DMP are closely associated with nerve varicosities (418) and electron microscopy suggests more nerve-ICC-IM contacts than nerve-SMC contacts (419). ICC-IM and ICC-DMP are believed to be the primary ICC that receive input from the ENS (418).

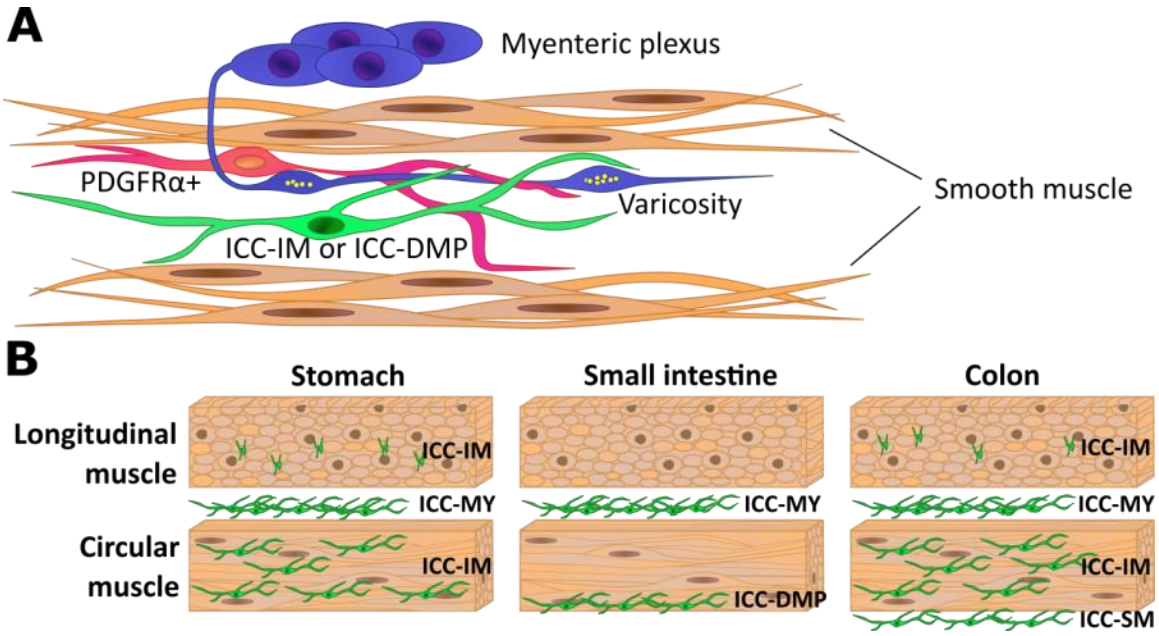

Figure 7-1: The SIP syncytium
(A) The SIP syncytium is composed of SMCs, ICCs, and PDGFR□+ cells which receive input from ENS varicosities. (B) ICC localization and composition varies with bowel region . Abbreviations: ICC-DMP, deep muscular plexus ICC; ICC-IM, intramuscular ICC; ICC-MY, myenteric ICC; ICC-SM, submucosal ICC.

To determine how ICC contribute to neuromuscular transmission, many early studies compared SMC recordings in wild type and ICC-IM-deficient animals during electric field stimulation (EFS). Although some investigators observed attenuated excitatory and/or inhibitory junction potentials in ICC-depleted smooth muscle, results were inconsistent (419-421). Possible explanations for the disparate findings include incomplete absence of ICC in certain model organisms (e.g., commonly used W/W^V mouse has inconsistent and incomplete ICC loss (29)), strain and species differences, differences in level of tissue pre-contraction or pre-relaxation (422), use of nifedipine (422), differences between bowel regions, and developmental changes in

innervation or smooth muscle reactivity in the absence of ICC. More recent studies test contributions of transduction pathways for specific neurotransmitters, often in genetically modified conditional knockout mice (51, 420, 422). These studies support the presence of parallel complementary pathways for signal transduction involving smooth muscle cells, ICC, and PDGFRα+ cells (**Figure 7-2A-B**).

7.2.1 - Inhibitory signaling

Inhibitory junctional potentials (IJPs) recorded from colon smooth muscle are composed of a fast purinergic phase that is followed by a slower nitrergic phase (51). The purinergic contribution to the IJP is probably mediated by PDGFRα+ cells, which express high levels of the purine receptor $P2Y_1$. The ligand for $P2Y_1$ receptors in the bowel was once thought to be adenosine triphosphate (ATP), but in recent years β-nicotinamide adenine dinucleotide (β-NAD) and adenosine 5-diphosphate-ribose (ADPR) have emerged as more likely candidates (34). Applying β-NAD and ADPR to PDGFRα+ cells activates apamin-sensitive small-conductance Ca^{2+}-activated K^+ (SK) channels, leading to potassium efflux and membrane hyperpolarization (423). The change in membrane potential spreads via gap junctions to nearby SMC. Purinergic receptors are also expressed on SMC and ICC, but they are unlikely to mediate the strong fast hyperpolarization associated with the IJP (34, 35).

Nitric oxide (NO) is a major signaling molecule in inhibitory motor neurons that acts on both ICC and SMC. NO binds and activates nitric oxide-sensitive guanylyl cyclase (NO-GC). Guanylate cyclase converts GTP to cGMP, which activates GMP-dependent protein kinase I (PRKG1). PRKG1 in turn phosphorylates serines and threonines on many intracellular proteins, causing hyperpolarizing via mechanisms that remain incompletely understood. Molecules downstream of NO (e.g. NO-GC, *Prkg1*) have been deleted from subsets of ICC and SMC using conditional knockout mice. Although inconsistent findings have been reported, the results suggest

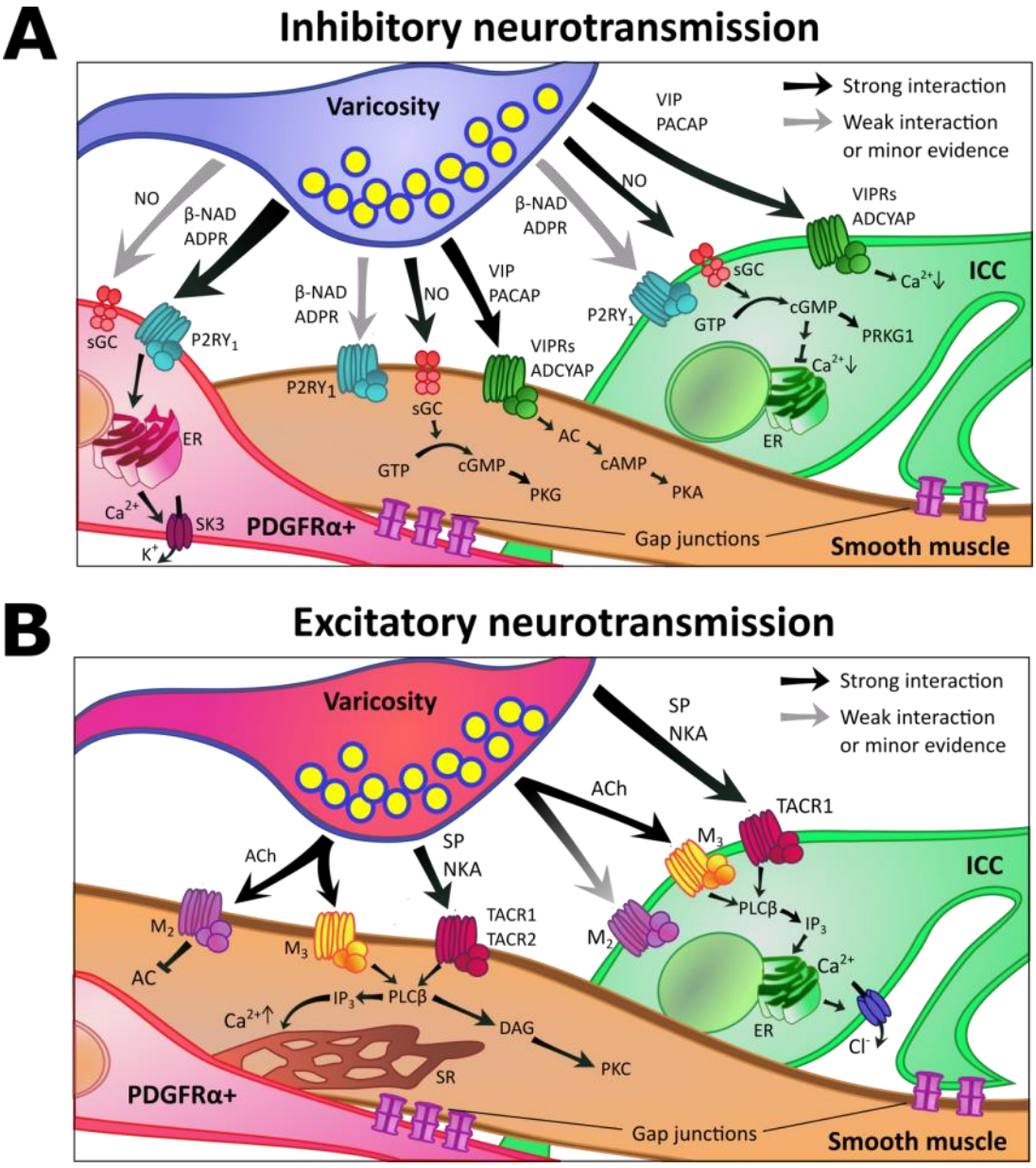

Figure 7-2: Inhibitory and excitatory motor neurotransmission.
(A) Inhibitory neurotransmission involves a combination of purine, NO, and VIP/PACAP signaling. (B) The primary neurotransmitters involved in excitatory neuromuscular transmission are acetylcholine and tachykinins. Abbreviations: AC, adenylate cyclase; ACh, acetylcholine; ADCYAP1R1, pituitary adenylate cyclase-activating polypeptide type 1 receptor; ADPR, ADP-Ribose; β-NAD, β-Nicotinamide adenine dinucleotide; cAMP, cyclic AMP; cGMP, cyclic GMP; DAG, diacylglycerol; GTP, guanosine triphosphate; ER, endoplasmic reticulum; ICC, interstitial cells of Cajal; IP_3, inositol triphosphate; M2, muscarinic receptor 2; M3, muscarinic receptor 3; NKA, neurokinin A; NO, nitric oxide; PACAP, pituitary adenylate cyclase-activating peptide; PKA, protein kinase A; PKC, protein kinase C; PRKG1, protein kinase G; PLCβ, phospholipase C beta; sGC, soluble guanylate cyclase; SK3, small conductance calcium-activated potassium channel 3; SP, substance P; SR, sarcoplasmic reticulum; TACR1, tachykinin receptor 1; TACR2, tachykinin receptor 2; VIP, vasoactive intestinal peptide; VIPR, VIP receptors.

that both ICC and SMC likely mediate NO signaling (51, 420). Interestingly, one study found that conditionally deleting NO-GC from ICC in mouse colon reduced IJP amplitude in response to EFS, but conditionally deleting NO-GC from ICC in mouse fundus completely abolished IJPs (51). This underscores an important and underemphasized issue in the literature: regulation of ICC, SMC, and PDGFRα+ cells by neural signaling may vary considerably depending on bowel region. Consistent with this observation, ICC localization and receptor expression differ in various bowel regions (**Figure 7-1B**). For instance, ICC-MY in stomach do not express the NO-GC subunit sGCβ1, whereas most ICC-MY in colon express sGCβ1, and some ICC-MY in colon express sGCβ1 at high levels (424).

A few recent papers suggest that PRKG1-independent (but NO-GC and cGMP dependent) NO signal transduction may occur in ICC (32, 33). Pacemaker rhythms in cultured colon ICC were slowed by NO donors and cGMP, but not by a PRKG1 inhibitor (32). Small-molecule activation of NO-GC decreased spontaneous calcium transients in ICC-DMP in mouse small intestine, but PRKG1 inhibition had no effect (33). These findings are difficult to reconcile with data showing absent NO-mediated IJPs in *Prkg1* conditional knockout mice (420). Possible explanations for the discrepancy include failure of the PRKG1 inhibitors to penetrate tissue, or differences between ICC subtypes studied.

Although the literature on how NO affects smooth muscle and ICC are sometimes contradictory, NO clearly has strong effects on both ICC and SMC in a guanylate cyclase-dependent manner. Further research is needed to determine (1) how members of the SIP syncytium in various bowel regions differ in receptor expression and response to signaling, (2) how innervation of the SIP syncytium differs in each bowel region, and (3) the significance of PRKG1-independent pathways in NO-mediated responses. Defining these characteristics may elucidate molecular mechanisms that generate diverse motility in each bowel region.

In addition to NO, inhibitory enteric neurons release vasoactive intestinal peptide (VIP) and pituitary adenylate cyclase activating peptide (PACAP). These neuropeptides likely signal through VIP receptors VIPR1 and VIPR2 and the PACAP receptor ADCYAP1R1, which are expressed on ICC and SMC (30). Typically, neuropeptides are released at high stimulus frequencies, so VIP and PACAP may play less prominent roles in direct motor neurotransmission than NO (30). In SMC, VIP/PACAP signaling is mediated via G_s which activates adenylyl cyclase, cyclic AMP(cAMP), and protein kinase A (PKA) (237). This increases Ca^{2+} transients that should increase the opening probability of Ca^{2+}-activated K^+ channels, causing membrane hyperpolarization (237). In ICC, VIP may act via a different pathway. VIP decreases calcium transients dramatically in some ICC, and calcium transients increase when a VIP inhibitor is added. These calcium transients likely control the activity of calcium-dependent chloride channels (CaCC) which regulate slow waves (33). The mechanism behind this response is currently unknown.

7.2.2 - Excitatory signaling

The major excitatory neurotransmitters involved in direct motor neurotransmission are acetylcholine (ACh) and tachykinins (neurokinin A (NKA), and substance P (SP)). ACh binds muscarinic M_2 and M_3 receptors on SMC and ICC, while tachykinins bind tachykinin receptor 1 (TACR1) and tachykinin receptor 2 (TACR2) receptors on SMC and TACR1 on ICC (**Figure 7-2B**). In ICC-DMP, signal transduction via M_3 receptors likely occurs through G_q leading to Ca^{2+} release from the endoplasmic reticulum and activation of CaCC such as anoctamin 1 (Ano1). Opening of CaCC causes a depolarizing current predicted to enhance the likelihood of action potential generation and increase contraction amplitude (36, 37). M_2 receptors are also expressed on ICC but may play a less important role than M_3 receptors (36, 38). In contrast, evidence from knockout mice suggests that both M_3 and M_2 receptors influence SMC contractility (39).

Like muscarinic signaling in ICC, tachykinin signaling via TACR1 is hypothesized to act via G_q signaling coupled to Ca^{2+} release and CaCC opening. Tachykinin signaling may be more important than muscarinic signaling in ICC-DMP. Applying TACR1 receptor antagonists attenuated basal Ca^{2+} transients in small intestine ICC-DMP, suggesting that ICC-DMP are tonically excited by tachykinins (36). The same may not be true in colonic ICC, which do not express TACR1 receptor as highly (36). In SMC, tachykinin signaling is transduced by both TACR2 and TACR1 receptors (40). Second messenger signaling likely occurs through protein kinase C (PKC) and IP_3 (30), although other pathways may be involved (40).

7.2.4 - ENS, the SIP syncytium, and bowel motility: putting it all together

When considering direct neural input to the SIP syncytium, it is important to remember that diverse motor patterns are needed for food to be digested and absorbed, and for waste to be eliminated. These motility patterns in human small intestine include peristalsis (waves of contraction and relaxation that propagate down the bowel), segmentation (alternating contraction and relaxation to mix food with digestive enzymes and bile), and the migrating motor complex (MMC) (where strong waves of contraction and relaxation propagate down the bowel during phase III to moves luminal contents toward distal bowel for elimination). In the colon there are high amplitude propagating contractions (HAPC) that move stool over long distances toward the rectum and occur only occasionally. Generation and maintenance of these motor patterns requires a complex interplay between neural signaling, ICC, PDGFRα+ cells, and SMC. In broad strokes, ICC continually produce oscillating electrical slow waves in the bowel that set the rhythm for many motor patterns. Slow wave electrical activity propagates from ICC to SMC, generating rhythmic SMC depolarization and contraction. Neural signaling onto the SIP syncytium generates and modulates ICC and SMC activity to produce the motor patterns described above. Stimuli from the environment alter ENS activity to determine which motor patterns should occur at

specific times (30). For example, segmentation in the small bowel occurs after meals, but phase III MMC predominates once most nutrients are absorbed. Although the ENS is not essential for generating some motor patterns, the ENS is probably the primary inducer of complex motility patterns needed for survival (31).

To "decide" what to do, sensory neurons of the ENS (called intrinsic primary afferent neurons, IPANs) respond to diverse stimuli including stretch and mucosal distortion (1, 2). Stretch sensing is mediated by mechanoreceptors located within the myenteric plexus, which fire in response to distention (24). Historically, it has been assumed that stimulation of enterochromaffin (EC) cells in the bowel mucosa and the resulting serotonin (5-HT) release onto IPANs play a major role in evoking enteric neural reflexes such as the peristaltic reflex. However, recent papers question the importance of serotonin release from EC cells for initiation of motility since mice lacking a critical enzyme involved in 5-HT biosynthesis in EC cells (tryptophan hydroxylase 1, or TPH1) survive to adulthood and have a normal gastrointestinal transit time (19). Further research has shown these mice have larger fecal pellets and aberrant colonic migrating motor complexes (15) suggesting that in the absence of 5-HT from EC cells, a higher degree of stretch is required to trigger contractions (16).

We have focused thus far on neurotransmission to the SIP syncytium, but enteric glia also influence bowel motility. Female mice lacking enteric glia have reduced gastrointestinal transit time and increased CMMC frequency compared to controls. Intriguingly, the same effect was not seen in males, suggesting potential glia-intrinsic sex-dependent differences, or sexual dimorphism in glial interacting partners (296). Other studies also suggest enteric glia influence bowel motility; for instance, mice lacking the glial-specific hemichannel connexin-43 had prolonged colonic transit, increased stool water content, and diminished contraction and relaxation amplitude (425). Mechanisms behind glial control of motility are not well understood. One hypothesis is that

trophic factors produced by glia may prevent ENS dysfunction. Another possibility is that enteric glia directly modulate ICC slow wave activity (426).

7.2.5 - Clinical relevance

Hirschsprung disease

The ENS forms from neural crest-derived precursor cells (ENCDC) that colonize the bowel during first trimester fetal development. In about 1:5000 children, ENCDC never reach the distal bowel resulting in a region where the ENS is completely absent. This problem is called Hirschsprung disease. In children with Hirschsprung disease, the region of bowel that lacks enteric ganglia (i.e. aganglionic bowel) is tonically contracted and does not have propagated motility, leading to functional obstruction. Because aganglionic bowel does not efficiently pass stool or air, Hirschsprung disease symptoms include distension, constipation, vomiting, abdominal pain, growth failure, and a predisposition to bowel inflammation (called enterocolitis) that may lead to death from sepsis. Hirschsprung disease provides absolute proof that the ENS is essential for life, since even a small region of aganglionosis can cause serious illness and premature death. Our recent review provides more detailed information about Hirschsprung disease symptoms and molecular mechanisms (57).

Chronic intestinal pseudo-obstruction syndrome (CIPO)

When the ENS is present throughout the bowel, but bowel motility does not consistently support survival or growth without at least intermittent intravenous nutrition, CIPO is the likely diagnosis. Symptoms of CIPO include repetitive episodes of abdominal distension and pain, vomiting, growth failure, and weight loss (89). CIPO may occur as a primary disorder, or it may be secondary to complications of another disease. CIPO should not be confused with transient

bowel motility defects such as ileus (the absence of bowel contractions) that commonly accompanies abdominal surgery, pancreatitis, appendicitis or sepsis.

The etiology of CIPO remains poorly understood, although clues are emerging from human and mouse genetics. Because so many cell types, transmitters, and signaling molecules impact ENS development and intestinal function, there are likely many underlying causes of CIPO, potentially including dysfunction of ENS, SMC, ICC, and/or PDGFRα+ cells. Unfortunately, even with advanced genetic tools like whole exome sequencing, causative genetic variants remain poorly defined. Only a few genetic causes of CIPO have been identified. These include mutations in the genes encoding filamin A (*FLNA*), DNA polymerase gamma (*POLG*), and gamma smooth muscle actin (*ACTG2*), leiomodin 1 (*LMOD*1), myosin heavy chain 11 (*MYH11*) and myosin light chain kinase (*MYLK*) (89, 91). Identifying more genetic causes of CIPO is critical as it will undoubtedly aid diagnosis. New medicines to treat CIPO are also desperately needed. Available prokinetic medications prevent ACh degradation (e.g. Pyridostigmine), activate 5-HT4 receptors (enhancing ACh release from excitatory motor neurons and increasing bowel motility; e.g. Cisapride, Tegeserod, Prucalopride), inhibit dopamine receptors (Metoclopramide, Domperidone), activate somatostatin receptors (Octreotide) or activate receptors for motilin, a peptide that increases GI motility (e.g. Erythromycin). Unfortunately, many of these medicines have serious side effects or are only minimally effective at enhancing small bowel motility and resolving symptoms for people with serious motility disorders like CIPO (89, 427).

7.3 – The ENS and vascular endothelium

During digestion, blood flow to intestinal mucosa increases as much as 2-fold owing in part to dilation of submucosal arterioles. Vasodilation and resulting hyperemia are needed to meet the high metabolic demands of the mucosa and to exchange nutrients, water, and solutes across

bowel epithelium. Neurogenic vasodilation of submucosal arterioles is mediated by extrinsic and intrinsic (ENS) innervation. In contrast, vasoconstriction of bowel arterioles is wholly under control of extrinsic sympathetic innervation. Here we briefly review ENS control of vasodilation, which has been extensively characterized.

Most studies of submucosal arteriole vasodilation evaluated guinea pig small intestine, using varied preparations including isolated submucosa and full thickness intact bowel. These studies suggest many triggers for ENS-mediated vasodilation, including gently stroking bowel mucosa, distorting the mucosa with puffs of gas, and distending smooth muscle with a balloon. Small distortions of the mucosa (stroking, puffing gas) cause enterochromaffin cells to release 5-HT onto enteric nerve terminals expressing 5-HT_3 (myenteric IPANS (428)) and 5-HT_4, and/or 5-HT_{1P} (submucosal IPANs (41)). Stimulation of these IPANs by 5-HT activates short (1-2 mm) reflex pathways within the submucosa, as well as longer reflex pathways that span submucosal and myenteric plexus (41). Stretching the bowel activates 5-HT_3 and 5-HT_4-insensitive mechanotransducers in the myenteric plexus (42) and possibly submucosal plexus (43) leading to vasodilation. Mechanical deformation of the gut activates neurites and soma of a large number of mechanosensitive enteric neurons within the myenteric plexus (24). These mechanosensitive neurons are multifunctional (i.e. they may be afferents, interneurons, or efferents) and their responses to mechanical stimulation may be rapid-adapting, slow-adapting, or ultra-slow-adapting (44).

A final common pathway for ENS-mediated vasodilation in guinea pig small intestine is release of ACh onto endothelial cells which activates muscarinic M_3 receptors, leading to NO release and vasodilation (45). In guinea pig distal colon, substance P and/or VIP release from submucosal plexus neurons may contribute to vasodilation (46). The ENS may also stimulate mast cells to release the vasodilator histamine directly onto submucosal blood vessels (45) via SP and/or calcitonin gene-related peptide (CGRP) (47).

7.3.1 - Clinical relevance

Impaired vascular control has been implicated in a number of inflammatory conditions, including necrotizing enterocolitis (NEC) and inflammatory bowel disease (IBD). NEC is a dangerous bowel disease in premature neonates, characterized by severe inflammation, ischemic necrosis, and sometimes bowel perforation. It is tempting to hypothesize that neuron dysfunction may contribute to development of necrotizing enterocolitis, for instance through dysregulation of vasodilation that occurs in response to feeding. Indeed, altered microcirculation involving constricted arterioles has been demonstrated in NEC (96) and damage to the ENS also occurs with NEC (97). However, there is not yet convincing evidence that ENS dysfunction is the primary cause of altered blood circulation in babies with NEC. Arguing against this hypothesis, vessel endothelial cells from bowel with NEC failed to generate NO in response to ACh, but vessels dilated in response to exogenous NO administration, suggesting dysfunction of endothelial cells may be paramount (98). This is similar to IBD, where vessel endothelium does not appropriately produce NO even when stimulated by ACh (99). Unfortunately, because defects seem intrinsic to endothelial cells, neuromodulators (e.g. AChE inhibitors) are unlikely to have therapeutic value in these disorders, although gut derived neural stem cells do appear to prevent NEC-like injury in a rodent model (97).

7.4 - Epithelial secretion and the ENS

5-HT released from enteroendocrine cells in response to mucosal stroking not only elicits peristalsis and supports vasodilation, but also activates fluid and electrolyte secretion into the gut lumen to facilitate digestion. 5-HT activates IPANS that in turn synapse on secretomotor neurons that release ACh or VIP. ACh acts via muscarinic receptors and VIP via VIPR1 receptors on crypt epithelial cells to increase intracellular Ca^{2+} (via phospholipase C and IP_3) and cAMP (via

G_s) respectively. Cyclic AMP activates the cystic fibrosis transmembrane regulator (CFTR) chloride channel. Calcium activates the HCLCA1 chloride channel inducing more transient chloride flux. Movement of chloride into the gut lumen is accompanied by sodium and water. The details of these circuits are much better understood than this brief description suggests, and they are beautifully described in reviews (48, 49).

Interestingly, a recent publication has also defined a role for enteric glia in the regulation of epithelial ion transport. When glial cells lack the glial-specific hemichannel connexin-43 neuron-regulated electrogenic ion transport was reduced while transmural conductance and epithelial permeability were not significantly changed. Activation of GFAP-expressing glial cells stimulated electrogenic ion transport similar to that observed with direct neuronal stimulation. Inhibiting neuronal activation with tetrodotoxin only partially reduced glial-induced electrogenic ion transport, indicating that the enteric glia interactions with the epithelium do not require neuronal activity (429).

7.4.1 - Clinical relevance

Dysfunctional regulation of epithelial secretion may lead to increased stool water content. VIP-producing tumors and SSRI-induced serotonin syndrome cause diarrhea by directly increasing neurotransmitters in the ENS circuit that controls epithelial secretion (100). Cholera, Rotavirus, Clostridium difficile, Cryptosporidium, and enterotoxin producing Escherichia coli all cause profuse watery diarrhea at least in part by activating ENS circuits (101, 102).

7.5 - The ENS, epithelial proliferation and repair

Bowel epithelium is replaced every few days via proliferation of stem cells and transit-amplifying cells in the crypt. Newly-generated cells differentiate into absorptive epithelial cells, goblet cells, and EC (among other cells types) before being lost via apoptosis. Regulation of

epithelial proliferation and differentiation is carefully controlled since too little epithelial replacement reduces absorptive capacity and too much epithelial proliferation causes cancer. Among other regulatory mechanisms, accumulating data suggest the ENS influences epithelial proliferation and repair, as well as epithelial barrier function, but that effects of the ENS on bowel epithelium are complex.

For example, chemical ablation of the myenteric plexus with benzalkonium chloride increases epithelial proliferation, crypt depth and villus height (430) suggesting inhibitory effects of the ENS on epithelial renewal. Consistent with the hypothesis that ENS components reduce epithelial proliferation, mice with a hypomorphic ENS because of mutations in the tyrosine kinase receptor *Ret* have enhanced small bowel epithelial proliferation after small bowel resection during the adaptive response (431). In contrast, loss of the hepatocyte growth factor receptor *Met* within the ENS leads to reduced epithelial proliferation after dextran sodium sulfate (DSS)-induced bowel injury (327). Because *Met* and *Ret* are expressed in different subsets of myenteric neurons, these observations suggest some enteric neurons enhance and others suppress bowel epithelial proliferation depending on context.

Consistent with this hypothesis, ACh activates muscarinic receptors on intestinal stem or progenitor cells to enhance epithelial proliferation (432-435). Neuron-derived serotonin activates 5-HT(2A) receptors on cholinergic neurons, enhancing ACh release (436) and also enhancing epithelial proliferation. Interestingly, glucagon-like peptide 2 (GLP-2), a potent stimulant for epithelial proliferation, might also work via the ENS since GLP-2 receptors are expressed by enteric neurons, but not intestinal epithelium (437). Alternatively, GLP-2 might support epithelial proliferation via subepithelial myofibroblasts that express GLP-2 receptor and release IGF-1 in response to GLP-2. In support of this hypothesis, IGF-1 is required for GLP-2 intestinotrophic effects and this mechanism could bypass the ENS (438).

In addition to regulating epithelial cell proliferation, enteric neurons appear to enhance epithelial barrier function. Co-culture of primary enteric neurons with primary intestinal epithelial stem cells, increases expression of tight junction associated protein zona occludens 1 (ZO-1), increases transepithelial resistance across the monolayer, and reduces apical to basolateral dextran permeability (105). Parallel studies suggest enteric glia may also influence intestinal epithelial barrier function (439-442). For these studies, enteric glia were eliminated using a transgenic GFAP-Cre driver to induce expression of HSV-TK or using the GFAP promoter to drive expression of the neoantigen haemagglutinin. In the former case, treatment with gancyclovir induced cell death in any cell that expressed the transgene by conversion of the antiviral agent to a toxic nucleotide analog. In the latter case, neoantigen expression led to CD8+-mediated cell death of any neoantigen-expressing cell. Eliminating glia in these ways led to massive bowel inflammation. Co-culture of epithelial cells and glia also changed gene expression (285) in epithelial cells, increasing tight junction proteins (like ZO1 and occludin) and decreasing transepithelial permeability in cultured epithelial monolayers (285, 441, 442). S-nitrosoglutathione was identified as a soluble glial-derived factor that increased epithelial barrier function *in vitro*. This compound drastically reduced the development of enterocolitis *in vivo* after HSV-TK-mediated damage to ENS and epithelium (441). Another study found that mucosal glia strongly upregulate their expression of GDNF in states of inflammation (443, 444). GDNF reduced epithelial apoptosis *in vitro* (445, 446) and in a mouse model of DSS-colitis, GDNF overexpression increased tight junction protein expression and decreased epithelial permeability (447). Collectively these studies provided substantial support for the hypothesis that enteric glia enhance epithelial barrier function. Interestingly, enteric glial cell-derived GDNF also activates RET on type 3 innate lymphoid cells (ILC3) to induce release of IL-22, which enhances epithelial expression of genes that reduce bacterial translocation (448). Collectively these studies provided substantial support for the hypothesis that enteric glia enhance epithelial barrier function.

Surprisingly, an elegant set of experiments showed that enteric glial cells are not required for maintenance of epithelial integrity in mice. The authors eliminated all enteric glia by inducing cholera toxin subunit A expression under the control of the PLP1 promoter. In this system, no enterocolitis developed and epithelial cell ultrastructure, proliferation and permeability were unaffected despite a dramatic loss of enteric glia. The absence of glia in the setting of DSS-induced colitis did not worsen symptom severity or specifically affect transepithelial permeability. Lastly, the authors showed that the discrepancy between their study and the previous *in vivo* studies could be explained by the aberrant GFAP-Cre transgene expression in a small number of epithelial cells which caused direct injury to the epithelial cell layer after ganciclovir treatment or induction of neoantigen expression (296).

Overall, it is clear the ENS influences intestinal barrier function in a normal physiologic state and during inflammation. The exact contributions of the different enteric neuron subtypes and of enteric glia have not yet been conclusively elucidated.

7.6 - The ENS and macrophages

Two broad classes of tissue-resident macrophages contribute to intestinal immune function. The most abundant macrophage (Mφ) class resides in the lamina propria (LpMφ) directly beneath bowel epithelium (413) and are surrounded by dense submucosal neuron projections that innervate the epithelial layer. Direct functional interactions between ENS and LpMφ have not yet been document, but seem plausible. The second, relatively understudied group called muscularis macrophages (MMφ) are very closely associated with the myenteric plexus and emerging literature suggests significant cross-talk and even developmental interdependence between these cell types (**Figure 7-3**).

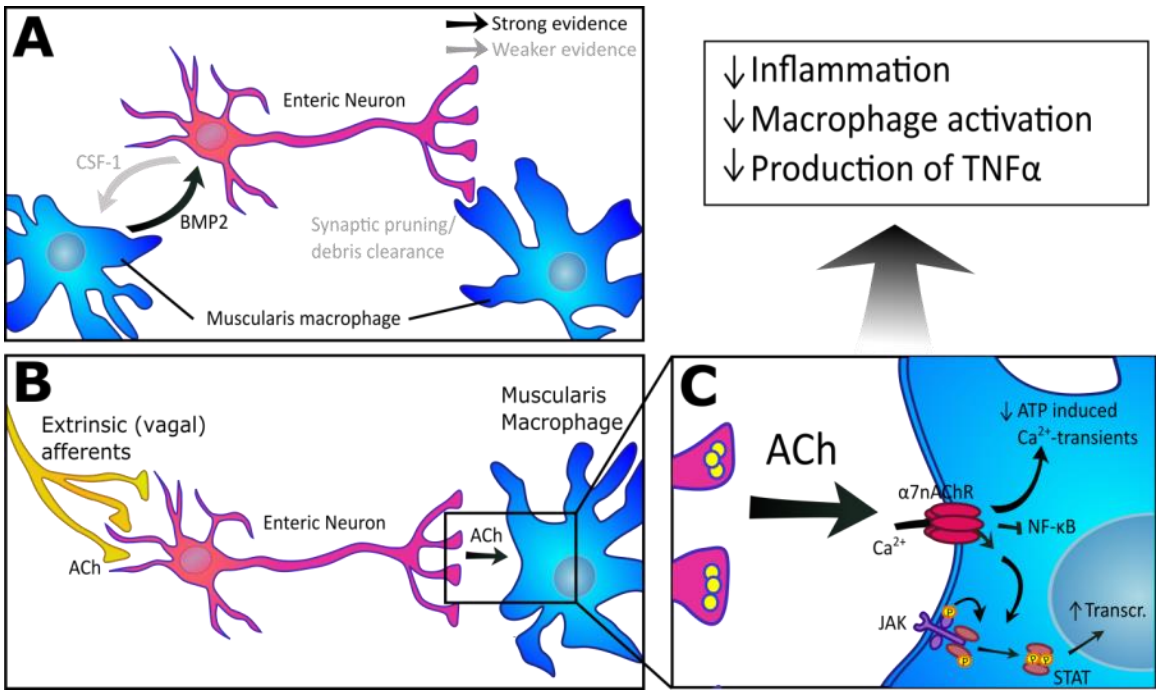

Figure 7-3: Interaction between muscularis macrophages and enteric neurons.
(A) Muscularis macrophages support enteric neurons through BMP2 signaling and possibly synaptic pruning and clearing of debris. (B) Enteric neurons are a key part of the cholinergic anti-inflammatory pathway (CAIP) reducing the activation of macrophages through vagal stimulation. (C) Activation of muscularis macrophages by ACh decreases macrophage activation and decreases production of TNFα. Abbreviations: α7nAChR, α7 nicotinic acetylcholine receptor; ACh, acetylcholine; ATP, adenosine triphosphate; BMP2, bone morphogenetic protein 2; CSF-1, colony stimulating factor 1; JAK, Janus kinase; NF-κB, nuclear factor kappa-light-chain-enhancer of activated B cells; STAT, signal transducer and activation of stimulation; TNFα, tumor necrosis factor alpha; Transcr., transcription.

7.7 - The ENS depends on MMφ for normal structure and function

MMφ produce bone morphogenetic protein 2 (BMP2), a morphogen that binds its receptor BMPRII on neurons and influences ENS precursor differentiation, neurite fasciculation, and ganglion formation (290, 449). Mice lacking MMφ during development have increased numbers of enteric neurons and a disorganized ENS. Interestingly, this phenotype is similar what occurs when the BMP antagonist noggin is over-expressed *in vivo* (449, 450). Acute depletion of MMφ from the bowel in adulthood enhanced colon contractility in response to stretch *ex vivo*, but delayed expulsion of a bead by the colon *in vivo*, suggesting problems with coordinating muscle activity. The motility changes were not limited to the colon since gastric emptying was also

accelerated two days after acute MMφ depletion. The effects of MMφ depletion on *ex vivo* colon contractility could be mimicked by dorsomorphin (a BMP signaling inhibitor) or rescued by adding BMP2. Consistent with these observations, nuclear localization of pSMAD1/5/8 (a downstream effector complex for BMP signaling) was reduced in enteric neurons from MMφ-depleted bowel. Interestingly, antibiotic treatment to reduce luminal microbes reduced bowel MMφ, BMP2 levels, and nuclear pSMAD1/5/8 in enteric neurons. Antibiotics increased whole-bowel transit time and enhanced colon contractility *ex vivo*, suggesting dysfunctional bowel motility (450). Taken together, these results offer strong evidence that enteric neurons rely on BMP2 produced by MMφ for normal morphology and function. These observations also suggest that postnatal acquisition of intestinal microbes critically shapes neuroimmune interactions in the bowel. Some authors have suggested that MMφ also contribute to normal ENS morphology by phagocytosing neuronal debris (115). This function of MMφ would be similar to that of microglia, the tissue-resident macrophages of the brain, which clear apoptotic neurons and eliminate unnecessary axons and synaptic connections (i.e. synaptic pruning). Further research is needed to determine the extent to which phagocytosis by MMφ shapes the ENS.

7.8 - Activated MMφ regulate enteric neuron excitability during inflammation

Activated murine MMφ release chemokines, cytokines (interleukin 1, monocyte chemoattractant protein 1, interleukin 6, tumor necrosis factor alpha (TNFα)) and other bioactive compounds (NO, prostaglandins) (414, 451). NO regulates neuron excitability and directly relaxes SMC, so it is not surprising that increased NO reduces bowel contractility. Some enteric neurons also produce TNFα receptors, and TNFα activates neuropeptide Y (NPY) expression. NPY increases bowel epithelial permeability during inflammation (452), suggesting a neuro-immune interaction that might be modulated to reduce intestinal inflammation.

7.9 - The ENS modulates MMφ activation, and may affect MMφ survival

Macrophages express many neurotransmitter receptors, including α7 nicotinic acetylcholine (α7nAChR), tachykinin, glycine, and P2 purine receptors, all of which may alter MMφ function (451). The most well-characterized example of ENS modulation of MMφ is the cholinergic anti-inflammatory pathway (CAIP), a circuit involving the vagus, ENS, and MMφ. Stimulating the vagus nerve activates cholinergic enteric neurons near MMφ, leading to release of ACh and stimulation of α7nAChR on MMφ. This reduces inflammation by decreasing the ATP-induced calcium transients in MMφ, decreasing macrophage activation (453) and reducing TNFα production by macrophages (454). α7nAChR also activates the Jak2-STAT3 signaling pathway, which likely plays a role in attenuating macrophage activation (455). ENS-MMφ signaling is likely not limited to ACh-α7nAChR interactions given the large number of neurotransmitter receptors expressed by macrophages. Extrinsic nerves also modulate MMφ activation directly through norepinephrine signaling onto adrenoreceptor β2, but this pathway is probably independent of the ENS (413).

Intriguingly, adult enteric neurons express colony stimulating factor 1 (CSF-1), the primary survival factor for MMφ (450). Since other CSF-1 expressing cell types had not been identified in the bowel, we hypothesized that MMφ rely on CSF-1 produced by enteric neurons for normal development. Surprisingly, MMφ appear normal in neonatal bowel even in the absence of an ENS. Other intestinal cell types (endothelial cells, ICC) produce CSF-1 perinatally and may be the main cells supplying MMφ with CSF-1 in early life (220). Since a considerable ENS development occurs after birth, ENS-MMφ interactions likely mature postnatally, and it remains possible that CSF-1 expressed by neurons is critical for MMφ survival in adulthood. Global knockout models of CSF-1 (i.e. *Csf1*$^{op/op}$ mice) lack all MMφ, but thus far conditional depletion of CSF-1 from enteric neurons has not been reported. This experiment would be needed to confirm that ENS-derived CSF-1 influences adult MMφ number or function.

7.9.1 - Clinical relevance

Post-operative paralytic ileus is a common condition characterized by transiently impaired bowel motility after abdominal surgery. Post-operative ileus may be partially mediated by low-grade inflammation leading to impairment of muscle contractility. Supporting a role for MMφ in post-operative ileus, depletion of MMφ by clodronate or genetic MMφ loss in *Csf1*$^{op/op}$ mice protects against post-operative ileus (456). Intriguingly, vagal nerve stimulation reduced inflammation and improved post-operative ileus (457). This is likely mediated by the vagal-ENS-MMφ anti-inflammatory pathway described previously (453). MMφ activation has also been implicated in other gastrointestinal motility disorders such as gastroparesis, which also may be helped by vagal stimulation. This topic is summarized in a number of excellent recent reviews (414, 451).

7.10 - ENS interactions with the microbiome

After birth, the bowel must grapple with drastic changes as it is exposed to a diverse array of microbes seeking to establish themselves within the gut lumen. Microbial colonization occurs while the ENS is still maturing, and we now believe these microbes substantially affect ENS development. At least two studies have shown reductions in neuron density in the small intestine and/or colon of young germ-free (GF) mice compared to age-matched gnotobiotic controls (54, 55). Oddly, one study reported an increased proportion of nitrergic myenteric neurons in their 3-day-old GF mice (54), while the other study, which used 4-week old GF mice, reported *decreased* nitrergic neuron numbers (55). The cause of this difference is unclear.

A few mechanisms for microbial effects on ENS development have been proposed. Interestingly, enteric neurons and glia express toll-like receptors (TLR), pattern recognition receptors that are activated by pathogen associated molecular patterns (PAMPs) as part of the

innate immune system. TLRs 3, 4, and 7 are expressed in enteric neurons and glia (458). Additionally, TLR2 may be expressed in ENS and in surrounding cells including SMC (198). Global deletion of TLR2 reduced the number of nitrergic neurons in colon, and accelerated gastrointestinal transit (198). Mice with a global deletion of TLR4, which detects lipopolysaccharide (LPS; a major component of gram-negative bacteria) had reduced numbers of nitrergic neurons, slow bowel motility, and reduced bowel relaxation in response to EFS. Conditional knockout mice missing *Myd88* selectively in neurons and glia also had delayed colon transit and reduced nitrergic neurons (55) MYD88 is a mediator of TLR4 activity. Finally, a high fat diet, which causes dysbiosis, also reduced NO-producing myenteric neuron number and slowed bowel motility in a TLR4-dependent fashion (199).

One possible explanation for these findings is that microbes could activate TLRs on enteric glia or mesenchymal cells, leading to release of the RET ligand glial cell line-derived neurotrophic factor (GDNF). GDNF provides trophic support for enteric neurons expressing RET and its co-receptor GDNF Family Receptor alpha 1 (GFRα1) during ENS development (124). In addition, GDNF contributes to motility by stimulating the ascending limb of the peristaltic response (320). In support of this theory, mice lacking TLR2 had significantly reduced GDNF in muscle. Administering recombinant GDNF to these mice subcutaneously for seven days restored neuron numbers and reversed dysmotility (198). Some evidence suggests enteric glia produce GDNF in response to inflammation (443), making them a plausible intermediary in this pathway, although SMCs or other mesenchymal cells could also be involved.

In addition to developmental effects, the microbiome can affect the ENS in adult life. Microbiome composition directly affects mature ENS function by altering electrophysiologic properties of neuron subtypes (459) and leading to changes in intestinal motility and neurally-mediated secretion (460, 461). Furthermore, giving mice antibiotics reduces neuron numbers and slows gastrointestinal transit (55). The ENS can also influence the composition of the

microbiome. In a zebrafish model of HSCR, the pathogenic over-abundance of pro-inflammatory bacterial strains could be corrected simply by restoring ENS function (103). These observations highlight just a few of the complex interactions between gut microbes and the ENS; a more detailed description of ENS-microbiome interactions can be found in recent reviews (462, 463).

7.11 - ENS interactions with the adaptive immune system

Enteric neuron projections can be found within mucosal lymphoid follicles (Peyer's patches) (464, 465). When lymphocytes from Peyer's patches were exposed to neuropeptides, they significantly increased their proliferation rate and immunoglobulin synthesis (104). This suggests the exciting possibility that enteric neurons can directly influence the adaptive immune system. For example, the Y1 receptor that binds neuropeptide Y is expressed on monocytes, macrophages, lymphocytes, and granulocytes (466). Y1-deficient mice have reduced antigen presenting cell function, reduced effector T cells, and reduced production of TNFα and IL-12 by macrophages. Similarly, *Npy-/-* mice have lower TNFα levels and *Y1-/-* mice resist colitis that occurs after epithelial injury with dextran sodium sulfate (DSS) (467). VIP is produced by inhibitory motor neurons, descending interneurons and secretomotor neurons of the ENS to control motility and epithelial function. The VIP receptor is also expressed by T-cells, where VIP promotes a T-reg phenotype (468), by dendritic cells where VIP induces a tolerogenic phenotype (469, 470), and by macrophages where VIP inhibits production of TNFα, IL-6 and IL-12p40 (468). These anti-inflammatory effects of VIP *in vitro* contrast with the observation that *VIP-/-* mice are resistant to TNBS-induced colitis (471) and LPS-induced endotoxemia (472). The reason for this discrepancy is not known.

7.12 - ENS interaction with enteroendocrine cells

Enteroendocrine cells (EEC) are a diverse group of neuroendocrine cells in the bowel epithelium that produce hormones and neuropeptides in response to stimulation from the gut lumen. The molecules produced by EEC act locally on cells within the mucosa, as well as systemically via the bloodstream (473). Significant cross-talk occurs between EEC and the ENS to modulate vasodilation, motility and epithelial secretion. We already alluded to one mechanism by which enterochromaffin cells (EC), a subtype of EEC, signal enteric neurons through release of 5-HT onto nerve terminals. The triggers for 5-HT release are incredibly diverse and include mechanical deformation of the mucosa, macromolecules (e.g. glucose, fatty acids, amino acids), chemical irritants (e.g. allyl isothiocyanate), injury or stress (e.g. norepinephrine), and changes in the bacterial milieu (e.g. butyrate and other short chain fatty acids) (13, 473). In response to stimulation, EC activate neurons through the release of 5-HT onto nerve terminals. In addition to 5-HT, EEC produce neuropeptides such as somatostatin, motilin, VIP, glucagon-like peptide-1 (GLP-1) and cholecystokinin (CCK), which modulate ENS activity (474-476). It has traditionally been assumed that these neuroactive peptides signal in a paracrine manner. However, presynaptic and postsynaptic markers have been identified on EC, suggesting that EC communicate with nerves via synapse-like structures (13, 477). Even more compelling, monosynaptic transmission of modified rabies virus confirms the presence of functional efferent synapses (477). Unfortunately, the *in vivo* data does not address the question of whether the EC form synapses with enteric or extrinsic neurons (477). There is a paucity of research regarding EEC-ENS connections and particularly efferent ENS signaling onto hormone-producing EEC. Given the similarity in signaling molecules and receptors between EECs and the ENS, it seems very likely that these cells communicate through additional pathways that remain to be discovered.

7.13 - The ENS, CNS and the autonomic nervous system

A variety of extrinsic nerves innervate the bowel, including sympathetic nerves, the parasympathetic vagus and sacral plexus nerves, and the dorsal root ganglia. Some of these nerves interact directly with their targets in the bowel, but they may also mediate their effects indirectly by synapsing on enteric neurons. We already mentioned the cholinergic anti-inflammatory (CAIP) pathway, where vagal nerve fibers signal ENS intermediaries that then signal macrophages to reduce inflammation. Here we provide a brief overview of other important ENS interactions with the autonomic nervous system. Please see the following reviews for a more in-depth discussion of this topic (2, 478).

7.14 - Sympathetic neuron-ENS interactions

Sympathetic nerve endings contact the vast majority of enteric neurons (479), and may also activate enteric glia via ATP release (480). Sympathetic nerves indirectly regulate epithelial secretion by inhibiting secretomotor neurons in the submucosal plexus. This inhibition is likely tonic since transepithelial secretion is greatly enhanced after sympathectomy (479), and acute sympathetic inhibition effects on secretion are most apparent when the secretomotor reflex has been activated (481, 482).

The sympathetic nervous system coordinates motility across large segments of bowel. The changes in motility are mediated by reflex arcs that involve afferent sensory neurons of the ENS and efferent inhibition of enteric neurotransmission by the sympathetic nervous system. These reflex arcs may include or bypass the CNS, depending on context. Sympathetic reflexes have been worked out in detail and are well described in the following review (479).

7.15 - Parasympathetic-ENS interactions

Parasympathetic innervation of the upper gastrointestinal tract is exclusively provided by

the vagus nerve and vagal projections are known to reach as far as the colon. Whether the entire bowel is innervated by the vagus nerve is still contested. Evidence suggests that the innervation includes the distal colon at least in some animal models (483). The pelvic nerves may provide additional parasympathetic innervation to the lower gastrointestinal tract. However, a recent study argues that these nerves are actually part of the sympathetic nervous system (484).

Most enteric ganglia in the small intestine and stomach are innervated by vagal nerve fibers (485). The vast majority of vagal nerve fibers are sensory and transmit afferent input to the CNS. It is unclear if afferent vagal signaling to the CNS is directly influenced by the ENS. Vagal-enteric (efferent) neurotransmission is predominantly cholinergic, although additional neurotransmitters have been identified in preganglionic vagal neurons (catecholamines and NO) and could have an auxiliary role (486, 487). Efferent vagal input affects all functions of the ENS, including the regulation of bowel motility, epithelial secretion, and vasoconstriction (2). Additionally, the vagus nerve mediates anti-inflammatory effects on the bowel through enteric neurons as part of the CAIP as described earlier (453).

7.15.1 - Clinical relevance

The pathways described above confirm bidirectional communication between the ENS and CNS that has important effects on bowel function, but the gut also influence the brain, an interaction referred to as the “Gut-Brain Axis” (488). An additional intriguing hypothesis is that these pathways may lead to CNS disease since protein misfolding events that occur in the ENS could be initiators for certain CNS diseases such as Parkinson’s disease (PD). PD involves the prion-like misfolding of α-synuclein which aggregates into deposits called Lewy bodies, leading to neurodegeneration and dementia. Genetic changes or ingested toxins like the pesticide rotenone could first cause α-synuclein aggregation in the ENS (489), which then travels to the CNS via the vagus, where they induce misfolding of additional α-synuclein to cause the

characteristic Lewy body pathology. Support for this hypothesis includes the observation that Lewy body-type pathology is found within enteric neurons of people with PD (490), bowel symptoms often precede CNS symptoms and correlate with disease severity (491), and that α-synuclein aggregates can travel from the bowel to the brain via the vagus nerve (492, 493). In humans, truncal vagotomy may reduce PD risk (494, 495). Similar transit of misfolded protein from the bowel to the brain could also explain the spread of prion diseases like kuru, variant Creutzfeldt-Jakob, scrapie, chronic wasting disease and spongiform encephalopathy where ingestion of misfolded prion proteins initiates disease pathogenesis (496). More details are provided in excellent reviews (497-499).

7.16 - ENS and the CNS

Since the ENS shares many neurotransmitters, receptors, and transcription factors with the CNS, it is not surprising that many people with CNS disease also have problems with bowel function. People with autism spectrum disorder (ASD) are 3-4 times more likely to have gastrointestinal symptoms than unaffected individuals; intriguingly, mutations in chromodomain-helicase-DNA binding protein 8 (CDH8), haploinsufficiency for the transcription factor TCF4, an activating mutation in the sodium-dependent 5-HT transporter (SERT/SLC6A4), and MET mutations are all directly linked to ASD and GI motility disorders (327, 500-503). Mice expressing mutant forms of amyloid precursor protein associated with familial Alzheimer disease accumulate amyloid beta in enteric neurons, have a reduced enteric neuron number, dysmotility and increased vulnerability to bowel inflammation (504, 505). Mutations in TAR DNA-binding protein 43 (TDP-43) that cause familial amyotrophic lateral sclerosis (ALS), may also cause ENS defects, including intestinal obstruction in the Prp-TDP43^{Ala315Thr} mouse model (506, 507). There is much more to learn about links between ENS and CNS disease.

7.17 - Summary

The enteric neurons and glia richly integrate sensory stimuli to control bowel motility, epithelial function, blood flow, and immune system activity. To do this, almost every cell of the bowel wall closely interacts with the ENS including smooth muscle, ICC, PDGFRα+ cells, EEC, epithelial cells, blood vessels, and many hematopoietic lineages. The ENS also interacts with extrinsic sympathetic, parasympathetic and sensory nerves, and is influenced by hormonal signals to modulate bowel function to meet systemic needs. Mechanisms and cell types that impact ENS activity remain under-investigated. Defining molecular and cellular mechanisms of ENS activity promises new approaches to dangerous bowel motility disorders (Hirschsprung disease, CIPO, gastroparesis), common and less dangerous motility problems (irritable bowel syndrome, chronic constipation, functional dyspepsia), inflammatory bowel disease, necrotizing enterocolitis, and ischemic bowel disease. Given links between gut microbes, bowel motility, epithelial function and CNS activity, ENS biology may also provide new approaches to addressing complex problems like anxiety, depression, autism, Parkinson's and ALS, and Alzheimer's disease as we begin to define the interplay along the gut brain axis.

7.18 - Acknowledgements

ROH is supported by the Irma and Norman Braman Endowment, the Suzi and Scott Lustgarten Center Endowment, The Children's Hospital of Philadelphia Research Institute, March of Dimes 6-FY15-235, FDA (1R01FD005312-01), Canadian Institute of Health Research (377028) and the NIH SPARC Program OT2OD023859. CMW is supported by NIH NIDDK (1F30 DK117546-01). CMW and SS would like to thank Sanja Popovic, Tiancheng Wang, Sohaib Hashmi, and Natania Field for their unwavering support and insightful feedback.

CHAPTER 8 : APPENDIX B: ROBUST VISUALIZATION OF HUMAN COLON ENTERIC NERVOUS SYSTEM WITHOUT TISSUE SECTIONING.

This chapter is currently under review at *Gastroenterology*. Authors: Kahleb D. Graham*, Silvia Huerta López*, Rajarshi Sengupta, Archana Shenoy, Sabine Schneider, Christina M. Wright, Michael Feldman, Emma Furth, Federico Valdivieso, Amanda Lemke, Benjamin J. Wilkins, Edward Doolin, Marthe J. Howard, Robert O. Heuckeroth. Copyright©2018 the authors.

* Co-first authors; contributed equally

8.1 - ABSTRACT

Background & Aims: Current understanding and management of bowel motility disorders is limited by histologic techniques that rarely yield valuable information about cells that control motility. These cells are deep in the bowel wall, not uniform in distribution, and impossible to see in sufficient detail in small two-dimensional sections routinely used for human pathology.

Methods: We developed a new technique to image in three dimensions the enteric nervous system (ENS) and other cells that control motility in human colon by combining tissue clearing, immunohistochemistry, confocal microscopy, and quantitative image analysis. Our methods do not require tissue sectioning and can be scaled to evaluate large bowel regions.

Results: Using human adult colon, one of the thickest bowel regions, we tested many approaches and dozens of antibodies until we established a method that worked consistently to visualize the human ENS in three dimensions. By imaging colon from people who do not have bowel motility disorders, we generated unprecedented images, and we provide detailed quantitative data about the density of neurons and glia, ratios of cholinergic and nitrergic neurons, and organization of the ENS. We also provide a two 4.5 cm x 0.6 cm regions from resected Hirschsprung disease

bowel demonstrating a hypoganglionic transition zone in an infant. Murine images for comparison highlight advantages of whole mount staining.

Conclusions: Most of what we need to know about ENS structure is only visible in three dimensions. Our new techniques and quantitative data provide the opportunity to radically change how we evaluate bowel dysmotility and may be applicable to other types of bowel disease.

8.2 - INTRODUCTION

Diverse enteric nervous system (ENS) structural variants that may have relevance for human bowel motility disorders are clearly documented in mice because wholemount staining allows exceptional ENS visualization(134, 263). Human ENS is thought to contain about as many neurons as spinal cord with ~20 neuron and 7 glia types(106, 401, 416, 508). Although ENS controls most bowel functions (106, 416), ENS comprises < 1:1000 bowel wall cells (our estimate), and is buried in opaque tissue making visualization challenging. A few approaches demonstrated elegant ENS structures in human bowel(509-512), but methods were not reproducible in our hands, or failed to demonstrate ENS in large intact regions. Clinical histology only detects dramatic ENS defects (e.g., neurons present or absent) and quantitative analyses provide highly variable results(387, 513, 514), impairing understanding bowel motility disorders. Defining defects causing human disease is essential to find new cures. We therefore sought to develop robust, highly reproducible methods to visualize cells controlling human colon motility. Our new approach provides three-dimensional ENS views in large colon regions without sectioning, preserving interactions with other bowel cells. This approach should provide novel insight into human disease, but first we must define “normal” human bowel.

Bowel motility disorders alter smooth muscle contraction and relaxation(515) governed by integrated circuits including enteric sensory neurons, interneurons, excitatory and inhibitory motor neurons (2, 106, 416, 516), pacemaker cells called Interstitial cells of Cajal (ICC)

(517),enteric glia, muscularis macrophages, platelet derived growth factor receptor alpha (PDGFRα+), and enteroendocrine cells (2, 106). Cell type-specific disease origins are not well understood for human bowel motility disorders, in part because thin sections provide limited views of important anatomy.

Defining cell type-specific defects that affect bowel motility is most important for life-threatening diseases like Hirschsprung's (57, 59), achalasia (518), gastroparesis (519), and chronic intestinal pseudo-obstruction (CIPO) (427). Improved imaging could provide new ideas about pathogenesis or treatment. We focused on human colon, which is frequently affected in Hirschsprung disease and CIPO. We provide 280 confocal Z-stacks, detailed quantitative data from 14 adults and show transition zone hypoganglionosis in one child with Hirschsprung disease.

8.3 - METHODS

All authors had access to data and approved final manuscript.

Mice: Studies adhere to ARRIVE guidelines (520) and Institutional Animal Care and Use Committee at Children's Hospital of Philadelphia (IACUC #16-001041). P0 *GFRα1-/-* (MGI Cat# 3715269, RRID:MGI:3715269)(125) and WT littermate (C57BL/6 background) were analyzed (9-12 AM). Dam was fed Mouse Diet 5015* (LabDiet), not fasted, housed on corncob (Anderssen) in Lab Products (Seaford, DE) caging.

Human Tissue: Colon was acquired with Institutional Review Board approval (Children's Hospital of Philadelphia (CHOP) IRB#13-010357, Perelman School of Medicine at University of Pennsylvania IRB#804376). Abramson Cancer Center Tumor Tissue Bank or CHOP pathology de-identified tissue providing limited clinical data.

Human colon staining: Detailed protocol is at protocols.io (Will add link at publication).

Tissue processing: Colons resected for clinical indications (Supplemental Table 2) remained at ambient temperature until arrival in pathology following routine hospital procedures. Transfer to sterile ice cold 1X phosphate buffered saline (PBS) occurred 61-112 minutes after resection. Staff pathologists provided regions without recognized abnormalities. Lab received coded specimens in PBS on ice. While covered with PBS, fat was removed. Tissue was pinned along edges (serosa up) to Sylgard® 184 Silicone Elastomer (Dow) using insect pins. We stretched while pinning making colon thin, flat, and uniform thickness. Pins were repositioned several times to stretch colon as muscles relaxed increasing area 2.6-fold (N = 3, SEM = 0.15) compared to un-stretched colon. Pinned tissue was fixed (4% paraformaldehyde, 4^{o}C overnight), then transferred to PBS. Edges with pin holes were trimmed. Full thickness colon was cut with scissors. Many specimens were 1 x 1 cm^2. Larger colon also worked well (e.g. 2 x 3 cm^2, 4.5 x 0.6 cm^2). Stored tissue (4^{o}C, 50% PBS/50% glycerol/0.05% sodium azide) could be stained months later without obvious tissue degradation.

Immunohistochemistry: 1 x 1 cm^2 fixed colon were processed in 24-well VWR Culture Plates (Non-treated), 2 cm diameter, Cat #10861-558). Reagent volumes: 500-1000μL/well (enough to cover tissue). After washing (PBS, 3 x 5 minutes, room temperature), incubating in 100% methanol (1 hour, on ice) to permeabilize and remove lipids, and treating with Dent's bleach (5 mL 30% hydrogen peroxide, 5 mL dimethylsulfoxide, 20 mL 100% methanol) (311) (2 hours, room temperature) to permeabilize and quench auto-fluorescence, colon was washed (PBS, 3 x 5 minutes, room temperature), transferred to 2 mL Eppendorf tubes containing 500-1000 μL blocking solution (4% normal donkey serum, 0.5% Triton X-100, 0.05% sodium azide in PBS) and incubated (3 days, 37^{o}C, New Brunswick Scientific I24 Incubator Shaker Series, 40-100

rpm). Next, we incubated with one or more primary antibodies (Supplemental Table 1) in blocking solution on shaker (14 days, 37ºC, 40-100 rpm) using Parafilm® sealed tubes. Unbound primary antibody was removed (PBS/0.05% sodium azide, 3 washes, 2 hours/wash, plus an additional overnight wash, on rocker). Secondary antibodies were in PBS/0.05% sodium azide (3 days, 37ºC, on rocker). Excess secondary was removed with PBS/0.05% sodium azide (3 washes, 2 hours per wash, plus additional wash overnight, room temperature, on rocker).

Dehydration, clearing and mounting after antibody staining: Colon was dehydrated in 24-well dishes in graded methanol/PBS (~ 500µL per well, extra if needed to cover, 30 minutes/wash: 50% methanol, then 70% methanol, then 80% methanol, then 95% methanol, then 100% methanol x 3, room temperature, on rocker). Dehydrated colon was incubated in Murray's Clear (2:1 benzyl benzoate: benzyl alcohol)(312) until translucent (15-30 min, room temperature). Completely transparent colon was mounted on glass slides in Murray's Clear and imaged within 48 hours.

Imaging: Using a Zeiss LSM 710 confocal microscope (10x and 20x Plan-Apochromat objectives, Zeiss Zen software (version 2.3 14.0.14.201)), Z-axis increments were 4 µm (10x objective) or 1 µm (20x objective). Each image slice was 900x900 (10x) or 1200x1200 pixels (20x). 10x Z-stacks were stitched to cover large regions. Laser-scanning operated under multi-track to sequentially acquire multi-channel images. Each channel used 100% laser power. Excitation/long-pass emission filters: Alexa Fluor 647 (excitation: 633 nm, emission: 656-755-nm filter), Alexa Flour 594 (excitation: 561 nm, emission: 588-656-nm filter), Alexa Flour 488 (excitation: 488 nm, emission: 493-584-nm filter). Tile scan and Zen stitching were used to assemble multi-field images. ImageJ (Java 1.8), Imaris 9.0.2 (Bitplane AG, Zurich Switzerland), Adobe Photoshop CS6, and Inkscape (0.92.3) manipulation was limited to uniform contrast

adjustment, cropping, rotating, stitching, assembling Z-stacks, generating three-dimensional projections and videos.

Quantitative data: Analyses employed manual and automated features. Imaris modules: Crop 3D, Imaging Processing, Thresholding, Background Subtraction, Surface, Manual Contour, Click Drawing Mode, and Detailed Statistics. ImageJ features: Regions of interest (ROIs), Polygon selection, Straight line tool, Measurements, Scale bar, Z-Project, Split channels, Merge channels, and Duplicate. Ganglia were manually circled in many Z-stack layers to identify ROIs. Cells were manually counted and measured in three-dimensional space. Quantitative analyses focused on myenteric plexus.

Myenteric plexus analysis:

Neurons (HuC/D+PHOX2B+) and glia (S100β+) were counted in ganglia using 39 randomly selected colon regions (4 right, 5 fields/subject; 3 left, 5 fields/subject; 1 left, 4 fields). Two-dimensional ganglion areas were manually outlined in flattened Z-stacks (4 right, 4 left colon). Using similar manual outlining, we determined percent colon containing myenteric plexus (defined as ganglia plus thick nerve fiber bundles connecting ganglia), and percent plexus occupied by ganglia (defined as regions with >2 myenteric neurons separated by <1 cell diameter). For three-dimensional analyses, individual ganglia volumes were determined by manually outlining at 5-7μm increments within 20X Z-stacks using Click Drawing mode (Surface Contour module, Imaris). Cell density within ganglia was determined by manually counting within defined volumes.

Neuron subtype analysis:

Myenteric neurons (HuC/D+ cells) expressing neuronal nitric oxide synthase (nNOS), choline acetyltransferase (ChAT) or vesicular acetylcholine transporter (VAChT), were identified by triple label immunohistochemistry. Neurons were manually counted within Z-stacks (5 random fields/subject, 4 right, 4 left, 40 total regions). Maximum neuron diameter was determined manually using ImageJ (6 nNOS+/image, 6 ChAT+/image, five 20X images/subject; 4 right, 4 left; forty 20X images total, 240 nNOS neurons, 240 ChAT neurons).

Statistics: We used GraphPad Prism 7 (GraphPad Software, San Diego, CA) D 'Agostino & Pearson and Shapiro-Wilk normality tests with unpaired t-tests to compare means. Volumes of manually contoured ganglia were obtained using Detailed Statistical Analysis (Imaris). Data are presented as mean +/- standard error.

8.4 - RESULTS

Whole mount staining

Human bowel analyses typically rely on thin sections (4-6 μm (paraffin) or 15-20 μm (frozen)) like **Figure 8-1A**. Epithelium, submucosa and muscle are easily seen. A few myenteric and submucosal neurons are recognizable, but sections provide limited data about cells that control bowel motility. Advantages of whole mount staining are easily demonstrated in mouse where WT have rich ENS networks in stomach, small bowel and colon (**Figure 8-1B,F,J**). *Gfrα1-/-* mice have much less dense ENS in stomach, and only extrinsic nerve fibers in small bowel and colon (**Figure 8-1E,I,M**). These differences are difficult to appreciate via hematoxylin and eosin (**Figure 8-1C,D,G,H,K,L**) or in antibody stained sections(521). Therefore, mouse analyses rely on whole mount staining to visualize elegant interconnected enteric neurons closely interacting with glia, smooth muscle, ICC, macrophages, PGDFRα+ cells, blood vessels and epithelium.

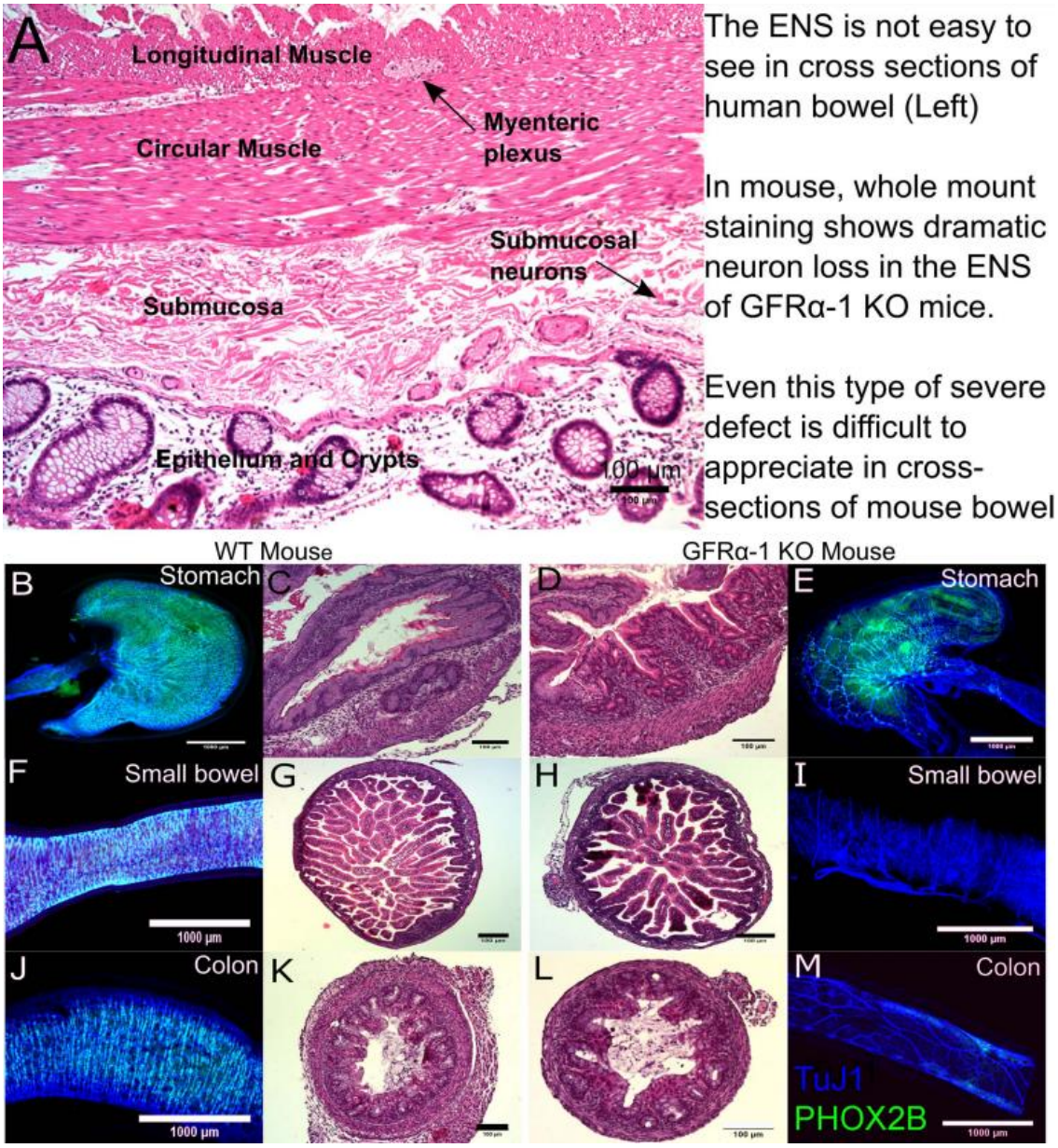

Figure 8-1: ENS is difficult to appreciate in bowel sections.
(A) Full thickness human colon. Hematoxylin and eosin (H&E) stained (5 µm paraffin) section, the most common method to evaluate bowel pathology. (B,F,J) Rich ENS networks in P0 *WT* mouse stomach (B), small bowel (F), and colon (J) are easily seen after TuJ1 (blue)/PHOX2B (green) whole mount immunohistochemistry. (E,I,M) P0 *GFRα1-/-* mice have few enteric neurons in stomach (E) and only extrinsic nerve fibers in small bowel (I) and colon (M) seen by whole mount TuJ1 (blue)/PHOX2B (green) immunohistochemistry. (C,D,G,H,K,L) ENS is difficult to appreciate in H&E stained 5 µm sections from P0 WT stomach (C), small bowel (G) or colon (K). ENS loss is difficult to appreciate in P0 *GFRα1-/-* stomach (D), small bowel (H) or colon (L) 5 µm sections even though magnification is ~5-7x higher in sections than whole mounts. (A,C,D,G,H,K,L) Scale bar = 100 µm. (B,E,F,I,J,M) Scale bar = 1000 µm.

Challenge of human analyses

Our goal was to establish highly reproducible, inexpensive, simple techniques to visualize human ENS in three dimensions to advance understanding of bowel motility disorders. The primary challenge is that human bowel is thick (**Figure 8-1A**) and ENS is buried between circular and longitudinal muscle (myenteric plexus) or between circular muscle and mucosa (submucosal plexus). Remarkable glimpses of human ENS were provided by micro-dissecting muscle off ENS and staining exposed areas(512, 522, 523). These dissections are challenging, time consuming, expose only small areas, damage structures of interest, and do not permit robust visualization of sparsely distributed submucosal neurons. Exceptional human small bowel ENS images were also generated using 300μm sections, tissue clearing and confocal imaging(509-511). Unfortunately, we were unable to reliably clear or consistently antibody stain human colon via published methods. We tried several other approaches(509, 511, 524-527), but human colon was incompletely penetrated by antibody or not transparent after clearing.

Optimal clearing, staining and imaging

We modified published methods (524, 526) to enhanced colon staining and translucency. Several principles guided our approach. We wanted to image full thickness bowel without dissection so cellular interactions remain intact. We found this could be achieved routinely with 1x1 cm^2 pieces and much larger regions. We reasoned antibodies and light would penetrate better if colon was as thin as possible. We therefore pinned and repeatedly stretched colon before fixation to average thickness 800-1000μm (**Figure 8-2A**). We kept colon as flat and uniform as possible and avoided drying. Stretched colon is probably similar to distended colon *in vivo*. After overnight fixation, tissue could be stored months without apparent degradation. We tried tissue fixed without careful preparation, but colon was thick, had poor reagent penetration, and images were difficult to interpret because tissue was folded.

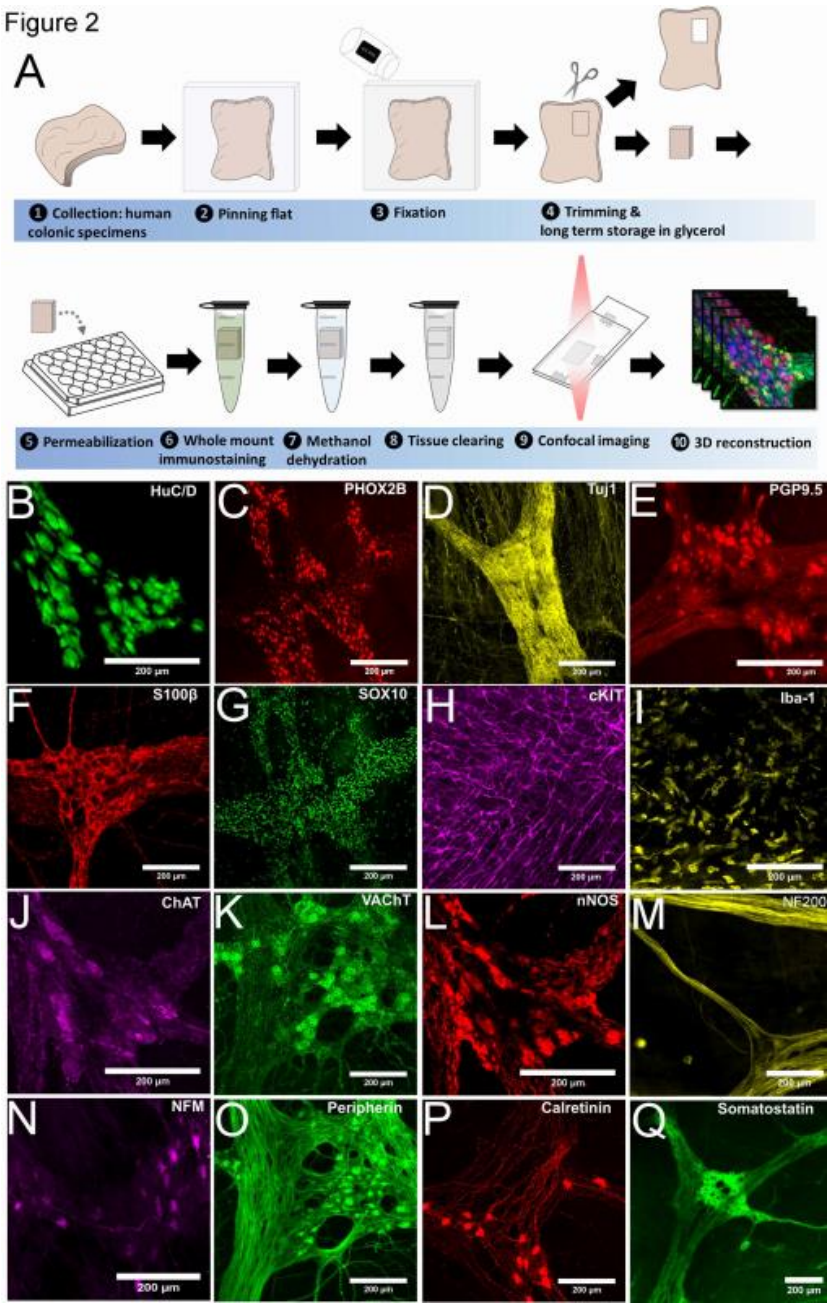

Figure 8-2: Tissue clearing permits imaging cells controlling human colon motility.
(A) Strategy to image without sectioning. (B-G,J-Q) Human colon myenteric plexus region was visualized with 14 antibodies. (H,I) Longitudinal muscle ICC and muscularis macrophages were visualized with cKIT (H) and Iba-1 (I) antibodies. Scale bars = 200 microns.

Methanol, Dent's bleach, prolonged incubation at 37ºC, and shaking enhanced staining. Murray's Clear closely matches tissue refractive index to make tissue translucent. These steps

collectively took 23 days (**Supplemental Figure 8-1**). Tissue was imaged in Murray's clear within 48 hours of immersion because fluorescence declined over time.

Imaging and antibody testing

Colon was easily imaged to 1000μm allowing full bowel thickness reconstruction. We identified antibodies binding nerve cell bodies (HuC/D), neuronal and some glial nuclei (PHOX2B), nerve fibers (TuJ1), nerve cell bodies and fibers (PGP9.5), enteric glia (S100β, SOX10), ICC (cKIT), muscularis macrophages (Iba1), and enteric neuron subsets (ChAT, VAchT, nNOS, neurofilament 200, neurofilament M, peripherin, calretinin, somatostatin) (**Figure 8-2B-Q**). We generated three-dimensional images of many cell types controlling human colon motility. 280 Z-stacks may be downloaded from Blackfynn (Link provided at publication or for reviewers at https://drive.google.com/drive/folders/1Tt_A979u7Q5oxFmrOB29SvaERb5nT_Ev?usp=sharing). Quantitative analyses focused on human colon myenteric plexus.

Human colon ENS in three dimensions

To identify ENS abnormalities causing dysmotility, we first need to understand ENS structure in people without known motility defects. Therefore, we acquired human colon resected for other clinical indications (Supplemental Table 2). Adult specimens analyzed may not be "normal", but did not have obvious pathology. Three-dimensional imaging of colon stained with HuC/D, PHOX2B and S100β antibodies showed enteric neurons clustered into ganglia in submucosal and myenteric plexus. Ganglia are separated by thick nerve fiber bundles (Supplemental Video 1). Myenteric ganglia were larger on average than submucosal ganglia. A few individual neuron cell bodies were found within thick circular muscle of all colons (Supplemental Video 1), an observation that surprised us. A rich network of fine nerve fibers and

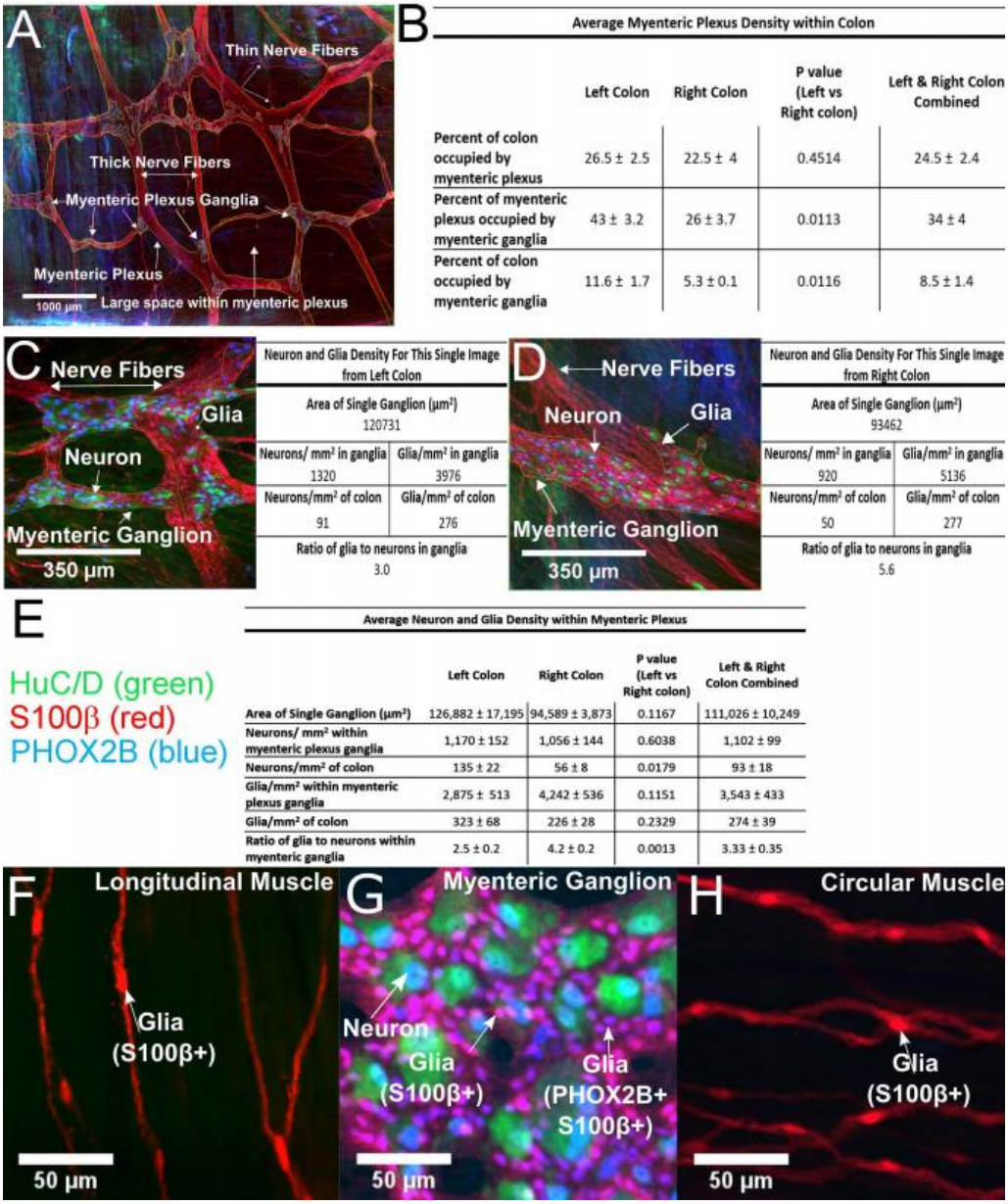

Figure 8-3: Human colon myenteric plexus two-dimensional analyses.
(A) Flattened Z-stack through myenteric plexus (10x objective, stitched fields, 4 x 5 mm^2). Small clustered ganglia have neurons stained for HuC/D (green) and PHOX2B (blue). Nerve fibers are visualized via glial S100β (red). Myenteric plexus and ganglia within plexus were outlined manually (yellow lines). (B) Quantitative data from 4 x 5 mm^2 images like (A). (C,D) Flattened Z-stack from colon myenteric ganglia (left (C) or right (D)) stained for HuC/D (green), S100β (red) and PHOX2B (blue) imaged with 20x objective. Table to right of each image shows quantitative data from that specific Z-stack. (E) Quantitative data (five 20x fields/subject; 4 left colon, 4 right colon; 40 fields). (F,G,H) Colon stained with HuC/D (green), S100 (red), and PHOX2B (blue) antibodies. PHOX2B immunoreactive nuclei include all myenteric neurons and glia within myenteric ganglia (G). Glia in longitudinal (F) and circular muscle (J) are not PHOX2B immunoreactive. (A) Scale bar = 1000 µm. (C,D) Scale bar = 350 µm. (F-H) Scale bar = 50 µM.

closely associated glia (S100β+) was present within circular and longitudinal muscle, with neurites largely parallel to smooth muscle (**Supplemental Video 8-1**). Glia were also closely associated with neuronal soma in ganglia (**Supplemental Video 8-2, Supplemental Figure 8-2**) and nerve fibers were dense near bowel mucosa.

Human colon myenteric plexus

To establish normal indices, full thickness human colon stained for HuC/D, PHOX2B and S100β was imaged parallel to bowel surface (**Figure 8-3A**). Confocal Z-stacks were stitched to evaluate large regions (**Figure 8-3A** is 4 x 5 mm^2). For quantitative analyses, we defined "myenteric plexus" as nerve fiber bundles (containing S100β+ glia) and embedded nerve soma (HuC/D+PHOX2B+). We defined "myenteric plexus ganglia" as regions within fiber bundles containing >2 adjacent neuron cell bodies. Using colon muscle flattened Z-stacks we determined percent colon containing myenteric plexus or ganglia (**Figure 8-3B**). Although myenteric plexus area was similar in left and right colon (left 26.5% ± 2.5, right 22.5% ± 4, p = 0.4514), more myenteric plexus was occupied by ganglia on left (left 43% ± 3.2, right 26% ± 3.7, P = 0.0113) and more image area was occupied by ganglia (left 11.6% ± 1.7, right 5.3% ± 0.1, P = 0.0116). Two-fold differences in density between left and right colon suggest region specific normal ranges.

We next determined neuronal and glial density in colon myenteric plexus by counting HuC/D, PHOX2B and S100β stained cells (**Figure 8-3C-E**). We discovered all myenteric neurons and all glia within myenteric ganglia or thick nerve fiber bundles had nuclear PHOX2B immunoreactivity (**Figure 8-3G**). In contrast, glia associated with thin nerve fibers throughout muscle were not PHOX2B immunoreactive (**Figure 8-3F, H**). Using 20X Z-stacks, we counted all stained cells in each image. Data are first presented based on two-dimensional areas, ignoring

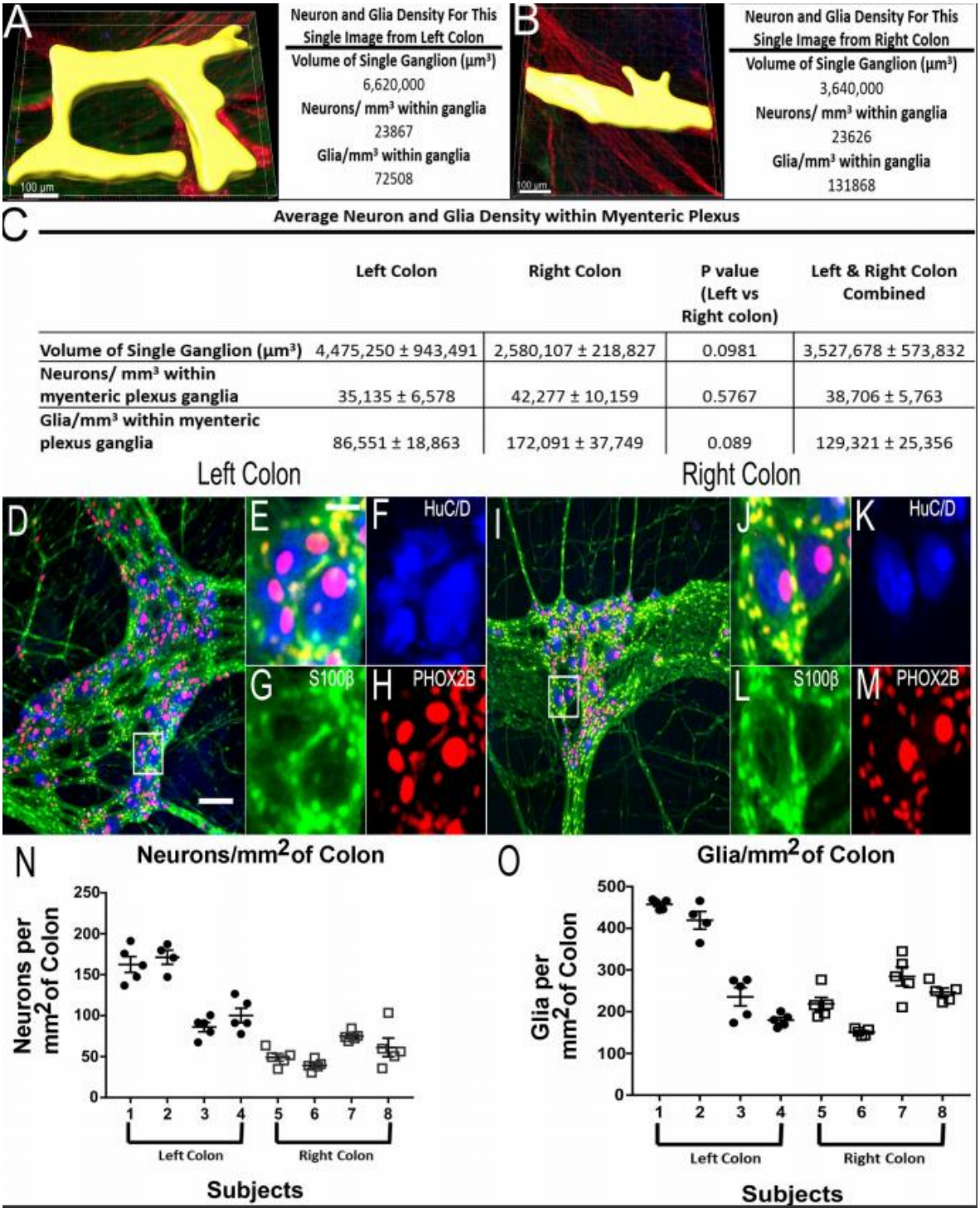

Figure 8-4: Human colon myenteric plexus three-dimensional analyses.
(A, B) Ganglia volumes in three-dimensional space (yellow regions) (Supplemental Videos 3 and 4 are from these regions). To right of each image are quantitative data from that specific region. (C) Cell density (N = five 20x objective fields/subject, 8 subjects (4 left, 4 right colon)). (D-M) Manual neuron and glia counts were obtained after HuC/D (blue), S100□ (green) and PHOX2B (red) staining. (D,I) Flattened Z-stacks. (E-H,J-M) Single slices and channels from Z-stack. (N,

O) To estimate cell density over large regions we multiplied density within small regions analyzed (like Figure 4D) by percentage of bowel with myenteric plexus (using images like 3A). We found little variability in cell density within ganglia, indicated by tight data clusters in individuals. Inter-individual differences primarily reflect percentage of bowel occupied by ganglia in each individual. (A,B,D,I) Scale bars =100 μm. (E,F,G,H,J,K,L,M) Use (E) scale bar = 25 μm.

Z-depth, since most clinicians think about human bowel this way. Quantitative data adjacent to each image were from that specific Z-stack (**Figure 8-3C, D**). Areas containing neurons were considered "ganglia" and outlined (yellow lines). Mean density data for evaluated regions are in **Figure 8-3E**. Although neuron density within myenteric ganglia was similar in left and right colon, neurons per mm^2 bowel was greater on left because ganglia occupy a larger percentage of bowel wall (left = 135 ± 22, right 56 ± 8, P = 0.0179). In contrast, glial density was not statistically different in right versus left colon (glia per mm^2: left = 323 ± 68, right = 226 ± 28, P = 0.2329) or within myenteric ganglia (left = 2,875 ± 513, right = 4,242 ± 536, P = 0.1151). Interestingly, within ganglia, ratio of glia to neurons was lower in left than right colon (left = 2.5 ± 0.2 glia/neuron, right = 4.2 ± 0.2, P = 0.0013). To define cell density within myenteric ganglia in three-dimensions, we manually outlined and counted cells in Z-stacks (**Figure 8-4A, B**). Quantitative data for two individual images are provided (**Figure 8-4A, B**). Pooled data indicate normal ranges for people without known bowel motility disorders (**Figure 8-4C**).

Estimates for large areas were generated by multiplying density of neurons or glia within ganglia (counted at high magnification in three-dimensional Z-stacks, **Figure 8-4D-M**) by percent colon containing ganglia (measured at low magnification, like **Figure 8-3**). Using five regions per individual, cell density estimates clustered within tight ranges (**Figure 8-4N,O**). Variation was greater between subjects and there was more variation in left versus right colon.

We next asked how biopsy size impacts neuron density estimates, recognizing ENS is not uniformly distributed. To do this we divided a single 4 mm x 5 mm region into 20 x 1 mm^2 zones and analyzed ganglion density in each zone (**Figure 8-5A, B**). If 1 mm^2 is evaluated, widely divergent estimates of ganglion density (0% to 17%) occur depending on zone evaluated. Using 4

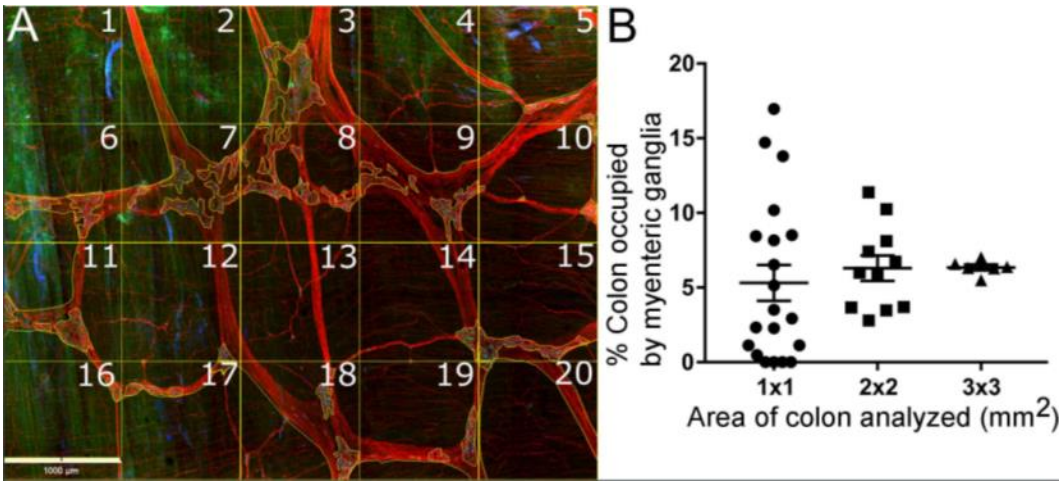

Figure 8-5: Size of region evaluated dramatically affects estimated myenteric plexus neuron density.
(A) Flattened Z-stack (Figure 3A) was divided into 20 squares (one mm^2 each). We determined percentage of each square occupied by ganglia (regions with nerve cell bodies). (B) Estimates of percent colon occupied by ganglia based on 1 x 1 mm^2, 2 x 2 mm^2, or 3 x 3 mm^2 regions. Some 1 x 1 mm^2 regions have no myenteric plexus whereas others have up to 17% of area occupied by ganglia. As size of region evaluated increases, estimates of percent area occupied by ganglia become more uniform. Scale bar = 1000μm.

mm^2 areas, ganglion density estimates were more tightly clustered, but still ranged 3.5% to 11.4%. In contrast, narrow ranges were generated analyzing 9 mm^2 regions. Thus, limited sampling causes diverse enteric neuron density estimates, with greater precision as area evaluated increases.

Neuron subtype ratios

Human intestinal motility disorders may result from quantitative or qualitative ENS defects (57, 134, 427, 513, 528, 529) and nitric oxide (NO)-producing enteric neurons are particularly susceptible to injury (94). Since most myenteric neurons express either nNOS or ChAT and VAChT (2, 417, 530-533) we defined ratios of these markers in human colon myenteric plexus using ChAT, nNOS and HuC/D (**Figure 8-6A-H**) or ChAT, VAChT and HuC/D staining (**Figure 8-6K-Q**). We determined percent neurons (HuC/D+) expressing nNOS, ChAT, both, or neither (N = 84 neurons/sample, 40 samples, 3360 total neurons, Supplemental

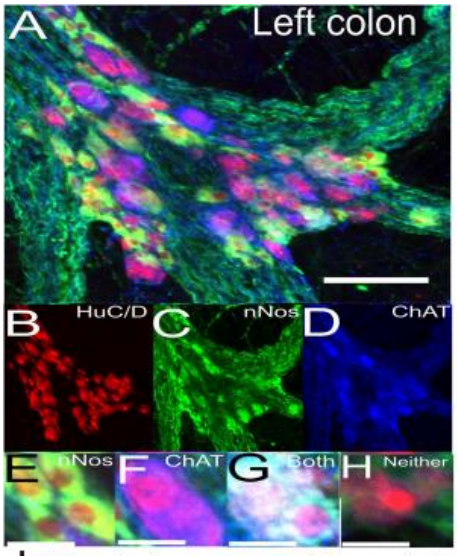

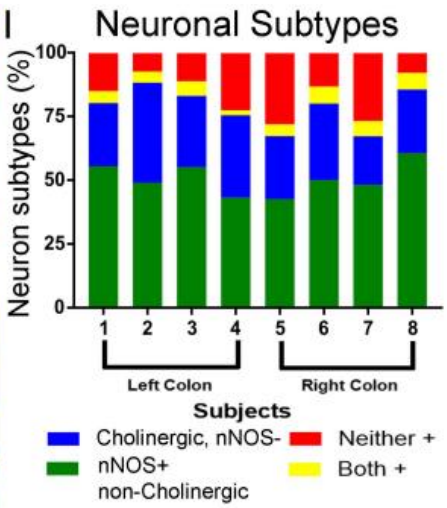

J. Myenteric neuron subtypes in human colon

Neuron Subtypes	Left Colon	Right Colon	P value (Left vs Right Colon)	Left and Right Colon Combined
Non-Cholinergic nNOS+	50.7 +/- 3.2	50.4 +/- 3.9	0.953	50.6 +/- 2.2
Cholinergic nNOS-	31.1 +/- 3.1	24.6 +/- 2.1	0.149	27.9 +/- 2.1
Cholinergic nNOS+	4.2 +/- 0.8	6.0 +/- 0.5	0.116	5.1 +/- 1.3
Non-Cholinergic nNOS-	14.0 +/- 3.0	19.1 +/- 4.5	0.656	16.6 +/- 1.6

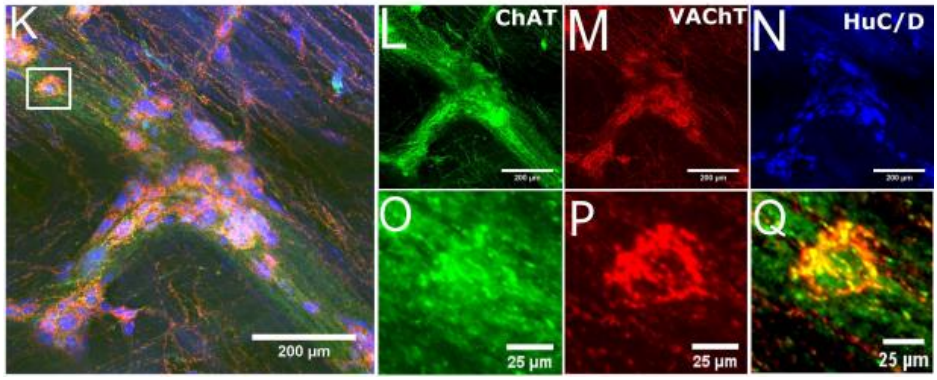

Figure 8-6 : Cholinergic and nitrergic neuron ratios.
(A) Flattened Z-stack, human colon myenteric ganglion stained for HuC/D (red), nNOS (green) and ChAT (blue). (B-D) Imaging channels for (A). (E-H) Examples of neurons from (A) we considered nNOS+ChAT+ (E), ChAT+nNOS- (F), ChAT+nNOS+ (G) or neither ChAT nor nNOS positive. (I) Proportion of each neuron class (8 individuals). (J) Average neuron percentages in each class. (I, J) Numbers reflect estimates based on VAChT/ChAT, nNOS and HuC/D staining. (K) Flattened Z-stack, human colon myenteric ganglion stained for ChAT (green), VAChT (red) and HuC/D (blue). (L-N) Imaging channels for (K). (O-Q) High magnification single confocal slice of neuron from boxed region in (K). We scored this neuron as VAChT+, but ChAT immunoreactivity alone was not well localized and ChAT background staining was too high for us to have scored this cell as ChAT+ without VAChT staining. (A) Scale bar = 100 µm. (B-H, O-Q) Scale bars = 25 µm. (K-N) Scale bars = 200 µm.

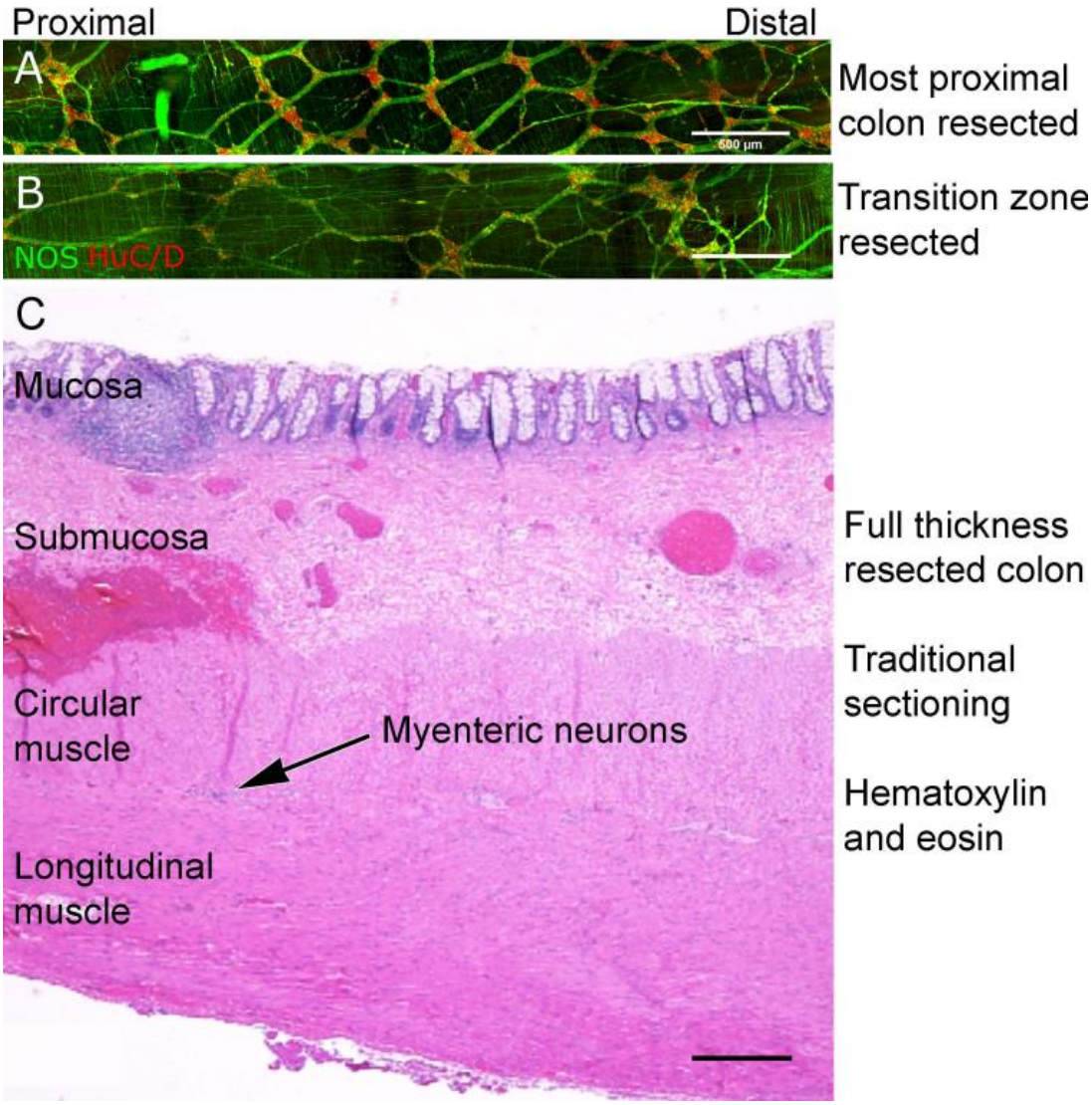

Figure 8-7: Whole mount staining in Hirschsprung disease.
(A, B) Colon resected from a two month old child with Hirschsprung disease stained for nNOS and HuC/D. Myenteric plexus is easily seen in flattened Z-stacks and denser in most proximal bowel resected (A) compared to more distal "transition zone" (B). (C) H&E stained full thickness colon ~ 4.5 cm from distal margin of resected bowel. Myenteric neurons are detectable, but little information is provided. Scale bars = 500 µm

Table 3) using Z-stacks to unambiguously distinguish cytoplasmic staining from overlying neurites. In parallel, we compared ChAT to VAChT staining, because murine data suggested ChAT staining is often weak. VAChT was considered "positive" in 1.62-fold more neurons than ChAT, but many VAChT+ cells had faint ChAT staining or high background (**Figure 8-6O-Q**). We hypothesize ChAT staining alone (at least with this antibody) led to systematic cholinergic

neuron undercounting. Original nNOS, ChAT, HuC/D counts are in **Supplemental Table 8-3**, which explains how we adjusted counts based on VAChT/ChAT data to establish "cholinergic" neuron counts (**Figure 8-6I, J**). We scored ~50% of myenteric neurons as nNOS+ non-cholinergic (**Figure 8-6I, J**), ~28% as cholinergic nNOS negative, ~5% nNOS+ cholinergic, and ~17% as neither nNOS+ nor cholinergic. **Figure 8-6I** shows inter-individual variability. We also measured largest diameter for nNOS+ and ChAT+ neurons (**Supplemental Figure 8-3**). On average, ChAT+ neuron diameters were 32% larger than nNOS+ neurons in left and right colon. Collectively our data provide the first detailed quantitative information about adult human colon ENS anatomy based on three-dimensional images.

Hirschsprung disease transition zone analysis

To highlight how our method might add clinical value, we stained long colon regions resected from a child with Hirschsprung disease, a problem where enteric neurons are absent from distal bowel. With whole mount staining, hypoganglionic transition zone is readily distinguished from denser ENS in proximal resected colon (**Figure 8-7A, B**). In contrast, ENS is much more difficult to appreciate in sectioned bowel from the same child (**Figure 8-7C**).

8.5 - DISCUSSION

Human bowel was estimated to have ~500 million enteric neurons controlling most aspects of bowel function (417). Our data suggest colon alone has ~55 million enteric neurons (~100 neurons/mm^2 x 1.4 m colon length x 0.15 m circumference (534) x 1,000,000 mm^2/m^2 x 2.6-fold stretching). When ENS is missing or defective, profound bowel dysfunction may occur causing life-threatening problems like Hirschsprung disease (HSCR)(57) and neuropathic chronic intestinal pseudo-obstruction (CIPO)(427). ENS defects may also underlie achalasia(518) and gastroparesis (535), where selective nNOS neurons loss was reported. Furthermore, ENS can be

damaged by toxins (e.g., chemotherapy) (536-538), systemic disease (diabetes, Parkinson's) (498, 539-541), or inflammation due to infection (542, 543), inflammatory bowel disease(544), or necrotizing enterocolitis (97), causing long-term dysmotility and visceral hypersensitivity(545). Unfortunately, until now, it has been difficult to visualize human ENS in three dimensions. This limited understanding of disease mechanisms because full thickness biopsies often appear "normal" unless changes are dramatic (e.g., complete enteric neuron loss) and many ENS defects cannot be seen in sectioned tissue.

Most of what we know about ENS comes from animal models where bowel is thin and muscle easily dissected from submucosa (134, 263, 546). Human bowel, in contrast, is thick (~1 mm even maximally stretched for colon) and muscle layers are difficult to separate from submucosa or each other. For this reason, essentially all human ENS analyses use thin cross-sections (e.g., 5 μm). The Gastro 2009 International Working Group nicely highlighted wide variation in prior studies for "ganglia per 10 mm" (13.5-fold range in rectum) and neurons per ganglia (9-fold range in colon)(387). Swaminathan and Kapur identified a ~150-fold range for "mean number of ganglion cells per cm" in normal colon (514) and then determined reproducible enteric neuron counts require >5 full circumference sections (estimated at 1.25 mm^2 = 5 sections x ~0.005 mm thick section x ~50 mm circumference in 8 week old). Our data suggest 1 mm^2 still yields quite variable estimates of neuron density and that >9 mm^2 provides more reliable data. Additional critical problems arise evaluating human ENS anatomy using thin sections. Arrangement of ENS is difficult to appreciate, so dramatic changes in ENS organization can be missed. Nerve fiber bundle orientation is impossible to discern in sections and small nerve fibers difficult to see, so changes in neurite density or organization are not appreciated. Decades of mouse work suggests three-dimensional imaging provides much greater insight into disease mechanisms and is essential to see many ENS defects. Thus, robust new three-dimensional methods to visualize human ENS may provide new insight into motility disorder mechanisms.

A few prior studies demonstrated human ENS in three-dimensions. Beautiful myenteric plexus images were produced by meticulous "fiber by fiber" removal of longitudinal muscle to expose ENS(512, 533, 547). We tried this method, but found it difficult to uncover even small regions, and only cells exposed by dissection could be imaged. Optical clearing, immunohistochemistry and imaging also generated spectacular human ENS images (509-511), but we had difficulty obtaining good images using their method even with significant effort. Furthermore, they used 300μm sections and did not visualize ENS in large regions or provide quantitative data.

To overcome these problems, we spent years optimizing clearing and antibody staining for human colon. Our goal was to establish methods that worked well, were easy, and did not require special skill (like microdissection). In addition, we wanted to visualize cells that control bowel motility in three dimensions without sectioning that disrupts connections, making it difficult to visualize ENS organization. We recognize for this approach to be useful, we need a large library of publically available images from people who do not have bowel motility disorders and need rigorous quantitative data for "normal" ENS anatomy. Our current studies meet many of these goals.

Our approach makes colon completely translucent. Large bowel pieces were stained and imaged without sectioning, up to 2 x 3 cm^2. We suspect larger regions would stain and clear equally well. Confocal imaging permitted visualization of stained cells from serosa to mucosa and three-dimensional analyses. We identified antibodies that stain neurons, glia, ICC and muscularis macrophages, neuron subtypes and nerve fibers. As expected, some antibodies do not work with our method. We provide 280 three-dimensional Z-stacks of stained human colon. These images highlight how much we are missing with traditional tissue sectioning. We performed substantial quantitative analyses to define "normal" adult human colon ENS anatomy. Finally, we show how easily the hypoganglionic transition zone can be identified in a child with Hirschsprung disease.

This is clinically relevant since “transition zone pull through” is thought to be a common cause of post-operative morbidity in children with Hirschsprung disease (57).

Several observations are worth highlighting. We estimate enteric neurons are < 0.1% of total cells in human colon. Myenteric and submucosal plexus resembles ENS in other species, but differences in ENS anatomy between species(548, 549) means we need human ENS normal values. Irregular ganglia spacing (e.g., **Figure 8-3A**) probably explains dramatic variability in reported enteric neuron densities (387, 514) since some thin sections include large ganglia and others encompass regions with no enteric neurons. Within myenteric ganglia, neuron density was fairly uniform (SEM < 25% of mean neurons/mm^3) and adult human colon had 137 +/- 20 neurons per myenteric ganglion (from **Figure 8-4C**: 38,706 neurons/mm^3 x 0.0035278 mm^3 per ganglion = 137 neurons/ganglion). Uniformity of neuron density within myenteric ganglia contrasts with the 1.65-fold difference in ganglion density within myenteric plexus of right and left colon (P = 0.0113), highlighting the need to establish region-specific normal ranges for most parameters.

Enteric gliaare much more abundant than neurons even within myenteric ganglia. Our estimates of glial index (glia to neuron ratio) within ganglia (2.5 for left; 4.2 for right colon) are lower than previously reported (5.9-7(547)), but S100β does not label all glia (550, 551). Furthermore, three left colons were from people with diverticulitis where loss of S100β labeled enteric glia has been reported (552). Strikingly, S100β nicely highlights ENS throughout bowel even though there are many enteric glia types. One novel observation was that PHOX2B immunoreactive nuclei included S100β+ glia and HuC/D+ neurons, but PHOX2B immunoreactivity was not detected in enteric glia outside ganglia. Murine data also show PHOX2B in adult enteric neurons and glia, although mouse images suggest PHOX2B expression in glia within and outside enteric ganglia (157). These data suggests *PHOX2B*, a gene mutated in some people with Hirschsprung disease (57), might influence glial diversity in human ENS.

Finally, we began to define neuron subtype ratios in human colon myenteric plexus. Because most myenteric neurons produce either nitric oxide or acetylcholine(417), we focused on these subgroups. We found little between-subject variability in non-cholinergic nNOS+ neuron prevalence, accounting for ~50% of myenteric neurons. Prior reports indicated 43-48% of human myenteric neurons were ChAT- nNOS+ myenteric neuron (530, 532, 533). Also consistent with past studies reporting 4-10% of human colon myenteric neurons produce nNOS and ChAT(531-533), we scored 4-6% of myenteric neurons as cholinergic nNOS+. We differed substantially from prior studies reporting 52-56% of human colon myenteric neurons were ChAT+ nNOS- and 6-7% ChAT-/nNOS-(531-533). Despite using ChAT and VAChT, we scored fewer myenteric neurons as cholinergic nNOS- (~28%) and more neurons as non-cholinergic nNOS- (14-19%). We do not know if differences reflect technical issues (e.g., antibody staining intensity), differences between investigator scoring approaches, or biological variation between subjects. Neuron subtype ratios vary between mouse strains and can be influenced by diet(53, 134, 337, 553, 554) so biological variability between subjects is plausible. Clearly, more remains to be done to define neuron subtype ratios in the human ENS.

Our study has limitations. Subjects were 28 to 80 years old, with the exception of one infant with Hirschsprung disease. Colon specimens were resected for clinical indications. Although we tried to evaluate only pathology-free regions, diverticulitis causes inflammation and inflammation affects the ENS. Exact colon regions are not known (i.e., “left” might be from splenic flexure or sigmoid). Specimens were randomly oriented. We cannot distinguish proximal from distal within specimens. We do not know specimen location along the circumferential colon axis. Finally, staining takes several weeks, so intraoperative decisions based on this method would require repeated procedures. Nonetheless, our work lays the foundation for future research and suggests new directions as we (and others) pursue human ENS analyses.

Conclusion:

We can now visualize human ENS in three-dimensions in large colon areas with minimal dissection and no sectioning. Our images make it easy to understand why previously reported enteric neuron density estimates vary up to 150-fold. We tested >40 antibodies and identified 16 antibodies that provide exceptional data with our new approach. We hope this method will become standard practice for defining ENS anatomy in adults and children with bowel motility disorders. The 280 Z-stacks we make freely available should provide valuable additional data. We invite others to help us perform quantitative analysis using our images.

8.6 - ACKNOWLEDGEMENTS

We thank Pierre Russo for ongoing support and encouragement. We are grateful for assistance of Deepika Kothakapa, Caitlin Feltcher, Lauren Schmucker, and Andrew Kromer. This work was supported by Irma and Norman Braman Endowment (ROH), Suzi and Scott Lustgarten Center Endowment (ROH), Children's Hospital of Philadelphia Research Institute (ROH), Abramson Cancer Center, NIH 5 F30 DK117546-02 (CMW), and NIH SPARC 3OT2OD023859-01 (MJH (PI), ROH (co-I)).

8.7 – AUTHOR CONTRIBUTIONS

KG, SHL, RS, and ROH planned the study. KG, SHL and ROH analyzed and interpreted data, performed statistical analyses, and drafted the manuscript. KG, SHL, RS, AS, SS, CMW, MF, EF, FV, AL, BJW, and ED were critically involved in acquisition of data. MH analyzed data and provided insightful guidance for project planning. MH and ROH obtained funding. ROH supervised the study. All authors revised and approved the manuscript.

8.8 – SUPPLEMENTARY MATERIALS

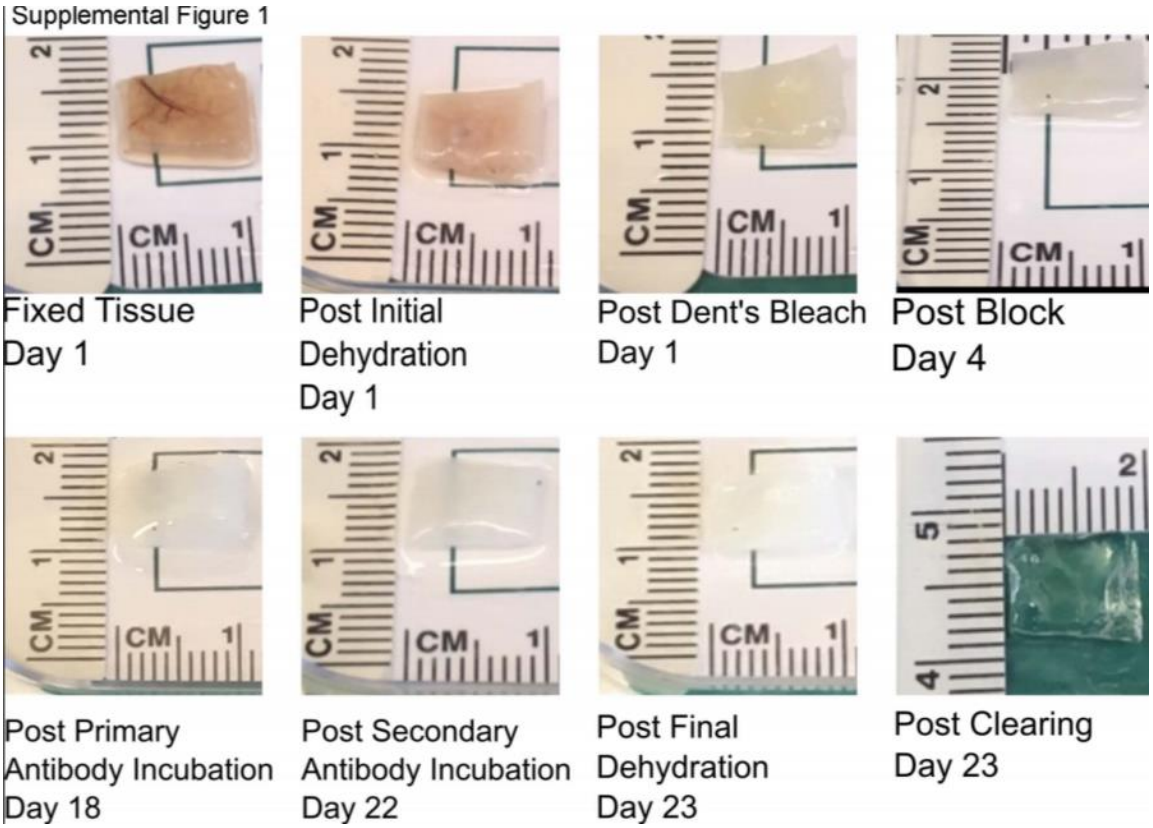

Supplementary Figure 8-1: Tissue processing.
A single piece of full thickness human colon on selected days of our procedure.

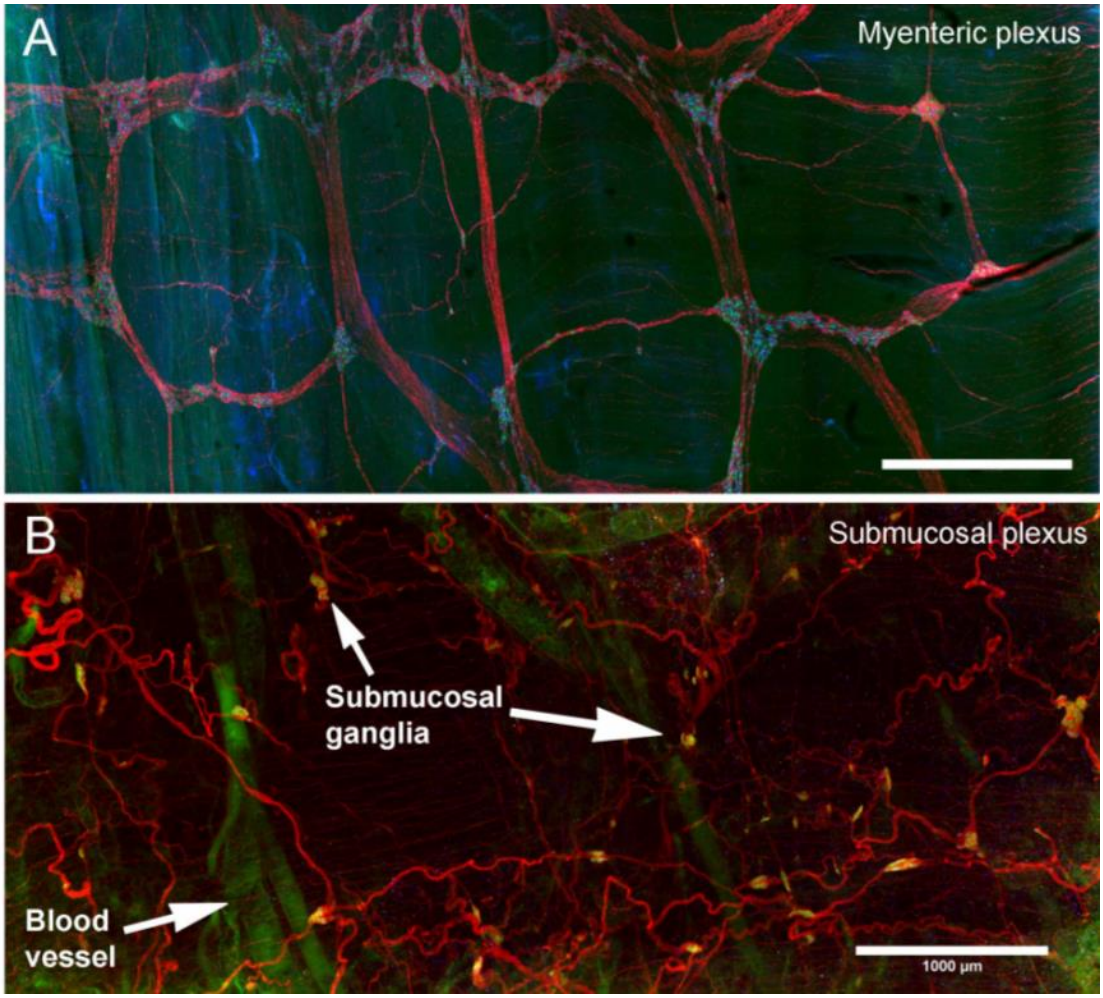

Supplementary Figure 8-2: Large (5.5 x 2.5 mm^2) confocal images.
(A, B) Flattened Z-stacks of human colon myenteric (A) and submucosal plexus (B) stained with HuC/D (green), PHOX2B (blue), and S100β (red) antibodies were acquired with 10X objective and stitched. Scale bars = 1000 μm.

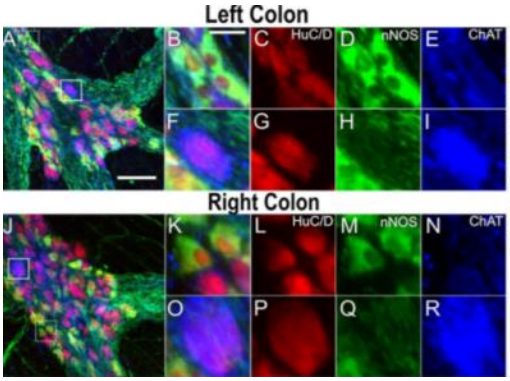

S

Diameter of Neuronal Subtypes

Diameter of neuron subtypes	Left Colon	Right Colon	P value (Left vs Right Colon)	Left and Right Colon Combined	P value (nNOS+/ChAT- vs ChAT+/nNOS-)
Diameter of nNOS+/CHAT- neurons (µm)	21.7 +/- 1.1	22 +/- 0.76	0.83	21.9 +/- 0.6	0.0003
Diameter of CHAT+/nNOS- neurons (µm)	28.9 +/- 1.8	28.8 +/- 2.3	0.99	28.9 +/- 1.3	

Supplementary Figure 8-3: Largest neuron soma diameter.
(A, J) Flattened Z-stack, single human myenteric ganglion from left (A) or right colon (J) stained for HuC/D (red), nNOS (green) and ChAT (blue). (B-I, K-R) Higher magnification images. (B-E) nNOS+ChAT- neurons from dotted line boxed region in (A). (F-I) ChAT+nNOS- neuron from solid line boxed region in (A) (K-N) nNOS+ChAT- neurons from dotted line boxed region in (J). (O-R) ChAT+ nNOS- neuron from solid line boxed region in (J). (S) Longest neuron diameter (N = 240 nNOS+ and 240 ChAT+ neurons (A, J) Scale bar A = 100 □m. (B-I, K-R) Scale bar = 25 µm.

Supplementary Table 8-1: List of antibodies

Primary Antibody	Category Number	Species	Source	Concentration	RRID
Hu (C,D)	A21271	Mouse	Invitrogen	1:200	AB_221448
nNOS	AB5380	Rabbit	Millipore	1:100	AB_91824
ChAT	AB144P	Goat	Millipore	1:100	AB_2079751
PGP9.5	AB108986	Rabbit	Abcam	1:50	AB_10891773
Tuj1 (β-Tubulin III)	PRB-435P	Rabbit	Covance	1:2500	AB_291637
C-Kit	AB32363	Rabbit	Abcam	1:100	AB_731513
S100β	AB52642	Rabbit	Abcam	1:100	AB_882426
Peripherin	MAB1527	Mouse	Fisher	1:300	AB_2284441
Iba-1	019-19741	Rabbit	Wako	1:500	AB_839504
Somatostatin	MAB354	Rat	Millipore	1:500	AB_2255365
Calretinin	18-0211	Rabbit	Invitrogen	1:100	AB_86712
Neurofilament 200	N4142	Rabbit	Sigma	1:2000	AB_477272
Neurofilament M	841001	Rabbit	Biolegend	1:1000	AB_2565457
VAChT	139 103	Rabbit	Synaptic Systems	1:1000	AB_887864
PHOX2B	AF4940	Goat	R&D Systems	1:200	AB_10889846
Sox10	AB5727	Rabbit	Millipore	1:50	AB_2195375

Secondary Antibody	Category Number	Species	Source	Concentration	RRID
Goat Alexa Fluor- 647	A21447	Donkey	Invitrogen	1:400	AB_141844
Goat Alexa Fluor- 594	A11058	Donkey	Invitrogen	1:400	AB_142540
Goat Alexa Fluor- 488	A11055	Donkey	Thermo Fisher Scientific	1:400	AB_2534102
Mouse Alexa Fluor- 647	A31571	Donkey	Invitrogen	1:400	AB_162542
Mouse Alexa Fluor- 594	A21203	Donkey	Invitrogen	1:400	AB_141633
Mouse Alexa Fluor- 488	A21202	Donkey	Invitrogen	1:400	AB_141607
Rabbit Alexa Fluor- 647	A31573	Donkey	Invitrogen	1:400	AB_2536183
Rabbit Alexa Fluor- 594	A21207	Donkey	Invitrogen	1:400	AB_141637
Rabbit Alexa Fluor- 488	A21206	Donkey	Thermo Fisher Scientific	1:400	AB_2535792
Rat Alexa Fluor- 594	A21209	Donkey	Thermo Fisher Scientific	1:400	AB_2535795

Supplementary Table 8-2: Demographics

Condition indicates the medical problem that led to colon resection.

Sample Number	Sex	Age	Colon region	Condition
Adult:				
4514	Male	77	Right	Polyp
4656	Male	70	Right	Adenocarcinoma
4504	Male	63	Right	Colon Cancer
4527	Male	63	Right	Crohn's disease
4755	Male	55	Right	Polyp
4506	Male	51	Right	Cancer
4790	Male	51	Right	Colonic mass
4689	Female	80	Left	Colovaginal fistula
4585	Female	63	Left	Sigmoid mass
4443	Female	60	Left	Diverticulitis
4566	Male	59	Left	Sigmoid mass
4557	Male	37	Left	Sessile polyp
4454	Male	36	Left	Diverticulitis
4445	Male	28	Left	Diverticulitis
Pediatric:				
1255	Male	2 months	Recto-sigmoid	Hirschsprung disease

Supplementary Table 8-3: VAChT-ChAT correction.

Myenteric neuron subtypes in human colon based on 3360 cells counted in full confocal Z-stacks after ChAT, nNOS and HuC/D antibody staining

Neuron Subtypes	Left Colon	Right Colon	P value (Left vs Right Colon)	Left and Right Colon Combined
nNOS+/ChAT-	52.3 +/- 3.2	52.7 +/- 3.9	0.953	52.5 +/- 2.3
ChAT+/nNOS-	19.2 +/- 1.9	15.2 +/- 1.3	0.149	17.2 +/- 1.3
nNOS+/ChAT+	2.6 +/- 0.5	3.7 +/- 0.3	0.116	3.2 +/- 0.3
nNOS-/ChAT-	25.9 +/- 3.0	28.5 +/- 4.5	0.656	27.2 +/- 2.6

ChAT staining for many neurons was weak and background ChAT staining was higher than desirable. By systematic analysis of human colon stained with antibodies to VAChT, ChAT and HuC/D we scored 1.62-fold more neurons (HuC/D+) as VAChT+ than ChAT+. Most VAChT+ cells had identifiable but weak ChAT+ staining (See Figure O-Q). We consider these cells to be cholinergic neurons. Data in Figure 6J reflect the 1.62-fold adjustment to numbers in the table above. The math is as follows:

Corrected "Cholinergic nNOS-" = ChAT+/nNOS- x 1.62
Corrected "Cholinergic nNOS+ = ChAT+/nNOS+ x 1.62
Corrected "Non-Cholinergic nNOS-" = ChAT-/nNOS- minus reclassified nNOS- neurons
Corrected "Non-Cholinergic nNOS+" = ChAT-/nNOS+ minus reclassified nNOS+ neurons

Myenteric neuron subtypes in human colon. Numbers are corrected for systematic undercounting when ChAT antibody is used alone. This table is reproduced in Figure 6J.

Neuron Subtypes	Left Colon	Right Colon	P value (Left vs Right Colon)	Left and Right Colon Combined
Non-Cholinergic nNOS+	50.7 +/- 3.2	50.4 +/- 3.9	0.953	50.6 +/- 2.2
Cholinergic nNOS-	31.1 +/- 3.1	24.6 +/- 2.1	0.149	27.9 +/- 2.1
Cholinergic nNOS+	4.2 +/- 0.8	6.0 +/- 0.5	0.116	5.1 +/- 1.3
Non-Cholinergic nNOS-	14 +/- 3.0	19.1 +/- 4.5	0.656	16.6 +/- 1.6

Supplemental Video 1: Human colon three-dimensional Z-stack imaged from serosa to mucosa after staining with HuC/D (green), S100β (red), and PHOX2B (blue) antibodies.

Supplemental Video 2: Human colon three-dimensional Z-stack imaged through a single myenteric plexus ganglion after staining with HuC/D (green), S100β (red), and PHOX2B (blue) antibodies.

Supplemental Video 3: Human colon three-dimensional Z-stack imaged through a single myenteric plexus ganglion after staining with HuC/D (green), S100β (red), and PHOX2B (blue) antibodies. Imaris was used to define ganglion region in 3-dimensional space. Video corresponds to Figure 4A image.

Supplemental Video 4: Human colon three-dimensional Z-stack imaged through a single myenteric plexus ganglion after staining with HuC/D (green), S100β (red), and PHOX2B (blue) antibodies. Imaris was used to define region of ganglion in 3-dimensional space. Video corresponds to Figure 4B image.

Supplemental Image Files: Original three-dimensional Z-stack .CZI image files were opened in ImageJ and converted to .TIF file format. Each fluorescent channel was assigned a color. We removed outer serosal and mucosal image planes that did not fill the full field of view. 280 image files are available at Blackfynn.com or at https://drive.google.com/drive/folders/1Tt_A979u7Q5oxFmrOB29SvaERb5nT_Ev?usp=sharing. Excel file provides metadata for each image. (We will provide specific links when the manuscript is accepted, making all files public). Using ImageJ, colors may be merged. Contrast or brightness adjustments will facilitate viewing stained cells.

REFERENCES

1. Furness JB. *The enteric nervous system.* Malden, MA.: Blackwell Publishing. ; 2006.
2. Furness JB, Callaghan BP, Rivera LR, and Cho HJ. The enteric nervous system and gastrointestinal innervation: integrated local and central control. *Adv Exp Med Biol.* 2014;817(39-71.
3. Ziegler MM, Ross AJ, 3rd, and Bishop HC. Total intestinal aganglionosis: a new technique for prolonged survival. *Journal of pediatric surgery.* 1987;22(1):82-3.
4. Qu ZD, Thacker M, Castelucci P, Bagyanszki M, Epstein ML, and Furness JB. Immunohistochemical analysis of neuron types in the mouse small intestine. *Cell and tissue research.* 2008;334(2):147-61.
5. Furness JB. Types of neurons in the enteric nervous system. *Journal of the autonomic nervous system.* 2000;81(1-3):87-96.
6. Kunze WA, and Furness JB. The enteric nervous system and regulation of intestinal motility. *Annual review of physiology.* 1999;61(117-42.
7. Nurgali K, Stebbing MJ, and Furness JB. Correlation of electrophysiological and morphological characteristics of enteric neurons in the mouse colon. *The Journal of comparative neurology.* 2004;468(1):112-24.
8. Furness JB, Alex G, Clark MJ, and Lal VV. Morphologies and projections of defined classes of neurons in the submucosa of the guinea-pig small intestine. *The anatomical record Part A, Discoveries in molecular, cellular, and evolutionary biology.* 2003;272(2):475-83.
9. Furness JB. Novel gut afferents: Intrinsic afferent neurons and intestinofugal neurons. *Autonomic neuroscience : basic & clinical.* 2006;125(1-2):81-5.
10. Kunze WA, Clerc N, Furness JB, and Gola M. The soma and neurites of primary afferent neurons in the guinea-pig intestine respond differentially to deformation. *The Journal of physiology.* 2000;526 Pt 2(375-85.
11. Mongardi Fantaguzzi C, Thacker M, Chiocchetti R, and Furness JB. Identification of neuron types in the submucosal ganglia of the mouse ileum. *Cell and tissue research.* 2009;336(2):179-89.
12. Furness JB, Jones C, Nurgali K, and Clerc N. Intrinsic primary afferent neurons and nerve circuits within the intestine. *Progress in neurobiology.* 2004;72(2):143-64.
13. Bellono NW, Bayrer JR, Leitch DB, Castro J, Zhang C, O'Donnell TA, Brierley SM, Ingraham HA, and Julius D. Enterochromaffin Cells Are Gut Chemosensors that Couple to Sensory Neural Pathways. *Cell.* 2017;170(1):185-98 e16.
14. Treichel AJ, Farrugia G, and Beyder A. The touchy business of gastrointestinal (GI) mechanosensitivity. *Brain research.* 2018;1693(Pt B):197-200.
15. Heredia DJ, Gershon MD, Koh SD, Corrigan RD, Okamoto T, and Smith TK. Important role of mucosal serotonin in colonic propulsion and peristaltic reflexes: in vitro analyses in mice lacking tryptophan hydroxylase 1. *The Journal of physiology.* 2013;591(23):5939-57.

16. Kendig DM, and Grider JR. Serotonin and colonic motility. *Neurogastroenterology and motility : the official journal of the European Gastrointestinal Motility Society.* 2015;27(7):899-905.
17. Smith TK, and Gershon MD. CrossTalk proposal: 5-HT is necessary for peristalsis. *The Journal of physiology.* 2015;593(15):3225-7.
18. Spencer NJ, Sia TC, Brookes SJ, Costa M, and Keating DJ. CrossTalk opposing view: 5-HT is not necessary for peristalsis. *The Journal of physiology.* 2015;593(15):3229-31.
19. Li Z, Chalazonitis A, Huang YY, Mann JJ, Margolis KG, Yang QM, Kim DO, Cote F, Mallet J, and Gershon MD. Essential roles of enteric neuronal serotonin in gastrointestinal motility and the development/survival of enteric dopaminergic neurons. *The Journal of neuroscience : the official journal of the Society for Neuroscience.* 2011;31(24):8998-9009.
20. Keating DJ, and Spencer NJ. Release of 5-hydroxytryptamine from the mucosa is not required for the generation or propagation of colonic migrating motor complexes. *Gastroenterology.* 2010;138(2):659-70 70 e1-2.
21. Spencer NJ, Nicholas SJ, Robinson L, Kyloh M, Flack N, Brookes SJ, Zagorodnyuk VP, and Keating DJ. Mechanisms underlying distension-evoked peristalsis in guinea pig distal colon: is there a role for enterochromaffin cells? *American journal of physiology Gastrointestinal and liver physiology.* 2011;301(3):G519-27.
22. Mazzuoli G, and Schemann M. Multifunctional rapidly adapting mechanosensitive enteric neurons (RAMEN) in the myenteric plexus of the guinea pig ileum. *The Journal of physiology.* 2009;587(Pt 19):4681-94.
23. Mazzuoli G, and Schemann M. Mechanosensitive enteric neurons in the myenteric plexus of the mouse intestine. *PloS one.* 2012;7(7):e39887.
24. Kugler EM, Michel K, Zeller F, Demir IE, Ceyhan GO, Schemann M, and Mazzuoli-Weber G. Mechanical stress activates neurites and somata of myenteric neurons. *Frontiers in cellular neuroscience.* 2015;9(342.
25. Tonini M, and Costa M. A pharmacological analysis of the neuronal circuitry involved in distension-evoked enteric excitatory reflex. *Neuroscience.* 1990;38(3):787-95.
26. Johnson PJ, Bornstein JC, Yuan SY, and Furness JB. Analysis of contributions of acetylcholine and tachykinins to neuro-neuronal transmission in motility reflexes in the guinea-pig ileum. *Br J Pharmacol.* 1996;118(4):973-83.
27. Lomax AE, and Furness JB. Neurochemical classification of enteric neurons in the guinea-pig distal colon. *Cell and tissue research.* 2000;302(1):59-72.
28. Nasser Y, Ho W, and Sharkey KA. Distribution of adrenergic receptors in the enteric nervous system of the guinea pig, mouse, and rat. *The Journal of comparative neurology.* 2006;495(5):529-53.
29. Sanders KM, Kito Y, Hwang SJ, and Ward SM. Regulation of Gastrointestinal Smooth Muscle Function by Interstitial Cells. *Physiology (Bethesda).* 2016;31(5):316-26.

30. Sanders KM, Koh SD, Ro S, and Ward SM. Regulation of gastrointestinal motility--insights from smooth muscle biology. *Nature reviews Gastroenterology & hepatology.* 2012;9(11):633-45.
31. Huizinga JD, Martz S, Gil V, Wang XY, Jimenez M, and Parsons S. Two independent networks of interstitial cells of cajal work cooperatively with the enteric nervous system to create colonic motor patterns. *Frontiers in neuroscience.* 2011;5(93.
32. Shahi PK, Choi S, Jeong YJ, Park CG, So I, and Jun JY. Basal cGMP regulates the resting pacemaker potential frequency of cultured mouse colonic interstitial cells of Cajal. *Naunyn Schmiedebergs Arch Pharmacol.* 2014;387(7):641-8.
33. Baker SA, Drumm BT, Cobine CA, Keef KD, and Sanders KM. Inhibitory Neural Regulation of the Ca (2+) Transients in Intramuscular Interstitial Cells of Cajal in the Small Intestine. *Front Physiol.* 2018;9(328.
34. Kurahashi M, Mutafova-Yambolieva V, Koh SD, and Sanders KM. Platelet-derived growth factor receptor-alpha-positive cells and not smooth muscle cells mediate purinergic hyperpolarization in murine colonic muscles. *Am J Physiol Cell Physiol.* 2014;307(6):C561-70.
35. Peri LE, Sanders KM, and Mutafova-Yambolieva VN. Differential expression of genes related to purinergic signaling in smooth muscle cells, PDGFRalpha-positive cells, and interstitial cells of Cajal in the murine colon. *Neurogastroenterology and motility : the official journal of the European Gastrointestinal Motility Society.* 2013;25(9):e609-20.
36. Baker SA, Drumm BT, Skowronek KE, Rembetski BE, Peri LE, Hennig GW, Perrino BA, and Sanders KM. Excitatory Neuronal Responses of Ca(2+) Transients in Interstitial Cells of Cajal in the Small Intestine. *eNeuro.* 2018;5(2).
37. Zhu MH, Sung IK, Zheng H, Sung TS, Britton FC, O'Driscoll K, Koh SD, and Sanders KM. Muscarinic activation of Ca2+-activated Cl- current in interstitial cells of Cajal. *The Journal of physiology.* 2011;589(Pt 18):4565-82.
38. So KY, Kim SH, Sohn HM, Choi SJ, Parajuli SP, Choi S, Yeum CH, Yoon PJ, and Jun JY. Carbachol regulates pacemaker activities in cultured interstitial cells of Cajal from the mouse small intestine. *Mol Cells.* 2009;27(5):525-31.
39. Unno T, Matsuyama H, Izumi Y, Yamada M, Wess J, and Komori S. Roles of M2 and M3 muscarinic receptors in cholinergic nerve-induced contractions in mouse ileum studied with receptor knockout mice. *Br J Pharmacol.* 2006;149(8):1022-30.
40. Lecci A, Capriati A, Altamura M, and Maggi CA. Tachykinins and tachykinin receptors in the gut, with special reference to NK2 receptors in human. *Autonomic neuroscience : basic & clinical.* 2006;126-127(232-49.
41. Vanner S, and Macnaughton WK. Submucosal secretomotor and vasodilator reflexes. *Neurogastroenterology and motility : the official journal of the European Gastrointestinal Motility Society.* 2004;16 Suppl 1(39-43.
42. Reed DE, and Vanner SJ. Long vasodilator reflexes projecting through the myenteric plexus in guinea-pig ileum. *The Journal of physiology.* 2003;553(Pt 3):911-24.

43. Weber E, Neunlist M, Schemann M, and Frieling T. Neural components of distension-evoked secretory responses in the guinea-pig distal colon. *The Journal of physiology.* 2001;536(Pt 3):741-51.
44. Mazzuoli-Weber G, and Schemann M. Mechanosensitivity in the enteric nervous system. *Frontiers in cellular neuroscience.* 2015;9(408.
45. Vanner S, and Surprenant A. Neural reflexes controlling intestinal microcirculation. *Am J Physiol.* 1996;271(2 Pt 1):G223-30.
46. Vanner S, and Surprenant A. Cholinergic and noncholinergic submucosal neurons dilate arterioles in guinea pig colon. *Am J Physiol.* 1991;261(1 Pt 1):G136-44.
47. Stead RH, Tomioka M, Quinonez G, Simon GT, Felten SY, and Bienenstock J. Intestinal mucosal mast cells in normal and nematode-infected rat intestines are in intimate contact with peptidergic nerves. *Proc Natl Acad Sci U S A.* 1987;84(9):2975-9.
48. Xue J, Askwith C, Javed NH, and Cooke HJ. Autonomic nervous system and secretion across the intestinal mucosal surface. *Autonomic neuroscience : basic & clinical.* 2007;133(1):55-63.
49. Banks MR, and Farthing MJ. Fluid and electrolyte transport in the small intestine. *Curr Opin Gastroenterol.* 2002;18(2):176-81.
50. Li Z, Hao MM, Van den Haute C, Baekelandt V, Boesmans W, and Vanden Berghe P. Regional complexity in enteric neuron wiring reflects diversity of motility patterns in the mouse large intestine. *eLife.* 2019;8(
51. Lies B, Gil V, Groneberg D, Seidler B, Saur D, Wischmeyer E, Jimenez M, and Friebe A. Interstitial cells of Cajal mediate nitrergic inhibitory neurotransmission in the murine gastrointestinal tract. *American journal of physiology Gastrointestinal and liver physiology.* 2014;307(1):G98-106.
52. Timmermans JP, Hens J, and Adriaensen D. Outer submucous plexus: an intrinsic nerve network involved in both secretory and motility processes in the intestine of large mammals and humans. *The Anatomical record.* 2001;262(1):71-8.
53. Fu M, Landreville S, Agapova OA, Wiley LA, Shoykhet M, Harbour JW, and Heuckeroth RO. Retinoblastoma protein prevents enteric nervous system defects and intestinal pseudo-obstruction. *The Journal of clinical investigation.* 2013;123(12):5152-64.
54. Collins J, Borojevic R, Verdu EF, Huizinga JD, and Ratcliffe EM. Intestinal microbiota influence the early postnatal development of the enteric nervous system. *Neurogastroenterology and motility : the official journal of the European Gastrointestinal Motility Society.* 2014;26(1):98-107.
55. Anitha M, Vijay-Kumar M, Sitaraman SV, Gewirtz AT, and Srinivasan S. Gut microbial products regulate murine gastrointestinal motility via Toll-like receptor 4 signaling. *Gastroenterology.* 2012;143(4):1006-16 e4.
56. Heuckeroth RO, and Schafer KH. Gene-environment interactions and the enteric nervous system: Neural plasticity and Hirschsprung disease prevention. *Developmental biology.* 2016;417(2):188-97.

57. Heuckeroth RO. Hirschsprung disease - integrating basic science and clinical medicine to improve outcomes. *Nature reviews Gastroenterology & hepatology.* 2018;15(3):152-67.
58. Tam PK. Hirschsprung's disease: A bridge for science and surgery. *Journal of pediatric surgery.* 2016;51(1):18-22.
59. McKeown SJ, Stamp L, Hao MM, and Young HM. Hirschsprung disease: a developmental disorder of the enteric nervous system. *Wiley interdisciplinary reviews Developmental biology.* 2013;2(1):113-29.
60. Heuckeroth RO. Even When You Know Everything, There Is Still More to Learn About Hirschsprung Disease. *Gastroenterology.* 2018;155(6):1681-4.
61. Lake JI, Tusheva OA, Graham BL, and Heuckeroth RO. Hirschsprung-like disease is exacerbated by reduced de novo GMP synthesis. *The Journal of clinical investigation.* 2013;123(11):4875-87.
62. Schill EM, Lake JI, Tusheva OA, Nagy N, Bery SK, Foster L, Avetisyan M, Johnson SL, Stenson WF, Goldstein AM, et al. Ibuprofen slows migration and inhibits bowel colonization by enteric nervous system precursors in zebrafish, chick and mouse. *Developmental biology.* 2016;409(2):473-88.
63. Fu M, Sato Y, Lyons-Warren A, Zhang B, Kane MA, Napoli JL, and Heuckeroth RO. Vitamin A facilitates enteric nervous system precursor migration by reducing Pten accumulation. *Development.* 2010;137(4):631-40.
64. Arshad A, Powell C, and Tighe MP. Hirschsprung's disease. *Bmj.* 2012;345(e5521.
65. Menezes M, and Puri P. Long-term outcome of patients with enterocolitis complicating Hirschsprung's disease. *Pediatric surgery international.* 2006;22(4):316-8.
66. Yanchar NL, and Soucy P. Long-term outcome after Hirschsprung's disease: patients' perspectives. *Journal of pediatric surgery.* 1999;34(7):1152-60.
67. Jarvi K, Laitakari EM, Koivusalo A, Rintala RJ, and Pakarinen MP. Bowel function and gastrointestinal quality of life among adults operated for Hirschsprung disease during childhood: a population-based study. *Annals of surgery.* 2010;252(6):977-81.
68. Neuvonen MI, Kyrklund K, Rintala RJ, and Pakarinen MP. Bowel Function and Quality of Life After Transanal Endorectal Pull-through for Hirschsprung Disease: Controlled Outcomes up to Adulthood. *Annals of surgery.* 2017;265(3):622-9.
69. Rintala RJ, and Pakarinen MP. Long-term outcomes of Hirschsprung's disease. *Seminars in pediatric surgery.* 2012;21(4):336-43.
70. Zaitoun I, Erickson CS, Barlow AJ, Klein TR, Heneghan AF, Pierre JF, Epstein ML, and Gosain A. Altered neuronal density and neurotransmitter expression in the ganglionated region of Ednrb null mice: implications for Hirschsprung's disease. *Neurogastroenterology and motility : the official journal of the European Gastrointestinal Motility Society.* 2013;25(3):e233-44.
71. Musser MA, Correa H, and Southard-Smith EM. Enteric neuron imbalance and proximal dysmotility in ganglionated intestine of the Sox10(Dom/+)

Hirschsprung mouse model. *Cellular and molecular gastroenterology and hepatology.* 2015;1(1):87-101.
72. Roberts RR, Bornstein JC, Bergner AJ, and Young HM. Disturbances of colonic motility in mouse models of Hirschsprung's disease. *American journal of physiology Gastrointestinal and liver physiology.* 2008;294(4):G996-G1008.
73. Coyle D, O'Donnell AM, Gillick J, and Puri P. Altered neurotransmitter expression profile in the ganglionic bowel in Hirschsprung's disease. *Journal of pediatric surgery.* 2016;51(5):762-9.
74. Cheng LS, Schwartz DM, Hotta R, Graham HK, and Goldstein AM. Bowel dysfunction following pullthrough surgery is associated with an overabundance of nitrergic neurons in Hirschsprung disease. *Journal of pediatric surgery.* 2016;51(11):1834-8.
75. Yamakawa K, Huot YK, Haendelt MA, Hubert R, Chen XN, Lyons GE, and Korenberg JR. DSCAM: a novel member of the immunoglobulin superfamily maps in a Down syndrome region and is involved in the development of the nervous system. *Human molecular genetics.* 1998;7(2):227-37.
76. Wang Y, He Q, Zhang R, Zhong W, Zhu D, Zhang Y, and Xia H. Association between DSCAM polymorphisms and non-syndromic Hirschsprung disease in Chinese population. *BMC medical genetics.* 2018;19(1):116.
77. Jannot AS, Pelet A, Henrion-Caude A, Chaoui A, Masse-Morel M, Arnold S, Sanlaville D, Ceccherini I, Borrego S, Hofstra RM, et al. Chromosome 21 scan in Down syndrome reveals DSCAM as a predisposing locus in Hirschsprung disease. *PloS one.* 2013;8(5):e62519.
78. Korbel JO, Tirosh-Wagner T, Urban AE, Chen XN, Kasowski M, Dai L, Grubert F, Erdman C, Gao MC, Lange K, et al. The genetic architecture of Down syndrome phenotypes revealed by high-resolution analysis of human segmental trisomies. *Proc Natl Acad Sci U S A.* 2009;106(29):12031-6.
79. Ehe BK, Lamson DR, Tarpley M, Onyenwoke RU, Graves LM, and Williams KP. Identification of a DYRK1A-mediated phosphorylation site within the nuclear localization sequence of the hedgehog transcription factor GLI1. *Biochemical and biophysical research communications.* 2017;491(3):767-72.
80. Liu JA, Lai FP, Gui HS, Sham MH, Tam PK, Garcia-Barcelo MM, Hui CC, and Ngan ES. Identification of GLI Mutations in Patients With Hirschsprung Disease That Disrupt Enteric Nervous System Development in Mice. *Gastroenterology.* 2015;149(7):1837-48 e5.
81. Yang JT, Liu CZ, Villavicencio EH, Yoon JW, Walterhouse D, and Iannaccone PM. Expression of human GLI in mice results in failure to thrive, early death, and patchy Hirschsprung-like gastrointestinal dilatation. *Molecular medicine.* 1997;3(12):826-35.
82. Najas S, Arranz J, Lochhead PA, Ashford AL, Oxley D, Delabar JM, Cook SJ, Barallobre MJ, and Arbones ML. DYRK1A-mediated Cyclin D1 Degradation in Neural Stem Cells Contributes to the Neurogenic Cortical Defects in Down Syndrome. *EBioMedicine.* 2015;2(2):120-34.
83. Soppa U, Schumacher J, Florencio Ortiz V, Pasqualon T, Tejedor FJ, and Becker W. The Down syndrome-related protein kinase DYRK1A

phosphorylates p27(Kip1) and Cyclin D1 and induces cell cycle exit and neuronal differentiation. *Cell cycle.* 2014;13(13):2084-100.
84. Stagni F, Giacomini A, Emili M, Guidi S, and Bartesaghi R. Neurogenesis impairment: An early developmental defect in Down syndrome. *Free radical biology & medicine.* 2018;114(15-32.
85. Travassos D, van Herwaarden-Lindeboom M, and van der Zee DC. Hirschsprung's disease in children with Down syndrome: a comparative study. *European journal of pediatric surgery : official journal of Austrian Association of Pediatric Surgery [et al] = Zeitschrift fur Kinderchirurgie.* 2011;21(4):220-3.
86. Friedmacher F, and Puri P. Hirschsprung's disease associated with Down syndrome: a meta-analysis of incidence, functional outcomes and mortality. *Pediatric surgery international.* 2013;29(9):937-46.
87. Moore SW. Down syndrome and the enteric nervous system. *Pediatric surgery international.* 2008;24(8):873-83.
88. Wallace RA. Clinical audit of gastrointestinal conditions occurring among adults with Down syndrome attending a specialist clinic. *Journal of intellectual & developmental disability.* 2007;32(1):45-50.
89. Antonucci A, Fronzoni L, Cogliandro L, Cogliandro RF, Caputo C, De Giorgio R, Pallotti F, Barbara G, Corinaldesi R, and Stanghellini V. Chronic intestinal pseudo-obstruction. *World journal of gastroenterology.* 2008;14(19):2953-61.
90. Gargiulo A, Auricchio R, Barone MV, Cotugno G, Reardon W, Milla PJ, Ballabio A, Ciccodicola A, and Auricchio A. Filamin A is mutated in X-linked chronic idiopathic intestinal pseudo-obstruction with central nervous system involvement. *American journal of human genetics.* 2007;80(4):751-8.
91. Ravenscroft G, Pannell S, O'Grady G, Ong R, Ee HC, Faiz F, Marns L, Goel H, Kumarasinghe P, Sollis E, et al. Variants in ACTG2 underlie a substantial number of Australasian patients with primary chronic intestinal pseudo-obstruction. *Neurogastroenterology and motility : the official journal of the European Gastrointestinal Motility Society.* 2018:e13371.
92. Bonora E, Bianco F, Cordeddu L, Bamshad M, Francescatto L, Dowless D, Stanghellini V, Cogliandro RF, Lindberg G, Mungan Z, et al. Mutations in RAD21 disrupt regulation of APOB in patients with chronic intestinal pseudo-obstruction. *Gastroenterology.* 2015;148(4):771-82 e11.
93. Pingault V, Girard M, Bondurand N, Dorkins H, Van Maldergem L, Mowat D, Shimotake T, Verma I, Baumann C, and Goossens M. SOX10 mutations in chronic intestinal pseudo-obstruction suggest a complex physiopathological mechanism. *Human genetics.* 2002;111(2):198-206.
94. Rivera LR, Poole DP, Thacker M, and Furness JB. The involvement of nitric oxide synthase neurons in enteric neuropathies. *Neurogastroenterology and motility : the official journal of the European Gastrointestinal Motility Society.* 2011;23(11):980-8.

95. Diers AR, Broniowska KA, and Hogg N. Nitrosative stress and redox-cycling agents synergize to cause mitochondrial dysfunction and cell death in endothelial cells. *Redox biology.* 2013;1(1-7.
96. Downard CD, Grant SN, Matheson PJ, Guillaume AW, Debski R, Fallat ME, and Garrison RN. Altered intestinal microcirculation is the critical event in the development of necrotizing enterocolitis. *Journal of pediatric surgery.* 2011;46(6):1023-8.
97. Zhou Y, Yang J, Watkins DJ, Boomer LA, Matthews MA, Su Y, and Besner GE. Enteric nervous system abnormalities are present in human necrotizing enterocolitis: potential neurotransplantation therapy. *Stem Cell Res Ther.* 2013;4(6):157.
98. Nowicki PT, Caniano DA, Hammond S, Giannone PJ, Besner GE, Reber KM, and Nankervis CA. Endothelial nitric oxide synthase in human intestine resected for necrotizing enterocolitis. *J Pediatr.* 2007;150(1):40-5.
99. Hatoum OA, Binion DG, Otterson MF, and Gutterman DD. Acquired microvascular dysfunction in inflammatory bowel disease: Loss of nitric oxide-mediated vasodilation. *Gastroenterology.* 2003;125(1):58-69.
100. Lane R, and Baldwin D. Selective serotonin reuptake inhibitor-induced serotonin syndrome: review. *J Clin Psychopharmacol.* 1997;17(3):208-21.
101. Jones SL, and Blikslager AT. Role of the enteric nervous system in the pathophysiology of secretory diarrhea. *J Vet Intern Med.* 2002;16(3):222-8.
102. Eklund S, Jodal M, and Lundgren O. The enteric nervous system participates in the secretory response to the heat stable enterotoxins of Escherichia coli in rats and cats. *Neuroscience.* 1985;14(2):673-81.
103. Rolig AS, Mittge EK, Ganz J, Troll JV, Melancon E, Wiles TJ, Alligood K, Stephens WZ, Eisen JS, and Guillemin K. The enteric nervous system promotes intestinal health by constraining microbiota composition. *PLoS Biol.* 2017;15(2):e2000689.
104. Stanisz AM, Befus D, and Bienenstock J. Differential effects of vasoactive intestinal peptide, substance P, and somatostatin on immunoglobulin synthesis and proliferations by lymphocytes from Peyer's patches, mesenteric lymph nodes, and spleen. *J Immunol.* 1986;136(1):152-6.
105. Puzan M, Hosic S, Ghio C, and Koppes A. Enteric Nervous System Regulation of Intestinal Stem Cell Differentiation and Epithelial Monolayer Function. *Sci Rep.* 2018;8(1):6313.
106. Schneider S, Wright CM, and Heuckeroth RO. Unexpected Roles for the Second Brain: Enteric Nervous System as Master Regulator of Bowel Function. *Annual review of physiology.* 2019;81(235-59.
107. Espinosa-Medina I, Jevans B, Boismoreau F, Chettouh Z, Enomoto H, Muller T, Birchmeier C, Burns AJ, and Brunet JF. Dual origin of enteric neurons in vagal Schwann cell precursors and the sympathetic neural crest. *Proc Natl Acad Sci U S A.* 2017;114(45):11980-5.
108. Uesaka T, Nagashimada M, and Enomoto H. Neuronal Differentiation in Schwann Cell Lineage Underlies Postnatal Neurogenesis in the Enteric

Nervous System. *The Journal of neuroscience : the official journal of the Society for Neuroscience.* 2015;35(27):9879-88.
109. Brokhman I, Xu J, Coles BLK, Razavi R, Engert S, Lickert H, Babona-Pilipos R, Morshead CM, Sibley E, Chen C, et al. Dual embryonic origin of the mammalian enteric nervous system. *Developmental biology.* 2019;445(2):256-70.
110. Pham TD, Gershon MD, and Rothman TP. Time of origin of neurons in the murine enteric nervous system: sequence in relation to phenotype. *The Journal of comparative neurology.* 1991;314(4):789-98.
111. Hao MM, and Young HM. Development of enteric neuron diversity. *Journal of cellular and molecular medicine.* 2009;13(7):1193-210.
112. Rothman TP, and Gershon MD. Phenotypic expression in the developing murine enteric nervous system. *The Journal of neuroscience : the official journal of the Society for Neuroscience.* 1982;2(3):381-93.
113. Bergner AJ, Stamp LA, Gonsalvez DG, Allison MB, Olson DP, Myers MG, Jr., Anderson CR, and Young HM. Birthdating of myenteric neuron subtypes in the small intestine of the mouse. *The Journal of comparative neurology.* 2014;522(3):514-27.
114. Jonscher R, and Belkind-Gerson J. Concise Review: Cellular and Molecular Mechanisms of Postnatal Injury-Induced Enteric Neurogenesis. *Stem cells.* 2019.
115. Kulkarni S, Micci MA, Leser J, Shin C, Tang SC, Fu YY, Liu L, Li Q, Saha M, Li C, et al. Adult enteric nervous system in health is maintained by a dynamic balance between neuronal apoptosis and neurogenesis. *Proceedings of the National Academy of Sciences of the United States of America.* 2017;114(18):E3709-E18.
116. Enomoto H, Hughes I, Golden J, Baloh RH, Yonemura S, Heuckeroth RO, Johnson EM, Jr., and Milbrandt J. GFRalpha1 expression in cells lacking RET is dispensable for organogenesis and nerve regeneration. *Neuron.* 2004;44(4):623-36.
117. Gianino S, Grider JR, Cresswell J, Enomoto H, and Heuckeroth RO. GDNF availability determines enteric neuron number by controlling precursor proliferation. *Development.* 2003;130(10):2187-98.
118. Heuckeroth RO, Lampe PA, Johnson EM, and Milbrandt J. Neurturin and GDNF promote proliferation and survival of enteric neuron and glial progenitors in vitro. *Developmental biology.* 1998;200(1):116-29.
119. Schuchardt A, D'Agati V, Larsson-Blomberg L, Costantini F, and Pachnis V. Defects in the kidney and enteric nervous system of mice lacking the tyrosine kinase receptor Ret. *Nature.* 1994;367(6461):380-3.
120. Cacalano G, Farinas I, Wang LC, Hagler K, Forgie A, Moore M, Armanini M, Phillips H, Ryan AM, Reichardt LF, et al. GFRalpha1 is an essential receptor component for GDNF in the developing nervous system and kidney. *Neuron.* 1998;21(1):53-62.

121. Moore MW, Klein RD, Farinas I, Sauer H, Armanini M, Phillips H, Reichardt LF, Ryan AM, Carver-Moore K, and Rosenthal A. Renal and neuronal abnormalities in mice lacking GDNF. *Nature.* 1996;382(6586):76-9.
122. Tomuschat C, and Puri P. RET gene is a major risk factor for Hirschsprung's disease: a meta-analysis. *Pediatric surgery international.* 2015;31(8):701-10.
123. Pini Prato A, Musso M, Ceccherini I, Mattioli G, Giunta C, Ghiggeri GM, and Jasonni V. Hirschsprung disease and congenital anomalies of the kidney and urinary tract (CAKUT): a novel syndromic association. *Medicine.* 2009;88(2):83-90.
124. Uesaka T, Nagashimada M, and Enomoto H. GDNF signaling levels control migration and neuronal differentiation of enteric ganglion precursors. *The Journal of neuroscience : the official journal of the Society for Neuroscience.* 2013;33(41):16372-82.
125. Uesaka T, Jain S, Yonemura S, Uchiyama Y, Milbrandt J, and Enomoto H. Conditional ablation of GFRalpha1 in postmigratory enteric neurons triggers unconventional neuronal death in the colon and causes a Hirschsprung's disease phenotype. *Development.* 2007;134(11):2171-81.
126. Lasrado R, Boesmans W, Kleinjung J, Pin C, Bell D, Bhaw L, McCallum S, Zong H, Luo L, Clevers H, et al. Lineage-dependent spatial and functional organization of the mammalian enteric nervous system. *Science.* 2017;356(6339):722-6.
127. Rossi J, Herzig KH, Voikar V, Hiltunen PH, Segerstrale M, and Airaksinen MS. Alimentary tract innervation deficits and dysfunction in mice lacking GDNF family receptor alpha2. *The Journal of clinical investigation.* 2003;112(5):707-16.
128. Heuckeroth RO, Enomoto H, Grider JR, Golden JP, Hanke JA, Jackman A, Molliver DC, Bardgett ME, Snider WD, Johnson EM, Jr., et al. Gene targeting reveals a critical role for neurturin in the development and maintenance of enteric, sensory, and parasympathetic neurons. *Neuron.* 1999;22(2):253-63.
129. Hosoda K, Hammer RE, Richardson JA, Baynash AG, Cheung JC, Giaid A, and Yanagisawa M. Targeted and natural (piebald-lethal) mutations of endothelin-B receptor gene produce megacolon associated with spotted coat color in mice. *Cell.* 1994;79(7):1267-76.
130. Pavan WJ, Liddell RA, Wright A, Thibaudeau G, Matteson PG, McHugh KM, and Siracusa LD. A high-resolution linkage map of the lethal spotting locus: a mouse model for Hirschsprung disease. *Mammalian genome : official journal of the International Mammalian Genome Society.* 1995;6(1):1-7.
131. Yanagisawa H, Yanagisawa M, Kapur RP, Richardson JA, Williams SC, Clouthier DE, de Wit D, Emoto N, and Hammer RE. Dual genetic pathways of endothelin-mediated intercellular signaling revealed by targeted disruption of endothelin converting enzyme-1 gene. *Development.* 1998;125(5):825-36.
132. Minami SB, Nara K, Mutai H, Morimoto N, Sakamoto H, Takiguchi T, Kaga K, and Matsunaga T. A clinical and genetic study of 16 Japanese families with Waardenburg syndrome. *Gene.* 2019;704(86-90.

133. Parisi MA, and Kapur RP. Genetics of Hirschsprung disease. *Current opinion in pediatrics.* 2000;12(6):610-7.
134. Lake JI, and Heuckeroth RO. Enteric nervous system development: migration, differentiation, and disease. *American journal of physiology Gastrointestinal and liver physiology.* 2013;305(1):G1-24.
135. Kapur RP. Early death of neural crest cells is responsible for total enteric aganglionosis in Sox10(Dom)/Sox10(Dom) mouse embryos. *Pediatric and developmental pathology : the official journal of the Society for Pediatric Pathology and the Paediatric Pathology Society.* 1999;2(6):559-69.
136. Van de Putte T, Maruhashi M, Francis A, Nelles L, Kondoh H, Huylebroeck D, and Higashi Y. Mice lacking ZFHX1B, the gene that codes for Smad-interacting protein-1, reveal a role for multiple neural crest cell defects in the etiology of Hirschsprung disease-mental retardation syndrome. *American journal of human genetics.* 2003;72(2):465-70.
137. Pattyn A, Morin X, Cremer H, Goridis C, and Brunet JF. The homeobox gene Phox2b is essential for the development of autonomic neural crest derivatives. *Nature.* 1999;399(6734):366-70.
138. Lang D, Chen F, Milewski R, Li J, Lu MM, and Epstein JA. Pax3 is required for enteric ganglia formation and functions with Sox10 to modulate expression of c-ret. *The Journal of clinical investigation.* 2000;106(8):963-71.
139. Leon TY, Ngan ES, Poon HC, So MT, Lui VC, Tam PK, and Garcia-Barcelo MM. Transcriptional regulation of RET by Nkx2-1, Phox2b, Sox10, and Pax3. *Journal of pediatric surgery.* 2009;44(10):1904-12.
140. Watanabe Y, Stanchina L, Lecerf L, Gacem N, Conidi A, Baral V, Pingault V, Huylebroeck D, and Bondurand N. Differentiation of Mouse Enteric Nervous System Progenitor Cells Is Controlled by Endothelin 3 and Requires Regulation of Ednrb by SOX10 and ZEB2. *Gastroenterology.* 2017;152(5):1139-50 e4.
141. Zhu L, Lee HO, Jordan CS, Cantrell VA, Southard-Smith EM, and Shin MK. Spatiotemporal regulation of endothelin receptor-B by SOX10 in neural crest-derived enteric neuron precursors. *Nature genetics.* 2004;36(7):732-7.
142. Britsch S, Goerich DE, Riethmacher D, Peirano RI, Rossner M, Nave KA, Birchmeier C, and Wegner M. The transcription factor Sox10 is a key regulator of peripheral glial development. *Genes & development.* 2001;15(1):66-78.
143. Lane PW, and Liu HM. Association of megacolon with a new dominant spotting gene (Dom) in the mouse. *The Journal of heredity.* 1984;75(6):435-9.
144. Bondurand N, Dastot-Le Moal F, Stanchina L, Collot N, Baral V, Marlin S, Attie-Bitach T, Giurgea I, Skopinski L, Reardon W, et al. Deletions at the SOX10 gene locus cause Waardenburg syndrome types 2 and 4. *American journal of human genetics.* 2007;81(6):1169-85.
145. Pingault V, Guiochon-Mantel A, Bondurand N, Faure C, Lacroix C, Lyonnet S, Goossens M, and Landrieu P. Peripheral neuropathy with hypomyelination, chronic intestinal pseudo-obstruction and deafness: a developmental "neural

crest syndrome" related to a SOX10 mutation. *Annals of neurology.* 2000;48(4):671-6.
146. Inoue K, Shilo K, Boerkoel CF, Crowe C, Sawady J, Lupski JR, and Agamanolis DP. Congenital hypomyelinating neuropathy, central dysmyelination, and Waardenburg-Hirschsprung disease: phenotypes linked by SOX10 mutation. *Annals of neurology.* 2002;52(6):836-42.
147. Paratore C, Eichenberger C, Suter U, and Sommer L. Sox10 haploinsufficiency affects maintenance of progenitor cells in a mouse model of Hirschsprung disease. *Human molecular genetics.* 2002;11(24):3075-85.
148. Kim J, Lo L, Dormand E, and Anderson DJ. SOX10 maintains multipotency and inhibits neuronal differentiation of neural crest stem cells. *Neuron.* 2003;38(1):17-31.
149. Bondurand N, Natarajan D, Barlow A, Thapar N, and Pachnis V. Maintenance of mammalian enteric nervous system progenitors by SOX10 and endothelin 3 signalling. *Development.* 2006;133(10):2075-86.
150. Stanchina L, Van de Putte T, Goossens M, Huylebroeck D, and Bondurand N. Genetic interaction between Sox10 and Zfhx1b during enteric nervous system development. *Developmental biology.* 2010;341(2):416-28.
151. Cacheux V, Dastot-Le Moal F, Kaariainen H, Bondurand N, Rintala R, Boissier B, Wilson M, Mowat D, and Goossens M. Loss-of-function mutations in SIP1 Smad interacting protein 1 result in a syndromic Hirschsprung disease. *Human molecular genetics.* 2001;10(14):1503-10.
152. Saunders CJ, Zhao W, and Ardinger HH. Comprehensive ZEB2 gene analysis for Mowat-Wilson syndrome in a North American cohort: a suggested approach to molecular diagnostics. *American journal of medical genetics Part A.* 2009;149A(11):2527-31.
153. Dastot-Le Moal F, Wilson M, Mowat D, Collot N, Niel F, and Goossens M. ZFHX1B mutations in patients with Mowat-Wilson syndrome. *Human mutation.* 2007;28(4):313-21.
154. Coyle D, and Puri P. Hirschsprung's disease in children with Mowat-Wilson syndrome. *Pediatric surgery international.* 2015;31(8):711-7.
155. Van de Putte T, Francis A, Nelles L, van Grunsven LA, and Huylebroeck D. Neural crest-specific removal of Zfhx1b in mouse leads to a wide range of neurocristopathies reminiscent of Mowat-Wilson syndrome. *Human molecular genetics.* 2007;16(12):1423-36.
156. Soret R, Mennetrey M, Bergeron KF, Dariel A, Neunlist M, Grunder F, Faure C, Silversides DW, Pilon N, and Ente-Hirsch Study G. A collagen VI-dependent pathogenic mechanism for Hirschsprung's disease. *The Journal of clinical investigation.* 2015;125(12):4483-96.
157. Corpening JC, Cantrell VA, Deal KK, and Southard-Smith EM. A Histone2BCerulean BAC transgene identifies differential expression of Phox2b in migrating enteric neural crest derivatives and enteric glia. *Developmental dynamics : an official publication of the American Association of Anatomists.* 2008;237(4):1119-32.

158. Amiel J, Laudier B, Attie-Bitach T, Trang H, de Pontual L, Gener B, Trochet D, Etchevers H, Ray P, Simonneau M, et al. Polyalanine expansion and frameshift mutations of the paired-like homeobox gene PHOX2B in congenital central hypoventilation syndrome. *Nature genetics.* 2003;33(4):459-61.
159. Nagashimada M, Ohta H, Li C, Nakao K, Uesaka T, Brunet JF, Amiel J, Trochet D, Wakayama T, and Enomoto H. Autonomic neurocristopathy-associated mutations in PHOX2B dysregulate Sox10 expression. *The Journal of clinical investigation.* 2012;122(9):3145-58.
160. Lang D, and Epstein JA. Sox10 and Pax3 physically interact to mediate activation of a conserved c-RET enhancer. *Human molecular genetics.* 2003;12(8):937-45.
161. Zhu J, Garcia-Barcelo MM, Tam PK, and Lui VC. HOXB5 cooperates with NKX2-1 in the transcription of human RET. *PloS one.* 2011;6(6):e20815.
162. Lui VC, Cheng WW, Leon TY, Lau DK, Garcia-Barcelo MM, Miao XP, Kam MK, So MT, Chen Y, Wall NA, et al. Perturbation of hoxb5 signaling in vagal neural crests down-regulates ret leading to intestinal hypoganglionosis in mice. *Gastroenterology.* 2008;134(4):1104-15.
163. Zhu JJ, Kam MK, Garcia-Barcelo MM, Tam PK, and Lui VC. HOXB5 binds to multi-species conserved sequence (MCS+9.7) of RET gene and regulates RET expression. *The international journal of biochemistry & cell biology.* 2014;51(142-9.
164. Carter TC, Kay DM, Browne ML, Liu A, Romitti PA, Kuehn D, Conley MR, Caggana M, Druschel CM, Brody LC, et al. Hirschsprung's disease and variants in genes that regulate enteric neural crest cell proliferation, migration and differentiation. *Journal of human genetics.* 2012;57(8):485-93.
165. Garcia-Barcelo M, Ganster RW, Lui VC, Leon TY, So MT, Lau AM, Fu M, Sham MH, Knight J, Zannini MS, et al. TTF-1 and RET promoter SNPs: regulation of RET transcription in Hirschsprung's disease. *Human molecular genetics.* 2005;14(2):191-204.
166. Rancourt DE, Tsuzuki T, and Capecchi MR. Genetic interaction between hoxb-5 and hoxb-6 is revealed by nonallelic noncomplementation. *Genes & development.* 1995;9(1):108-22.
167. Kam MK, Cheung MC, Zhu JJ, Cheng WW, Sat EW, Tam PK, and Lui VC. Perturbation of Hoxb5 signaling in vagal and trunk neural crest cells causes apoptosis and neurocristopathies in mice. *Cell death and differentiation.* 2014;21(2):278-89.
168. Teng L, Mundell NA, Frist AY, Wang Q, and Labosky PA. Requirement for Foxd3 in the maintenance of neural crest progenitors. *Development.* 2008;135(9):1615-24.
169. Bates MD, Dunagan DT, Welch LC, Kaul A, and Harvey RP. The Hlx homeobox transcription factor is required early in enteric nervous system development. *BMC developmental biology.* 2006;6(33.
170. Cantrell VA, Owens SE, Chandler RL, Airey DC, Bradley KM, Smith JR, and Southard-Smith EM. Interactions between Sox10 and EdnrB modulate

penetrance and severity of aganglionosis in the Sox10Dom mouse model of Hirschsprung disease. *Human molecular genetics.* 2004;13(19):2289-301.
171. Ngan ES, Garcia-Barcelo MM, Yip BH, Poon HC, Lau ST, Kwok CK, Sat E, Sham MH, Wong KK, Wainwright BJ, et al. Hedgehog/Notch-induced premature gliogenesis represents a new disease mechanism for Hirschsprung disease in mice and humans. *The Journal of clinical investigation.* 2011;121(9):3467-78.
172. Mundell NA, Plank JL, LeGrone AW, Frist AY, Zhu L, Shin MK, Southard-Smith EM, and Labosky PA. Enteric nervous system specific deletion of Foxd3 disrupts glial cell differentiation and activates compensatory enteric progenitors. *Developmental biology.* 2012;363(2):373-87.
173. Bergeron KF, Nguyen CM, Cardinal T, Charrier B, Silversides DW, and Pilon N. Upregulation of the Nr2f1-A830082K12Rik gene pair in murine neural crest cells results in a complex phenotype reminiscent of Waardenburg syndrome type 4. *Disease models & mechanisms.* 2016;9(11):1283-93.
174. Charrier B, and Pilon N. Toward a better understanding of enteric gliogenesis. *Neurogenesis.* 2017;4(1):e1293958.
175. Lopez SH, Avetisyan M, Wright CM, Mesbah K, Kelly RG, Moon AM, and Heuckeroth RO. Loss of Tbx3 in murine neural crest reduces enteric glia and causes cleft palate, but does not influence heart development or bowel transit. *Developmental biology.* 2018;444 Suppl 1(S337-S51.
176. D'Autreaux F, Morikawa Y, Cserjesi P, and Gershon MD. Hand2 is necessary for terminal differentiation of enteric neurons from crest-derived precursors but not for their migration into the gut or for formation of glia. *Development.* 2007;134(12):2237-49.
177. Hendershot TJ, Liu H, Sarkar AA, Giovannucci DR, Clouthier DE, Abe M, and Howard MJ. Expression of Hand2 is sufficient for neurogenesis and cell type-specific gene expression in the enteric nervous system. *Developmental dynamics : an official publication of the American Association of Anatomists.* 2007;236(1):93-105.
178. D'Autreaux F, Margolis KG, Roberts J, Stevanovic K, Mawe G, Li Z, Karamooz N, Ahuja A, Morikawa Y, Cserjesi P, et al. Expression level of Hand2 affects specification of enteric neurons and gastrointestinal function in mice. *Gastroenterology.* 2011;141(2):576-87, 87 e1-6.
179. Lei J, and Howard MJ. Targeted deletion of Hand2 in enteric neural precursor cells affects its functions in neurogenesis, neurotransmitter specification and gangliogenesis, causing functional aganglionosis. *Development.* 2011;138(21):4789-800.
180. Pollak J, Wilken MS, Ueki Y, Cox KE, Sullivan JM, Taylor RJ, Levine EM, and Reh TA. ASCL1 reprograms mouse Muller glia into neurogenic retinal progenitors. *Development.* 2013;140(12):2619-31.
181. Kim EJ, Ables JL, Dickel LK, Eisch AJ, and Johnson JE. Ascl1 (Mash1) defines cells with long-term neurogenic potential in subgranular and subventricular zones in adult mouse brain. *PloS one.* 2011;6(3):e18472.
182. Battiste J, Helms AW, Kim EJ, Savage TK, Lagace DC, Mandyam CD, Eisch AJ, Miyoshi G, and Johnson JE. Ascl1 defines sequentially generated lineage-

restricted neuronal and oligodendrocyte precursor cells in the spinal cord. *Development.* 2007;134(2):285-93.
183. Zeisel A, Munoz-Manchado AB, Codeluppi S, Lonnerberg P, La Manno G, Jureus A, Marques S, Munguba H, He L, Betsholtz C, et al. Brain structure. Cell types in the mouse cortex and hippocampus revealed by single-cell RNA-seq. *Science.* 2015;347(6226):1138-42.
184. Guillemot F. Spatial and temporal specification of neural fates by transcription factor codes. *Development.* 2007;134(21):3771-80.
185. Blaugrund E, Pham TD, Tennyson VM, Lo L, Sommer L, Anderson DJ, and Gershon MD. Distinct subpopulations of enteric neuronal progenitors defined by time of development, sympathoadrenal lineage markers and Mash-1-dependence. *Development.* 1996;122(1):309-20.
186. Memic F, Knoflach V, Sadler R, Tegerstedt G, Sundstrom E, Guillemot F, Pachnis V, and Marklund U. Ascl1 Is Required for the Development of Specific Neuronal Subtypes in the Enteric Nervous System. *The Journal of neuroscience : the official journal of the Society for Neuroscience.* 2016;36(15):4339-50.
187. Chalazonitis A, Tang AA, Shang Y, Pham TD, Hsieh I, Setlik W, Gershon MD, and Huang EJ. Homeodomain interacting protein kinase 2 regulates postnatal development of enteric dopaminergic neurons and glia via BMP signaling. *The Journal of neuroscience : the official journal of the Society for Neuroscience.* 2011;31(39):13746-57.
188. Chalazonitis A, D'Autreaux F, Guha U, Pham TD, Faure C, Chen JJ, Roman D, Kan L, Rothman TP, Kessler JA, et al. Bone morphogenetic protein-2 and -4 limit the number of enteric neurons but promote development of a TrkC-expressing neurotrophin-3-dependent subset. *The Journal of neuroscience : the official journal of the Society for Neuroscience.* 2004;24(17):4266-82.
189. Memic F, Knoflach V, Morarach K, Sadler R, Laranjeira C, Hjerling-Leffler J, Sundstrom E, Pachnis V, and Marklund U. Transcription and Signaling Regulators in Developing Neuronal Subtypes of Mouse and Human Enteric Nervous System. *Gastroenterology.* 2018;154(3):624-36.
190. Hatano M, Aoki T, Dezawa M, Yusa S, Iitsuka Y, Koseki H, Taniguchi M, and Tokuhisa T. A novel pathogenesis of megacolon in Ncx/Hox11L.1 deficient mice. *The Journal of clinical investigation.* 1997;100(4):795-801.
191. Shirasawa S, Yunker AM, Roth KA, Brown GA, Horning S, and Korsmeyer SJ. Enx (Hox11L1)-deficient mice develop myenteric neuronal hyperplasia and megacolon. *Nature medicine.* 1997;3(6):646-50.
192. Nakai S, Sugitani Y, Sato H, Ito S, Miura Y, Ogawa M, Nishi M, Jishage K, Minowa O, and Noda T. Crucial roles of Brn1 in distal tubule formation and function in mouse kidney. *Development.* 2003;130(19):4751-9.
193. Chevalier J, Derkinderen P, Gomes P, Thinard R, Naveilhan P, Vanden Berghe P, and Neunlist M. Activity-dependent regulation of tyrosine hydroxylase expression in the enteric nervous system. *The Journal of physiology.* 2008;586(7):1963-75.

194. Hao MM, Moore RE, Roberts RR, Nguyen T, Furness JB, Anderson RB, and Young HM. The role of neural activity in the migration and differentiation of enteric neuron precursors. *Neurogastroenterology and motility : the official journal of the European Gastrointestinal Motility Society.* 2010;22(5):e127-37.
195. Li Z, Caron MG, Blakely RD, Margolis KG, and Gershon MD. Dependence of serotonergic and other nonadrenergic enteric neurons on norepinephrine transporter expression. *The Journal of neuroscience : the official journal of the Society for Neuroscience.* 2010;30(49):16730-40.
196. Raghavan S, and Bitar KN. The influence of extracellular matrix composition on the differentiation of neuronal subtypes in tissue engineered innervated intestinal smooth muscle sheets. *Biomaterials.* 2014;35(26):7429-40.
197. Turner KN, Schachner M, and Anderson RB. Cell adhesion molecule L1 affects the rate of differentiation of enteric neurons in the developing gut. *Developmental dynamics : an official publication of the American Association of Anatomists.* 2009;238(3):708-15.
198. Brun P, Giron MC, Qesari M, Porzionato A, Caputi V, Zoppellaro C, Banzato S, Grillo AR, Spagnol L, De Caro R, et al. Toll-like receptor 2 regulates intestinal inflammation by controlling integrity of the enteric nervous system. *Gastroenterology.* 2013;145(6):1323-33.
199. Reichardt F, Chassaing B, Nezami BG, Li G, Tabatabavakili S, Mwangi S, Uppal K, Liang B, Vijay-Kumar M, Jones D, et al. Western diet induces colonic nitrergic myenteric neuropathy and dysmotility in mice via saturated fatty acid- and lipopolysaccharide-induced TLR4 signalling. *The Journal of physiology.* 2017;595(5):1831-46.
200. Suply E, de Vries P, Soret R, Cossais F, and Neunlist M. Butyrate enemas enhance both cholinergic and nitrergic phenotype of myenteric neurons and neuromuscular transmission in newborn rat colon. *American journal of physiology Gastrointestinal and liver physiology.* 2012;302(12):G1373-80.
201. Neunlist M, and Schemann M. Nutrient-induced changes in the phenotype and function of the enteric nervous system. *The Journal of physiology.* 2014;592(14):2959-65.
202. Kapoor A, Auer DR, Lee D, Chatterjee S, and Chakravarti A. Testing the Ret and Sema3d genetic interaction in mouse enteric nervous system development. *Human molecular genetics.* 2017;26(10):1811-20.
203. Reid JE, and Wernisch L. Pseudotime estimation: deconfounding single cell time series. *Bioinformatics.* 2016;32(19):2973-80.
204. Trapnell C, Cacchiarelli D, Grimsby J, Pokharel P, Li S, Morse M, Lennon NJ, Livak KJ, Mikkelsen TS, and Rinn JL. The dynamics and regulators of cell fate decisions are revealed by pseudotemporal ordering of single cells. *Nature biotechnology.* 2014;32(4):381-6.
205. Ueno T, and Fukuzawa M. Current status of intestinal transplantation. *Surgery today.* 2010;40(12):1112-22.
206. De Giorgio R, Ricciardiello L, Naponelli V, Selgrad M, Piazzi G, Felicani C, Serra M, Fronzoni L, Antonucci A, Cogliandro RF, et al. Chronic intestinal pseudo-

obstruction related to viral infections. *Transplantation proceedings.* 2010;42(1):9-14.
207. Van Goethem G, Schwartz M, Lofgren A, Dermaut B, Van Broeckhoven C, and Vissing J. Novel POLG mutations in progressive external ophthalmoplegia mimicking mitochondrial neurogastrointestinal encephalomyopathy. *European journal of human genetics : EJHG.* 2003;11(7):547-9.
208. De Giorgio R, Bianco F, Latorre R, Caio G, Clavenzani P, and Bonora E. Enteric neuropathies: Yesterday, Today and Tomorrow. *Advances in experimental medicine and biology.* 2016;891(123-33.
209. Qiu M, Bulfone A, Martinez S, Meneses JJ, Shimamura K, Pedersen RA, and Rubenstein JL. Null mutation of Dlx-2 results in abnormal morphogenesis of proximal first and second branchial arch derivatives and abnormal differentiation in the forebrain. *Genes & development.* 1995;9(20):2523-38.
210. Thomas BL, Tucker AS, Qui M, Ferguson CA, Hardcastle Z, Rubenstein JL, and Sharpe PT. Role of Dlx-1 and Dlx-2 genes in patterning of the murine dentition. *Development.* 1997;124(23):4811-8.
211. Qiu M, Bulfone A, Ghattas I, Meneses JJ, Christensen L, Sharpe PT, Presley R, Pedersen RA, and Rubenstein JL. Role of the Dlx homeobox genes in proximodistal patterning of the branchial arches: mutations of Dlx-1, Dlx-2, and Dlx-1 and -2 alter morphogenesis of proximal skeletal and soft tissue structures derived from the first and second arches. *Developmental biology.* 1997;185(2):165-84.
212. Anderson SA, Eisenstat DD, Shi L, and Rubenstein JL. Interneuron migration from basal forebrain to neocortex: dependence on Dlx genes. *Science.* 1997;278(5337):474-6.
213. Anderson SA, Qiu M, Bulfone A, Eisenstat DD, Meneses J, Pedersen R, and Rubenstein JL. Mutations of the homeobox genes Dlx-1 and Dlx-2 disrupt the striatal subventricular zone and differentiation of late born striatal neurons. *Neuron.* 1997;19(1):27-37.
214. Cobos I, Calcagnotto ME, Vilaythong AJ, Thwin MT, Noebels JL, Baraban SC, and Rubenstein JL. Mice lacking Dlx1 show subtype-specific loss of interneurons, reduced inhibition and epilepsy. *Nature neuroscience.* 2005;8(8):1059-68.
215. Vohra BP, Tsuji K, Nagashimada M, Uesaka T, Wind D, Fu M, Armon J, Enomoto H, and Heuckeroth RO. Differential gene expression and functional analysis implicate novel mechanisms in enteric nervous system precursor migration and neuritogenesis. *Developmental biology.* 2006;298(1):259-71.
216. Visel A, Thaller C, and Eichele G. GenePaint.org: an atlas of gene expression patterns in the mouse embryo. *Nucleic acids research.* 2004;32(Database issue):D552-6.
217. Lopez SH, Avetisyan M, Wright CM, Mesbah K, Kelly RG, Moon AM, and Heuckeroth RO. Loss of Tbx3 in murine neural crest reduces enteric glia and causes cleft palate, but does not influence heart development or bowel transit. *Developmental biology.* 2018.

218. McKinsey GL, Lindtner S, Trzcinski B, Visel A, Pennacchio LA, Huylebroeck D, Higashi Y, and Rubenstein JL. Dlx1&2-dependent expression of Zfhx1b (Sip1, Zeb2) regulates the fate switch between cortical and striatal interneurons. *Neuron.* 2013;77(1):83-98.
219. Baxter AL, Vivian JL, Hagelstrom RT, Hossain W, Golden WL, Wassman ER, Vanzo RJ, and Butler MG. A Novel Partial Duplication of ZEB2 and Review of ZEB2 Involvement in Mowat-Wilson Syndrome. *Molecular syndromology.* 2017;8(4):211-8.
220. Avetisyan M, Rood JE, Huerta Lopez S, Sengupta R, Wright-Jin E, Dougherty JD, Behrens EM, and Heuckeroth RO. Muscularis macrophage development in the absence of an enteric nervous system. *Proc Natl Acad Sci U S A.* 2018;115(18):4696-701.
221. Enomoto H, Crawford PA, Gorodinsky A, Heuckeroth RO, Johnson EM, Jr., and Milbrandt J. RET signaling is essential for migration, axonal growth and axon guidance of developing sympathetic neurons. *Development.* 2001;128(20):3963-74.
222. Creedon DJ, Tansey MG, Baloh RH, Osborne PA, Lampe PA, Fahrner TJ, Heuckeroth RO, Milbrandt J, and Johnson EM, Jr. Neurturin shares receptors and signal transduction pathways with glial cell line-derived neurotrophic factor in sympathetic neurons. *Proceedings of the National Academy of Sciences of the United States of America.* 1997;94(13):7018-23.
223. Wright-Jin EC, Grider JR, Duester G, and Heuckeroth RO. Retinaldehyde dehydrogenase enzymes regulate colon enteric nervous system structure and function. *Developmental biology.* 2013;381(1):28-37.
224. Tabara H, Naito Y, Ito A, Katsuma A, Sakurai MA, Ohno S, Shimizu H, Yabuta N, and Nojima H. Neonatal lethality in knockout mice expressing the kinase-dead form of the gefitinib target GAK is caused by pulmonary dysfunction. *PloS one.* 2011;6(10):e26034.
225. Schill EM, Wright CM, Jamil A, LaCombe JM, Roper RJ, and Heuckeroth RO. Down syndrome mouse models have an abnormal enteric nervous system. *JCI insight.* 2019;5(
226. Dobin A, Davis CA, Schlesinger F, Drenkow J, Zaleski C, Jha S, Batut P, Chaisson M, and Gingeras TR. STAR: ultrafast universal RNA-seq aligner. *Bioinformatics.* 2013;29(1):15-21.
227. Lahens NF, Ricciotti E, Smirnova O, Toorens E, Kim EJ, Baruzzo G, Hayer KE, Ganguly T, Schug J, and Grant GR. A comparison of Illumina and Ion Torrent sequencing platforms in the context of differential gene expression. *BMC genomics.* 2017;18(1):602.
228. Ritchie ME, Phipson B, Wu D, Hu Y, Law CW, Shi W, and Smyth GK. limma powers differential expression analyses for RNA-sequencing and microarray studies. *Nucleic acids research.* 2015;43(7):e47.
229. Law CW, Chen Y, Shi W, and Smyth GK. voom: Precision weights unlock linear model analysis tools for RNA-seq read counts. *Genome biology.* 2014;15(2):R29.

230. Jeong J, Cesario J, Zhao Y, Burns L, Westphal H, and Rubenstein JL. Cleft palate defect of Dlx1/2-/- mutant mice is caused by lack of vertical outgrowth in the posterior palate. *Developmental dynamics : an official publication of the American Association of Anatomists.* 2012;241(11):1757-69.
231. Roberts RR, Ellis M, Gwynne RM, Bergner AJ, Lewis MD, Beckett EA, Bornstein JC, and Young HM. The first intestinal motility patterns in fetal mice are not mediated by neurons or interstitial cells of Cajal. *The Journal of physiology.* 2010;588(Pt 7):1153-69.
232. Cobos I, Borello U, and Rubenstein JL. Dlx transcription factors promote migration through repression of axon and dendrite growth. *Neuron.* 2007;54(6):873-88.
233. Mowat DR, Wilson MJ, and Goossens M. Mowat-Wilson syndrome. *Journal of medical genetics.* 2003;40(5):305-10.
234. Le TN, Zhou QP, Cobos I, Zhang S, Zagozewski J, Japoni S, Vriend J, Parkinson T, Du G, Rubenstein JL, et al. GABAergic Interneuron Differentiation in the Basal Forebrain Is Mediated through Direct Regulation of Glutamic Acid Decarboxylase Isoforms by Dlx Homeobox Transcription Factors. *The Journal of neuroscience : the official journal of the Society for Neuroscience.* 2017;37(36):8816-29.
235. Pla R, Stanco A, Howard MA, Rubin AN, Vogt D, Mortimer N, Cobos I, Potter GB, Lindtner S, Price JD, et al. Dlx1 and Dlx2 Promote Interneuron GABA Synthesis, Synaptogenesis, and Dendritogenesis. *Cerebral cortex.* 2018;28(11):3797-815.
236. Krantis A. GABA in the Mammalian Enteric Nervous System. *News in physiological sciences : an international journal of physiology produced jointly by the International Union of Physiological Sciences and the American Physiological Society.* 2000;15(284-90.
237. Hagen BM, Bayguinov O, and Sanders KM. VIP and PACAP regulate localized Ca2+ transients via cAMP-dependent mechanism. *Am J Physiol Cell Physiol.* 2006;291(2):C375-85.
238. Fung C, Unterweger P, Parry LJ, Bornstein JC, and Foong JP. VPAC1 receptors regulate intestinal secretion and muscle contractility by activating cholinergic neurons in guinea pig jejunum. *American journal of physiology Gastrointestinal and liver physiology.* 2014;306(9):G748-58.
239. Chandrasekharan B, Nezami BG, and Srinivasan S. Emerging neuropeptide targets in inflammation: NPY and VIP. *American journal of physiology Gastrointestinal and liver physiology.* 2013;304(11):G949-57.
240. Lelievre V, Favrais G, Abad C, Adle-Biassette H, Lu Y, Germano PM, Cheung-Lau G, Pisegna JR, Gressens P, Lawson G, et al. Gastrointestinal dysfunction in mice with a targeted mutation in the gene encoding vasoactive intestinal polypeptide: a model for the study of intestinal ileus and Hirschsprung's disease. *Peptides.* 2007;28(9):1688-99.
241. El-Chammas K, and Sood MR. Chronic Intestinal Pseudo-obstruction. *Clinics in colon and rectal surgery.* 2018;31(2):99-107.

242. Pichel JG, Shen L, Sheng HZ, Granholm AC, Drago J, Grinberg A, Lee EJ, Huang SP, Saarma M, Hoffer BJ, et al. Defects in enteric innervation and kidney development in mice lacking GDNF. *Nature.* 1996;382(6586):73-6.
243. Ngan ES, Shum CK, Poon HC, Sham MH, Garcia-Barcelo MM, Lui VC, and Tam PK. Prokineticin-1 (Prok-1) works coordinately with glial cell line-derived neurotrophic factor (GDNF) to mediate proliferation and differentiation of enteric neural crest cells. *Biochimica et biophysica acta.* 2008;1783(3):467-78.
244. Denning GM, Ackermann LW, Barna TJ, Armstrong JG, Stoll LL, Weintraub NL, and Dickson EW. Proenkephalin expression and enkephalin release are widely observed in non-neuronal tissues. *Peptides.* 2008;29(1):83-92.
245. Kumar PP, Franklin S, Emechebe U, Hu H, Moore B, Lehman C, Yandell M, and Moon AM. TBX3 regulates splicing in vivo: a novel molecular mechanism for Ulnar-mammary syndrome. *PLoS genetics.* 2014;10(3):e1004247.
246. Rowley M, Grothey E, and Couch FJ. The role of Tbx2 and Tbx3 in mammary development and tumorigenesis. *Journal of mammary gland biology and neoplasia.* 2004;9(2):109-18.
247. Kumar PP, Emechebe U, Smith R, Franklin S, Moore B, Yandell M, Lessnick SL, and Moon AM. Coordinated control of senescence by lncRNA and a novel T-box3 co-repressor complex. *eLife.* 2014;3(
248. Tada M, and Smith JC. T-targets: clues to understanding the functions of T-box proteins. *Development, growth & differentiation.* 2001;43(1):1-11.
249. Bamshad M, Lin RC, Law DJ, Watkins WC, Krakowiak PA, Moore ME, Franceschini P, Lala R, Holmes LB, Gebuhr TC, et al. Mutations in human TBX3 alter limb, apocrine and genital development in ulnar-mammary syndrome. *Nature genetics.* 1997;16(3):311-5.
250. Heanue TA, and Pachnis V. Expression profiling the developing mammalian enteric nervous system identifies marker and candidate Hirschsprung disease genes. *Proceedings of the National Academy of Sciences of the United States of America.* 2006;103(18):6919-24.
251. Amiel J, Sproat-Emison E, Garcia-Barcelo M, Lantieri F, Burzynski G, Borrego S, Pelet A, Arnold S, Miao X, Griseri P, et al. Hirschsprung disease, associated syndromes and genetics: a review. *Journal of medical genetics.* 2008;45(1):1-14.
252. Bergeron KF, Silversides DW, and Pilon N. The developmental genetics of Hirschsprung's disease. *Clinical genetics.* 2013;83(1):15-22.
253. Goldstein AM, Hofstra RM, and Burns AJ. Building a brain in the gut: development of the enteric nervous system. *Clinical genetics.* 2013;83(4):307-16.
254. Gui H, Schriemer D, Cheng WW, Chauhan RK, Antinolo G, Berrios C, Bleda M, Brooks AS, Brouwer RW, Burns AJ, et al. Whole exome sequencing coupled with unbiased functional analysis reveals new Hirschsprung disease genes. *Genome biology.* 2017;18(1):48.
255. Kapoor A, Jiang Q, Chatterjee S, Chakraborty P, Sosa MX, Berrios C, and Chakravarti A. Population variation in total genetic risk of Hirschsprung

disease from common RET, SEMA3 and NRG1 susceptibility polymorphisms. *Human molecular genetics.* 2015;24(10):2997-3003.
256. Luzon-Toro B, Gui H, Ruiz-Ferrer M, Sze-Man Tang C, Fernandez RM, Sham PC, Torroglosa A, Kwong-Hang Tam P, Espino-Paisan L, Cherny SS, et al. Exome sequencing reveals a high genetic heterogeneity on familial Hirschsprung disease. *Scientific reports.* 2015;5(16473.
257. Obermayr F, Hotta R, Enomoto H, and Young HM. Development and developmental disorders of the enteric nervous system. *Nature reviews Gastroenterology & hepatology.* 2013;10(1):43-57.
258. Zhu B, Zhang M, Williams EM, Keller C, Mansoor A, and Davie JK. TBX2 represses PTEN in rhabdomyosarcoma and skeletal muscle. *Oncogene.* 2016;35(32):4212-24.
259. Burgucu D, Guney K, Sahinturk D, Ozbudak IH, Ozel D, Ozbilim G, and Yavuzer U. Tbx3 represses PTEN and is over-expressed in head and neck squamous cell carcinoma. *BMC cancer.* 2012;12(481.
260. Emechebe U, Kumar PP, Rozenberg JM, Moore B, Firment A, Mirshahi T, and Moon AM. T-box3 is a ciliary protein and regulates stability of the Gli3 transcription factor to control digit number. *eLife.* 2016;5(
261. Osterwalder M, Speziale D, Shoukry M, Mohan R, Ivanek R, Kohler M, Beisel C, Wen X, Scales SJ, Christoffels VM, et al. HAND2 targets define a network of transcriptional regulators that compartmentalize the early limb bud mesenchyme. *Developmental cell.* 2014;31(3):345-57.
262. Rallis C, Del Buono J, and Logan MP. Tbx3 can alter limb position along the rostrocaudal axis of the developing embryo. *Development.* 2005;132(8):1961-70.
263. Sasselli V, Pachnis V, and Burns AJ. The enteric nervous system. *Dev Biol.* 2012;366(1):64-73.
264. Bakker ML, Boukens BJ, Mommersteeg MT, Brons JF, Wakker V, Moorman AF, and Christoffels VM. Transcription factor Tbx3 is required for the specification of the atrioventricular conduction system. *Circulation research.* 2008;102(11):1340-9.
265. Frank DU, Carter KL, Thomas KR, Burr RM, Bakker ML, Coetzee WA, Tristani-Firouzi M, Bamshad MJ, Christoffels VM, and Moon AM. Lethal arrhythmias in Tbx3-deficient mice reveal extreme dosage sensitivity of cardiac conduction system function and homeostasis. *Proc Natl Acad Sci U S A.* 2012;109(3):E154-63.
266. Frank DU, Emechebe U, Thomas KR, and Moon AM. Mouse TBX3 mutants suggest novel molecular mechanisms for Ulnar-mammary syndrome. *PloS one.* 2013;8(7):e67841.
267. Lake JI, Avetisyan M, Zimmermann AG, and Heuckeroth RO. Neural crest requires Impdh2 for development of the enteric nervous system, great vessels, and craniofacial skeleton. *Developmental biology.* 2016;409(1):152-65.

268. Jiang X, Iseki S, Maxson RE, Sucov HM, and Morriss-Kay GM. Tissue origins and interactions in the mammalian skull vault. *Developmental biology.* 2002;241(1):106-16.
269. Lee HY, Kleber M, Hari L, Brault V, Suter U, Taketo MM, Kemler R, and Sommer L. Instructive role of Wnt/beta-catenin in sensory fate specification in neural crest stem cells. *Science.* 2004;303(5660):1020-3.
270. Fu X, Xu J, Chaturvedi P, Liu H, Jiang R, and Lan Y. Identification of Osr2 Transcriptional Target Genes in Palate Development. *Journal of dental research.* 2017;96(12):1451-8.
271. Lan Y, Ovitt CE, Cho ES, Maltby KM, Wang Q, and Jiang R. Odd-skipped related 2 (Osr2) encodes a key intrinsic regulator of secondary palate growth and morphogenesis. *Development.* 2004;131(13):3207-16.
272. Srinivas S, Watanabe T, Lin CS, William CM, Tanabe Y, Jessell TM, and Costantini F. Cre reporter strains produced by targeted insertion of EYFP and ECFP into the ROSA26 locus. *BMC developmental biology.* 2001;1(4.
273. Danielian PS, Muccino D, Rowitch DH, Michael SK, and McMahon AP. Modification of gene activity in mouse embryos in utero by a tamoxifen-inducible form of Cre recombinase. *Current biology : CB.* 1998;8(24):1323-6.
274. McLeod MJ. Differential staining of cartilage and bone in whole mouse fetuses by alcian blue and alizarin red S. *Teratology.* 1980;22(3):299-301.
275. Butchbach ME, Edwards JD, Schussler KR, and Burghes AH. A novel method for oral delivery of drug compounds to the neonatal SMNDelta7 mouse model of spinal muscular atrophy. *Journal of neuroscience methods.* 2007;161(2):285-90.
276. Miller MS, Galligan JJ, and Burks TF. Accurate measurement of intestinal transit in the rat. *Journal of pharmacological methods.* 1981;6(3):211-7.
277. Carvalho BS, and Irizarry RA. A framework for oligonucleotide microarray preprocessing. *Bioinformatics.* 2010;26(19):2363-7.
278. Gentleman RC, Carey VJ, Bates DM, Bolstad B, Dettling M, Dudoit S, Ellis B, Gautier L, Ge Y, Gentry J, et al. Bioconductor: open software development for computational biology and bioinformatics. *Genome biology.* 2004;5(10):R80.
279. Turgeon B, and Meloche S. Interpreting neonatal lethal phenotypes in mouse mutants: insights into gene function and human diseases. *Physiological reviews.* 2009;89(1):1-26.
280. Mesbah K, Harrelson Z, Theveniau-Ruissy M, Papaioannou VE, and Kelly RG. Tbx3 is required for outflow tract development. *Circulation research.* 2008;103(7):743-50.
281. Bush JO, and Jiang R. Palatogenesis: morphogenetic and molecular mechanisms of secondary palate development. *Development.* 2012;139(2):231-43.
282. Walker BE, Fraser, F.C. Closure of the Secondary Palate in Three Strains of Mice. *J Embryol Exp Morphol.* 1956;4(176-89.
283. Goudy S, Law A, Sanchez G, Baldwin HS, and Brown C. Tbx1 is necessary for palatal elongation and elevation. *Mechanisms of development.* 2010;127(5-6):292-300.

284. Huang X, Goudy SL, Ketova T, Litingtung Y, and Chiang C. Gli3-deficient mice exhibit cleft palate associated with abnormal tongue development. *Developmental dynamics : an official publication of the American Association of Anatomists.* 2008;237(10):3079-87.
285. Van Landeghem L, Mahe MM, Teusan R, Leger J, Guisle I, Houlgatte R, and Neunlist M. Regulation of intestinal epithelial cells transcriptome by enteric glial cells: impact on intestinal epithelial barrier functions. *BMC Genomics.* 2009;10(507.
286. Mo R, Freer AM, Zinyk DL, Crackower MA, Michaud J, Heng HH, Chik KW, Shi XM, Tsui LC, Cheng SH, et al. Specific and redundant functions of Gli2 and Gli3 zinc finger genes in skeletal patterning and development. *Development.* 1997;124(1):113-23.
287. Lee JM, Kim JY, Cho KW, Lee MJ, Cho SW, Zhang Y, Byun SK, Yi CK, and Jung HS. Modulation of cell proliferation during palatogenesis by the interplay between Tbx3 and Bmp4. *Cell and tissue research.* 2007;327(2):285-92.
288. Zhang Z, Song Y, Zhao X, Zhang X, Fermin C, and Chen Y. Rescue of cleft palate in Msx1-deficient mice by transgenic Bmp4 reveals a network of BMP and Shh signaling in the regulation of mammalian palatogenesis. *Development.* 2002;129(17):4135-46.
289. Zirzow S, Ludtke TH, Brons JF, Petry M, Christoffels VM, and Kispert A. Expression and requirement of T-box transcription factors Tbx2 and Tbx3 during secondary palate development in the mouse. *Developmental biology.* 2009;336(2):145-55.
290. Fu M, Vohra BP, Wind D, and Heuckeroth RO. BMP signaling regulates murine enteric nervous system precursor migration, neurite fasciculation, and patterning via altered Ncam1 polysialic acid addition. *Developmental biology.* 2006;299(1):137-50.
291. Goldstein AM, Brewer KC, Doyle AM, Nagy N, and Roberts DJ. BMP signaling is necessary for neural crest cell migration and ganglion formation in the enteric nervous system. *Mechanisms of development.* 2005;122(6):821-33.
292. Puig I, Champeval D, De Santa Barbara P, Jaubert F, Lyonnet S, and Larue L. Deletion of Pten in the mouse enteric nervous system induces ganglioneuromatosis and mimics intestinal pseudoobstruction. *The Journal of clinical investigation.* 2009;119(12):3586-96.
293. Suzuki T, Takeuchi J, Koshiba-Takeuchi K, and Ogura T. Tbx Genes Specify Posterior Digit Identity through Shh and BMP Signaling. *Developmental cell.* 2004;6(1):43-53.
294. Singh R, Hoogaars WM, Barnett P, Grieskamp T, Rana MS, Buermans H, Farin HF, Petry M, Heallen T, Martin JF, et al. Tbx2 and Tbx3 induce atrioventricular myocardial development and endocardial cushion formation. *Cellular and molecular life sciences : CMLS.* 2012;69(8):1377-89.
295. Weidgang CE, Russell R, Tata PR, Kuhl SJ, Illing A, Muller M, Lin Q, Brunner C, Boeckers TM, Bauer K, et al. TBX3 Directs Cell-Fate Decision toward Mesendoderm. *Stem cell reports.* 2014;2(5):747.

296. Rao M, Rastelli D, Dong L, Chiu S, Setlik W, Gershon MD, and Corfas G. Enteric Glia Regulate Gastrointestinal Motility but Are Not Required for Maintenance of the Epithelium in Mice. *Gastroenterology.* 2017;153(4):1068-81 e7.
297. Chai Y, Jiang X, Ito Y, Bringas P, Jr., Han J, Rowitch DH, Soriano P, McMahon AP, and Sucov HM. Fate of the mammalian cranial neural crest during tooth and mandibular morphogenesis. *Development.* 2000;127(8):1671-9.
298. Chai Y, and Maxson RE, Jr. Recent advances in craniofacial morphogenesis. *Developmental dynamics : an official publication of the American Association of Anatomists.* 2006;235(9):2353-75.
299. Ferguson MW. Palate development. *Development.* 1988;103 Suppl(41-60.
300. Jin JZ, Li Q, Higashi Y, Darling DS, and Ding J. Analysis of Zfhx1a mutant mice reveals palatal shelf contact-independent medial edge epithelial differentiation during palate fusion. *Cell and tissue research.* 2008;333(1):29-38.
301. Aanhaanen WT, Brons JF, Dominguez JN, Rana MS, Norden J, Airik R, Wakker V, de Gier-de Vries C, Brown NA, Kispert A, et al. The Tbx2+ primary myocardium of the atrioventricular canal forms the atrioventricular node and the base of the left ventricle. *Circulation research.* 2009;104(11):1267-74.
302. Harrelson Z, Kelly RG, Goldin SN, Gibson-Brown JJ, Bollag RJ, Silver LM, and Papaioannou VE. Tbx2 is essential for patterning the atrioventricular canal and for morphogenesis of the outflow tract during heart development. *Development.* 2004;131(20):5041-52.
303. Hoogaars WM, Engel A, Brons JF, Verkerk AO, de Lange FJ, Wong LY, Bakker ML, Clout DE, Wakker V, Barnett P, et al. Tbx3 controls the sinoatrial node gene program and imposes pacemaker function on the atria. *Genes & development.* 2007;21(9):1098-112.
304. Douglas NC, and Papaioannou VE. The T-box transcription factors TBX2 and TBX3 in mammary gland development and breast cancer. *Journal of mammary gland biology and neoplasia.* 2013;18(2):143-7.
305. van den Boogaard M, Wong LY, Tessadori F, Bakker ML, Dreizehnter LK, Wakker V, Bezzina CR, t Hoen PA, Bakkers J, Barnett P, et al. Genetic variation in T-box binding element functionally affects SCN5A/SCN10A enhancer. *The Journal of clinical investigation.* 2012;122(7):2519-30.
306. Hotta R, Stamp LA, Foong JP, McConnell SN, Bergner AJ, Anderson RB, Enomoto H, Newgreen DF, Obermayr F, Furness JB, et al. Transplanted progenitors generate functional enteric neurons in the postnatal colon. *The Journal of clinical investigation.* 2013;123(3):1182-91.
307. Brehmer A, Rupprecht H, and Neuhuber W. Two submucosal nerve plexus in human intestines. *Histochemistry and cell biology.* 2010;133(2):149-61.
308. Sang Q, Williamson S, and Young HM. Projections of chemically identified myenteric neurons of the small and large intestine of the mouse. *Journal of anatomy.* 1997;190 (Pt 2)(209-22.

309. Stuart T, Butler A, Hoffman P, Hafemeister C, Papalexi E, Mauck WM, 3rd, Hao Y, Stoeckius M, Smibert P, and Satija R. Comprehensive Integration of Single-Cell Data. *Cell.* 2019;177(7):1888-902 e21.
310. Butler A, Hoffman P, Smibert P, Papalexi E, and Satija R. Integrating single-cell transcriptomic data across different conditions, technologies, and species. *Nature biotechnology.* 2018;36(5):411-20.
311. Dent JA, Polson AG, and Klymkowsky MW. A whole-mount immunocytochemical analysis of the expression of the intermediate filament protein vimentin in Xenopus. *Development.* 1989;105(1):61-74.
312. Dodt HU, Leischner U, Schierloh A, Jahrling N, Mauch CP, Deininger K, Deussing JM, Eder M, Zieglgansberger W, and Becker K. Ultramicroscopy: three-dimensional visualization of neuronal networks in the whole mouse brain. *Nature methods.* 2007;4(4):331-6.
313. Smith-Edwards KM, Najjar SA, Edwards BS, Howard MJ, Albers KM, and Davis BM. Extrinsic Primary Afferent Neurons Link Visceral Pain to Colon Motility Through a Spinal Reflex in Mice. *Gastroenterology.* 2019;157(2):522-36 e2.
314. Smith-Edwards KM, DeBerry JJ, Saloman JL, Davis BM, and Woodbury CJ. Profound alteration in cutaneous primary afferent activity produced by inflammatory mediators. *eLife.* 2016;5(
315. Grindberg RV, Yee-Greenbaum JL, McConnell MJ, Novotny M, O'Shaughnessy AL, Lambert GM, Arauzo-Bravo MJ, Lee J, Fishman M, Robbins GE, et al. RNA-sequencing from single nuclei. *Proc Natl Acad Sci U S A.* 2013;110(49):19802-7.
316. Habib N, Li Y, Heidenreich M, Swiech L, Avraham-Davidi I, Trombetta JJ, Hession C, Zhang F, and Regev A. Div-Seq: Single-nucleus RNA-Seq reveals dynamics of rare adult newborn neurons. *Science.* 2016;353(6302):925-8.
317. Krishnaswami SR, Grindberg RV, Novotny M, Venepally P, Lacar B, Bhutani K, Linker SB, Pham S, Erwin JA, Miller JA, et al. Using single nuclei for RNA-seq to capture the transcriptome of postmortem neurons. *Nature protocols.* 2016;11(3):499-524.
318. Lake BB, Codeluppi S, Yung YC, Gao D, Chun J, Kharchenko PV, Linnarsson S, and Zhang K. A comparative strategy for single-nucleus and single-cell transcriptomes confirms accuracy in predicted cell-type expression from nuclear RNA. *Sci Rep.* 2017;7(1):6031.
319. Lake BB, Ai R, Kaeser GE, Salathia NS, Yung YC, Liu R, Wildberg A, Gao D, Fung HL, Chen S, et al. Neuronal subtypes and diversity revealed by single-nucleus RNA sequencing of the human brain. *Science.* 2016;352(6293):1586-90.
320. Grider JR, Heuckeroth RO, Kuemmerle JF, and Murthy KS. Augmentation of the ascending component of the peristaltic reflex and substance P release by glial cell line-derived neurotrophic factor. *Neurogastroenterology and motility : the official journal of the European Gastrointestinal Motility Society.* 2010;22(7):779-86.
321. Thompson CL, Ng L, Menon V, Martinez S, Lee CK, Glattfelder K, Sunkin SM, Henry A, Lau C, Dang C, et al. A high-resolution spatiotemporal atlas of gene expression of the developing mouse brain. *Neuron.* 2014;83(2):309-23.

322. Dominguez MH, Ayoub AE, and Rakic P. POU-III transcription factors (Brn1, Brn2, and Oct6) influence neurogenesis, molecular identity, and migratory destination of upper-layer cells of the cerebral cortex. *Cerebral cortex.* 2013;23(11):2632-43.
323. Barber K, Studer L, and Fattahi F. Derivation of enteric neuron lineages from human pluripotent stem cells. *Nature protocols.* 2019;14(4):1261-79.
324. Manousiouthakis E, Chen Y, Cairns DM, Pollard R, Gerlovin K, Dente MJ, Razavi Y, and Kaplan DL. Bioengineered in vitro enteric nervous system. *Journal of tissue engineering and regenerative medicine.* 2019.
325. McCann CJ, and Thapar N. Enteric neural stem cell therapies for enteric neuropathies. *Neurogastroenterology and motility : the official journal of the European Gastrointestinal Motility Society.* 2018;30(10):e13369.
326. McCann CJ, Cooper JE, Natarajan D, Jevans B, Burnett LE, Burns AJ, and Thapar N. Transplantation of enteric nervous system stem cells rescues nitric oxide synthase deficient mouse colon. *Nature communications.* 2017;8(15937.
327. Avetisyan M, Wang H, Schill EM, Bery S, Grider JR, Hassell JA, Stappenbeck T, and Heuckeroth RO. Hepatocyte Growth Factor and MET Support Mouse Enteric Nervous System Development, the Peristaltic Response, and Intestinal Epithelial Proliferation in Response to Injury. *The Journal of neuroscience : the official journal of the Society for Neuroscience.* 2015;35(33):11543-58.
328. Swaminathan M, Hill-Yardin EL, Bornstein JC, and Foong JPP. Endogenous Glutamate Excites Myenteric Calbindin Neurons by Activating Group I Metabotropic Glutamate Receptors in the Mouse Colon. *Frontiers in neuroscience.* 2019;13(426.
329. Taniguchi H, He M, Wu P, Kim S, Paik R, Sugino K, Kvitsiani D, Fu Y, Lu J, Lin Y, et al. A resource of Cre driver lines for genetic targeting of GABAergic neurons in cerebral cortex. *Neuron.* 2011;71(6):995-1013.
330. Allan DW, and Thor S. Transcriptional selectors, masters, and combinatorial codes: regulatory principles of neural subtype specification. *Wiley interdisciplinary reviews Developmental biology.* 2015;4(5):505-28.
331. Zhang Z, Li Q, Diao M, Liu N, Cheng W, Xiao P, Zou J, Su L, Yu K, Wu J, et al. Sporadic Hirschsprung Disease: Mutational Spectrum and Novel Candidate Genes Revealed by Next-generation Sequencing. *Sci Rep.* 2017;7(1):14796.
332. Oishi K, Aramaki M, and Nakajima K. Mutually repressive interaction between Brn1/2 and Rorb contributes to the establishment of neocortical layer 2/3 and layer 4. *Proc Natl Acad Sci U S A.* 2016;113(12):3371-6.
333. Castro DS, Skowronska-Krawczyk D, Armant O, Donaldson IJ, Parras C, Hunt C, Critchley JA, Nguyen L, Gossler A, Gottgens B, et al. Proneural bHLH and Brn proteins coregulate a neurogenic program through cooperative binding to a conserved DNA motif. *Developmental cell.* 2006;11(6):831-44.
334. Jin Z, Liu L, Bian W, Chen Y, Xu G, Cheng L, and Jing N. Different transcription factors regulate nestin gene expression during P19 cell neural differentiation

and central nervous system development. *J Biol Chem.* 2009;284(12):8160-73.
335. Pruunsild P, Bengtson CP, and Bading H. Networks of Cultured iPSC-Derived Neurons Reveal the Human Synaptic Activity-Regulated Adaptive Gene Program. *Cell reports.* 2017;18(1):122-35.
336. Stoll C, Dott B, Alembik Y, and Roth MP. Associated congenital anomalies among cases with Down syndrome. *European journal of medical genetics.* 2015;58(12):674-80.
337. Avetisyan M, Schill EM, and Heuckeroth RO. Building a second brain in the bowel. *J Clin Invest.* 2015;125(3):899-907.
338. Jiang Y, Liu MT, and Gershon MD. Netrins and DCC in the guidance of migrating neural crest-derived cells in the developing bowel and pancreas. *Dev Biol.* 2003;258(2):364-84.
339. Arnold S, Pelet A, Amiel J, Borrego S, Hofstra R, Tam P, Ceccherini I, Lyonnet S, Sherman S, and Chakravarti A. Interaction between a chromosome 10 RET enhancer and chromosome 21 in the Down syndrome-Hirschsprung disease association. *Hum Mutat.* 2009;30(5):771-5.
340. Heuckeroth RO. In: Christophe Faure CDL, and Nikhil Thepar ed. *Pedaitric Neurogastroenterology: Gastrointestinal Motility And Functional Disorders In Children*. New York: Springer; 2013:271-83.
341. Jain S, Naughton CK, Yang M, Strickland A, Vij K, Encinas M, Golden J, Gupta A, Heuckeroth R, Johnson EM, Jr., et al. Mice expressing a dominant-negative Ret mutation phenocopy human Hirschsprung disease and delineate a direct role of Ret in spermatogenesis. *Development.* 2004;131(21):5503-13.
342. Quinn FM, Surana R, and Puri P. The influence of trisomy 21 on outcome in children with Hirschsprung's disease. *J Pediatr Surg.* 1994;29(6):781-3.
343. Ly A, Nikolaev A, Suresh G, Zheng Y, Tessier-Lavigne M, and Stein E. DSCAM is a netrin receptor that collaborates with DCC in mediating turning responses to netrin-1. *Cell.* 2008;133(7):1241-54.
344. Lai Wing Sun K, Correia JP, and Kennedy TE. Netrins: versatile extracellular cues with diverse functions. *Development.* 2011;138(11):2153-69.
345. Ponten F, Jirstrom K, and Uhlen M. The Human Protein Atlas--a tool for pathology. *The Journal of pathology.* 2008;216(4):387-93.
346. Reeves RH, Irving NG, Moran TH, Wohn A, Kitt C, Sisodia SS, Schmidt C, Bronson RT, and Davisson MT. A mouse model for Down syndrome exhibits learning and behaviour deficits. *Nat Genet.* 1995;11(2):177-84.
347. Gupta M, Dhanasekaran AR, and Gardiner KJ. Mouse models of Down syndrome: gene content and consequences. *Mamm Genome.* 2016;27(11-12):538-55.
348. Williams AD, Mjaatvedt CH, and Moore CS. Characterization of the cardiac phenotype in neonatal Ts65Dn mice. *Dev Dyn.* 2008;237(2):426-35.
349. Gutierrez-Castellanos N, Winkelman BH, Tolosa-Rodriguez L, Devenney B, Reeves RH, and De Zeeuw CI. Size does not always matter: Ts65Dn Down syndrome mice show cerebellum-dependent motor learning deficits that

cannot be rescued by postnatal SAG treatment. *J Neurosci.* 2013;33(39):15408-13.
350. Trazzi S, Fuchs C, Valli E, Perini G, Bartesaghi R, and Ciani E. The amyloid precursor protein (APP) triplicated gene impairs neuronal precursor differentiation and neurite development through two different domains in the Ts65Dn mouse model for Down syndrome. *J Biol Chem.* 2013;288(29):20817-29.
351. Trazzi S, Mitrugno VM, Valli E, Fuchs C, Rizzi S, Guidi S, Perini G, Bartesaghi R, and Ciani E. APP-dependent up-regulation of Ptch1 underlies proliferation impairment of neural precursors in Down syndrome. *Hum Mol Genet.* 2011;20(8):1560-73.
352. Contestabile A, Greco B, Ghezzi D, Tucci V, Benfenati F, and Gasparini L. Lithium rescues synaptic plasticity and memory in Down syndrome mice. *J Clin Invest.* 2013;123(1):348-61.
353. Kida E, Rabe A, Walus M, Albertini G, and Golabek AA. Long-term running alleviates some behavioral and molecular abnormalities in Down syndrome mouse model Ts65Dn. *Exp Neurol.* 2013;240(178-89.
354. Blazek JD, Billingsley CN, Newbauer A, and Roper RJ. Embryonic and not maternal trisomy causes developmental attenuation in the Ts65Dn mouse model for Down syndrome. *Dev Dyn.* 2010;239(6):1645-53.
355. O'Doherty A, Ruf S, Mulligan C, Hildreth V, Errington ML, Cooke S, Sesay A, Modino S, Vanes L, Hernandez D, et al. An aneuploid mouse strain carrying human chromosome 21 with Down syndrome phenotypes. *Science.* 2005;309(5743):2033-7.
356. Gribble SM, Wiseman FK, Clayton S, Prigmore E, Langley E, Yang F, Maguire S, Fu B, Rajan D, Sheppard O, et al. Massively parallel sequencing reveals the complex structure of an irradiated human chromosome on a mouse background in the Tc1 model of Down syndrome. *PLoS One.* 2013;8(4):e60482.
357. Fotaki V, Dierssen M, Alcantara S, Martinez S, Marti E, Casas C, Visa J, Soriano E, Estivill X, and Arbones ML. Dyrk1A haploinsufficiency affects viability and causes developmental delay and abnormal brain morphology in mice. *Mol Cell Biol.* 2002;22(18):6636-47.
358. Blazek JD, Abeysekera I, Li J, and Roper RJ. Rescue of the abnormal skeletal phenotype in Ts65Dn Down syndrome mice using genetic and therapeutic modulation of trisomic Dyrk1a. *Hum Mol Genet.* 2015;24(20):5687-96.
359. Viader A, Wright-Jin EC, Vohra BP, Heuckeroth RO, and Milbrandt J. Differential regional and subtype-specific vulnerability of enteric neurons to mitochondrial dysfunction. *PLoS One.* 2011;6(11):e27727.
360. Vilz TO, Overhaus M, Stoffels B, Websky M, Kalff JC, and Wehner S. Functional assessment of intestinal motility and gut wall inflammation in rodents: analyses in a standardized model of intestinal manipulation. *Journal of visualized experiments : JoVE.* 201267).

361. Sasselli V, Boesmans W, Vanden Berghe P, Tissir F, Goffinet AM, and Pachnis V. Planar cell polarity genes control the connectivity of enteric neurons. *The Journal of clinical investigation.* 2013;123(4):1763-72.
362. Roper RJ, St John HK, Philip J, Lawler A, and Reeves RH. Perinatal loss of Ts65Dn Down syndrome mice. *Genetics.* 2006;172(1):437-43.
363. de Pontual L, Pelet A, Clement-Ziza M, Trochet D, Antonarakis SE, Attie-Bitach T, Beales PL, Blouin JL, Dastot-Le Moal F, Dollfus H, et al. Epistatic interactions with a common hypomorphic RET allele in syndromic Hirschsprung disease. *Hum Mutat.* 2007;28(8):790-6.
364. Wang H, Hughes I, Planer W, Parsadanian A, Grider JR, Vohra BP, Keller-Peck C, and Heuckeroth RO. The timing and location of glial cell line-derived neurotrophic factor expression determine enteric nervous system structure and function. *The Journal of neuroscience : the official journal of the Society for Neuroscience.* 2010;30(4):1523-38.
365. Uesaka T, Young HM, Pachnis V, and Enomoto H. Development of the intrinsic and extrinsic innervation of the gut. *Developmental biology.* 2016;417(2):158-67.
366. Foong JP, Tough IR, Cox HM, and Bornstein JC. Properties of cholinergic and non-cholinergic submucosal neurons along the mouse colon. *J Physiol.* 2014;592(4):777-93.
367. Swenson O, and Bill AH, Jr. Resection of rectum and rectosigmoid with preservation of the sphincter for benign spastic lesions producing megacolon; an experimental study. *Surgery.* 1948;24(2):212-20.
368. Swenson O, Rheinlander HF, and Diamond I. Hirschsprung's disease; a new concept of the etiology; operative results in 34 patients. *N Engl J Med.* 1949;241(15):551-6.
369. Cammarata-Scalisi F, Paoli-Valeri M, Cammarata-Scalisi G, Diaz JJ, Nasre R, and Cammarata-Scalisi ME. [Frequency of imperforate anus and associated risk factors in patients with Down syndrome]. *Acta gastroenterologica Latinoamericana.* 2012;42(1):40-5.
370. Freeman SB, Torfs CP, Romitti PA, Royle MH, Druschel C, Hobbs CA, and Sherman SL. Congenital gastrointestinal defects in Down syndrome: a report from the Atlanta and National Down Syndrome Projects. *Clinical genetics.* 2009;75(2):180-4.
371. Deitz SL, and Roper RJ. Trisomic and allelic differences influence phenotypic variability during development of Down syndrome mice. *Genetics.* 2011;189(4):1487-95.
372. Das I, and Reeves RH. The use of mouse models to understand and improve cognitive deficits in Down syndrome. *Disease models & mechanisms.* 2011;4(5):596-606.
373. Currier DG, Polk RC, and Reeves RH. A Sonic hedgehog (Shh) response deficit in trisomic cells may be a common denominator for multiple features of Down syndrome. *Progress in brain research.* 2012;197(223-36.

374. Roper RJ, Baxter LL, Saran NG, Klinedinst DK, Beachy PA, and Reeves RH. Defective cerebellar response to mitogenic Hedgehog signaling in Down [corrected] syndrome mice. *Proc Natl Acad Sci U S A.* 2006;103(5):1452-6.
375. Roper RJ, VanHorn JF, Cain CC, and Reeves RH. A neural crest deficit in Down syndrome mice is associated with deficient mitotic response to Sonic hedgehog. *Mechanisms of development.* 2009;126(3-4):212-9.
376. Yamagata M, and Sanes JR. Dscam and Sidekick proteins direct lamina-specific synaptic connections in vertebrate retina. *Nature.* 2008;451(7177):465-9.
377. Fuerst PG, Bruce F, Tian M, Wei W, Elstrott J, Feller MB, Erskine L, Singer JH, and Burgess RW. DSCAM and DSCAML1 function in self-avoidance in multiple cell types in the developing mouse retina. *Neuron.* 2009;64(4):484-97.
378. Amano K, Fujii M, Arata S, Tojima T, Ogawa M, Morita N, Shimohata A, Furuichi T, Itohara S, Kamiguchi H, et al. DSCAM deficiency causes loss of pre-inspiratory neuron synchroneity and perinatal death. *The Journal of neuroscience : the official journal of the Society for Neuroscience.* 2009;29(9):2984-96.
379. Yabut O, Domogauer J, and D'Arcangelo G. Dyrk1A overexpression inhibits proliferation and induces premature neuronal differentiation of neural progenitor cells. *J Neurosci.* 2010;30(11):4004-14.
380. Fattahi F, Steinbeck JA, Kriks S, Tchieu J, Zimmer B, Kishinevsky S, Zeltner N, Mica Y, El-Nachef W, Zhao H, et al. Deriving human ENS lineages for cell therapy and drug discovery in Hirschsprung disease. *Nature.* 2016;531(7592):105-9.
381. Tang CS, Li P, Lai FP, Fu AX, Lau ST, So MT, Lui KN, Li Z, Zhuang X, Yu M, et al. Identification of Genes Associated With Hirschsprung Disease, Based on Whole-Genome Sequence Analysis, and Potential Effects on Enteric Nervous System Development. *Gastroenterology.* 2018;155(6):1908-22 e5.
382. Grossman TR, Gamliel A, Wessells RJ, Taghli-Lamallem O, Jepsen K, Ocorr K, Korenberg JR, Peterson KL, Rosenfeld MG, Bodmer R, et al. Over-expression of DSCAM and COL6A2 cooperatively generates congenital heart defects. *PLoS genetics.* 2011;7(11):e1002344.
383. Li JC, Mi KH, Zhou JL, Busch L, and Kuhnel W. The development of colon innervation in trisomy 16 mice and Hirschsprung's disease. *World journal of gastroenterology.* 2001;7(1):16-21.
384. Leffler A, Wedel T, and Busch LC. Congenital colonic hypoganglionosis in murine trisomy 16--an animal model for Down's syndrome. *Eur J Pediatr Surg.* 1999;9(6):381-8.
385. Walters LC, Cantrell VA, Weller KP, Mosher JT, and Southard-Smith EM. Genetic background impacts developmental potential of enteric neural crest-derived progenitors in the Sox10Dom model of Hirschsprung disease. *Human molecular genetics.* 2010;19(22):4353-72.
386. Reinholdt LG, Ding Y, Gilbert GJ, Czechanski A, Solzak JP, Roper RJ, Johnson MT, Donahue LR, Lutz C, and Davisson MT. Molecular characterization of the

translocation breakpoints in the Down syndrome mouse model Ts65Dn. *Mamm Genome.* 2011;22(11-12):685-91.
387. Knowles CH, Veress B, Kapur RP, Wedel T, Farrugia G, Vanderwinden JM, Geboes K, Smith VV, Martin JE, Lindberg G, et al. Quantitation of cellular components of the enteric nervous system in the normal human gastrointestinal tract--report on behalf of the Gastro 2009 International Working Group. *Neurogastroenterol Motil.* 2011;23(2):115-24.
388. Belichenko NP, Belichenko PV, Kleschevnikov AM, Salehi A, Reeves RH, and Mobley WC. The "Down syndrome critical region" is sufficient in the mouse model to confer behavioral, neurophysiological, and synaptic phenotypes characteristic of Down syndrome. *The Journal of neuroscience : the official journal of the Society for Neuroscience.* 2009;29(18):5938-48.
389. Becker W, and Sippl W. Activation, regulation, and inhibition of DYRK1A. *The FEBS journal.* 2011;278(2):246-56.
390. McElyea SD, Starbuck JM, Tumbleson-Brink DM, Harrington E, Blazek JD, Ghoneima A, Kula K, and Roper RJ. Influence of prenatal EGCG treatment and Dyrk1a dosage reduction on craniofacial features associated with Down syndrome. *Human molecular genetics.* 2016;25(22):4856-69.
391. Parisi MA, Baldessari AE, Iida MH, Clarke CM, Doggett B, Shirasawa S, and Kapur RP. Genetic background modifies intestinal pseudo-obstruction and the expression of a reporter gene in Hox11L1-/- mice. *Gastroenterology.* 2003;125(5):1428-40.
392. Gao X, Hu D, Gogol M, and Li H. ClusterMap: Compare multiple Single Cell RNA-Seq datasets across different experimental conditions. *Bioinformatics.* 2019.
393. Takahashi K, and Yamanaka S. Induction of pluripotent stem cells from mouse embryonic and adult fibroblast cultures by defined factors. *Cell.* 2006;126(4):663-76.
394. Vanhoutteghem A, Delhomme B, Herve F, Nondier I, Petit JM, Araki M, Araki K, and Djian P. The importance of basonuclin 2 in adult mice and its relation to basonuclin 1. *Mechanisms of development.* 2016;140(53-73.
395. Chi P, Chen Y, Zhang L, Guo X, Wongvipat J, Shamu T, Fletcher JA, Dewell S, Maki RG, Zheng D, et al. ETV1 is a lineage survival factor that cooperates with KIT in gastrointestinal stromal tumours. *Nature.* 2010;467(7317):849-53.
396. Mattar P, Ericson J, Blackshaw S, and Cayouette M. A conserved regulatory logic controls temporal identity in mouse neural progenitors. *Neuron.* 2015;85(3):497-504.
397. Mattar P, Stevanovic M, Nad I, and Cayouette M. Casz1 controls higher-order nuclear organization in rod photoreceptors. *Proc Natl Acad Sci U S A.* 2018;115(34):E7987-E96.
398. Wamsley B, Jaglin XH, Favuzzi E, Quattrocolo G, Nigro MJ, Yusuf N, Khodadadi-Jamayran A, Rudy B, and Fishell G. Rbfox1 Mediates Cell-type-Specific Splicing in Cortical Interneurons. *Neuron.* 2018;100(4):846-59 e7.
399. Higashi Y, Maruhashi M, Nelles L, Van de Putte T, Verschueren K, Miyoshi T, Yoshimoto A, Kondoh H, and Huylebroeck D. Generation of the floxed allele of

the SIP1 (Smad-interacting protein 1) gene for Cre-mediated conditional knockout in the mouse. *Genesis.* 2002;32(2):82-4.
400. Chen Y, Shi J, Xia TC, Xu R, He X, and Xia Y. Preservation Solutions for Kidney Transplantation: History, Advances and Mechanisms. *Cell transplantation.* 2019:963689719872699.
401. Zeisel A, Hochgerner H, Lonnerberg P, Johnsson A, Memic F, van der Zwan J, Haring M, Braun E, Borm LE, La Manno G, et al. Molecular Architecture of the Mouse Nervous System. *Cell.* 2018;174(4):999-1014 e22.
402. Workman MJ, Mahe MM, Trisno S, Poling HM, Watson CL, Sundaram N, Chang CF, Schiesser J, Aubert P, Stanley EG, et al. Engineered human pluripotent-stem-cell-derived intestinal tissues with a functional enteric nervous system. *Nature medicine.* 2017;23(1):49-59.
403. Choudhury A, Rahyead A, Kammermeier J, and Mutalib M. The Use of Pyridostigmine in a Child With Chronic Intestinal Pseudo-Obstruction. *Pediatrics.* 2018;141(Suppl 5):S404-S7.
404. Collins RRJ, Barth B, Megison S, Pfeifer CM, Rice LM, Harris S, Timmons CF, and Rakheja D. ACTG2-Associated Visceral Myopathy With Chronic Intestinal Pseudoobstruction, Intestinal Malrotation, Hypertrophic Pyloric Stenosis, Choledochal Cyst, and a Novel Missense Mutation. *International journal of surgical pathology.* 2019;27(1):77-83.
405. Dong W, Baldwin C, Choi J, Milunsky JM, Zhang J, Bilguvar K, Lifton RP, and Milunsky A. Identification of a dominant MYH11 causal variant in chronic intestinal pseudo-obstruction: Results of whole-exome sequencing. *Clinical genetics.* 2019.
406. Boeckxstaens GE, Rumessen JJ, de Wit L, Tytgat GN, and Vanderwinden JM. Abnormal distribution of the interstitial cells of cajal in an adult patient with pseudo-obstruction and megaduodenum. *The American journal of gastroenterology.* 2002;97(8):2120-6.
407. Isozaki K, Hirota S, Miyagawa J, Taniguchi M, Shinomura Y, and Matsuzawa Y. Deficiency of c-kit+ cells in patients with a myopathic form of chronic idiopathic intestinal pseudo-obstruction. *The American journal of gastroenterology.* 1997;92(2):332-4.
408. De Giorgio R, Sarnelli G, Corinaldesi R, and Stanghellini V. Advances in our understanding of the pathology of chronic intestinal pseudo-obstruction. *Gut.* 2004;53(11):1549-52.
409. Lee MY, Ha SE, Park C, Park PJ, Fuchs R, Wei L, Jorgensen BG, Redelman D, Ward SM, Sanders KM, et al. Transcriptome of interstitial cells of Cajal reveals unique and selective gene signatures. *PloS one.* 2017;12(4):e0176031.
410. Ha SE, Lee MY, Kurahashi M, Wei L, Jorgensen BG, Park C, Park PJ, Redelman D, Sasse KC, Becker LS, et al. Transcriptome analysis of PDGFRalpha+ cells identifies T-type Ca2+ channel CACNA1G as a new pathological marker for PDGFRalpha+ cell hyperplasia. *PloS one.* 2017;12(8):e0182265.
411. Breland A, Ha SE, Jorgensen BG, Jin B, Gardner TA, Sanders KM, and Ro S. Smooth Muscle Transcriptome Browser: offering genome-wide references

and expression profiles of transcripts expressed in intestinal SMC, ICC, and PDGFRalpha(+) cells. *Sci Rep.* 2019;9(1):387.
412. Batista Lobo S, Denyer M, Britland S, and Javid FA. Development of an intestinal cell culture model to obtain smooth muscle cells and myenteric neurones. *Journal of anatomy.* 2007;211(6):819-29.
413. Gabanyi I, Muller PA, Feighery L, Oliveira TY, Costa-Pinto FA, and Mucida D. Neuro-immune Interactions Drive Tissue Programming in Intestinal Macrophages. *Cell.* 2016;164(3):378-91.
414. De Schepper S, Stakenborg N, Matteoli G, Verheijden S, and Boeckxstaens GE. Muscularis macrophages: Key players in intestinal homeostasis and disease. *Cellular immunology.* 2017.
415. Vanner S, Greenwood-Van Meerveld B, Mawe G, Shea-Donohue T, Verdu EF, Wood J, and Grundy D. Fundamentals of Neurogastroenterology: Basic Science. *Gastroenterology.* 2016.
416. Furness JB. Integrated Neural and Endocrine Control of Gastrointestinal Function. *Adv Exp Med Biol.* 2016;891(159-73.
417. Furness JB. The enteric nervous system and neurogastroenterology. *Nature reviews Gastroenterology & hepatology.* 2012;9(5):286-94.
418. Sanders KM, Hwang SJ, and Ward SM. Neuroeffector apparatus in gastrointestinal smooth muscle organs. *The Journal of physiology.* 2010;588(Pt 23):4621-39.
419. Beckett EA, Horiguchi K, Khoyi M, Sanders KM, and Ward SM. Loss of enteric motor neurotransmission in the gastric fundus of Sl/Sl(d) mice. *The Journal of physiology.* 2002;543(Pt 3):871-87.
420. Klein S, Seidler B, Kettenberger A, Sibaev A, Rohn M, Feil R, Allescher HD, Vanderwinden JM, Hofmann F, Schemann M, et al. Interstitial cells of Cajal integrate excitatory and inhibitory neurotransmission with intestinal slow-wave activity. *Nature communications.* 2013;4(1630.
421. Huizinga JD, Liu LW, Fitzpatrick A, White E, Gill S, Wang XY, Zarate N, Krebs L, Choi C, Starret T, et al. Deficiency of intramuscular ICC increases fundic muscle excitability but does not impede nitrergic innervation. *American journal of physiology Gastrointestinal and liver physiology.* 2008;294(2):G589-94.
422. Groneberg D, Lies B, Konig P, Jager R, Seidler B, Klein S, Saur D, and Friebe A. Cell-specific deletion of nitric oxide-sensitive guanylyl cyclase reveals a dual pathway for nitrergic neuromuscular transmission in the murine fundus. *Gastroenterology.* 2013;145(1):188-96.
423. Kurahashi M, Zheng H, Dwyer L, Ward SM, Koh SD, and Sanders KM. A functional role for the 'fibroblast-like cells' in gastrointestinal smooth muscles. *The Journal of physiology.* 2011;589(Pt 3):697-710.
424. Iino S, Horiguchi K, and Nojyo Y. Interstitial cells of Cajal are innervated by nitrergic nerves and express nitric oxide-sensitive guanylate cyclase in the guinea-pig gastrointestinal tract. *Neuroscience.* 2008;152(2):437-48.
425. McClain J, Grubisic V, Fried D, Gomez-Suarez RA, Leinninger GM, Sevigny J, Parpura V, and Gulbransen BD. Ca2+ responses in enteric glia are mediated

by connexin-43 hemichannels and modulate colonic transit in mice. *Gastroenterology.* 2014;146(2):497-507 e1.
426. Bassotti G, Villanacci V, Antonelli E, Morelli A, and Salerni B. Enteric glial cells: new players in gastrointestinal motility? *Lab Invest.* 2007;87(7):628-32.
427. Di Nardo G, Di Lorenzo C, Lauro A, Stanghellini V, Thapar N, Karunaratne TB, Volta U, and De Giorgio R. Chronic intestinal pseudo-obstruction in children and adults: diagnosis and therapeutic options. *Neurogastroenterology and motility : the official journal of the European Gastrointestinal Motility Society.* 2017;29(1).
428. Bertrand PP, Kunze WA, Furness JB, and Bornstein JC. The terminals of myenteric intrinsic primary afferent neurons of the guinea-pig ileum are excited by 5-hydroxytryptamine acting at 5-hydroxytryptamine-3 receptors. *Neuroscience.* 2000;101(2):459-69.
429. Grubisic V, and Gulbransen BD. Enteric glial activity regulates secretomotor function in the mouse colon but does not acutely affect gut permeability. *The Journal of physiology.* 2017;595(11):3409-24.
430. Hernandes L, Zucoloto S, and Alvares EP. Effect of myenteric denervation on intestinal epithelium proliferation and migration of suckling and weanling rats. *Cell Prolif.* 2000;33(3):127-38.
431. Hitch MC, Leinicke JA, Wakeman D, Guo J, Erwin CR, Rowland KJ, Merrick EC, Heuckeroth RO, and Warner BW. Ret heterozygous mice have enhanced intestinal adaptation after massive small bowel resection. *American journal of physiology Gastrointestinal and liver physiology.* 2012;302(10):G1143-50.
432. Takahashi T, Shiraishi A, and Murata J. The Coordinated Activities of nAChR and Wnt Signaling Regulate Intestinal Stem Cell Function in Mice. *Int J Mol Sci.* 2018;19(3).
433. Greig CJ, and Cowles RA. Muscarinic acetylcholine receptors participate in small intestinal mucosal homeostasis. *Journal of pediatric surgery.* 2017;52(6):1031-4.
434. Lundgren O, Jodal M, Jansson M, Ryberg AT, and Svensson L. Intestinal epithelial stem/progenitor cells are controlled by mucosal afferent nerves. *PloS one.* 2011;6(2):e16295.
435. Muise ED, Gandotra N, Tackett JJ, Bamdad MC, and Cowles RA. Distribution of muscarinic acetylcholine receptor subtypes in the murine small intestine. *Life Sci.* 2017;169(6-10.
436. Gross ER, Gershon MD, Margolis KG, Gertsberg ZV, Li Z, and Cowles RA. Neuronal serotonin regulates growth of the intestinal mucosa in mice. *Gastroenterology.* 2012;143(2):408-17 e2.
437. Bjerknes M, and Cheng H. Modulation of specific intestinal epithelial progenitors by enteric neurons. *Proc Natl Acad Sci U S A.* 2001;98(22):12497-502.
438. Leen JL, Izzo A, Upadhyay C, Rowland KJ, Dube PE, Gu S, Heximer SP, Rhodes CJ, Storm DR, Lund PK, et al. Mechanism of action of glucagon-like peptide-2 to increase IGF-I mRNA in intestinal subepithelial fibroblasts. *Endocrinology.* 2011;152(2):436-46.

439. Cornet A, Savidge TC, Cabarrocas J, Deng WL, Colombel JF, Lassmann H, Desreumaux P, and Liblau RS. Enterocolitis induced by autoimmune targeting of enteric glial cells: a possible mechanism in Crohn's disease? *Proc Natl Acad Sci U S A.* 2001;98(23):13306-11.
440. Aube AC, Cabarrocas J, Bauer J, Philippe D, Aubert P, Doulay F, Liblau R, Galmiche JP, and Neunlist M. Changes in enteric neurone phenotype and intestinal functions in a transgenic mouse model of enteric glia disruption. *Gut.* 2006;55(5):630-7.
441. Savidge TC, Newman P, Pothoulakis C, Ruhl A, Neunlist M, Bourreille A, Hurst R, and Sofroniew MV. Enteric glia regulate intestinal barrier function and inflammation via release of S-nitrosoglutathione. *Gastroenterology.* 2007;132(4):1344-58.
442. Bush TG, Savidge TC, Freeman TC, Cox HJ, Campbell EA, Mucke L, Johnson MH, and Sofroniew MV. Fulminant jejuno-ileitis following ablation of enteric glia in adult transgenic mice. *Cell.* 1998;93(2):189-201.
443. von Boyen GB, Schulte N, Pfluger C, Spaniol U, Hartmann C, and Steinkamp M. Distribution of enteric glia and GDNF during gut inflammation. *BMC Gastroenterol.* 2011;11(3.
444. Xiao WD, Chen W, Sun LH, Wang WS, Zhou SW, and Yang H. The protective effect of enteric glial cells on intestinal epithelial barrier function is enhanced by inhibiting inducible nitric oxide synthase activity under lipopolysaccharide stimulation. *Mol Cell Neurosci.* 2011;46(2):527-34.
445. Xiao W, Wang W, Chen W, Sun L, Li X, Zhang C, and Yang H. GDNF is involved in the barrier-inducing effect of enteric glial cells on intestinal epithelial cells under acute ischemia reperfusion stimulation. *Mol Neurobiol.* 2014;50(2):274-89.
446. Steinkamp M, Geerling I, Seufferlein T, von Boyen G, Egger B, Grossmann J, Ludwig L, Adler G, and Reinshagen M. Glial-derived neurotrophic factor regulates apoptosis in colonic epithelial cells. *Gastroenterology.* 2003;124(7):1748-57.
447. Zhang DK, He FQ, Li TK, Pang XH, Cui DJ, Xie Q, Huang XL, and Gan HT. Glial-derived neurotrophic factor regulates intestinal epithelial barrier function and inflammation and is therapeutic for murine colitis. *J Pathol.* 2010;222(2):213-22.
448. Ibiza S, Garcia-Cassani B, Ribeiro H, Carvalho T, Almeida L, Marques R, Misic AM, Bartow-McKenney C, Larson DM, Pavan WJ, et al. Glial-cell-derived neuroregulators control type 3 innate lymphoid cells and gut defence. *Nature.* 2016;535(7612):440-3.
449. Chalazonitis A, Pham TD, Li Z, Roman D, Guha U, Gomes W, Kan L, Kessler JA, and Gershon MD. Bone morphogenetic protein regulation of enteric neuronal phenotypic diversity: relationship to timing of cell cycle exit. *The Journal of comparative neurology.* 2008;509(5):474-92.
450. Muller PA, Koscso B, Rajani GM, Stevanovic K, Berres ML, Hashimoto D, Mortha A, Leboeuf M, Li XM, Mucida D, et al. Crosstalk between muscularis

macrophages and enteric neurons regulates gastrointestinal motility. *Cell.* 2014;158(2):300-13.
451. Cipriani G, Gibbons SJ, Kashyap PC, and Farrugia G. Intrinsic Gastrointestinal Macrophages: Their Phenotype and Role in Gastrointestinal Motility. *Cellular and molecular gastroenterology and hepatology.* 2016;2(2):120-30 e1.
452. Chandrasekharan B, Jeppsson S, Pienkowski S, Belsham DD, Sitaraman SV, Merlin D, Kokkotou E, Nusrat A, Tansey MG, and Srinivasan S. Tumor necrosis factor-neuropeptide Y cross talk regulates inflammation, epithelial barrier functions, and colonic motility. *Inflamm Bowel Dis.* 2013;19(12):2535-46.
453. Matteoli G, Gomez-Pinilla PJ, Nemethova A, Di Giovangiulio M, Cailotto C, van Bree SH, Michel K, Tracey KJ, Schemann M, Boesmans W, et al. A distinct vagal anti-inflammatory pathway modulates intestinal muscularis resident macrophages independent of the spleen. *Gut.* 2014;63(6):938-48.
454. Wang H, Yu M, Ochani M, Amella CA, Tanovic M, Susarla S, Li JH, Wang H, Yang H, Ulloa L, et al. Nicotinic acetylcholine receptor alpha7 subunit is an essential regulator of inflammation. *Nature.* 2003;421(6921):384-8.
455. de Jonge WJ, van der Zanden EP, The FO, Bijlsma MF, van Westerloo DJ, Bennink RJ, Berthoud HR, Uematsu S, Akira S, van den Wijngaard RM, et al. Stimulation of the vagus nerve attenuates macrophage activation by activating the Jak2-STAT3 signaling pathway. *Nat Immunol.* 2005;6(8):844-51.
456. Wehner S, Behrendt FF, Lyutenski BN, Lysson M, Bauer AJ, Hirner A, and Kalff JC. Inhibition of macrophage function prevents intestinal inflammation and postoperative ileus in rodents. *Gut.* 2007;56(2):176-85.
457. The F, Cailotto C, van der Vliet J, de Jonge WJ, Bennink RJ, Buijs RM, and Boeckxstaens GE. Central activation of the cholinergic anti-inflammatory pathway reduces surgical inflammation in experimental post-operative ileus. *Br J Pharmacol.* 2011;163(5):1007-16.
458. Barajon I, Serrao G, Arnaboldi F, Opizzi E, Ripamonti G, Balsari A, and Rumio C. Toll-like receptors 3, 4, and 7 are expressed in the enteric nervous system and dorsal root ganglia. *J Histochem Cytochem.* 2009;57(11):1013-23.
459. McVey Neufeld KA, Mao YK, Bienenstock J, Foster JA, and Kunze WA. The microbiome is essential for normal gut intrinsic primary afferent neuron excitability in the mouse. *Neurogastroenterology and motility : the official journal of the European Gastrointestinal Motility Society.* 2013;25(2):183-e88.
460. Lomasney KW, Cryan JF, and Hyland NP. Converging effects of a Bifidobacterium and Lactobacillus probiotic strain on mouse intestinal physiology. *American journal of physiology Gastrointestinal and liver physiology.* 2014;307(2):G241-7.
461. Wang B, Mao YK, Diorio C, Wang L, Huizinga JD, Bienenstock J, and Kunze W. Lactobacillus reuteri ingestion and IK(Ca) channel blockade have similar effects on rat colon motility and myenteric neurones. *Neurogastroenterology and motility : the official journal of the European Gastrointestinal Motility Society.* 2010;22(1):98-107, e33.

462. Hyland NP, and Cryan JF. Microbe-host interactions: Influence of the gut microbiota on the enteric nervous system. *Developmental biology.* 2016;417(2):182-7.
463. Kabouridis PS, and Pachnis V. Emerging roles of gut microbiota and the immune system in the development of the enteric nervous system. *The Journal of clinical investigation.* 2015;125(3):956-64.
464. Chiocchetti R, Mazzuoli G, Albanese V, Mazzoni M, Clavenzani P, Lalatta-Costerbosa G, Lucchi ML, Di Guardo G, Marruchella G, and Furness JB. Anatomical evidence for ileal Peyer's patches innervation by enteric nervous system: a potential route for prion neuroinvasion? *Cell and tissue research.* 2008;332(2):185-94.
465. Vulchanova L, Casey MA, Crabb GW, Kennedy WR, and Brown DR. Anatomical evidence for enteric neuroimmune interactions in Peyer's patches. *J Neuroimmunol.* 2007;185(1-2):64-74.
466. Farzi A, Reichmann F, and Holzer P. The homeostatic role of neuropeptide Y in immune function and its impact on mood and behaviour. *Acta Physiol (Oxf).* 2015;213(3):603-27.
467. Wheway J, Mackay CR, Newton RA, Sainsbury A, Boey D, Herzog H, and Mackay F. A fundamental bimodal role for neuropeptide Y1 receptor in the immune system. *J Exp Med.* 2005;202(11):1527-38.
468. Gonzalez-Rey E, Fernandez-Martin A, Chorny A, and Delgado M. Vasoactive intestinal peptide induces CD4+,CD25+ T regulatory cells with therapeutic effect in collagen-induced arthritis. *Arthritis Rheum.* 2006;54(3):864-76.
469. Gonzalez-Rey E, Chorny A, Fernandez-Martin A, Ganea D, and Delgado M. Vasoactive intestinal peptide generates human tolerogenic dendritic cells that induce CD4 and CD8 regulatory T cells. *Blood.* 2006;107(9):3632-8.
470. Delgado M, Gonzalez-Rey E, and Ganea D. The neuropeptide vasoactive intestinal peptide generates tolerogenic dendritic cells. *J Immunol.* 2005;175(11):7311-24.
471. Abad C, Cheung-Lau G, Coute-Monvoisin AC, and Waschek JA. Vasoactive intestinal peptide-deficient mice exhibit reduced pathology in trinitrobenzene sulfonic acid-induced colitis. *Neuroimmunomodulation.* 2015;22(3):203-12.
472. Abad C, Tan YV, Cheung-Lau G, Nobuta H, and Waschek JA. VIP deficient mice exhibit resistance to lipopolysaccharide induced endotoxemia with an intrinsic defect in proinflammatory cellular responses. *PloS one.* 2012;7(5):e36922.
473. Latorre R, Sternini C, De Giorgio R, and Greenwood-Van Meerveld B. Enteroendocrine cells: a review of their role in brain-gut communication. *Neurogastroenterology and motility : the official journal of the European Gastrointestinal Motility Society.* 2016;28(5):620-30.
474. He Y, Wang H, Yang D, Wang C, Yang L, and Jin C. Differential expression of motilin receptor in various parts of gastrointestinal tract in dogs. *Gastroenterol Res Pract.* 2015;2015(970940.

475. Amato A, Cinci L, Rotondo A, Serio R, Faussone-Pellegrini MS, Vannucchi MG, and Mule F. Peripheral motor action of glucagon-like peptide-1 through enteric neuronal receptors. *Neurogastroenterology and motility : the official journal of the European Gastrointestinal Motility Society.* 2010;22(6):664-e203.
476. Sayegh AI, and Ritter RC. Cholecystokinin activates specific enteric neurons in the rat small intestine. *Peptides.* 2003;24(2):237-44.
477. Bohorquez DV, Shahid RA, Erdmann A, Kreger AM, Wang Y, Calakos N, Wang F, and Liddle RA. Neuroepithelial circuit formed by innervation of sensory enteroendocrine cells. *The Journal of clinical investigation.* 2015;125(2):782-6.
478. Berthoud HR, Jedrzejewska A, and Powley TL. Simultaneous labeling of vagal innervation of the gut and afferent projections from the visceral forebrain with dil injected into the dorsal vagal complex in the rat. *The Journal of comparative neurology.* 1990;301(1):65-79.
479. Lomax AE, Sharkey KA, and Furness JB. The participation of the sympathetic innervation of the gastrointestinal tract in disease states. *Neurogastroenterology and motility : the official journal of the European Gastrointestinal Motility Society.* 2010;22(1):7-18.
480. Gulbransen BD, Bains JS, and Sharkey KA. Enteric glia are targets of the sympathetic innervation of the myenteric plexus in the guinea pig distal colon. *The Journal of neuroscience : the official journal of the Society for Neuroscience.* 2010;30(19):6801-9.
481. Sjovall H, Redfors S, Hallback DA, Eklund S, Jodal M, and Lundgren O. The effect of splanchnic nerve stimulation on blood flow distribution, villous tissue osmolality and fluid and electrolyte transport in the small intestine of the cat. *Acta Physiol Scand.* 1983;117(3):359-65.
482. Sjovall H, Redfors S, Jodal M, and Lundgren O. On the mode of action of the sympathetic fibres on intestinal fluid transport: evidence for the existence of a glucose-stimulated secretory nervous pathway in the intestinal wall. *Acta Physiol Scand.* 1983;119(1):39-48.
483. Altschuler SM, Escardo J, Lynn RB, and Miselis RR. The central organization of the vagus nerve innervating the colon of the rat. *Gastroenterology.* 1993;104(2):502-9.
484. Espinosa-Medina I, Saha O, Boismoreau F, Chettouh Z, Rossi F, Richardson WD, and Brunet JF. The sacral autonomic outflow is sympathetic. *Science.* 2016;354(6314):893-7.
485. Walter GC, Phillips RJ, Baronowsky EA, and Powley TL. Versatile, high-resolution anterograde labeling of vagal efferent projections with dextran amines. *J Neurosci Methods.* 2009;178(1):1-9.
486. Kalia M, Fuxe K, Goldstein M, Harfstrand A, Agnati LF, and Coyle JT. Evidence for the existence of putative dopamine-, adrenaline- and noradrenaline-containing vagal motor neurons in the brainstem of the rat. *Neurosci Lett.* 1984;50(1-3):57-62.

487. Hyland NP, Abrahams TP, Fuchs K, Burmeister MA, and Hornby PJ. Organization and neurochemistry of vagal preganglionic neurons innervating the lower esophageal sphincter in ferrets. *The Journal of comparative neurology.* 2001;430(2):222-34.
488. Powell N, Walker MM, and Talley NJ. The mucosal immune system: master regulator of bidirectional gut-brain communications. *Nature reviews Gastroenterology & hepatology.* 2017;14(3):143-59.
489. Pan-Montojo F, Anichtchik O, Dening Y, Knels L, Pursche S, Jung R, Jackson S, Gille G, Spillantini MG, Reichmann H, et al. Progression of Parkinson's disease pathology is reproduced by intragastric administration of rotenone in mice. *PloS one.* 2010;5(1):e8762.
490. Braak H, de Vos RA, Bohl J, and Del Tredici K. Gastric alpha-synuclein immunoreactive inclusions in Meissner's and Auerbach's plexuses in cases staged for Parkinson's disease-related brain pathology. *Neurosci Lett.* 2006;396(1):67-72.
491. Edwards LL, Pfeiffer RF, Quigley EM, Hofman R, and Balluff M. Gastrointestinal symptoms in Parkinson's disease. *Mov Disord.* 1991;6(2):151-6.
492. Holmqvist S, Chutna O, Bousset L, Aldrin-Kirk P, Li W, Bjorklund T, Wang ZY, Roybon L, Melki R, and Li JY. Direct evidence of Parkinson pathology spread from the gastrointestinal tract to the brain in rats. *Acta Neuropathol.* 2014;128(6):805-20.
493. Ulusoy A, Rusconi R, Perez-Revuelta BI, Musgrove RE, Helwig M, Winzen-Reichert B, and Di Monte DA. Caudo-rostral brain spreading of alpha-synuclein through vagal connections. *EMBO Mol Med.* 2013;5(7):1119-27.
494. Liu B, Fang F, Pedersen NL, Tillander A, Ludvigsson JF, Ekbom A, Svenningsson P, Chen H, and Wirdefeldt K. Vagotomy and Parkinson disease: A Swedish register-based matched-cohort study. *Neurology.* 2017;88(21):1996-2002.
495. Svensson E, Horvath-Puho E, Thomsen RW, Djurhuus JC, Pedersen L, Borghammer P, and Sorensen HT. Vagotomy and subsequent risk of Parkinson's disease. *Annals of neurology.* 2015;78(4):522-9.
496. Kaatz M, Fast C, Ziegler U, Balkema-Buschmann A, Hammerschmidt B, Keller M, Oelschlegel A, McIntyre L, and Groschup MH. Spread of classic BSE prions from the gut via the peripheral nervous system to the brain. *Am J Pathol.* 2012;181(2):515-24.
497. Rao M, and Gershon MD. The bowel and beyond: the enteric nervous system in neurological disorders. *Nature reviews Gastroenterology & hepatology.* 2016;13(9):517-28.
498. Del Tredici K, and Braak H. Review: Sporadic Parkinson's disease: development and distribution of alpha-synuclein pathology. *Neuropathol Appl Neurobiol.* 2016;42(1):33-50.
499. Natale G, Ferrucci M, Lazzeri G, Paparelli A, and Fornai F. Transmission of prions within the gut and towards the central nervous system. *Prion.* 2011;5(3):142-9.

500. Bernier R, Golzio C, Xiong B, Stessman HA, Coe BP, Penn O, Witherspoon K, Gerdts J, Baker C, Vulto-van Silfhout AT, et al. Disruptive CHD8 mutations define a subtype of autism early in development. *Cell.* 2014;158(2):263-76.
501. Grubisic V, Kennedy AJ, Sweatt JD, and Parpura V. Pitt-Hopkins Mouse Model has Altered Particular Gastrointestinal Transits In Vivo. *Autism Res.* 2015;8(5):629-33.
502. Margolis KG, Li Z, Stevanovic K, Saurman V, Israelyan N, Anderson GM, Snyder I, Veenstra-VanderWeele J, Blakely RD, and Gershon MD. Serotonin transporter variant drives preventable gastrointestinal abnormalities in development and function. *The Journal of clinical investigation.* 2016;126(6):2221-35.
503. Peng Y, Huentelman M, Smith C, and Qiu S. MET receptor tyrosine kinase as an autism genetic risk factor. *Int Rev Neurobiol.* 2013;113(135-65.
504. Puig KL, Lutz BM, Urquhart SA, Rebel AA, Zhou X, Manocha GD, Sens M, Tuteja AK, Foster NL, and Combs CK. Overexpression of mutant amyloid-beta protein precursor and presenilin 1 modulates enteric nervous system. *J Alzheimers Dis.* 2015;44(4):1263-78.
505. Semar S, Klotz M, Letiembre M, Van Ginneken C, Braun A, Jost V, Bischof M, Lammers WJ, Liu Y, Fassbender K, et al. Changes of the enteric nervous system in amyloid-beta protein precursor transgenic mice correlate with disease progression. *J Alzheimers Dis.* 2013;36(1):7-20.
506. Guo Y, Wang Q, Zhang K, An T, Shi P, Li Z, Duan W, and Li C. HO-1 induction in motor cortex and intestinal dysfunction in TDP-43 A315T transgenic mice. *Brain research.* 2012;1460(88-95.
507. Esmaeili MA, Panahi M, Yadav S, Hennings L, and Kiaei M. Premature death of TDP-43 (A315T) transgenic mice due to gastrointestinal complications prior to development of full neurological symptoms of amyotrophic lateral sclerosis. *Int J Exp Pathol.* 2013;94(1):56-64.
508. Furness JB. *The enteric nervous system.* Malden, MA: Blackwell Publishing; 2006.
509. Liu YA, Chung YC, Pan ST, Shen MY, Hou YC, Peng SJ, Pasricha PJ, and Tang SC. 3-D imaging, illustration, and quantitation of enteric glial network in transparent human colon mucosa. *Neurogastroenterol Motil.* 2013;25(5):e324-38.
510. Fu YY, Peng SJ, Lin HY, Pasricha PJ, and Tang SC. 3-D imaging and illustration of mouse intestinal neurovascular complex. *Am J Physiol Gastrointest Liver Physiol.* 2013;304(1):G1-11.
511. Liu YA, Chen Y, Chiang AS, Peng SJ, Pasricha PJ, and Tang SC. Optical clearing improves the imaging depth and signal-to-noise ratio for digital analysis and three-dimensional projection of the human enteric nervous system. *Neurogastroenterol Motil.* 2011;23(10):e446-57.
512. Nemeth L, Yoneda A, Kader M, Devaney D, and Puri P. Three-dimensional morphology of gut innervation in total intestinal aganglionosis using whole-mount preparation. *J Pediatr Surg.* 2001;36(2):291-5.

513. Knowles CH, De Giorgio R, Kapur RP, Bruder E, Farrugia G, Geboes K, Lindberg G, Martin JE, Meier-Ruge WA, Milla PJ, et al. The London Classification of gastrointestinal neuromuscular pathology: report on behalf of the Gastro 2009 International Working Group. *Gut.* 2010;59(7):882-7.
514. Swaminathan M, and Kapur RP. Counting myenteric ganglion cells in histologic sections: an empirical approach. *Hum Pathol.* 2010;41(8):1097-108.
515. Keller J, Bassotti G, Clarke J, Dinning P, Fox M, Grover M, Hellstrom PM, Ke M, Layer P, Malagelada C, et al. Expert consensus document: Advances in the diagnosis and classification of gastric and intestinal motility disorders. *Nat Rev Gastroenterol Hepatol.* 2018;15(5):291-308.
516. Chambers JD, Bornstein JC, and Thomas EA. Insights into mechanisms of intestinal segmentation in guinea pigs: a combined computational modeling and in vitro study. *Am J Physiol Gastrointest Liver Physiol.* 2008;295(3):G534-41.
517. Blair PJ, Rhee PL, Sanders KM, and Ward SM. The Significance of Interstitial Cells in Neurogastroenterology. *J Neurogastroenterol Motil.* 2014.
518. Bredenoord AJ, Fox M, Kahrilas PJ, Pandolfino JE, Schwizer W, and Smout AJ. Chicago classification criteria of esophageal motility disorders defined in high resolution esophageal pressure topography. *Neurogastroenterol Motil.* 2012;24 Suppl 1(57-65.
519. Nguyen LA, and Snape WJ, Jr. Clinical presentation and pathophysiology of gastroparesis. *Gastroenterol Clin North Am.* 2015;44(1):21-30.
520. Kilkenny C, Browne WJ, Cuthill IC, Emerson M, and Altman DG. Improving bioscience research reporting: the ARRIVE guidelines for reporting animal research. *Osteoarthritis Cartilage.* 2012;20(4):256-60.
521. Enomoto H, Araki T, Jackman A, Heuckeroth RO, Snider WD, Johnson EM, Jr., and Milbrandt J. GFR alpha1-deficient mice have deficits in the enteric nervous system and kidneys. *Neuron.* 1998;21(2):317-24.
522. Krammer HJ, Karahan ST, Rumpel E, Klinger M, and Kuhnel W. Immunohistochemical visualization of the enteric nervous system using antibodies against protein gene product (PGP) 9.5. *Anat Anz.* 1993;175(4):321-5.
523. Wedel T, Roblick U, Gleiss J, Schiedeck T, Bruch HP, Kuhnel W, and Krammer HJ. Organization of the enteric nervous system in the human colon demonstrated by wholemount immunohistochemistry with special reference to the submucous plexus. *Ann Anat.* 1999;181(4):327-37.
524. Workman MJ, Mahe MM, Trisno S, Poling HM, Watson CL, Sundaram N, Chang CF, Schiesser J, Aubert P, Stanley EG, et al. Engineered human pluripotent-stem-cell-derived intestinal tissues with a functional enteric nervous system. *Nat Med.* 2016.
525. Hama H, Kurokawa H, Kawano H, Ando R, Shimogori T, Noda H, Fukami K, Sakaue-Sawano A, and Miyawaki A. Scale: a chemical approach for fluorescence imaging and reconstruction of transparent mouse brain. *Nat Neurosci.* 2011;14(11):1481-8.

526. Belle M, Godefroy D, Couly G, Malone SA, Collier F, Giacobini P, and Chedotal A. Tridimensional Visualization and Analysis of Early Human Development. *Cell.* 2017;169(1):161-73 e12.
527. Erturk A, Mauch CP, Hellal F, Forstner F, Keck T, Becker K, Jahrling N, Steffens H, Richter M, Hubener M, et al. Three-dimensional imaging of the unsectioned adult spinal cord to assess axon regeneration and glial responses after injury. *Nat Med.* 2011;18(1):166-71.
528. Knowles CH, De Giorgio R, Kapur RP, Bruder E, Farrugia G, Geboes K, Gershon MD, Hutson J, Lindberg G, Martin JE, et al. Gastrointestinal neuromuscular pathology: guidelines for histological techniques and reporting on behalf of the Gastro 2009 International Working Group. *Acta Neuropathol.* 2009;118(2):271-301.
529. Uranga-Ocio JA, Bastus-Diez S, Delkader-Palacios D, Garcia-Cristobal N, Leal-Garcia MA, and Abalo-Delgado R. Enteric neuropathy associated to diabetes mellitus. *Rev Esp Enferm Dig.* 2015;107(6):366-73.
530. Porter AJ, Wattchow DA, Brookes SJ, and Costa M. The neurochemical coding and projections of circular muscle motor neurons in the human colon. *Gastroenterology.* 1997;113(6):1916-23.
531. Murphy EM, Defontgalland D, Costa M, Brookes SJ, and Wattchow DA. Quantification of subclasses of human colonic myenteric neurons by immunoreactivity to Hu, choline acetyltransferase and nitric oxide synthase. *Neurogastroenterol Motil.* 2007;19(2):126-34.
532. Wattchow D, Brookes S, Murphy E, Carbone S, de Fontgalland D, and Costa M. Regional variation in the neurochemical coding of the myenteric plexus of the human colon and changes in patients with slow transit constipation. *Neurogastroenterol Motil.* 2008;20(12):1298-305.
533. Ng KS, Montes-Adrian NA, Mahns DA, and Gladman MA. Quantification and neurochemical coding of the myenteric plexus in humans: No regional variation between the distal colon and rectum. *Neurogastroenterol Motil.* 2018;30(3).
534. Helander HF, and Fandriks L. Surface area of the digestive tract - revisited. *Scand J Gastroenterol.* 2014;49(6):681-9.
535. Farrugia G. Histologic changes in diabetic gastroparesis. *Gastroenterol Clin North Am.* 2015;44(1):31-8.
536. Costa DVS, Bon-Frauches AC, Silva A, Lima-Junior RCP, Martins CS, Leitao RFC, Freitas GB, Castelucci P, Bolick DT, Guerrant RL, et al. 5-Fluorouracil Induces Enteric Neuron Death and Glial Activation During Intestinal Mucositis via a S100B-RAGE-NFkappaB-Dependent Pathway. *Sci Rep.* 2019;9(1):665.
537. Macchioni L, Petricciuolo M, Davidescu M, Fettucciari K, Scarpelli P, Vitale R, Gatticchi L, Orvietani PL, Marchegiani A, Marconi P, et al. Palmitate lipotoxicity in enteric glial cells: Lipid remodeling and mitochondrial ROS are responsible for cyt c release outside mitochondria. *Biochim Biophys Acta Mol Cell Biol Lipids.* 2018;1863(8):895-908.

538. Stojanovska V, Sakkal S, and Nurgali K. Platinum-based chemotherapy: gastrointestinal immunomodulation and enteric nervous system toxicity. *Am J Physiol Gastrointest Liver Physiol.* 2015;308(4):G223-32.
539. Chalazonitis A, and Rao M. Enteric nervous system manifestations of neurodegenerative disease. *Brain Res.* 2018;1693(Pt B):207-13.
540. Yarandi SS, and Srinivasan S. Diabetic gastrointestinal motility disorders and the role of enteric nervous system: current status and future directions. *Neurogastroenterol Motil.* 2014;26(5):611-24.
541. Azpiroz F, and Malagelada C. Diabetic neuropathy in the gut: pathogenesis and diagnosis. *Diabetologia.* 2016;59(3):404-8.
542. Mawe GM. Colitis-induced neuroplasticity disrupts motility in the inflamed and post-inflamed colon. *J Clin Invest.* 2015;125(3):949-55.
543. White JP, Xiong S, Malvin NP, Khoury-Hanold W, Heuckeroth RO, Stappenbeck TS, and Diamond MS. Intestinal Dysmotility Syndromes following Systemic Infection by Flaviviruses. *Cell.* 2018;175(5):1198-212 e12.
544. Margolis KG, and Gershon MD. Enteric Neuronal Regulation of Intestinal Inflammation. *Trends Neurosci.* 2016;39(9):614-24.
545. Klem F, Wadhwa A, Prokop LJ, Sundt WJ, Farrugia G, Camilleri M, Singh S, and Grover M. Prevalence, Risk Factors, and Outcomes of Irritable Bowel Syndrome After Infectious Enteritis: A Systematic Review and Meta-analysis. *Gastroenterology.* 2017;152(5):1042-54 e1.
546. Young HM, Stamp LA, and McKeown SJ. ENS Development Research Since 1983: Great Strides but Many Remaining Challenges. *Adv Exp Med Biol.* 2016;891(53-62.
547. Hoff S, Zeller F, von Weyhern CW, Wegner M, Schemann M, Michel K, and Ruhl A. Quantitative assessment of glial cells in the human and guinea pig enteric nervous system with an anti-Sox8/9/10 antibody. *J Comp Neurol.* 2008;509(4):356-71.
548. Olsson C, and Holmgren S. Autonomic control of gut motility: a comparative view. *Auton Neurosci.* 2011;165(1):80-101.
549. Christensen J, Stiles MJ, Rick GA, and Sutherland J. Comparative anatomy of the myenteric plexus of the distal colon in eight mammals. *Gastroenterology.* 1984;86(4):706-13.
550. Rao M, Nelms BD, Dong L, Salinas-Rios V, Rutlin M, Gershon MD, and Corfas G. Enteric glia express proteolipid protein 1 and are a transcriptionally unique population of glia in the mammalian nervous system. *Glia.* 2015.
551. Boesmans W, Lasrado R, Vanden Berghe P, and Pachnis V. Heterogeneity and phenotypic plasticity of glial cells in the mammalian enteric nervous system. *Glia.* 2015;63(2):229-41.
552. Bassotti G, Battaglia E, Bellone G, Dughera L, Fisogni S, Zambelli C, Morelli A, Mioli P, Emanuelli G, and Villanacci V. Interstitial cells of Cajal, enteric nerves, and glial cells in colonic diverticular disease. *Journal of clinical pathology.* 2005;58(9):973-7.

553. De Quelen F, Chevalier J, Rolli-Derkinderen M, Mourot J, Neunlist M, and Boudry G. n-3 polyunsaturated fatty acids in the maternal diet modify the postnatal development of nervous regulation of intestinal permeability in piglets. *J Physiol.* 2011;589(Pt 17):4341-52.
554. Musser MA, Correa H, and Southard-Smith EM. Enteric neuron imbalance and proximal dysmotility in ganglionated intestine of the Sox10Dom/+ Hirschsprung mouse model. *Cellular and molecular gastroenterology and hepatology.* 2015;1(1):87-101.